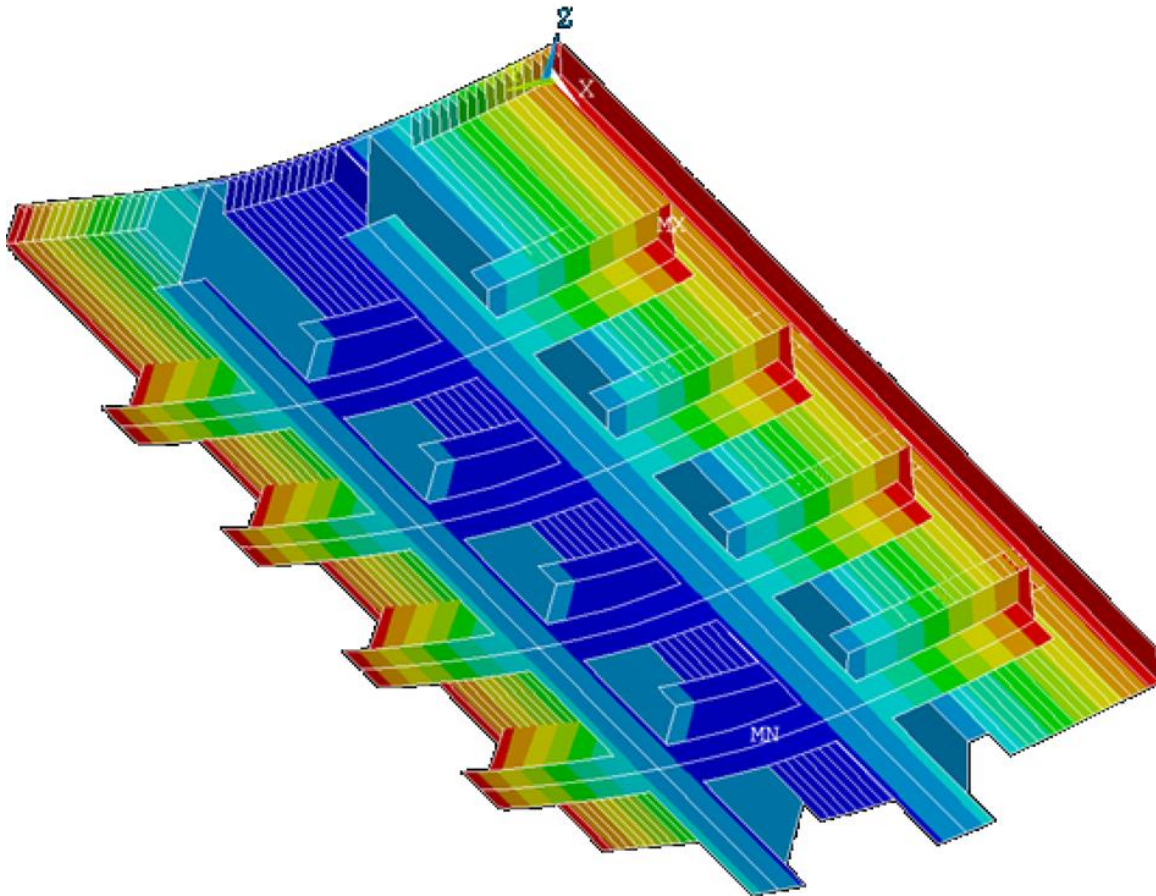


# Composite Bridge Design

---

Analysis of Realizing Composite Action in an FRP-Steel Bridge



Peter Flink

December 2015



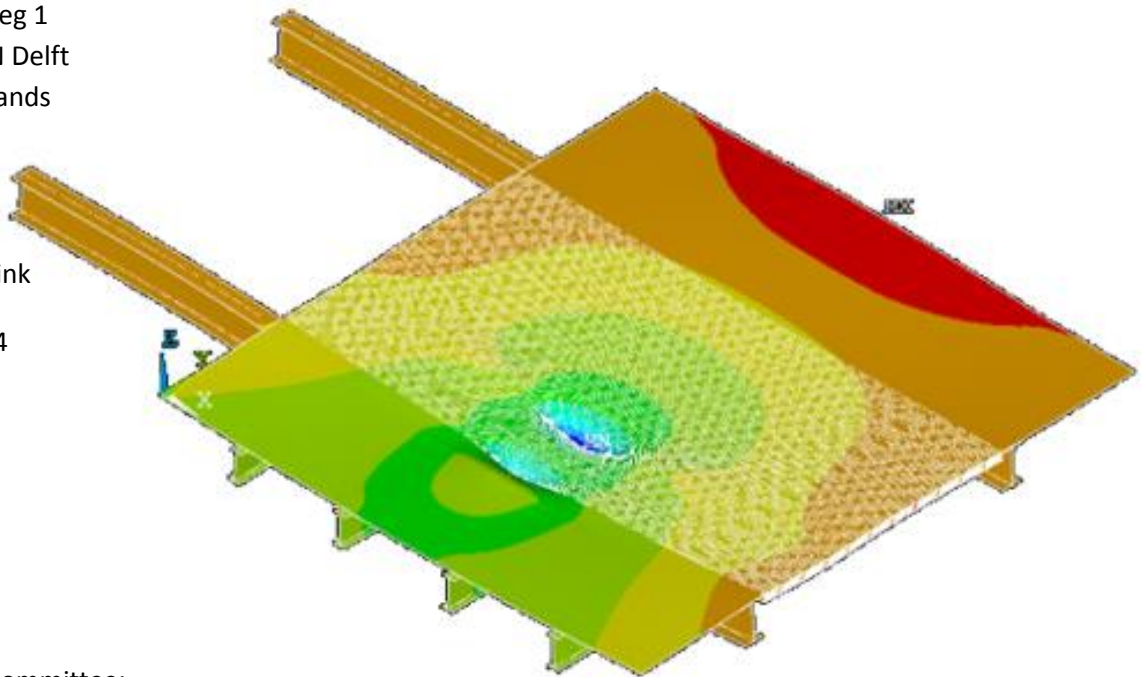
December 7, 2015

Master's Thesis

Delft University of Technology  
Civil Engineering and Geosciences: Structural Engineering  
Stevinweg 1  
2628 CN Delft  
Netherlands

Peter Flink

4007034



Thesis Committee:

**Prof. Dr. Ir. J.G. Rots** (Chairman), Professor at Delft University of Technology, Faculty of Civil Engineering and Geosciences, Department of Structural Engineering, Section Structural Mechanics

**Dr. M.H. Kolstein**, Associate Professor at Delft University of Technology, Faculty of Civil Engineering and Geosciences, Department of Structural Engineering, Section Structural and Building Engineering: Steel, Hybrid, and Composite Structures

**Ir. R. Abspoel**, Assistant Professor at Delft University of Technology, Department of Structural Engineering, Section Structural and Building Engineering: Steel, Hybrid, and Composite Structures

**Ir. L.J.M. Houben**, Associate Professor at Delft University of Technology, Department of Structural Engineering, Section Pavement Engineering

**Ing. M. van Almen**, Senior Constructor at Iv-Infra B.V., Section Movable Bridges

## Abstract

Many old moveable bridges have exceeded their technical lifetime. Replacement of the foundations is expensive and often unnecessary if the new bridge superstructure is lighter than the old one. With stricter design guidelines being in effect nowadays, a conventional orthotropic steel deck design will end up being heavier. A lightweight fiber reinforced polymer deck supported by steel girders is proposed as a solution. In this thesis the potential mass reduction resulting from a lightweight FRP deck is analyzed.

Analyses are initially performed under the assumption that realizing composite action will generate the best results. However, a finite element model of a bolted connection between an FRP deck and steel girders indicates that the strength of such a connection is too low to efficiently realize composite action. An alternate solution where the deck is draped over the main girders with a thin FRP layer is considered and outperforms the composite action design.

The design with FRP but without composite action is compared with a standard orthotropic steel design. The FRP design weighs order of magnitude 10% less than its orthotropic counterpart. However, it is still significantly heavier than the original component in need of replacing.

---

## Preface

The thesis before you has been established as one of the requirements for the master structural engineering at the Technical University Delft. The subject was offered by Iv-Infra, following their experience with a project with a fiber reinforced polymer deck. The purpose of this thesis was to design an FRP-steel hybrid bridge with composite action, with the hope of showing that significant weight savings could be obtained by designing bridges in this manner. Along the way a large portion of this paper became dedicated to the design and modeling of a bolted connection in FRP.

The subject of FRP was foreign to me at the start of this project. Therefore, this thesis gave me the opportunity to familiarize myself with a new material; one gaining in popularity in civil engineering. While not all information was transferred to paper, hopefully the reader can learn about FRP, its benefits, and its limitations from this thesis.

## Acknowledgements

At this point I would like to take the time to offer my gratitude to the people who have supported me throughout the completion of my thesis and my studies.

To start, I would like to thank Matthijs van Almen, who acted as my daily supervisor at Iv-Infra. He was always available made time for any and all questions I wanted to ask him and his advice and practical approach were instrumental in guiding this thesis to completion.

I am grateful for the exertion of my thesis committee. Prof. Rots, Ir. Abspoel, and Dr. Kolstein have added invaluable professional knowledge to this thesis.

I would like to distinguish everyone in the place where I worked. Erika, Harris, Stephan, Yirui, Dirk, Jeremy and Dennis welcomed me to the offices in Sliedrecht and made my time there more enjoyable. I would also like to thank Michel Koop, who provided me with the topic of this thesis as well as the opportunity to carry it out.

I would like to acknowledge my appreciation for my friends in Delft, who have ensured that my studies have been filled with entertainment and enjoyment.

Finally, I would like to thank my family. They have been loving and supportive throughout my studies, and have always pushed me to do my best.

## Summary

Fiber reinforced polymers (FRP) are recognized for their high strength and low weight. While, typically used in specialized functions where price is of the second order, their use is slowly becoming more prevalent in civil engineering. Considering the large quantities of material needed for structures, the relatively cheap E-glass fiber composites have dominated the market. Within civil engineering FRP is still only applied in situations where reduced mass will lead to benefits greater than solely a reduction in dead weight.

The expected reduction in mass offered so many additional benefits, that it drove the use of FRP in the renovation of the Julianabrug in Alphen aan den Rijn. The Julianabrug had reached the end of its life, as it was plagued by fatigue damage and corrosion. The use of FRP was specified under the belief that a bridge with an FRP deck could be executed lighter than the old bridge, and hence the foundations could be reused. The reuse of the foundations would easily compensate for the use of expensive composite materials.

The current design of the Julianabrug features a glass fiber reinforced polymer deck that does not act compositely with the steel girders below. This represents an inefficient use of material. Using the theory of inhomogeneous cross sections, the influence of compositely connecting the deck to the girders was analyzed. This was followed by a mass minimization procedure, focused on reducing the mass of the steel profiles, while maintaining the stiffness and strength of the current design. The mass minimization was repeated for three variants in which the material properties of the deck were altered to correspond to different lamination directions. This process indicated that realizing the optimal laminate stiffness in longitudinal direction led to the largest mass reduction of the considered variants.

In order to realize composite action between the two materials, a connection method needed to be designed. Adhesive connections were rejected based on questions regarding longevity. A bolted connection was decided upon, based on its simplicity and the widespread experience with such a joint. Hand calculations indicated that such a connection would be possible, but required an extremely thick laminate, with many connections. However, a finite element analysis of the joint was desired in order to determine whether the hand calculation was accurate or not.

A calibration study was performed to set up a failure criterion for the finite element results. This was done in order to establish a failure criterion which corresponds to reality. Both in reality, and numerically, peak stresses arise along the contact interface between a bolt and the laminate, so that looking at maximum values in models would lead to extremely low failure loads. The process to establish a failure criterion was started by finding a set of laboratory experiments from literature which thoroughly detailed the material and specimen properties. Models were made for these experiments, and the Tsai-Wu failure criterion was calculated within the laminate. The results of the experiments were set against trial failure criteria which accounted for distance from the interface and different

measurement methods in the cross section. The trial failure criterion which best matches the experimental results was then set as the failure criterion for the full scale model of the connection.

A full scale model of the bolted connection was created. This was tested against the failure criterion established with the small scale model. However, this indicated that the strength of the connection was significantly lower than the hand calculations had indicated. This meant that the design based on the hand calculations was no longer feasible, as too many bolts would be needed.

The construction was redesigned taking into account the modeled strength of the joint. Taking into account the joint strength led to an increase in thickness and height of the steel profile, and a reduction in height of the FRP deck. However, this design became so focused around the connection that the gains of establishing composite action were nearly entirely nullified. A comparison was made between how much mass could be saved in the composite action variant, and a variant in which composite action was not realized but the steel profile was increased to nearly the entire available construction height. The variant without composite action could be executed significantly lighter. Additionally, this variant would have a reduced complexity, since the connections were not necessary.

A problem with designing the construction in such a manner that the height of the steel profile is maximized, is that the deck and steel profile must be continuous. In other words, no relative vertical displacement between the two is allowed. To solve this, a detail was created in which a layer of FRP was draped over the top flange of the steel profile, guaranteeing a continuous displacement field. With wheel loads expected to pass over the bridge in close proximity to this detail, it is highly sensitive to fatigue loading. A design with glass fibers proved to be impractical due to the required thickness. This was solved through the application of a CFRP layer, which has been demonstrated to have significantly better properties under fatigue loading. With the better fatigue properties, the detail can be executed as a layer of the same thickness as the top layer of the deck draped over the girder. This leads to a relatively simple geometry of the detail design.

The current standard in the design of moveable bridges is the use of a steel orthotropic bridge deck. To truly understand the gains that can be had by applying an FRP deck, it should be compared with an orthotropic deck. This shows that an orthotropic deck will typically be significantly stiffer. The FRP deck on the other hand has been demonstrated to be less sensitive to local load carrying mechanisms due to its finer structure. Additionally, a bridge with an FRP deck can be executed significantly lighter than its steel counterpart. Since this is felt both in the weight of the leaf as well as in the counterweight, the effect of this on the total mass is even larger.

While an FRP design is lighter, this does not mean that it is lighter than a bridge designed according to 60 year old codes, i.e. designed for lower and less frequent loads. The increased traffic loading on bridges affects a bridge's mass more than FRP can compensate for. Hence, it appears that the desired effect that a modern design in FRP can be executed lighter than an steel design according to old design



---

loads is not obtained. This means that even if a bridge is executed with an FRP deck, the foundations must be verified for strength and potentially replaced or strengthened.

## Table of Contents

Abstract.....	4
Preface .....	5
Acknowledgements.....	6
Summary .....	7
1 Introduction .....	18
1.1 Problem Statement.....	19
1.2 Proposed Solution.....	20
1.3 Objectives and Aim .....	21
2 Glossary.....	22
3 Koningin Julianabrug.....	25
3.1 General Information About Movable Bridges.....	25
3.1.1 Types of Movable Bridges.....	25
3.1.2 Trunnion Bascule Bridges.....	25
3.2 Background Information Regarding Koningin Julianabrug .....	27
3.3 Variant Study for New Koningin Julianabrug .....	30
3.4 Current Design of the Koningin Julianabrug .....	32
4 Basics, Components and Properties of Fiber Reinforced Polymers.....	35
4.1 Basics of Fiber Reinforced Polymers.....	35
4.2 Components of Fiber Reinforced Polymers .....	35
4.3 Determination of Properties of Fiber Reinforced Polymers .....	37
4.3.1 Determination of Fiber Properties.....	37
4.3.2 Determination of Resin Properties .....	37
4.3.3 Determination of Lamella Properties.....	38
4.3.4 Failure Criterion to be Applied.....	39
4.3.5 Determination of Laminate Properties .....	41
5 Laminate Orientation.....	42
5.1 Basis of Laminate Orientation Determination .....	42
5.2 Procedure Description of Laminate Orientation Determination .....	43

5.3	Effective Width of FRP Deck .....	45
5.4	Composite Stiffness of Girders.....	47
5.5	Section Modulus of Connected Cross Section .....	49
5.6	Mass Change Due to Composite Action.....	51
5.7	Thermal Loading Between Deck and Girder .....	52
5.7.1	Thermal Force Between due to Uniform Temperature Change .....	52
5.7.2	Thermal Force due to Non-Uniform Temperature Change .....	54
5.7.3	Distribution of Thermal Shear Stress .....	56
5.8	Shear Flow Due to Vertical Loading .....	57
5.9	Conclusion Laminate Orientation .....	58
6	Joints Between FRP Deck and Steel Girders .....	60
6.1	Design of an FRP to Steel Joint.....	60
6.1.1	Considerations in the Design of FRP-Steel Joints.....	61
6.1.2	Preliminary Calculations of a Bolted Connection.....	62
6.1.3	Visualization of Main Girder to Deck Connection.....	65
6.2	Calibration of Model by Comparison to Experiments.....	66
6.2.1	Geometry of Pinned Joint Laminate .....	66
6.2.2	Supports and Loading of Calibration Model .....	67
6.2.3	Visualization of Results of Calibration Model .....	68
6.2.4	Interpretation of Calculation Results of Calibration Model.....	69
6.2.5	Verification of Hand Calculations.....	75
6.2.6	Conclusion of Calibration Study .....	76
6.3	Full Scale Joint Model .....	76
6.3.1	Materials Applied in Full Scale Model.....	76
6.3.2	Supports and Loading of Full Scale Model .....	77
6.3.3	Visualization of Full Scale Results .....	78
6.3.4	Convergence Study of Full Scale Model.....	80
6.3.5	Scaling Measurement Distances to Bolt Size .....	81
6.3.6	Determination of Strength of Full Scale Joint .....	82

6.3.7	Determination of Stiffness of Full Scale Joint .....	83
6.4	Redesign of Girder-Deck System.....	83
6.4.1	Redesign with Reduced Deck Height .....	84
6.4.2	Redesign with No Composite Action.....	86
6.4.3	Comparison between Redesign Variants .....	87
6.5	Connection Conclusion .....	87
6.6	Caveats to the Connection Design .....	89
7	Analysis of FRP Decks.....	91
7.1	Basic Information of Deck Types.....	91
7.2	Setup of FRP Deck Models .....	92
7.3	Displacements of Decks Resulting From Models .....	92
7.4	Conclusion Regarding FRP Deck Study.....	94
8	Evaluation of Main Girder to Deck Detail .....	95
8.1	Hand Calculations of Girder to Deck Detail .....	95
8.1.1	S-N Curve for FRP .....	96
8.1.2	Cycles until Failure .....	98
8.1.3	Miner’s Rule .....	98
8.1.4	Determination of Governing Failure Criterion.....	98
8.1.5	Schematization of Detail For Determination of Stresses.....	99
8.1.6	Determination of Laminate Height Required .....	100
8.2	Finite Element Model of Girder to Deck Detail.....	100
8.2.1	Geometry of Model for Main Girder to Deck Detail Calculation .....	101
8.2.2	Simplifications Applied in Model of Detail.....	102
8.2.3	Visualization of Model of Girder to Deck Detail .....	102
8.2.4	Results of Girder to Deck Detail Calculations .....	103
8.2.5	Cumulative Fatigue Damage Utilizing Finite Element Model .....	105
8.2.6	Alternative Solution to Fatigue Loading.....	106
8.3	Conclusion Regarding Girder to Deck Detail.....	107
9	Case Study.....	109

9.1	Design of Orthotropic Bridge Deck .....	109
9.1.1	Design of the Deck Plate and Stiffeners.....	110
9.1.2	Effective Width.....	110
9.1.3	Stiffness of Orthotropic Deck Girders .....	112
9.1.4	Section Modulus of Orthotropic Deck Girders.....	112
9.1.5	Mass of Orthotropic Deck Compared to FRP Deck .....	113
9.2	Orthotropic Deck Model .....	115
9.2.1	Loading and Supports .....	115
9.3	Orthotropic Deck Results .....	116
9.3.1	Stresses in FRP and Orthotropic Variants .....	117
9.3.2	Displacements in FRP and Orthotropic Variants.....	119
9.4	Conclusions Regarding Case Study .....	121
10	Conclusion.....	122
10.1	Conclusions of Considered Topics.....	122
10.2	Recommended Future Areas of Study .....	123
10.2.1	Experimental Verification of Joint Strength.....	123
10.2.2	Local Application of Different Materials .....	124
10.2.3	Verification of Scaling of the Measurement Distances for the Failure Criterion.....	124
10.2.4	Application of Alternate Failure Criterion.....	124
10.2.5	Calibration against Last Ply Failure .....	125
10.2.6	Flexural Fatigue Behavior of FRP .....	125
10.2.7	Optimization of Deck Geometry .....	125
10.2.8	Influence of Moment in Bolted Joint .....	125
10.2.9	Influence of Consecutive Bolts on One Another.....	126
10.2.10	Eurocomp .....	126
10.2.11	Injection Bolts .....	127
Appendix A:	Codes and Guidelines.....	128
A.1	Thermal Load .....	128
A.2	Vertical Traffic Load .....	129

A.2.1 Ultimate Limit State Load .....	130
A.2.2 Fatigue Loading.....	131
A.3 Serviceability Limit State (SLS) .....	133
Appendix B: Movable Bridge Types.....	135
Appendix C: Current Bridge Design .....	139
Appendix D: Design Requirements of the Case Study .....	142
D.1 Girders and Supports .....	142
D.2 Height Requirements .....	144
Appendix E: Basics of Fiber Reinforced Polymers .....	145
E.1 Fiber Reinforced Polymer Configuration .....	145
E.2 History Of Fiber Reinforced Polymers.....	145
E.2.1 Polymer History.....	146
E.2.2 Fiber History .....	147
E.2.3 Fiber Reinforced Polymer History .....	148
E.2.4 Previous Applications.....	148
Appendix F: Components of Fiber Reinforced Polymers .....	156
F.1 Fibers.....	156
F.1.1 Fiber Products .....	159
F.1.2 Fiber Prices .....	162
F.2 Matrix Phase .....	162
F.2.1 Thermosetting Polymers .....	163
F.2.2 Resin Costs .....	165
F.3 Production Process .....	165
Appendix G: Lamella Properties .....	171
G.1 Fiber Volume Fraction.....	172
G.2 Stiffness.....	174
G.2.1 Parallel Model Stiffness .....	174
G.2.2 Series Model Stiffness .....	175
G.2.3 Halpin-Tsai Stiffness Correction .....	176

G.3	Strength.....	177
G.3.1	Longitudinal Tensile Strength.....	177
G.3.2	Longitudinal Compressive Strength.....	179
G.3.3	Transverse Tensile Strength.....	182
G.3.4	Transverse Compressive Strength.....	183
G.3.5	Shear Strength.....	183
G.4	Failure Criteria.....	185
G.4.1	Tsai-Hill Criterion.....	185
G.4.2	Tsai-Wu Criterion.....	186
G.5	Correction Factors.....	191
G.5.1	Material Factor.....	191
G.5.2	Conversion Factors.....	192
G.5.3	Stiffness Reduction Factor.....	197
G.6	Thermal Expansion.....	197
G.6.1	Axial Thermal Expansion.....	197
G.6.2	Transverse Thermal Expansion.....	200
G.7	Summary of Lamella Properties.....	201
Appendix H:	Laminate Properties.....	202
H.1	Classic Plate Theory.....	202
H.1.1	Kinematic Equations.....	203
H.1.2	Constitutive Equations.....	205
H.1.3	Equilibrium Equations.....	206
H.2	Classical Laminate Theory.....	208
H.2.1	Thermal Stresses inside Laminates.....	209
H.2.2	Thermal Expansion of Laminates.....	213
H.3	Engineering Constants of Laminate.....	214
Appendix I:	Stability of Girders.....	221
Appendix J:	Comparing the Influence of Composite Action to Concrete.....	224
Appendix K:	Possible Connection Method Sketches.....	227

Appendix L: Joint Literature .....	228
L.1 Mechanical Joints.....	228
L.1.1 Net Tension .....	229
L.1.2 Bearing.....	231
L.1.3 Unquantified Effects.....	233
L.1.4 Disadvantages of Mechanical Connections.....	236
L.2 Adhesive Joints.....	237
L.2.1 Linear Method .....	237
L.2.2 Disadvantages of Adhesive Bonds.....	239
L.3 Conclusion.....	240
Appendix M: Contact Between a Cylinder and Groove.....	241
Appendix N: Calibration Study.....	243
N.1 Bolted Laminate Geometry.....	243
N.2 Supports and Loading .....	244
N.3 Materials .....	245
N.4 Mesh .....	245
N.5 Mesh Size .....	246
N.5.1 End Effect.....	247
N.5.2 Global Convergence .....	248
N.6 Results.....	249
N.6.1 Calculation Methods .....	249
N.6.2 Analysis.....	251
N.6.3 Conclusions.....	252
N.7 Scaling .....	253
Appendix O: Joint Influence Studies .....	256
O.1 Bolt Clearance .....	256
O.1.1 Injection Bolts.....	258
O.2 Bolt Head.....	261
O.3 Tension Effect.....	262



O.4	Alternative Materials For Connection.....	263
O.5	Comparison to Connections in Concrete .....	264
O.5.1	Assumed Values for Calculations of Connections in Concrete.....	266
O.5.2	Relationship Between Connections in Concrete and FRP .....	266
O.6	Influence of Connection Strength on Mass .....	267
Appendix P:	Comparison to Eurocomp Handbook.....	269
P.1	Simplifications and Assumptions of Eurocomp .....	269
P.2	Comparison of Eurocomp and Calibration Experiments.....	269
P.3	Comparison of Eurocomp and Full Scale Model .....	271
Appendix Q:	Model Validation.....	273
Q.1	Main Girders .....	274
Q.2	Crossbeams .....	275
Q.3	Deck.....	276
Q.4	Connections .....	277
Q.4.1	Free Horizontal Motion .....	277
Q.4.2	Restrained Vertical Motion .....	278
Q.4.3	Influence of Connection Stiffness .....	278
Q.5	Validation of Plate Approximation.....	280
Appendix R:	Verification of Loading Distance in Model.....	283
Appendix S:	Influence of Reduced Stiffness of Rear Abutment.....	285
Appendix T:	Bibliography .....	286

## 1 Introduction

Steel bridges are commonplace in the Netherlands. These bridges range in size from very small to very large. Their flexibility in application is largely due to the high strength of steel, compared to other materials. This was clear five decades ago, when many steel bridges were built across rivers and canals. Wear and tear over the years has weakened these bridges through fatigue damage, and in addition, many of these bridges were designed according to traffic conditions and regulations of those times. Therefore regular inspections and maintenance of these bridges is a necessity.

Inspections show an ever increasing number of bridges which are either structurally deficient or functionally obsolete. Structurally deficient refers to bridges which have damaged or deteriorated components, due to for instance fatigue loading, erosion, or corrosion. Whereas functionally obsolete regards a change in requirements which cannot be met, such as the increase in the design loading resulting from heavier and more frequent traffic. Bridges which are deficient and/or obsolete have become a systematic problem. Figures from the US and France indicate that 40% and 50% of the bridges in these countries are overdue for repairs, respectively.<sup>1</sup>

Clearly, repairs need to be made. Yet this leads to complications. Repairing the bridges in steel or concrete may be possible in some cases, but corrosion, fatigue and high maintenance requirements will continue to trouble the structures. In addition, some bridges are not suitable for repairs with steel and concrete. A common problem is that extra material is needed to strengthen bridges to handle the greater usage, increasing the weight on the foundations. Having to rebuild the foundations of a bridge is an expensive solution, and therefore repairs to solely the superstructure are to be preferred.

Synthetic composite materials have been suggested as a possible alternative to steel and concrete. Composites offer a lightweight, durable alternative to traditional construction materials. This means that these elements are expected to have a longer lifetime, lower maintenance costs, and should be sufficiently light to increase structural strength without increasing weight. The feasibility of these materials will be analyzed in this thesis.

The application of composite elements as bridge components is analyzed with regards to the *Koningin Julianabrug*. This bridge crosses the Old Rhine in Alphen aan den Rijn, The Netherlands. The bridge was built in the 1950s, but during emergency repairs in 2012 it became apparent that the leaf of the bascule bridge had reached the end of its lifetime. The decision was made to replace the leaf and the movement mechanism of the bridge.<sup>2</sup> The goal of this thesis is to find a design with composite materials which would suffice as a replacement leaf.

---

<sup>1</sup> (Hewson & Parke, 2008, pp. 509-510)

<sup>2</sup> (Gemeente Alphen aan den Rijn)

## 1.1 Problem Statement

Old bridges around the world are in dire need of repairs. Many of them have become structurally deficient as they may not have been properly maintained or have exceeded their design lifetime. A lack of maintenance and the surpassing of the design lifetime typically result in corrosion damage and fatigue cracking, respectively. If these effects become too large, the structure will no longer be safe.

In addition to the deficiency, many bridges have also become functionally obsolete. Older bridges are unable to cope with increased traffic loading because they were never designed for it. Increased traffic loading, in the form of increased frequency and mass of vehicles, has led to a faster accumulation of fatigue damage than expected. This has resulted in many bridges developing fatigue cracks. Bridges that are obsolete, will typically become structurally deficient at an alarmingly fast rate.

A few reasons for bridges becoming deficient and obsolete are given below:

- Fatigue damage
  - Increasing traffic loads
  - Increasing traffic Intensity
  - Structures exceeding design lifetime
- Corrosion
  - Inadequate maintenance
  - Due to moisture
  - Due to (deicing) salts
- Creep
  - Stress relaxation in prestressed structures
- Damage
  - Due to accidents

The fact that bridges being deficient and/or obsolete has become an all too common phenomenon, means a widely applicable solution is required. Steel and concrete repair methods typically result in an increase in the mass of the bridge, largely the result of modern design requirements being tougher than those originally governing in the bridge's design. Increasing the bridge mass has the consequence that the foundation must also be strengthened, leading to large additional costs. To prevent this, the use of synthetic composites has been suggested.

## 1.2 Proposed Solution

The proposed solution is to use fiber reinforced polymers to repair structurally deficient and functionally obsolete bridges. FRPs have some key advantages over steel and concrete as building materials, but also have several disadvantages. Table 1 lists these properties.

Advantages and Disadvantages of FRPs	
Advantages	Disadvantages
Lightweight	High Material Costs
Low Maintenance	High Production Costs
Long Fatigue Life	Low Stiffness
High Corrosion Resistance	Brittle Failure
Modular Production (Possible)	Sensitive to Fire
Modular Installation (Possible)	

Table 1: Advantages and Disadvantages of FRPs

Given the disadvantages listed in Table 1, especially the high cost and low stiffness, the application of a full FRP bridge seems unattractive. A bridge consisting of FRP and steel however, might benefit from the advantages of both, while discounting the disadvantages.

Applying a combination of the two materials, a combination of their properties is to be expected in the compositely designed structure. The main reasons for applying FRP are weight reduction and corrosion resistance. The weight reduction could lead to monetary savings if it leads to salvaging of the foundations. The corrosion due to the natural wear as well as the corrosion due to de-icing salts, will typically be concentrated at the FRP deck. The steel superstructure would be protected from these influences since the deck will shield the girders from above. Since the FRP is more resistant to the corrosion, and the steel is protected, the maintenance required to prevent damage will decrease.

Big disadvantages of FRP are that it is expensive, and lacking in stiffness. In comparison, steel is cheap and stiff. Therefore, the superstructure will be executed in steel. The long span elements can be produced out of the stiffer material, to ensure the global stiffness of the bridge is sufficient. The local spans, where stiffness is not equally critical, can be made out of FRP. This way, the two materials are used to complement one another.

### 1.3 Objectives and Aim

The objective of this thesis is to design a competitive alternative to traditional construction materials for the repair of heavily loaded movable bridges utilizing fiber reinforced polymers. To this end, several objectives were established in order to arrive at a successful design.

- This thesis aims at creating composite action between the FRP deck and the main load bearing structure of movable bridges under heavy traffic loading. Hence, an analysis should be made of the advantage this holds over non-composite decks. To this end, a comparison should be made between an integrated solution, and one where the deck does not contribute to the main load bearing structure.
- Although several bridges have already been built in composites, these have only recently started to feature steel-FRP interaction. The connection methods between these two are still being researched, and oftentimes over dimensioned in the field. Therefore, an analysis should be made regarding the optimal method with which to combine the FRP and the steel.
- Since the use of FRP over conventional methods is generally motivated by weight reduction, minimizing the mass of the bridge should be an integral criterion throughout the design process.
- The use of FRP materials in civil engineering applications has been limited due to the high costs. In this case quite some costs can be saved by reducing the mass of the bridge so that the foundations can be saved. However, a tradeoff between the savings on foundation upgrades and the extra material costs need to be made to determine the economic pragmatism of this solution.
- Considering that structural deficiency is the main driving force behind bridge repairs, the design featuring FRP must be analyzed for fatigue damage accumulation throughout its lifetime. This will illustrate the behavior of the bridge under long term repetitive loading.

The objectives above are combined to form the following research question:

*The aim of this master's thesis is to analyze the practicality of a compositely acting fiber reinforced polymer deck on steel main girders for a trunnion bascule type of movable bridge under heavy traffic loading, taking into account the static behavior, fatigue behavior, weight, and economics, through a numerical analysis applied to the case study of the Koningin Julianabrug.*

## 2 Glossary

In this chapter one can find a list of terms used throughout this thesis with a short description of their meaning.

Anisotropic	: Adjective describing material which has different properties in all directions
Aramid	: Aromatic Polyamide. A material used to create reinforcing fibers. Typically used for specialized applications.
CFM	: Continuous Filament Mat. A type of mat with long, randomly oriented fibers swirled together.
CFRP	: Carbon Fiber Reinforced Polymer. A type of FRP with the fiber reinforcement consisting of carbon fibers.
CLT	: Classical Laminate Theory. A mechanics model describing the behavior of a laminate based on the properties of its lamellas.
Composite	: A material consisting of two constituent materials. Typically, but not necessarily, referring to synthetic composites.
Counterweight	: CWT. The mass applied to the back end of a leaf to create a more balanced leaf around the axis of rotation.
CPT	: Classic Plate Theory. A mechanics model describing the behavior of thin plates. Used as a building block in the CLT.
CSM	: Chopped Strand Mat. A type of mat with short, randomly oriented fibers.
E-Glass	: A type of glass (fiber) with high electrical resistance. Oftentimes also applied for strength due to its relatively low cost.
Epoxy	: A common type of resin consisting of two components.
Fiber	: Long, thin filaments of a material such as glass, carbon or aramid. Synonymous with filament. In British English: "Fibre."
Filament	: Long, thin filaments of a material such as glass, carbon or aramid. Synonymous with fiber.
FRP	: Fiber Reinforced Polymer. A material consisting of two constituent synthetic materials. Synonymous with synthetic composite.

FVF	: Fiber Volume Fraction. The percentage of FRP, by volume, which is fibrous material.
GFRP	: Glass Fiber Reinforced Polymer. A type of FRP with the fiber reinforcement consisting of glass fibers.
Isotropic	: Adjective describing material which has identical properties in all directions.
Lamella	: A single layer consisting of mixed resin and fibers. The properties of this layer are constant over its height (including properties of its constituent materials, and its orientation).
Laminate	: A stack of multiple lamellas, where the properties of consecutive lamellas will almost exclusively vary. Typically the orientation is the main difference, but differing constituent materials may also be applied.
Leaf	: Component of a bridge which moves during opening and closing.
Mat	: A plate-shaped fiber product with constant fiber properties. Fibers may be randomly oriented or systematically woven together.
Matrix	: The material used as a binding agent in creating FRP. Also referred to as resin, polymer.
Polyester	: A common type of resin.
Polymer	: The material used as a binding agent in creating FRP. Also referred to as resin, matrix material.
Quasi-Isotropic	: Adjective describing material which approaches having identical properties in all directions.
Resin	: The material used as a binding agent in creating FRP. Also referred to as matrix material, polymer.
S-Glass	: A type of glass (fiber) with high strength properties.
SLS	: Serviceability Limit State. Conditions under which the maximum displacement and acceleration criteria may not be exceeded.
Strand	: A bundle of filaments, sometimes twisted, sometimes not.
Synthetic Composites	: A material consisting of two constituent synthetic materials. Synonymous with FRP.

- 
- Transversely Isotropic : Adjective describing material which has the same properties in two directions (the transverse directions), but different properties in the third direction (axial direction).
- Tsai-Hill : A failure criteria failing to take into account the difference in tensile and compressive behavior.
- Tsai-Wu : A failure criteria taking into account the difference in tensile and compressive behavior.
- UD : Unidirectional. A woven mat or lamella with (nearly) all fibers oriented in the same direction.
- ULS : Ultimate Limit State. Conditions under which the maximum strength of the construction may not be exceeded.
- Vinylester : A common type of resin
- Woven Mat : A mat with long fibers woven together into a systematic pattern.



### 3 Koningin Julianabrug

The design of a bridge superstructure consisting of FRP on steel, as described above, will be related to a specific case. This case will be that of the *Koningin Julianabrug* in Alphen aan den Rijn, The Netherlands. The *Koningin Julianabrug* is a movable bridge which underwent emergency repairs in 2012 after which it was determined that parts were irreparably damaged and needed to be replaced.<sup>3</sup>

#### 3.1 General Information About Movable Bridges

Bridges can be stationary or movable. Since this thesis the case study regards a movable bridge, some general information regarding movable bridges is given in this chapter.

##### 3.1.1 Types of Movable Bridges

There are many types of movable bridges, categorized by their type of movement. The main types are given below. A short description of each type of bridge mentioned below can be found in Appendix B: Movable Bridge Types.

- Trunnion Bascule: Rotates around a fixed transverse horizontal axis
- Rolling Bascule: Rotates around a moving transverse horizontal axis
- Swing: Rotates around a fixed vertical axis
- Vertical Lift: Translates upwards along a fixed vertical axis
- Submersible bridge: Translates downwards along a fixed vertical axis
- Retractable: Translates along a fixed longitudinal horizontal axis, where the bridge attaches to both ends of the roadway when closed
- Transporter: Translates along a fixed longitudinal horizontal axis, where the bridge never attaches to both ends of the roadway simultaneously, i.e. the movable part carries cars across the river like a ferry
- Gyrotory: Rotation around a fixed longitudinal axis
- Folding: Rotation around multiple transverse horizontal axes, consecutive rotations in opposite directions.
- Curling: Rotation around multiple transverse horizontal axes, consecutive rotations in equivalent directions<sup>4,5</sup>

##### 3.1.2 Trunnion Bascule Bridges

The case study of this thesis regards a trunnion bascule bridge. Hence, this type of bridge will be explained in more detail. As mentioned, a trunnion bascule bridge rotates about a fixed transverse horizontal axis. To balance the moment the bridge deck causes about the axis of rotation, a counterweight is typically applied. In some cases the counterweight is not applied and a more powerful

---

<sup>3</sup> (Gemeente Alphen aan den Rijn)

<sup>4</sup> (Hewson & Parke, 2008)

<sup>5</sup> (Wikipedia, 2015)

mechanical system is applied. If a counterweight is applied it is almost always designed to be lighter than a perfectly balanced case, to ease the operation of the bridge.<sup>6</sup> Two schematics of a trunnion bascule bridge can be seen in Figure 1 and Figure 2.



Figure 1: Double Trunnion Bascule Bridge<sup>7</sup>

Note the indicated components of the bridge in Figure 2:

- Trunnion bearing: The bearing which allows for rotation of the bridge
- Axis of rotation: The axis about which the bridge rotates (coincides with the center of the trunnion bearing)
- Bascule Leaf: The span of the bridge, i.e. the roadway and its supporting structure
- Centre of rotation: Coincides with the axis of rotation
- CWT: The counterweight; used to balance the leaf
- Bascule pier: foundation for the trunnion bearings

<sup>6</sup> (Hewson & Parke, 2008)

<sup>7</sup> (Wikipedia, 2015)

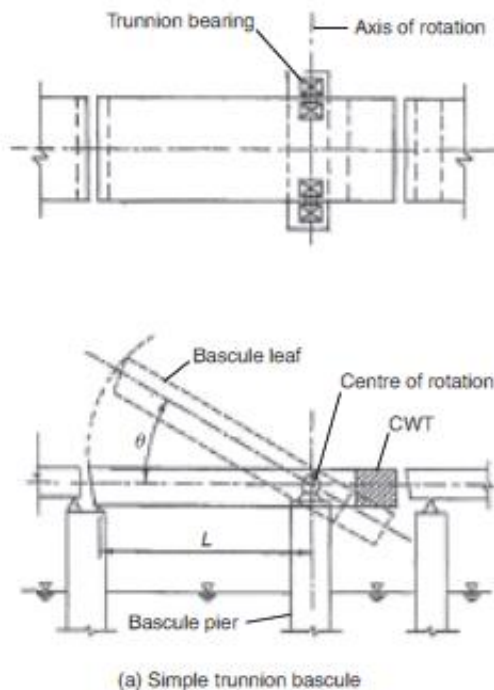


Figure 2: Schematic of a Trunnion Bascule Bridge<sup>8</sup>

### 3.2 Background Information Regarding Koningin Julianabrug

The *Koningin Julianabrug* is a trunnion bascule bridge located in Alphen aan den Rijn, The Netherlands. The locations of the bridge can be seen in Figure 3. The bridge itself is shown in Figure 4. It was built in the early 1950s and hence its age has exceeded 60 years, while its design lifetime was merely 50 years. With its advancing age it has been a constant source of problems for the past half-decade. As such the leaf is currently (2015) being replaced. A design goal of the new leaf is for it to be lighter than or equal in weight to the original leaf. The original leaf weighed approximately 57 tonnes, excluding fixtures, and its counterweight weighed 80 tonnes.

<sup>8</sup> (Hewson & Parke, 2008)

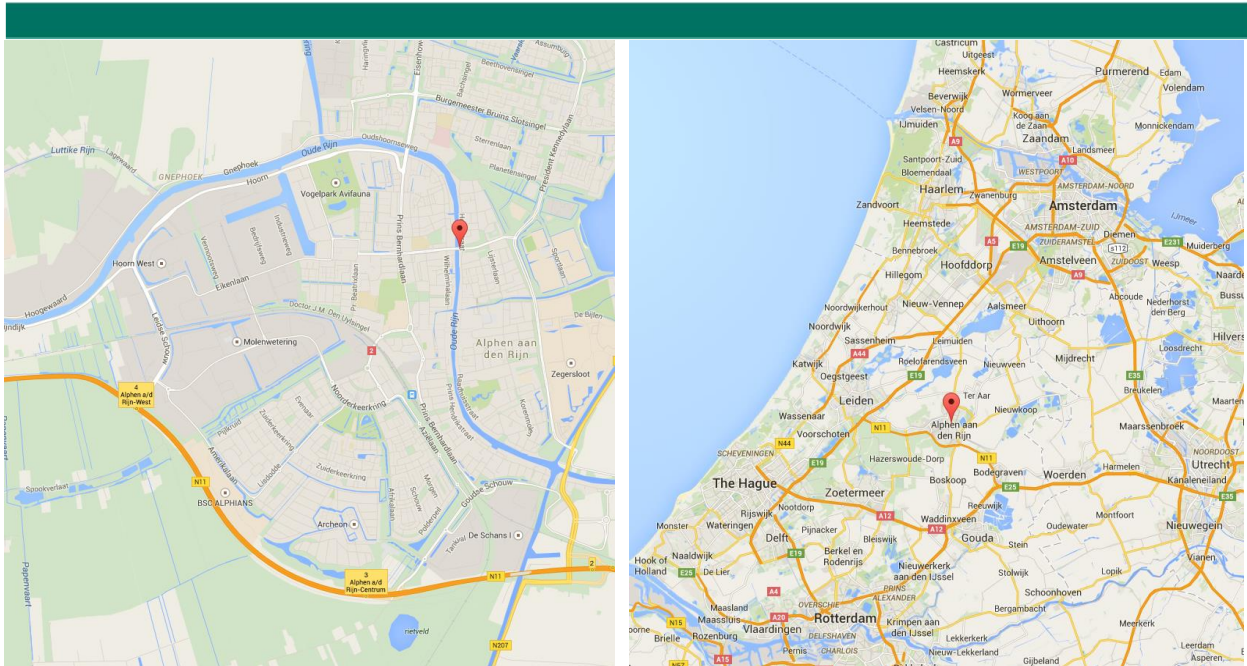


Figure 3: Location of Koningin Julianabrug<sup>9</sup>



Figure 4: View of the Koningin Julianabrug in open position<sup>10</sup>

<sup>9</sup> (Google)

Built in the 1950s the structure has become structurally deficient. Over the past few years malfunctions and closures have plagued the bridge. These are given in Table 2. The problems listed there have led to the decision to replace the bridge leaf completely. As part of the renovation process of the bridge other aspects of the bridge will be (re)placed or upgraded outside of the leaf; such as the stairs, the bridgetender's house, sound screens, handrails and coatings. These will not be considered in this thesis, solely the construction aspects of the leaf will be considered.

Problems with the Koningin Julianabrug	
Date	Event
16-8-2010	Bridge closed to replace deck asphalt (typical maintenance)
10-11-2011	Inspection of bridge shows severe rust formation around the trunnion bearings. Bridge is immediately closed to traffic over and under.
11-11-2011	Bridge is opened to ships. Only those which fit under the bridge are allowed through
22-11-2011	Independent research into maintenance is started.
26-11-2011	Bridge leaf is removed and shipped for repair of the deck
3-12-2011	During repairs damage appears worse than presumed. Trunnion bearings rusted over and need replacements. Concrete deck to be completely replaced
19-12-2011	Vandalism to bridge safety coverings and materials on site
31-1-2012	Repaired bridge leaf replaced, new expected lifetime is 3-5 years
11-2-2012	Tanker hits bottom of bridge. Damage to bridge is aesthetic only
14-2-2012	Another ship hits the bridge. Damage is minor; bridge remains functional during repairs
16-2-2012	Independent research concludes maintenance was insufficient. Inspections had repeatedly shown the bridge was in a poor state, and repairs were yet to come.
2-6-2013	Braking system for the lifting mechanism breaks. Bridge unable to open
9-1-2014	Lifting mechanism fails. Bridge gets locked in open position
28-4-2015	Bridge is closed for replacement of bridge leaf

Table 2: Problems with the Koningin Julianabrug<sup>11</sup>

One can see from Table 2, that the bridge suffered from many problems. Many of these could have been prevented with regular inspection and maintenance. The bridge was closed when excessive rust was discovered near the bearings. Proper inspection would have easily indicated that the steel needed to be repainted well prior to the formation of rust. One can imagine that if a problem as visible as worn paint is not discovered, then micro cracking due to fatigue or other difficult to see damages will definitely not be discovered. Proof of this can immediately be found in the concrete deck, which was damaged beyond repair when the rust was discovered near the bearings. However, the inspection that revealed the rust missed this damage entirely, and it was not until repairs on the steel were already underway that this damage was discovered.

<sup>10</sup> (VVD, 2014)

<sup>11</sup> (Redactie Omroep West, 2010-2015)

### 3.3 Variant Study for New Koningin Julianabrug

As part of the design process of the new bridge, the municipality of Alphen aan den Rijn ordered a variant study to be done of 5 preliminary concepts. The five concepts are listed below:

1. Variant 1
  - a. Renovation of the river crossing,
  - b. Foundations and secondary structures will be largely spared
  - c. Bridge leaf and mechanical components will be completely replaced.
  - d. Bridge deck will be applied in composite materials
    - i. Prevent weight increase
    - ii. Prevent foundation replacements.
2. Variant 2
  - a. Underpass,
  - b. Will not exceed 220 meters in length, so as to fall outside of tunnel laws
  - c. Useable by all forms of traffic
  - d. Sub variants
    - i. Open roof
    - ii. Closed roof
      1. Reuse of land above the underpass.
3. Variant 3
  - a. New bridge
  - b. All traffic
  - c. New foundations
  - d. New abutments
  - e. Superstructure and deck applied in steel.
4. Variant 4
  - a. Underpass
  - b. Will not exceed 220 meters in length, so as to fall outside of tunnel laws
  - c. Useable only by pedestrians, cyclists, busses, and emergency services
  - d. Sub variants
    - i. Open roof
    - ii. Closed roof
      1. Reuse of land above the underpass.
5. Variant 5
  - a. New bridge
  - b. Useable only by pedestrians, cyclists, busses, and emergency services
  - c. New foundations
  - d. New abutments.

e. Superstructure and deck applied in steel.<sup>12</sup>

Variant Characteristics					
	Variants				
	1	2	3	4	5
<b>Building Costs [Million €]</b>	10	45	19	44	18.5
<b>Lifespan [year]</b>	50 <sup>13</sup>	80	80	80	80
<b>Lead Time [years]</b>	2.5	5	4.5	5	4.5
<b>- During which traffic is hindered [years]</b>	0.5	2	1.5	2	1.5

Table 3: Variant Characteristics

For these five variants, a few characteristics have been given in Table 3. These properties were critical in deciding which of the variants to choose. The supervisory board named 4 criteria to the councilmembers of Alphen aan den Rijn which were pivotal in selecting their preference. These are:

- Costs
- Nuisance to traffic and people living in the vicinity
- Accessibility
- Planning<sup>14</sup>

While the costs are relatively self-explanatory criteria, the nuisance, the accessibility and planning will be enlightened further. The nuisance was based on the hindrance people would experience. The complete rebuild variants were projected to take a longer time, and hence submit people to more nuisance.

The two underpass variants were rejected based on the accessibility criterion. The slope required to pass under the waterway without exceeding the 220 meter maximum length, was deemed too steep for comfortable bicycle traffic. This eliminated the underpass variants.

The planning was much more important than usual because the municipality has plans to replace the *Steekterbrug*, another of the 3 traffic bridges in Alphen aan den Rijn which cross the Oude Rijn. The municipality feared major traffic delays if the bridges were out of commission simultaneously. The belief reigned that variant 1; leaf replacement rather than a complete rebuild, would be finished prior to the *Steekterbrug* being closed. Hence, the lead time of this shorter project was very beneficial.

In summation, Koningin Julianabrug will be designed according to variant 1, due to lower costs and shorter build times. Where the composite deck was specified solely on a preliminary technical

<sup>12</sup> (van Beek & Vrieling, 2012)

<sup>13</sup> Following the variant study, the municipality was given more information regarding composites. Here the life expectancy of composite components in traffic bridges was estimated as 60-100 years. (Rhijn, 2012)

<sup>14</sup> (Velzen, 2012)

assessment of feasibility based on mass. When the decision for an FRP deck was made, very little about the material itself had been taken into consideration, other than that it was lighter than steel and would therefore allow the foundations to remain in place, reducing costs and shortening build time.

### 3.4 Current Design of the Koningin Julianabrug

As mentioned, the bridge leaf already has a replacement design. This design will briefly be presented here. Additional detailed drawings of the current design are presented in Appendix C: Current Bridge Design. First, a schematic representation of the design is given in Figure 5.

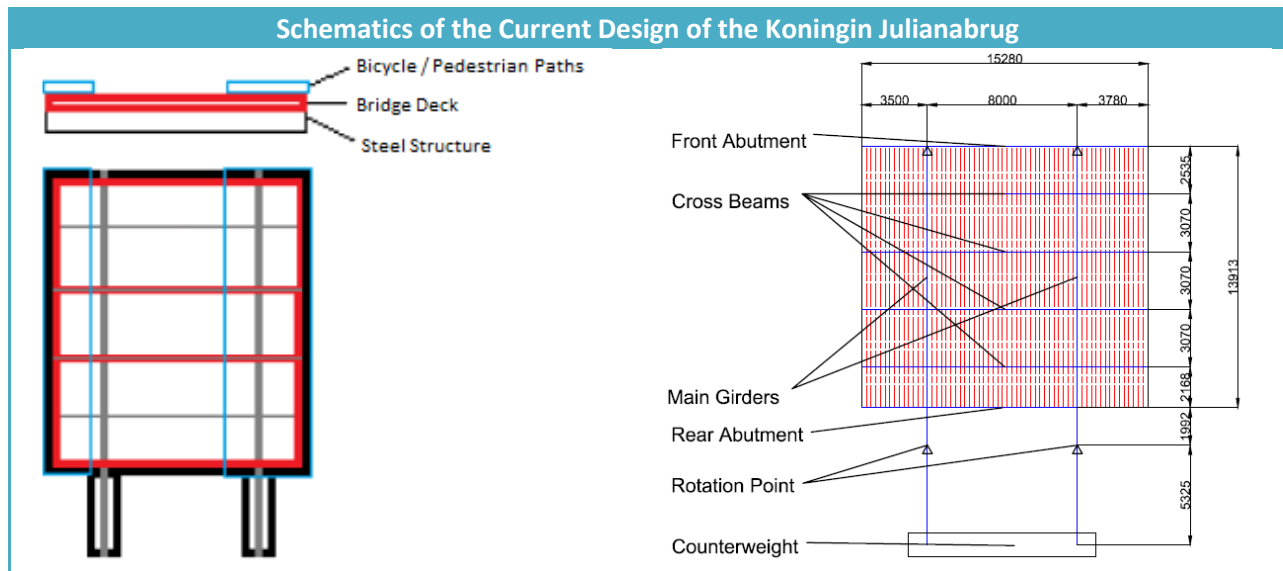


Figure 5: (Left): Schematic Representation of Current Bridge Design.<sup>15</sup> (Right) Global Geometry of Bridge.

As one can see in Figure 5, the current bridge design has two longitudinal steel beams. The design has six transverse steel beams, and three transverse bridge deck components. The design of the main beams is led in terms of dimensioning and placement by spatial limitations. The cross girder spacing is determined largely based on experience and practicality. The geometrical limitations which were adopted for this case study are presented in Appendix D: Design Requirements of the Case Study.

The bridge deck components were applied as an FRP deck system, rigidly connected in-situ. However, the deck has been loosely connected to steel girders, so that there will be no composite action between the steel and the deck. This seems like an ineffective use of material, since the bridge deck could add strength and stiffness to the bridge if it were to be fully connected. Basic information regarding the applied deck is given in Figure 6. Two screenshots of a 3-D model of the bridge have been presented in Figure 7 and Figure 8.

<sup>15</sup> (Hattink, 2014)



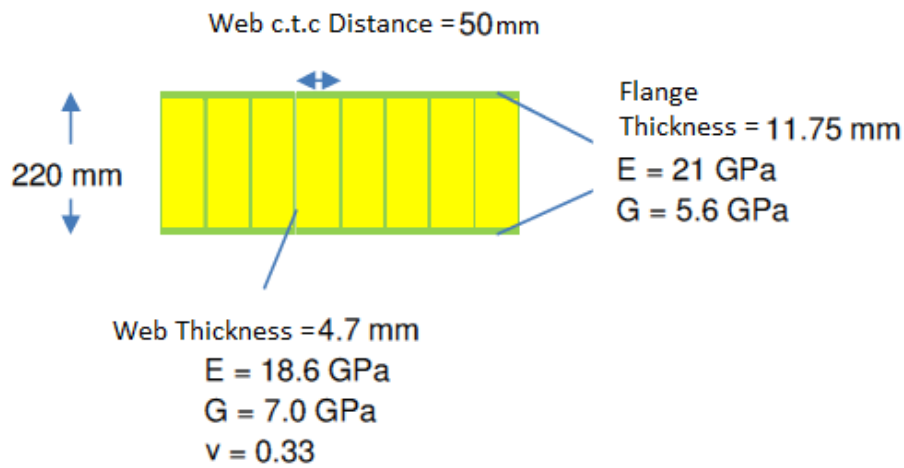


Figure 6: Current FRP Bridge Deck Information<sup>16</sup>

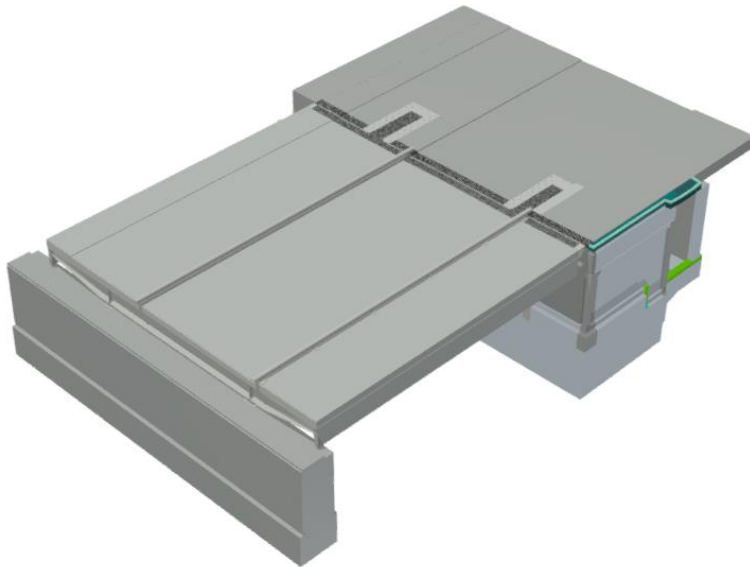


Figure 7: 3-D Model of Koningin Julianabrug, Closed<sup>17</sup>

<sup>16</sup> (Hattink, 2014)

<sup>17</sup> (Offereins)

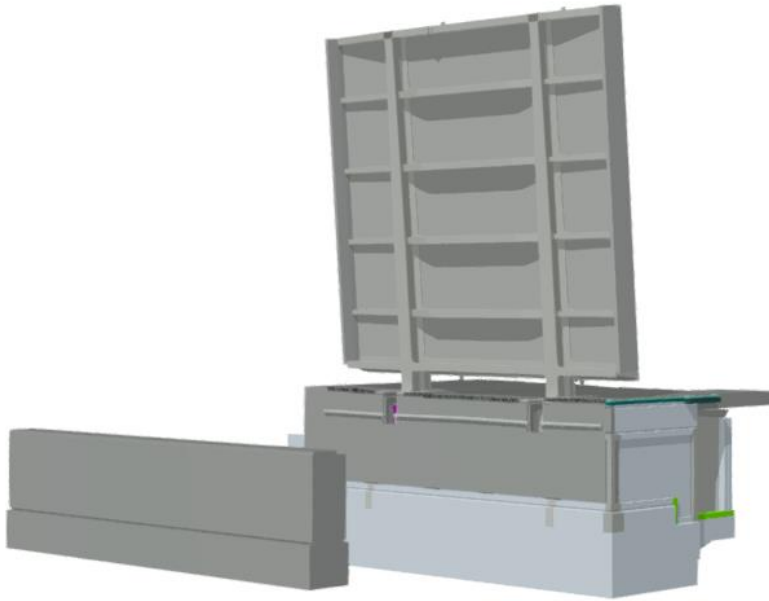


Figure 8: 3-D Model of Koningin Julianabrug, Open<sup>18</sup>

---

<sup>18</sup> (Offereins)

## 4 Basics, Components and Properties of Fiber Reinforced Polymers

Since the bridge deck will be executed in FRP, background information regarding the material will be useful. To this end a short summary regarding the basics of FRP, the components of FRP, and the mechanical properties will be given in this chapter.

### 4.1 Basics of Fiber Reinforced Polymers

Fiber reinforced polymers are a form of composite material. The building blocks of FRP are the fibers and the polymers (also known as the resin or the matrix). The fibers and polymers are combined into lamellas, which are layered into laminates, as shown in Figure 9. While FRP has been dated as far back as 3000 years ago, the modern day FRP materials are much more advanced. This is due to the development of many new types of resins and improvement in the production of the fibers.

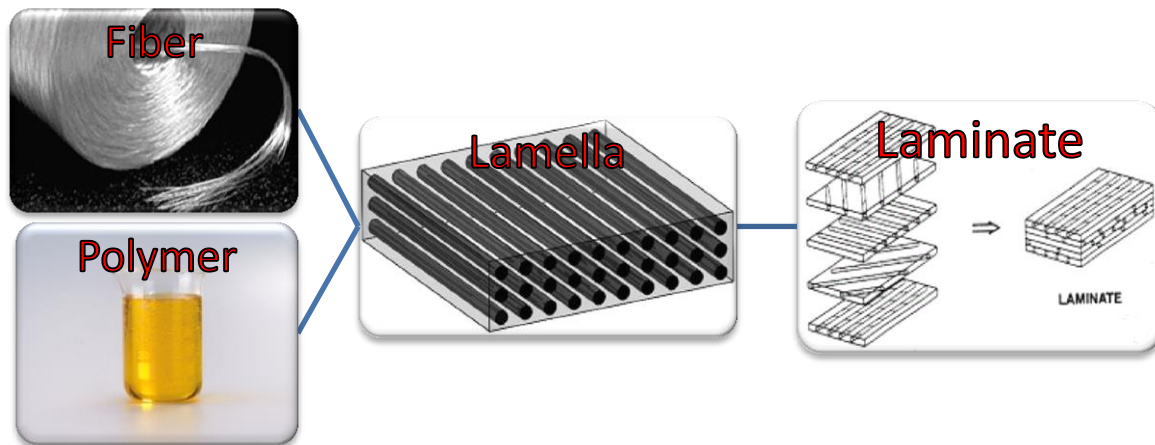


Figure 9: Laminate Build Up<sup>19</sup>

Nowadays, fiber reinforced polymers are sufficient in quality to be applied in structural purposes. FRP has been used in airplanes and boats for decades now, but the structural engineering world is still weary of their performance. Due to their promising attributes in terms of good strength and light weight, some pilot bridges have been (partially) created out of FRP. Examples of these include the Aberfeldy Footbridge, the Bonds Mill Roadbridge, and the Frieberg Bridge. For more information regarding the basics of fiber reinforced polymers see Basics of Fiber Reinforced Polymers.

### 4.2 Components of Fiber Reinforced Polymers

There are two components to fiber reinforced polymers: the fibers and the polymer. FRP derives most of its strength from the fibers. These typically have much better mechanical properties than the

<sup>19</sup> Pictures from: (Direct Industry, 2015), (Core Systems), (Allred & Associates Inc., 2015), (Rijswijk, Brouwer, & Beukers, 2003)

resin. There are three common types of fibers in modern FRP: carbon fibers, glass fibers, and aramid fibers. The differences in mechanical properties between the fibers is shown in Figure 10. Even though it appears that carbon and aramid fibers outperform glass fibers, glass fibers are much more frequently applied in structural application. This is because the cost of E-glass fibers is approximately 12-40 times lower than the other fiber types.

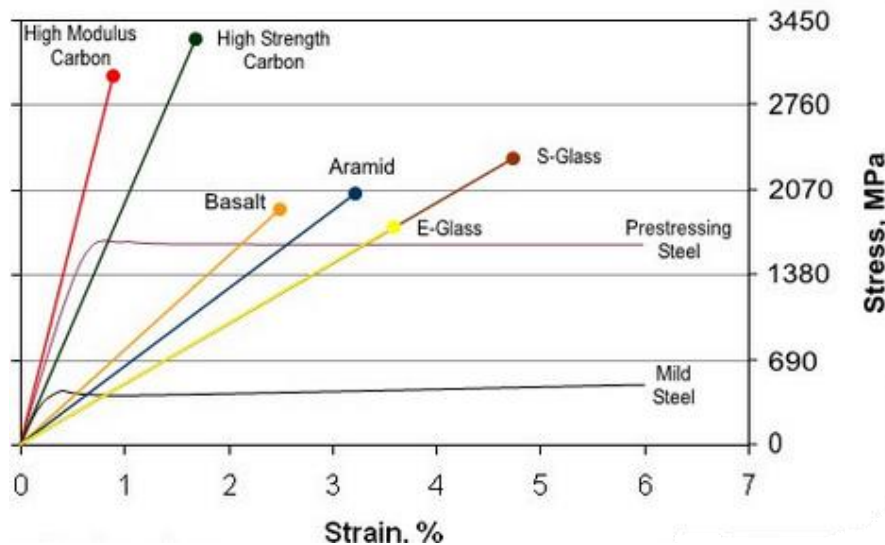


Figure 10: Stress-Strain Curve Various Fiber Materials and Steels<sup>20</sup>

The second constituent of FRP is the polymer, also known as the resin or the matrix. The polymer is responsible for the following points:

- Locking the fibers in place
- Coating the fibers to protect against corrosion and erosion
- Transferring the stresses between fibers
- Preventing fibers from buckling

There are three common types of matrix materials available. These are, in order of increasing quality and price, polyesters, vinylesters, and epoxies. Where for structural purposes, typically either polyesters or vinylesters are used as the main matrix material, and epoxies are used when joining FRP segments together. For more information regarding the components of FRP, see Components of Fiber Reinforced Polymers.

<sup>20</sup> (Prince Engineering, 2015)

### 4.3 Determination of Properties of Fiber Reinforced Polymers

The properties of FRP follow largely from its constituent materials. Therefore, the fiber and matrix properties must be determined. Based on the fiber and resin chosen, the lamella properties can be calculated.

#### 4.3.1 Determination of Fiber Properties

The first choice to be made is which fiber to apply. Based on cost considerations the use of E-glass is specified. E-glass has properties which are similar to S-glass and aramid fibers, but at a much lower cost. Similarly, while the properties of carbon fibers are typically better, their prices make them ill-suited for anything but specialized applications. The properties which have been assumed for the glass fibers are given in Table 4.

E-Glass Fiber Material Properties			
Property	Unit	Value	Value for Steel
Material Cost	€/kg	2	1
Young's Modulus	GPa	72	210
Poisson's Ratio	-	0.2	0.3
Shear Modulus	GPa	35	79
Axial Strength	MPa	2400	355
Density	kg/m <sup>3</sup>	2550	7850
Coefficient of Thermal Expansion	1/K	5*10 <sup>-6</sup>	12*10 <sup>-6</sup>

Table 4: Assumed Properties of E-Glass Fibers

#### 4.3.2 Determination of Resin Properties

With regards to the resin, the properties of all resins applied in civil engineering suffice with regards to the case study. The environment which is expected, is considered to be relatively mild considering FRP resistance to corrosion. The material will be exposed to occasional deicing salts, periodic moisture exposure, relatively little UV exposure, and no exposure to base substances. As a result all of the thermosetting polymers described should suffice. Therefore, the decision here also came down to costs, and the lowest cost material was selected. This was the polyester resin. The properties which were assumed for this material are given in Table 5.

Polyester Resin Material Properties		
Property	Unit	Value
Material Cost	€/kg	2
Young's Modulus	GPa	3
Poisson's Ratio	-	0.35
Shear Modulus	GPa	1.3
Tensile Strength	MPa	70
Compressive Strength	MPa	100
Shear Strength	MPa	34
Density	kg/m <sup>3</sup>	1200
Coefficient of Thermal Expansion	1/K	105*10 <sup>-6</sup>

Table 5: Assumed Properties of Polyester Resin

### 4.3.3 Determination of Lamella Properties

The properties associated with the two different materials are combined according to the descriptions in Appendix G: Lamella Properties. To this end, some assumptions needed to be made regarding the lamellas. One is that each lamella is considered to be unidirectional. The other assumptions are listed in Table 6. Note that the shear strength is also listed as an assumption. There are no known models to accurately predict the shear strength of lamellas. Experimental data for shear strength typically ranges between 60-100 MPa.<sup>21</sup> In order to remain conservative, a value of 55 MPa has been assumed.

The results of the lamella property calculations are listed in Table 7. The contrast between the strength in the axial and transverse direction are worth noting, as these vary more than a factor 10. This extreme anisotropy is largely responsible for the recommendations regarding minimal fiber fractions per direction.<sup>22</sup>

Assumptions Regarding Lamellas		
Property	Unit	Value
Fiber Volume Fraction	-	0.6
Stiffness Reduction Factor	-	0.97
Shear Strength	MPa	55

Table 6: Assumptions Regarding Lamella Properties

<sup>21</sup> (Kaw, 2006), (Torabizadeh, 2013), (Purslow, 1977), (Performance Composites Ltd., 2009)

<sup>22</sup> (Civieltechnisch Centrum Uitvoering Research en Regelgeving-onderzoekcommissie C 124, 2003-6)

Calculated Lamella Properties		
Property	Unit	Value
Density	kg/m <sup>3</sup>	1875
Axial Young's Modulus	GPa	43.1
Transverse Young's Modulus	GPa	12.8
Shear Modulus	GPa	4.4
Primary Poisson's Ratio	-	0.26
Secondary Poisson's Ratio	-	0.077
Axial Tensile Strength	MPa	1036
Axial Compressive Strength	MPa	846
Transverse Tensile Strength	MPa	48
Transverse Compressive Strength	MPa	69
Axial Thermal Expansion	1/K	7.6*10 <sup>-6</sup>
Transverse Thermal Expansion	1/K	43*10 <sup>-6</sup>

Table 7: Calculated Lamella Properties

#### 4.3.4 Failure Criterion to be Applied

For this thesis, the Tsai-Wu failure criterion will be utilized as described in G.4.2 Tsai-Wu Criterion. This failure criterion is lamella based, meaning that each lamella should be tested against the Tsai-Wu criterion. The Tsai-Wu criterion is given in Equation 1, with the constants given in Equation 2. If the Tsai-Wu Value reaches 1, the lamella fails.

$$F(\sigma_1, \sigma_2, \tau_{12}) = F_1\sigma_1 + F_2\sigma_2 + F_{11}\sigma_1^2 + F_{22}\sigma_2^2 + F_{66}\tau_{12}^2 - \sqrt{F_{11}F_{22}}\sigma_1\sigma_2$$

Equation 1: Tsai-Wu Failure Criterion<sup>23</sup>

$$F_1 = \frac{1}{\sigma_{1,u,t}} + \frac{1}{\sigma_{1,u,c}}$$

$$F_{11} = -\frac{1}{\sigma_{1,u,t}\sigma_{1,u,c}}$$

$$F_2 = \frac{1}{\sigma_{2,u,t}} + \frac{1}{\sigma_{2,u,c}}$$

$$F_{22} = -\frac{1}{\sigma_{2,u,t}\sigma_{2,u,c}}$$

$$F_{66} = \left(\frac{1}{\tau_{12,u}}\right)^2$$

Equation 2: Tsai-Wu Constants

<sup>23</sup> (Indian Institute of Technology)

With:

- $\sigma_{1,u,t}$ : Ultimate tensile stress in longitudinal direction
- $\sigma_{1,u,c}$ : Ultimate compressive stress in longitudinal direction
- $\sigma_{2,u,t}$ : Ultimate tensile stress in transverse direction
- $\sigma_{2,u,c}$ : Ultimate compressive stress in transverse direction
- $\tau_{12,u}$ : Ultimate shear stress

A plot of the Tsai-Wu failure surface is visible in Figure 11. Figure 12 shows several contour plots of this failure surface. Note the oblong shape, which is a result of anisotropy. Also note that biaxial tension and biaxial compression actually increases the strength, while having tension in one direction and compression in the other reduces strength.

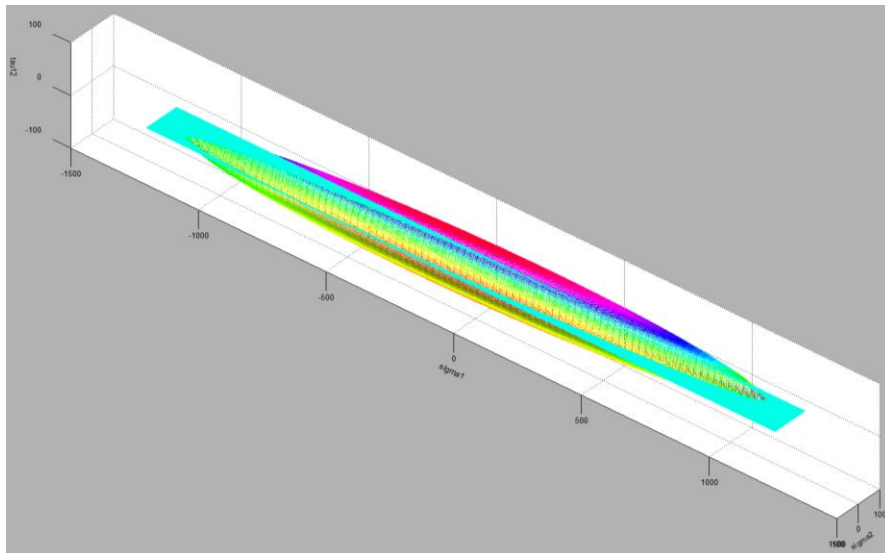


Figure 11: Tsai-Wu Failure Surface. Stresses in MPa.

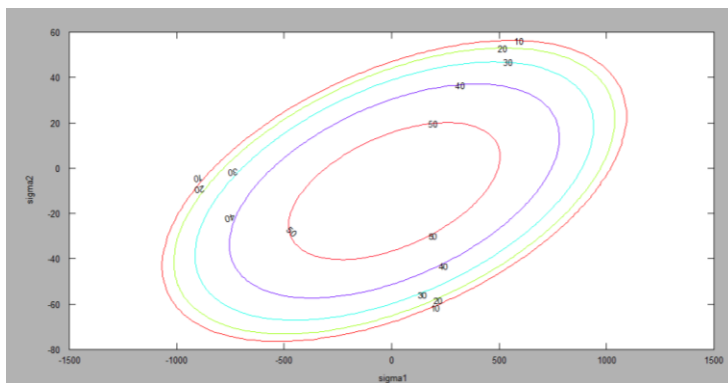


Figure 12: Contour Plot of Tsai-Wu Failure Criterion. Contours Represent Shear Stresses. Stresses in MPa.



#### 4.3.5 Determination of Laminate Properties

Following the calculation of lamella properties, the next logical step is to calculate the laminate properties. This has been done as explained in Appendix H: Laminate Properties. In order to avoid undesirable bending and torsional effects, the laminate will be created symmetrically about its neutral axis. Additionally, the decision must be made whether to create a quasi-isotropic laminate or a laminate with distinct primary and secondary directions. A quasi-isotropic laminate is built up with 25% of the fibers oriented in each of the four directions (0, 90, 45 and -45 degrees), while the directional laminate generally contains 55% in the primary direction and 15% in each of the three remaining directions. The choice has been made to deviate slightly from this in order to balance the coefficient of thermal expansion, so that 52.5% is oriented in the primary direction, 17.5% in the secondary direction, and 15% in each of the tertiary directions. Calculations in Chapter 5 Laminate Orientation indicate that the oriented laminate is better for this case study. Therefore, the properties of the oriented laminate are presented in Table 8.

Calculated Laminate Properties		
Property	Unit	Value
Material Cost	€/kg	5.50 <sup>24</sup>
Density	kg/m <sup>3</sup>	1875
Fibers Primary Direction	%	52.5
Fibers Secondary Direction	%	17.5
Fibers Tertiary Direction	%	15
Axial Young's Modulus	GPa	30
Transverse Young's Modulus	GPa	19.6
Shear Modulus	GPa	6.9
Primary Poisson's Ratio	-	0.28
Secondary Poisson's Ratio	-	0.19
Axial Thermal Expansion	1/K	12*10 <sup>-6</sup>
Transverse Thermal Expansion	1/K	23.3*10 <sup>-6</sup>

Table 8: Calculated Laminate Properties

<sup>24</sup> In addition to the material cost, a labor cost of 3.5 €/kg has been included. This has been done accordance with (Kok, 2013).

## 5 Laminate Orientation

One of the benefits of FRP is that it can be laminated according to specification. This chapter focusses on the influence of lamination direction on potential mass savings. This is done by varying the lamination direction to change the material properties of the deck.

### 5.1 Basis of Laminate Orientation Determination

To begin the design process, preliminary calculations need to be made. The calculations are needed to determine the strength requirements for the joints, estimate the sizes of the steel girders required, and orientate the laminate. In order to do this, several assumptions have been made:

- The global geometry is consistent with the current design (Shown on the left in Figure 13)
- The FRP deck
  - Has unchanged geometrical dimensions
  - Remains oriented with its webs in the longitudinal direction
  - Has material properties which are anisotropic and dependent on laminate composition, leading to different behavior dependent on laminate orientation
- A perfect shear connection exists between deck and girders for all variants other than the current design
- Stability of the elements has been largely excluded from analysis. A sample stability problem is shown in Appendix I: Stability of Girders.
- Only an effective width of the deck above each girder contributes to composite action

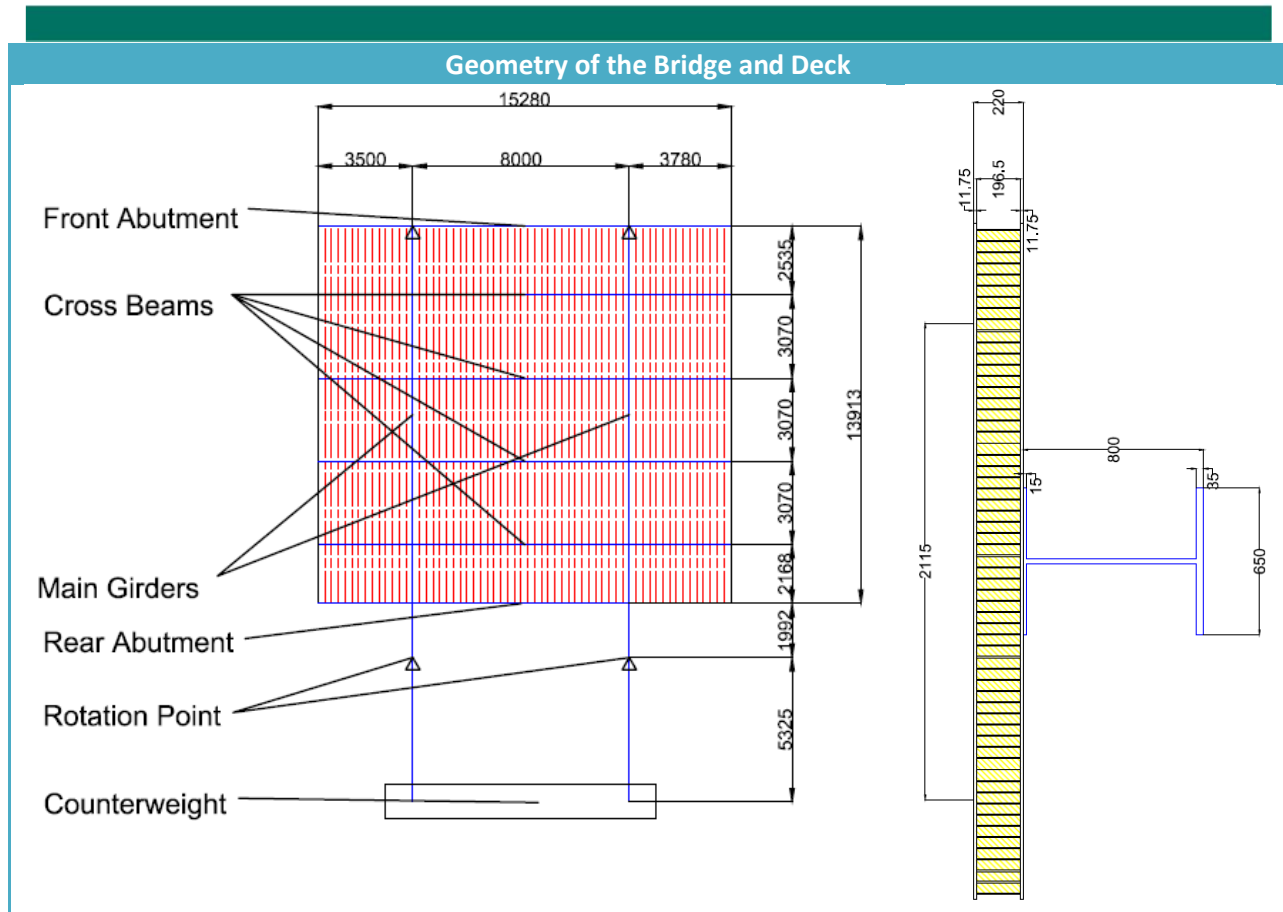


Figure 13: (Left) The Geometry of the Bridge. (Right) The Geometry of the Deck. The Yellow Shading Represents Foam Filling. Note That The Girder Dimensions Correspond to the Main Girder in the Lengthwise Laminated Variant, which will be Analyzed in this Chapter.

## 5.2 Procedure Description of Laminate Orientation Determination

For the analysis of the optimal laminate orientation, 5 variants will be considered. These are listed below.

1. The current design, i.e. the control situation: No composite action is included.
2. The current-composite situation: the current dimensions are used, but full composite action is assumed.
3. The Quasi-Isotropic solution: the FRP laminate is created in such a manner that it has equal properties in all directions.
4. The Crosswise Solution: the FRP laminate is created in such a manner that its stiffness in the crosswise direction of the bridge is largest.
5. The Lengthwise Solution: the FRP laminate is created in such a manner that its stiffness in the lengthwise direction of the bridge is largest.

The purpose of analyzing the laminate orientation is to minimize the mass of the superstructure, while maintaining structural integrity. Structural integrity has been maintained by requiring that the stiffness (Measured as  $EI_{zz}$ ) and the section modulus (simplified to  $z/EI_{zz}$ ) of each variant may not be less than of the current design.<sup>25</sup>

The result of composite action is an increase in stiffness and section modulus. Since the requirement is that they are not reduced and mass minimization is the ultimate goal, the dimensions of the steel girder are reduced.

Two forms of shear force are considered which are not present when the deck is not compositely connected to the girders. These are the shear force due to restrained thermal expansion and the shear flow due to vertical loading.

The results of the analysis are presented in six segments according to the outline below.

1. Effective Width of FRP
  - a. The width of the deck which works compositely with the steel is determined
2. Stiffness
  - a. The stiffness of the current situation is calculated.
  - b. The stiffness of the current situation, with composite action between the deck and the girders is calculated.
3. Stress ratio
  - a. The value of  $z/EI_{zz}$  is presented, normalized to the current design.
4. Mass
  - a. The mass of the current situation is calculated.
  - b. The mass of three alternatives is calculated assuming the stiffness may not decrease.
5. Thermal Force
  - a. The thermal force is calculated for the current situation if deck and steel were integrated.
  - b. The thermal force for the deck with new dimensions is calculated.
6. Shear Flow
  - a. The shear flow along the interface resulting from vertical loading is calculated based on the current situation if the deck and steel were integrated.
  - b. The shear force along the interface resulting from the vertical loading is calculated with the new girder sizes.

---

<sup>25</sup> The limiting value for the stiffness of the rear abutment was different (30% larger). See A.3 Serviceability Limit State (SLS) for more information.

### 5.3 Effective Width of FRP Deck

The width of the FRP deck which acts compositely with the girders plays an important role in how much it increases the stiffness and strength of the girders. Hence, this also plays an important role in determining how much can be gained by creating a shear connection between the two materials. If a girder is compositely connected to the deck and subjected to a moment, a normal stress arises in the deck. This normal stress dissipates as the distance to the girder gets larger, as visible in Figure 14. The stress is compressed into a certain width with a constant stress, so that the sum of the forces remains unchanged. This width is referred to as the effective width. Determination of the effective width is done for both the crossbeams and the main girders.

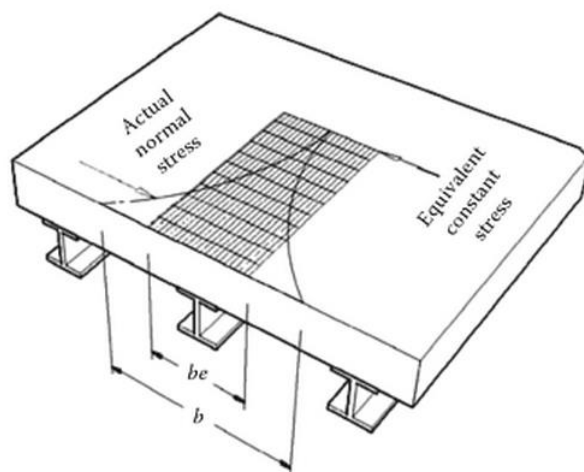


Figure 14: Representation of Effective Width of a Deck on Girders<sup>26</sup>

A comparison with the effective width of a concrete flange on a steel girder can be made. A concrete deck is not a viable alternative for this case study, since the weight of a concrete deck is approximately 5 times higher than that of an FRP deck. However, the comparison to a concrete deck is introduced as a reference for effective width in a different material. Additional comparisons to a steel-concrete solution are given in Appendix J: Comparing the Influence of Composite Action to Concrete. The rule for steel-concrete constructions is that the effective width may not exceed  $1/8^{\text{th}}$  of the effective length on either side of the shear connection.<sup>27</sup> Assuming that the shear connection is half as wide as the top flange, and the width of the deck exceeds  $1/8^{\text{th}}$  of the length to either side of the profile, the maximum effective width of a casted concrete flange is given by Equation 3.

<sup>26</sup> (Davalos, Chen, & Qiao, 2013)

<sup>27</sup> (Johnson, 2012)

$$b_e = 2 * \frac{L_e}{8} + \frac{1}{2} b_{flange}$$

### Equation 3: Effective Width of a Concrete Flange on a Steel Girder

With:

$L_e$ : Effective length of the considered span

$b_{flange}$ : Width of the steel flange

FRP behaves differently than concrete. Most notably, it has a much lower shear modulus; a typical shear modulus for concrete is approximately 20 GPa. When comparing this to the laminate calculated in 4.3.5 Determination of Laminate Properties the shear modulus of concrete is a factor 3 higher, while the size of the Young's moduli is nearly the same. However, research has shown that the value of the effective width decreases as the ratio E/G increases.<sup>28</sup> Therefore, the expected value for the effective width for FRP is lower than that for concrete. As such a model has been established specifically for the effective width of FRP decks on steel girders. The model is given in Equation 4.

$$b_{eff} = R \frac{\int_0^{\frac{b}{2}} \cosh(\xi y) dy}{\cosh\left(\frac{\xi b}{2}\right)}$$

$$\xi = \frac{\pi}{L} \sqrt{\frac{E}{G}}$$

### Equation 4: Effective Width model for FRP Decks on Steel Girders<sup>29</sup>

With:

R: Reduction Factor (Assumed as 1)

L: Span Length

b: Width of

E: Young's Modulus

G: Shear Modulus

Using Equation 4, the effective widths of the Main Girders and Crossbeams can be determined. The effective widths of the abutments will be assumed to be half of the width of the crossbeams, since the

<sup>28</sup> (Davalos, Chen, & Qiao, 2013)

<sup>29</sup> (Davalos, Chen, & Qiao, 2013). Note that (Davalos, Chen, & Qiao) replace the Young's Modulus with A(1,1) or A(2,2), and the shear modulus with A(3,3), where A is the stiffness matrix calculated in H.2 Classical Laminate Theory. This is a simplification to prevent having to calculate the true values. Since the true values are calculated in H.3 Engineering Constants of Laminate, they have been applied here.

FRP deck only extends to one side of these girders. The values are given in Table 9. Note that, as expected, the values of the effective width are lower for the FRP deck than they would be for an equivalent concrete deck. Note that while the lengthwise and crosswise laminated decks show a trade-off between effective widths in perpendicular directions, the quasi-isotropic laminate has a larger effective width for all locations. This is due to the fact that the shear modulus of a laminate is larger for a quasi-isotropic laminate than for an oriented laminate.

Effective Width of Deck				
Location	FRP Theory [m]			Concrete [m]
	Crosswise Laminated	Quasi-Isotropic	Lengthwise Laminated	Isotropic
<b>Rear Abutment</b>	0.4051	0.4881	0.474	1.11
<b>Main Girders</b>	2.4723	2.5458	2.115	4.05
<b>Front Abutment</b>	0.4051	0.4881	0.474	1.00
<b>Crossbeams</b>	0.8101	0.9763	0.9479	1.70

Table 9: Effective Width of an FRP Deck Based on Lamination Direction, with the Effective Width of a Concrete Deck for Comparison

## 5.4 Composite Stiffness of Girders

The stiffness is an important aspect of the current design. Typically for FRP structures, the stiffness is a limiting criteria. This is because while strength of FRP laminates is of the same order as that of steel, the Young's Modulus can be a factor 10 smaller. This is especially relevant for this case study, because in the current design the deformation requirements for the rear abutment are critical. Hence, in order to achieve a successful design, the stiffness of the construction must be increased.

The stiffness has been calculated for each variant in accordance with mechanics theory of inhomogeneous cross sections.<sup>30</sup> First the location of the normal force center, measured from the bottom of the cross section, is determined; shown in Equation 5.

$$\begin{aligned}
 z_{NC} &= \frac{\sum(E_i A_i z_i)}{\sum(E_i A_i)} = \frac{\sum(E_{FRP} A_{FRP} z_{FRP}) + \sum(E_{Steel} A_{Steel} z_{Steel})}{\sum(E_{FRP} A_{FRP}) + \sum(E_{Steel} A_{Steel})} \\
 &= \frac{(30)(88767)(910) + (210)(47500)(301)}{(30)(88767) + (210)(47500)} = 429mm
 \end{aligned}$$

Equation 5: Determination of the Height of the Normal Force Center. Numbers Correspond to The Main Girder Laminated in Lengthwise Direction.

<sup>30</sup> (Hartsuijker & Welleman, 2011)

With:

$E_i$ : Young's Modulus of Component "i"

$A_i$ : Area of Component "i"

$z_i$ : Distance from reference height (bottom of steel profile) of component "i."

After the normal force center has been determined, the "double letter symbol"  $EI_{zz}$  can be determined according to Equation 6.

$$EI_{zz} = \sum E_i * \left( \frac{1}{12} b_i h_i^3 + b_i h_i (z_i - z_{NC})^2 \right)$$

$$EI_{zz} = E_{FRP} * \left( 2 * \frac{1}{12} * b_{eff} * t_{face}^3 + b_{eff} (t_{face}) * (z_{upper\ face} - z_{NC})^2 + b_{eff} (t_{face}) * (z_{lower\ face} - z_{NC})^2 \right. \\ \left. + \frac{1}{12} * \frac{b_{eff}}{b_{web\ spacing}} * t_{web} * h_{web}^3 + \frac{b_{eff}}{b_{web\ spacing}} * t_{web} * h_{web} * (z_{web} - z_{NC})^2 \right) +$$

$$E_{steel} * \left( \frac{1}{12} * b_{top\ flange} * t_{top\ flange}^3 + b_{top\ flange} (t_{top\ flange}) * (z_{top\ flange} - z_{NC})^2 + \frac{1}{12} \right. \\ \left. * b_{bottom\ flange} * t_{bottom\ flange}^3 + b_{bottom\ flange} (t_{bottom\ flange}) \right. \\ \left. * (z_{bottom\ flange} - z_{NC})^2 + \frac{1}{12} * t_{web} * h_{web}^3 + t_{web} * h_{web} * (z_{web} - z_{NC})^2 \right)$$

$$EI_{zz} = 30 * \left( 2 * \frac{1}{12} * 2115 * 11.75^3 + 2115 * 11.75 * (1014 - 429)^2 + 2115 * 11.75 * (806 - 429)^2 + \frac{1}{12} \right. \\ \left. * \frac{2115}{50} * 4.7 * 197^3 + \frac{2115}{50} * 4.7 * 197 * (910 - 429)^2 \right) +$$

$$210 * \left( \frac{1}{12} * 650 * 15^3 + 650(15) * (793 - 429)^2 + \frac{1}{12} * 650 * 35^3 + 650(35) * (18 - 429)^2 + \frac{1}{12} \right. \\ \left. * 20 * 750^3 + 20 * 750 * (410 - 429)^2 \right) = 1.89 * 10^{12} \text{ Nmm}^2$$

$$EI_{zz} = EI_{zz,FRP} + EI_{zz,Steel} = 6.52 * 10^{11} + 1.24 * 10^{12} = 1.89 * 10^{12} \text{ Nmm}^2$$

**Equation 6:  $EI_{zz}$  of the FRP-Steel Composite Cross Section. The numbers correspond to the Main Girders in the Lengthwise Laminated Situation**

With:

$E_i$ : Young's Modulus of Component "i"

$b_i$ : Width of Component "i"

$h_i$ : Height of Component "i"

$z_i$ : Distance from reference height (bottom of steel profile) of component "i."

$z_{NC}$ : Height of Normal Force Center of the Cross Section



Figure 15 shows the results of determining the stiffness. Several points worth noting are listed below. Recall that a comparison to the increase in stiffness resulting from composite action in concrete is available in Appendix J: Comparing the Influence of Composite Action to Concrete.

- The differences between the current and composite variants indicate where the most gains are to be found. The main girder shows a large increase in stiffness, while the crossbeams show a slight increase in stiffness. The abutments show barely any increase in stiffness. This is because the abutments have been stiffened with steel up to the top of the deck.
- The stiffness of the rear abutment increases 30% between the current variant and the three directionally laminated variants. In the current design the rear abutment exceeded its allowable deformation. To resolve this in the new design, the stiffness requirement is 30% higher.
- For the three directionally laminated variants, the stiffness was known a priori, resulting from the current variant calculations. This means that the dimensions of the steel profile became the variables in the calculations of the stiffness.
- The stiffness of the other three girders changes little between the current variant and the three directionally laminated variants. This is because as much material as possible was removed from the girders without falling below the current design values.

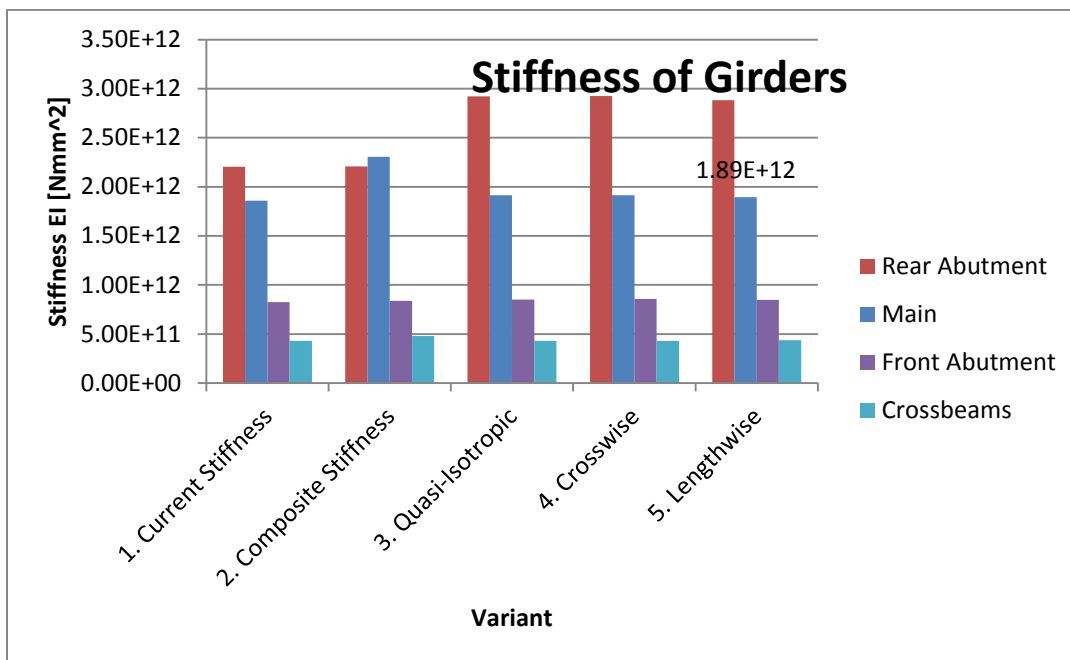


Figure 15: Stiffness of the Variants

## 5.5 Section Modulus of Connected Cross Section

In addition to maintaining a certain stiffness when minimizing the mass, the expected stress levels should also be maintained or reduced. To this end a ratio has been set up comparing the section moduli

of the different variants to the current design. This ratio may not exceed 1 as the mass of the elements are minimized. The values of this factor, calculated according to Equation 7, are shown in Figure 16.

Several points worth noting:

- As expected, the current situation shows unity for all girders.
- For the composite version of the current variant, the abutments show practically no change. This follows from a lack of improvement in the stiffness as outlined in 5.4 Composite Stiffness of Girders.
- There is a sizeable reduction in the stress in the rear abutment for the three directional variants. This follows from the large prescribed increase in  $EI_{zz}$ , combined with an unchanged height.
- The other girders show much smaller reductions for the directional variants. Where the small differences are largely due to rounding member sizes to standard values.
- Appendix J: Comparing the Influence of Composite Action to Concrete gives a comparison with the section modulus change expected in concrete.

$$W_{variant} = \frac{EI_{zz,variant}}{E_{Steel}z_{max,variant}}$$

$$Stress\ Ratio = \frac{W_{current\ design}}{W_{variant}}$$

Equation 7: (Top) The Calculation of the Section Moduli. (Bottom) The Stress Ratio; Determined as a Ratio between the Section Modulus of the Considered Variant and the Current Design.

With:

$EI_{zz}$ : Double Letter Stiffness Symbol According to Equation 6.

$W$ : Section Modulus

$z$ : Maximum Vertical Distance from the Normal Force Center of Steel

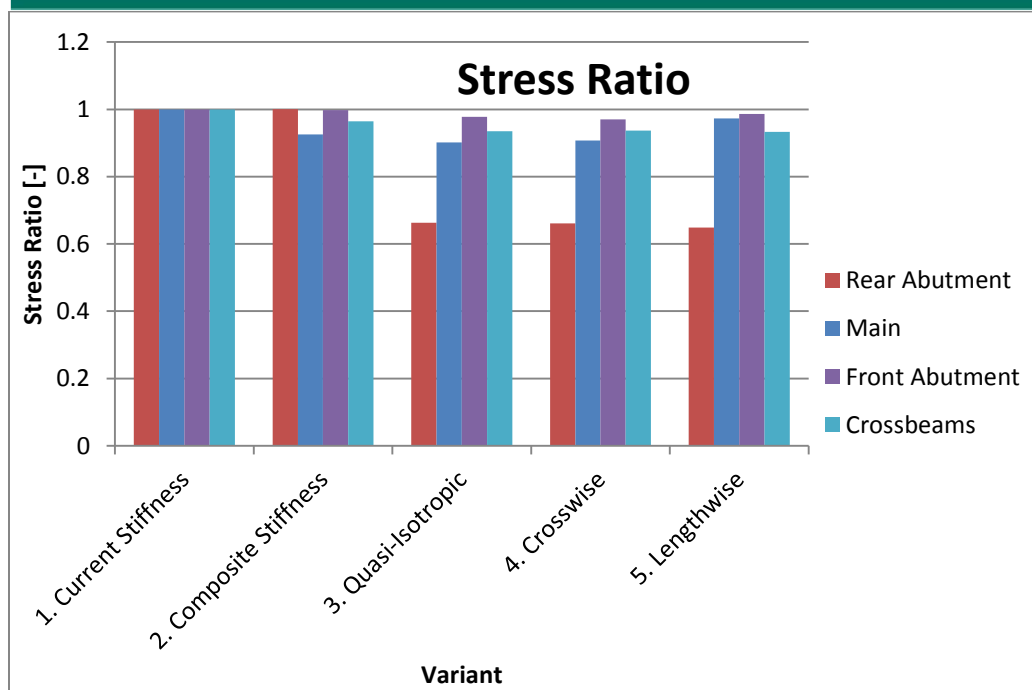


Figure 16: Stress Ratios of the Variants

## 5.6 Mass Change Due to Composite Action

The mass of the structure is important. Not only is a reduction in mass one of the key driving factors for using FRP, it also directly relates to the material costs for construction. The current design of the bridge failed to meet the mass reduction requirements, so that a reduction of the mass over the current situation is desired. The same variants described in 5.2 Procedure Description of Laminate Orientation Determination are calculated according to Equation 8 (note that original and composite stiffness variants have the same mass, and hence are not presented twice).

$$M_{steel} = A_{steel} \rho_{steel} L_{girder}$$

$$M = 47900e^{-6} * 7850 * 14.643 = 5506kg$$

Equation 8: Determination of Girder Mass. Numbers Correspond the Main Girder in the Lengthwise Laminated Variant.<sup>31</sup>

With:

$A_{steel}$ : Cross Sectional Area of Steel Girder

$\rho_{steel}$ : Density of Steel

$L_{girder}$ : Length of Steel Girder

<sup>31</sup> The mass of the deck has been excluded from the mass consideration. This has been done because the mass of the deck remains unchanged. Also, the length of the girder considered here is slightly larger than the measurements given in Figure 13. This is because exterior measurements, as opposed to heart to heart measurements have been used here.

The results of the mass minimization is shown in Figure 17. There are 3 things worth noting. First, the mass of the rear abutment barely decreased. In order to obtain the required increase in stiffness, the reduction of material allowed after including composite action is smaller than for the other members. Secondly, for all variants, the majority of the gain is obtained in the main girders. Thirdly, the largest gains are obtained when the laminate is oriented in the direction of the main girders.

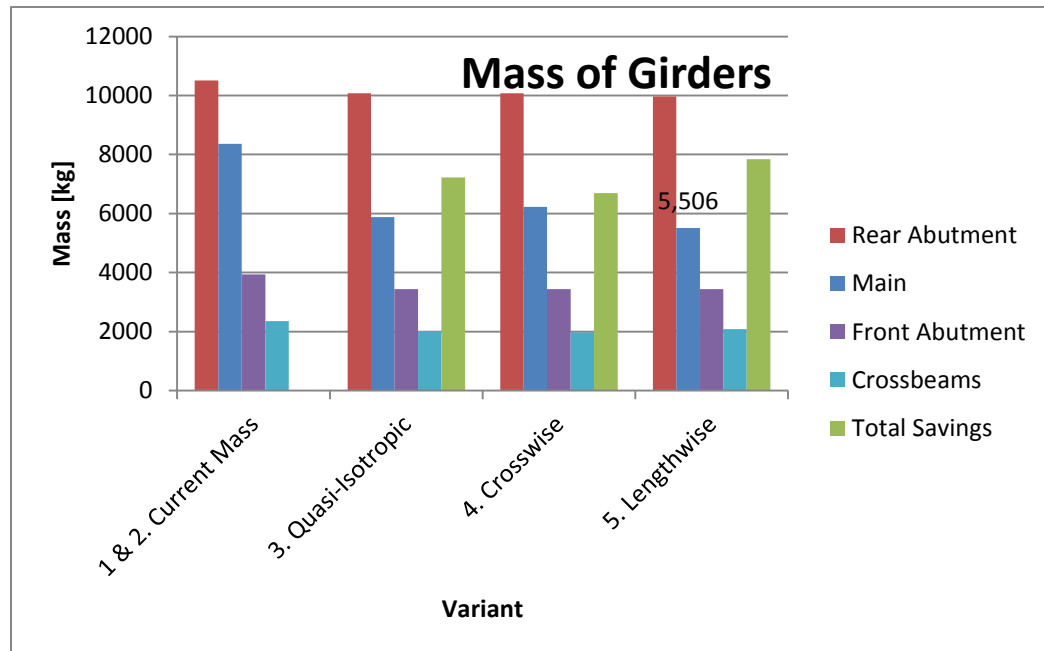


Figure 17: Mass of Girders

## 5.7 Thermal Loading Between Deck and Girder

In G.6 Thermal Expansion and H.2.2 Thermal Expansion of Laminates the behavior of FRP under thermal loading is analyzed, with the purpose of obtaining thermal expansion coefficients. The reason for this is that if the deck and the steel are to behave in a composite manner, the two must be connected in such a manner that they can transfer shear stresses. Creating a slip resistant joint leads to restricted thermal expansion, causing a force along the interface. This force can be divided into two components: that arising due to uniform temperature increase, and that arising due to a temperature gradient. The force and stress arising due to thermal expansion are analyzed in the following sections.

### 5.7.1 Thermal Force Between due to Uniform Temperature Change

The forces resulting from a uniform increase in temperature can be calculated according to Equation 9, while the transfer mechanism is shown in Figure 18. The values of the uniform thermal forces for the different variants are presented in Figure 19.

$$Q = \frac{(\alpha_{FRP} - \alpha_{steel}) * \Delta T}{\frac{1}{A_{deck} E_{FRP}} + \frac{1}{A_{steel} E_{steel}} + \frac{(h_{deck} + h_{steel})^2}{4 * (E_{FRP} * I_{deck} + E_{steel} * I_{steel})}}$$

$$Q = \frac{(2.33e^{-5} - 1.2e^{-5}) * 38}{\frac{1}{22276 * 19.6} + \frac{1}{17360 * 210} + \frac{(220 + 800)^2}{4 * (19.6 * 2.42e^8 + 210 * 1.69e^9)}} = 130.5kN$$

Equation 9: Calculation of Uniform Thermal Force. Numbers Correspond to Crossbeams under the Lengthwise Laminated Variant.<sup>32</sup>

With:

- $\alpha$ : Thermal Expansion Coefficient of Subscript Material
- $\Delta T$ : Change in Temperature
- $h$ : Height of Subscript Component
- $A$ : Area of Subscript Component
- $E$ : Young's Modulus of Subscript Material
- $I$ : Moment of Inertia of Subscript Component

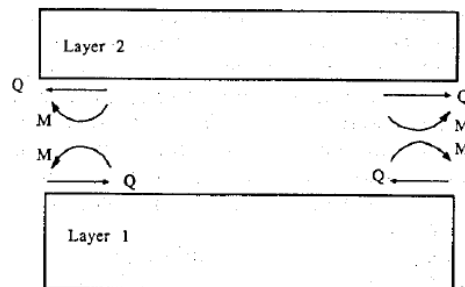


Figure 18: Load Transfer Mechanism for Bimaterial Strip Under Thermal Expansion<sup>33</sup>

<sup>32</sup> (Eischen, Chung, & Kim, 1990)

<sup>33</sup> (Eischen, Chung, & Kim, 1990)

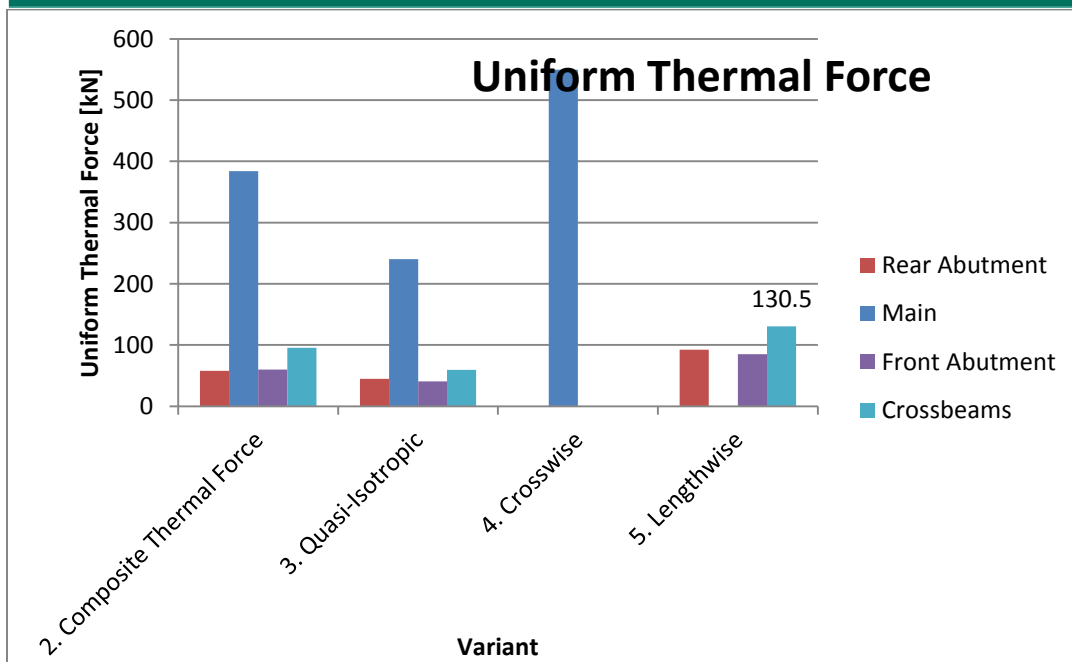


Figure 19: Uniform Thermal Forces for the Variants

Note that in Figure 19 some of the thermal forces for the crosswise and lengthwise laminated variants are zero. This is because when the FRP is laminated with one main direction, the coefficient of thermal expansion in that direction becomes nearly identical to that of steel. In other words, orienting the laminate in lengthwise direction means that there will be no restricted thermal expansion in lengthwise direction.

### 5.7.2 Thermal Force due to Non-Uniform Temperature Change

The temperature is not necessarily constant throughout the cross section. Therefore, there will also be a thermal force resulting from a difference in temperature between the deck and the girder. The simplified method explained in A.1 Thermal Load is applied. The calculation method for the force which arises due to the non-uniform thermal loading is given by Equation 10. The results of the calculations are presented in Figure 20.

$$Q = \frac{\alpha_1 * (\Delta T_1)}{\frac{1}{A_{deck} E_{FRP}} + \frac{1}{A_{steel} E_{steel}} + \frac{(h_{deck} + h_{steel})^2}{4 * (E_{FRP} * I_{deck} + E_{steel} * I_{steel})}}$$

$$Q = \frac{(1.2e^{-5}) * 10}{\frac{1}{22276 * 19.6} + \frac{1}{17360 * 210} + \frac{(220 + 800)^2}{4 * (19.6 * 2.42e^8 + 210 * 1.69e^9)}} = 36.5kN$$

Equation 10: Calculation of Non-Uniform Thermal Force. Numbers Correspond to Crossbeams under the Lengthwise Laminated Variant.<sup>34</sup>

With:

- $\alpha$ : Thermal Expansion Coefficient of Subscript Material
- $\Delta T_1$ : Change in Temperature of One Material
- $h$ : Height of Subscript Component
- $A$ : Area of Subscript Component
- $E$ : Young's Modulus of Subscript Material
- $I$ : Moment of Inertia of Subscript Component

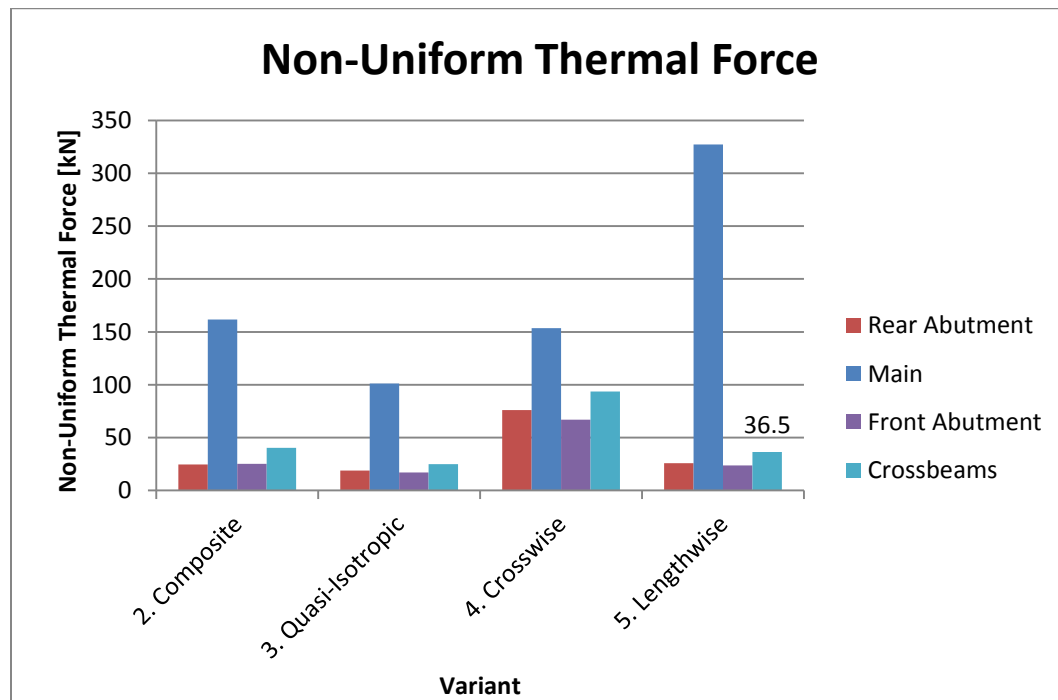


Figure 20: Non-Uniform Thermal Forces for the Variants

In all cases where a uniform thermal force is present, see Figure 19, the combination of uniform and non-uniform force is governing. Therefore, the non-uniform thermal force presented is based on the thermal expansion coefficient of steel. For the other cases, the non-uniform thermal force is based on the thermal expansion coefficient of FRP. This is done, because the uniform thermal force is

<sup>34</sup> (Eischen, Chung, & Kim, 1990)

calculated using the extreme temperature the system will obtain. Therefore, the additional force due to non-uniform heating follows from a less extreme temperature in the steel.

### 5.7.3 Distribution of Thermal Shear Stress

The force calculated above must be transferred between the composite deck and the steel girder if they are connected in a manner that allows composite action. The thermal force will be transferred near the end of the deck, resulting in a large peak shear stress. The shear stress has been determined using Suhir's theory, given in Equation 11. Suhir's theory assumes that the connection has uniform stiffness along the interface. See Figure 21 for the development of shear stress over half of the length of a crossbeam. One can see that the shear stress develops very quickly towards the end of the interface, and that there is no stress in a large region around the center of the interface.

$$\tau(x) = \frac{[(1 + \nu_1)\alpha_1 - (1 + \nu_2)\alpha_2]\Delta T}{\sqrt{\lambda s}} (e^{-k(L-x)} + e^{-k(L+x)})$$

$$\lambda = \frac{1 - \nu_1^2}{E_1 h_1} + \frac{1 - \nu_2^2}{E_2 h_2} + \frac{(h_1 + h_2)^2}{4 \left( \frac{E_1 h_1^3}{1 - \nu_1^2} + \frac{E_2 h_2^3}{1 - \nu_2^2} \right)}$$

$$s_1 = \frac{2(1 + \nu_1) h_1}{3E_1 b}$$

$$s_2 = \frac{2(1 + \nu_2) h_2}{3E_2 b}$$

$$s = b(s_1 + s_2)$$

$$k = \sqrt{\frac{\lambda}{s}}$$

Equation 11: Suhir Theory for Shear Stress Between Two Materials with Different Thermal Expansion Coefficients.<sup>35</sup>

With:

$\nu$ : Poisson's Ratio

$E$ : Young's Modulus

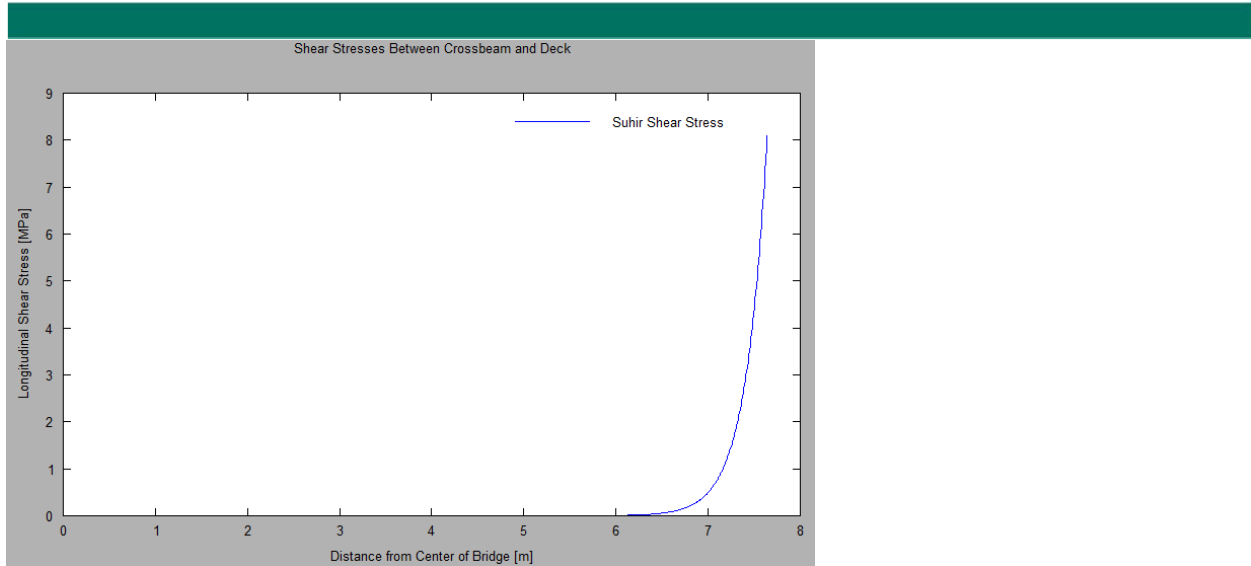
$h$ : Height

$b$ : Width

$x$ : Distance from Center of the Interface Towards Outside

<sup>35</sup> (Eischen, Chung, & Kim, 1990)





**Figure 21: Shear Stress Development Between Bridge Deck and Crossbeam Under Thermal Loading as Measured from the Center of the Bridge, Assuming a Perfectly Stiff Connection.**

The Suhir method is displayed mainly to illustrate the location where the shear stresses are active. The method is, unfortunately, quite inaccurate since it does not account for end-effects of the interface. At the edge of the beam, the shear stresses should return to zero, but since this is not taken into account, the method overestimates the total force transfer through the interface. When comparing the force calculated in Equation 9 to the integral of the shear stress shown in Figure 21, the integral of the shear stress shows an overestimation by a factor 2. Clearly, the Suhir method overestimates for the shear stress present and hence should only be viewed as illustrative. The most important thing to take away from Figure 21, is that the thermal force is concentrated at the end of the beam.

### 5.8 Shear Flow Due to Vertical Loading

The shear flow needs to be calculated in order to determine the force which must be transferred by the joints between the girders and the deck. The shear flow is determined for each of the variants according to Equation 12. It is presented in Figure 22 as a function of the vertical shear force acting on the composite cross section. Note that the shear flow is larger for all variants when compared to the composite version of the current design. This means that extra care should be taken while designing the joints.

$$s_x = \frac{\sum E_i S_i^{(a)}}{EI_{zz}} V_z$$

$$\frac{s_x}{V_z} = \frac{\sum E_i S_i^{(a)}}{EI_{zz}} = \frac{E_{FRP} A_{FRP} (z_{deck} - z_{NC})}{EI_{zz}} = \frac{(30)(88767)(910 - 429)}{1.89 * 10^{12}} = 0.677 \frac{N}{mmkN}$$

Equation 12: Shear flow Between the Deck and the Steel Girder as a Function of Shear Force acting on the Cross Section.<sup>36</sup>

With:

E: Young's Modulus

$S_i^{(a)}$ : Static Moment of Shear Section With Respect to Neutral Axis

$EI_{zz}$ : Double Letter Symbol For Stiffness According to Equation 6

$V_z$ : Vertical Shear Force

A: Area

z: Vertical Coordinate

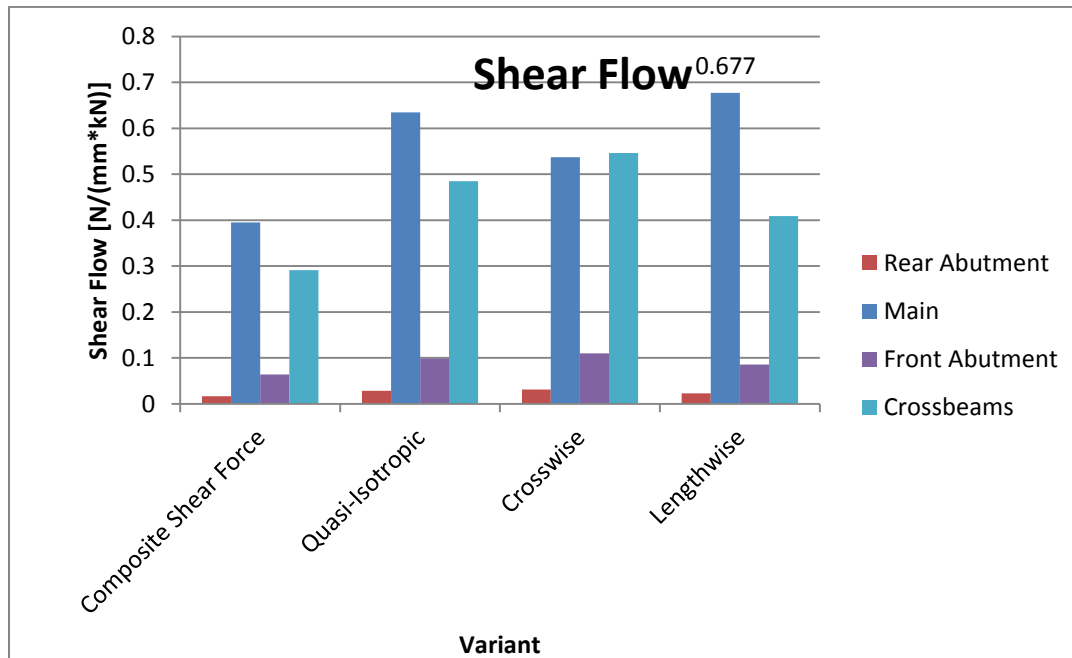


Figure 22: Shear Flow Along FRP-Steel Interface as a Factor of Vertical Shear Force

## 5.9 Conclusion Laminate Orientation

For all three of the variants considered in this chapter, it appears possible to reduce the mass of the structure while maintaining structural integrity. However, a choice must be made regarding the orientation of the laminate. The mass reduction is considered the most important criterion, but the thermal and shear forces will also be considered.

<sup>36</sup> (Hartsuijker & Welleman, 2011)

The lamination direction is chosen to be parallel to the main girders. This choice has been made based on the following reasons:

- The largest reduction in mass occurs for this variant
- The shear flow along the main girder is slightly higher than for the other variants, but the shear flow for the perpendicular direction, especially the crossbeams, is reduced.
- This variant has no thermal force acting in the direction of the main girder
  - No connection needs to be realized at the supports, reducing complexity.

## 6 Joints Between FRP Deck and Steel Girders

This thesis is directed towards designing a FRP-steel integrated bridge, calling for these two materials to be connected. The design requirements are such that the FRP will be placed on top of steel girders. In order to achieve composite action between the two materials, shear stresses must be transferable at the interface. The process of designing a shear connection is outlined below:

1. Literature Review (See Appendix L: Joint Literature)
  - a. Mechanical Joints
  - b. Adhesive Joints
2. Design of an FRP to Steel Joint
  - a. Design Considerations
  - b. Hand Calculations
  - c. Geometry Determination
3. Finite Element Analysis
  - a. Small Scale Model
  - b. Calibration against Experiments
    - i. Choose Failure Criteria
    - ii. Determine Optimal Failure Criteria Parameters
  - c. Full Scale Model
    - i. Determination of Failure Load
    - ii. Determination of Stiffness
    - iii. Check the Influence of Scaling Failure Criteria Parameters
4. Redesign of System
  - a. Reduced Deck Height
  - b. No Composite Action
5. Influence Studies (See Appendix O: Joint Influence Studies)
  - a. Hole Clearance
  - b. Bolt Head
  - c. Tension Effect
  - d. Alternative Materials
  - e. Relationship Between Connection Strength and Mass
6. Conclusion

### 6.1 Design of an FRP to Steel Joint

A design must be made for the connection between the FRP deck and the steel girder. There are two loads which impose different stresses along the interface. These are thermal loading, and vertical loading of the deck. Some properties based on which to design are given below.

- Thermal Connections

- End of beam
  - Need not be flush with the deck
    - Does not hinder traffic
- High peak stresses at end of bridge
  - More robust
  - No load spreading over length
- Vertical Loading Connections
  - Entire length of bridge
    - Must be flush with the deck
      - May not hinder traffic
  - No peak at end of bridge
    - More smaller connections possible
    - Load spreading over length

Considering the different requirements for each type of loading, it would be beneficial to design two types of connections. The design vertical shear force is 1308kN in the main girder<sup>37</sup> and the shear flow factor is  $0.677 \frac{kN}{m \cdot kN}$  as shown in Figure 22. This leads to a design shear flow of 885kN/m.<sup>38</sup> The thermal force has a maximum value in the cross beams of 130.5 kN. Since the shear flow due to vertical loading is significantly larger than the thermal force, this shear flow will be considered leading during the connection design process.

### 6.1.1 Considerations in the Design of FRP-Steel Joints

The connections responsible for transferring the shear stress which arises due to vertical loading must be applied over the entire length of the beam. The design shear flow is at a maximum near the ends of the deck, and at a minimum near the middle of the deck. The criteria based on which this connection method will be chosen are given below.

1. Flush with Deck
  - a. Since the connection will be utilized over the length of the bridge, it needs to be realized in such a manner that it does not protrude above the deck.
2. Stiffness
  - a. A connection with a large stiffness is preferred, since any slippage will reduce the composite action between the deck and the girder. See Q.4.3 Influence of Connection Stiffness, for an indication of the influence connection stiffness has on the global behavior of a system.
3. Weight

<sup>37</sup> (Hattink, 2014)

<sup>38</sup> Note that for the connection, a local thickening of the laminate will be applied. This will increase the static moment of the deck and so that the shear flow will increase by 16.5% to 1031 kN/m.

- a. Local thickening of the FRP laminate will lead to an increase in weight. This should be limited if possible.
- 4. Quantity
  - a. The realization of connections is expensive, therefore the number of connections should be minimized.
- 5. Applicability
  - a. Installation should be quick and easy.
  - b. These connections should be capable of being placed with reasonable spacing since more connections yield a better composite action.
- 6. Dependability
  - a. Adhesive connections are prohibited based on a lack of long term data regarding their strength.

Based on the design considerations above, a bolted connection through the bottom flange of the FRP deck appears to be the best solution. Attaching the bolt through only the bottom flange will make the bolts flush with the deck. Bolted connections also have the benefits of being stiff, low weight, and very applicable. Additionally, the experience with bolted connections in steel structures will reduce the learning curve for the application of such connections in FRP. Some additional connections which were considered are presented in Appendix K: Possible Connection Method Sketches.

### 6.1.2 Preliminary Calculations of a Bolted Connection

Some simplified calculations are performed to obtain an idea for the strength of a connection. There are design guidelines for bolted connections, however, the calculations will be performed by hand here. A comparison between these hand calculated values and the design guidelines is made in Appendix P: Comparison to Eurocomp Handbook. The hand calculations are based on the following assumptions:

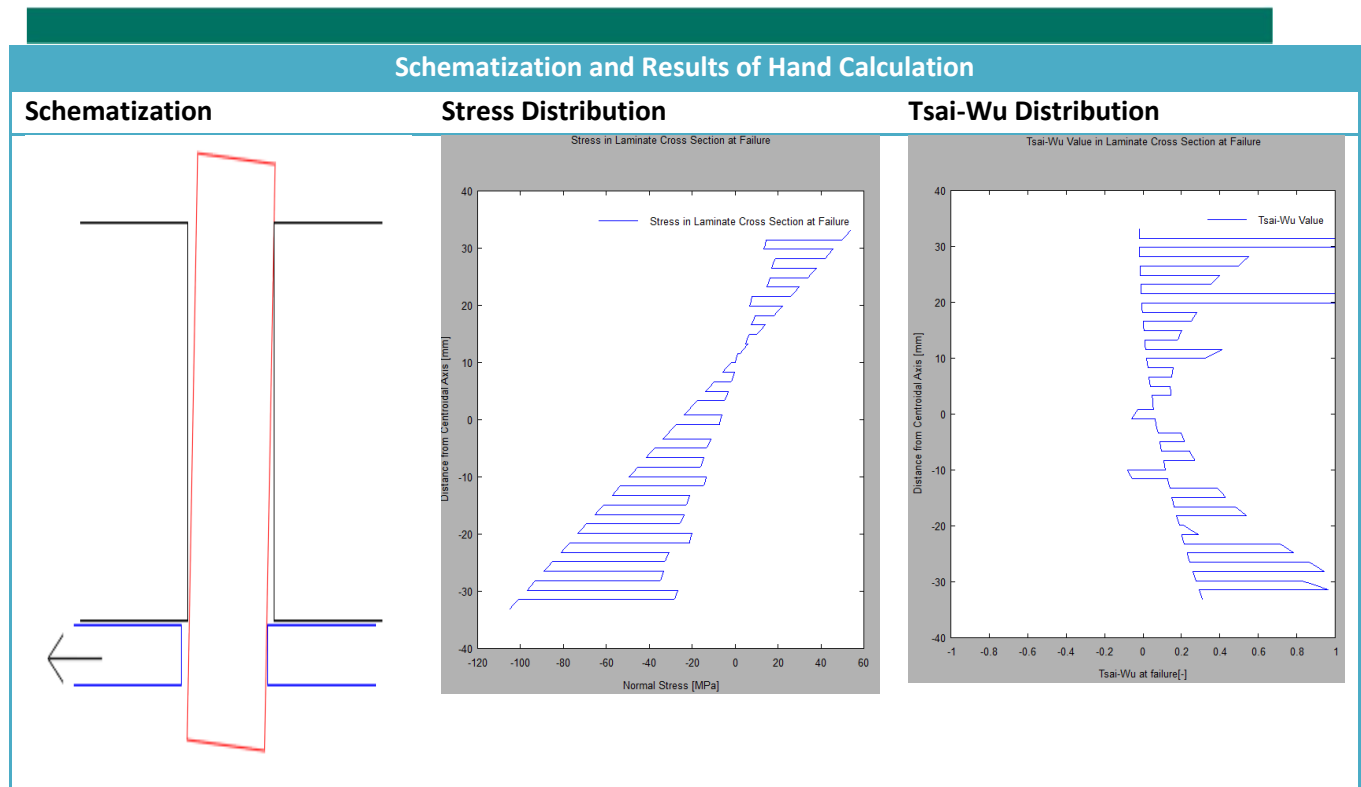
1. The bolt is rigid and free to rotate at its ends
  - a. The strain distribution in the connection is linear
2. All forces must be transferred through compression
  - a. Regions where tension arises are not tested against the failure criterion, since this will not actually occur
3. The stress distribution across the width of the hole can be approached with a sinusoidal distribution
  - a. Sinusoidal approach more accepted than linear theory as found in Appendix M: Contact Between a Cylinder and Groove.
4. The magnitude of the splitting stress equals one fourth of the compressive stress
  - a. This follows from a sinusoidal approximation. See O.3 Tension Effect for more information

5. The ULS conversion factors are applied
6. The Tsai-Wu Failure criterion is applied
7. Failure occurs in the laminate, not in the steel plate or the bolt
8. The laminate layup is been chosen in accordance with 5.9 Conclusion Laminate Orientation, and given in Table 10.

Ply Layup Properties		
Number	Thickness [mm]	Orientation [°]
1	1.66	0
2	1.66	90
3	1.66	0
4	1.66	45
5	1.66	0
6	1.66	-45
7	1.66	0
8	1.66	90
9	1.66	0
10	1.66	45
11	1.66	0
12	1.66	-45
13	1.66	0
14	1.66	90
15	1.66	0
16	1.66	45
17	1.66	0
18	1.66	-45
19	2.49	0
20	0.83	90
<b>40</b>	<b>66.25</b>	

Table 10: The Ply Layup Properties of the Upper Half of the Connection Laminate, the Laminate is Symmetric about its Central Axis

The schematization, and resulting stress and Tsai-Wu distributions are presented in Figure 23. Tension arises in the top of the laminate. Since this is not realistic, the Tsai-Wu values in this region are not taken into consideration.



**Figure 23:** From left to right: (1) Schematization of connection for hand calculations, (2) Resulting Stress Distribution in the Laminate, (3) Tsai-Wu values over the height of the cross section

In the preliminary calculations described above, several parameters may be altered to achieve a functional design. These include the force transfer per bolt (and hence the number of bolts), the diameter of the bolt, the thickness of the steel plate, the thickness of the laminate, and the ply orientation.

The ply orientation should result in the laminate-directionality described in Chapter 5 Laminate Orientation. Additionally as described in L.1.3 Unquantified Effects, grouping plies of the same direction together actually severely reduces the strength of bolted connections. Hence, applying more 0° oriented plies near the outside of the laminate is not an option to increase strength.

The force transferred per bolt, the bolt diameter, number of bolts, and the thickness of the laminate are all intertwined. Some initial requirements are set to limit the number of combinations which are possible.

- The bolt spacing requirements in FRP are such that each bolt requires 4 diameters of longitudinal space (pitch) and transverse space (gage).<sup>39</sup>
- No more than 4 bolts should be placed side by side
  - This follows from both space limitations and quantity minimization

<sup>39</sup> (Bank, 2006)



- The yield stress of steel should not be exceeded within the bolt due to the assumed moment which occurs in the connection.

With the requirements listed above, a large majority of smaller bolts must be discarded as options. Many of these bolts do not have the capacity to transfer the required force within the number of bolts which fit within the region under the given spacing requirements. For some of the medium to large sized bolts, the moment created between the laminate and the steel plate is sufficiently large that the yield stress of steel is exceeded in the bolt. Hence, these options must be eliminated as well. The only bolts which suffice on the grounds of the criteria above, are the M36 and M40 bolts.

The M36 bolt is chosen as the best solution for this case study. The M36 bolt can transfer 46kN in a laminate thickness of 66.25mm. The M36 bolt is chosen because it requires a thinner laminate than the M40 bolt. This has the following advantages:

- The thicknesses required for either bolt push the boundaries of current production techniques. The thinner laminate requirement of the M36 bolt will cause fewer difficulties during production .
- The thinner laminate requires less material, reducing material costs.
- The thinner laminate weighs less, so that mass can be saved on the entire construction.

### 6.1.3 Visualization of Main Girder to Deck Connection

The connection calculated in the previous section is show in Figure 24, Figure 25, and Figure 26.

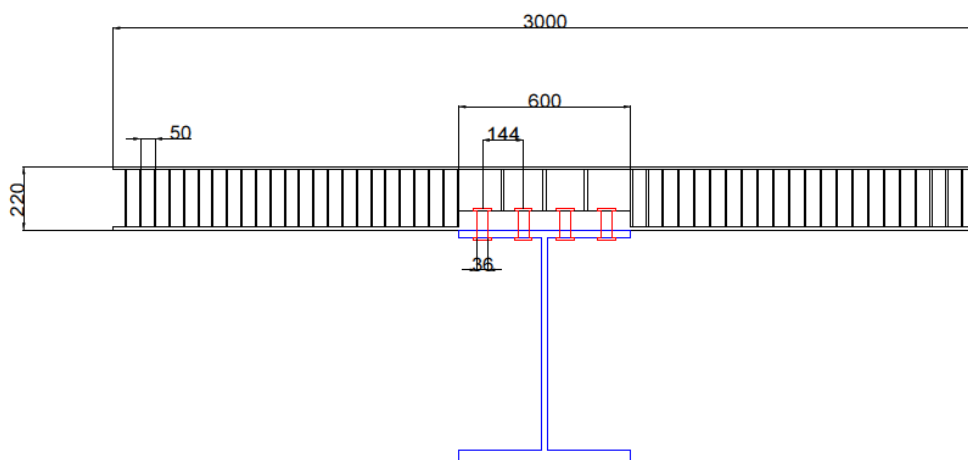


Figure 24: Front View of Connection Design. Note that the Top Flange of the Steel Profile has been Drawn out of Scale to Improve Visibility.

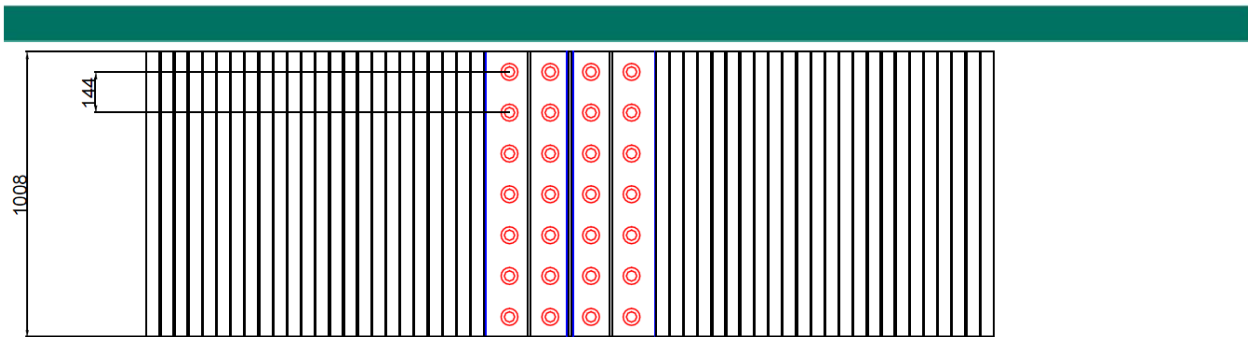


Figure 25: Top View of Connection Design

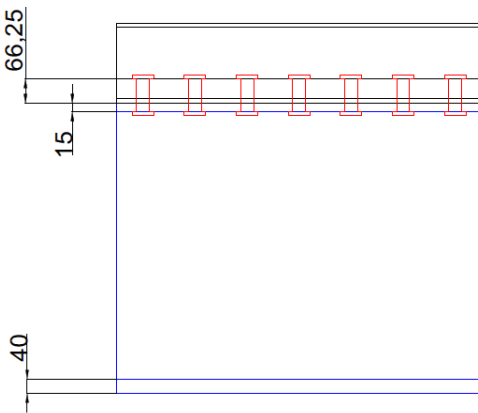


Figure 26: Side View of Connection Design. Note that the Top Flange of the Steel Profile has been Drawn out of Scale to Improve Visibility.

## 6.2 Calibration of Model by Comparison to Experiments

Prior to modeling a full sized connection, model accuracy should be demonstrated. In order to do this, a series of previously performed experiments has been found. The experiments were done on small scale, symmetrically loaded specimens. The model is run and compared to the results of these experiments. During this process, several model elements, and physical characteristics were checked. For a detailed description of the calibration, see Appendix N: Calibration Study. Here one can find information such as applied materials (N.3), applied elements (N.4), and mesh size (N.5).

### 6.2.1 Geometry of Pinned Joint Laminate

A series of experiments has been found, which measure the bearing strength of a bolt in a glass fiber reinforced polymer laminate. These experiments include a variety of geometries and laminate buildups which have been tested. As such, this makes for a good basis for creating a model which corresponds with reality. The setup of said experiments is shown in Figure 136. For these experiments, the bolt size was constant at 5mm and the laminates ranged from 1.4 to 4.8 mm in thickness, with varying lamella layups, and given in Table 11. The measurements of the specimens are much smaller than applicable for the case study, so that these experiments can only be used as calibration of the model.

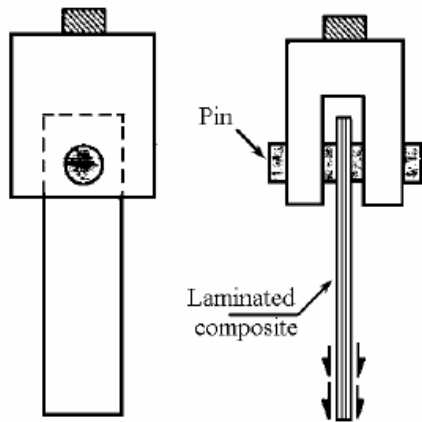


Figure 27: Calibration Experiment Set Up<sup>40</sup>

Layups of Experiment Specimens			
Specimen Number	Layup	Lamella Type	Thickness
1	[0/±45]s	UD	4.4
2	[90/±45]s	UD	4.4
3	[0/90/0]s	UD	3.3
4	[90/0/90]s	UD	3.3
5	[90/0]2s	UD	4.8
6	[±45]2s	UD	4.8
7	[0/90]6	Woven	1.4
8	[±45]6	Woven	1.4

Table 11: Layups, Lamella Types, and Thickness of Experimental Specimens<sup>41</sup>

### 6.2.2 Supports and Loading of Calibration Model

For the calibration experiment the bolt was held in place, and the laminate was subjected to displacement controlled loading, at a certain distance below the bolt. As such, displacements have been assigned to nodes corresponding to these locations. The model of the bolted laminate is shown in Figure 137 and Figure 138, with assigned displacements being numbered and indicated by the light blue markers. The displacements assigned at each location are listed in Table 12.

<sup>40</sup> (Okutan, 2001)

<sup>41</sup> (Okutan, 2001)

Displacements Assigned in Model			
Location	Ux	Uy	Uz
1	Fixed	Fixed	Fixed
2	Fixed	Fixed	Fixed
3	Variable	Free	Free
4	Variable	Fixed	Fixed

Table 12: Displacements Assigned to Calibration Model. Locations Correspond to Figure 28 and Figure 29.

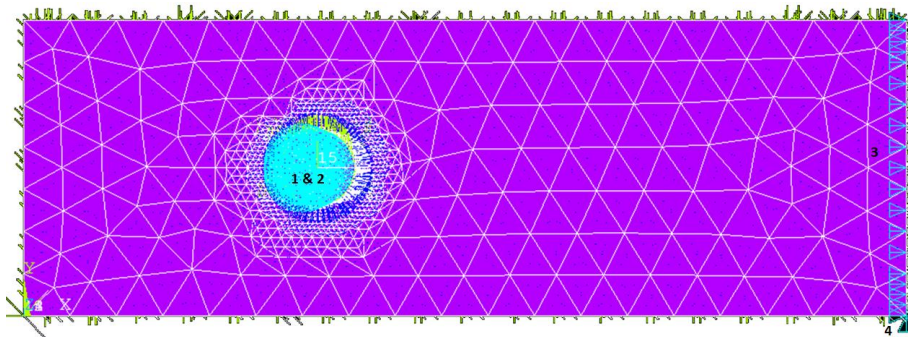


Figure 28: Top View of Calibration Model

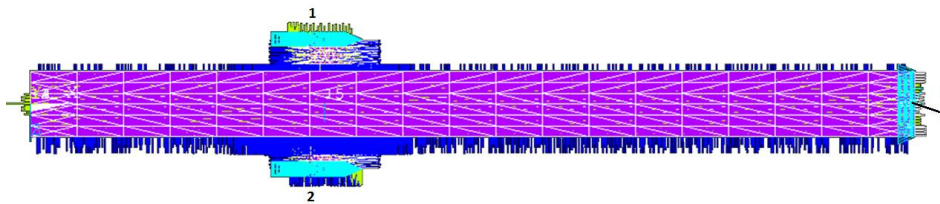


Figure 29: Side View of Calibration Model

### 6.2.3 Visualization of Results of Calibration Model

A typical result is shown in Figure 30. The model shows that the highest Tsai-Wu values occur near the contact interface between the bolt and laminate, as expected. The stresses dissipate as one gets further away from this interface. Note that the Tsai-Wu value far exceeds 1.

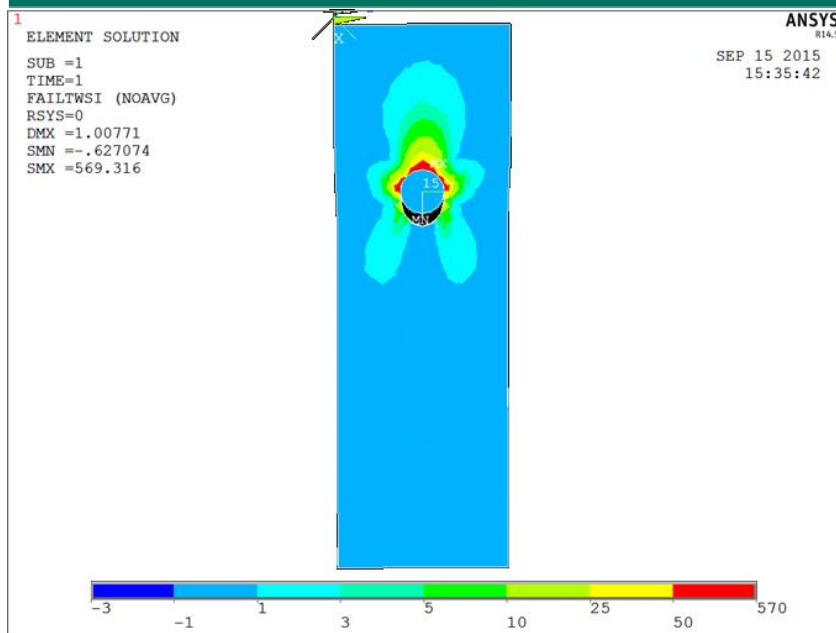


Figure 30: Tsai-Wu Value for a Laminate with a 5mm Pin Joint Undergoing a 1mm Displacement. The Peaking Tsai-Wu Criterion is Typical for all Modelled Specimens.

#### 6.2.4 Interpretation of Calculation Results of Calibration Model

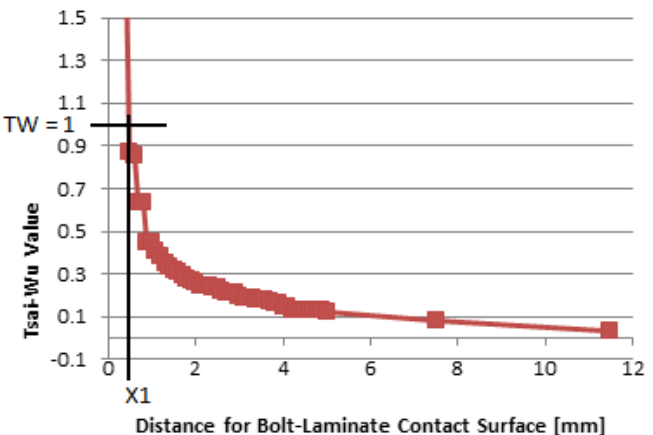
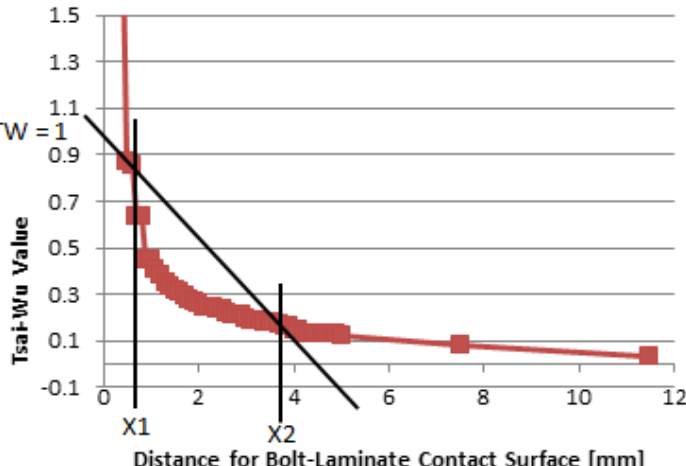
The data from the calibration models are used to determine the accuracy of the model and will be used to interpret the data obtained from a full-scale model. To analyze the data from the small scale models, an accurate method for determining failure should be established. The process by which the failure criterion will be established is outlined below, with more information to follow in the coming sections.

1. Three distance based methods for determining the relevant Tsai-Wu value are established.
2. Three cross section based methods are established for determining how to measure failure within the laminate.
3. The distance and cross section based methods are combined into 9 trial methods for establishing a failure criterion.
4. The modelled results are set against the experimental results for each of the 9 trial methods. Measurement distances are chosen for each trial method such that the highest possible correlation between modelled and experimental results are obtained.
5. The trial methods are compared with one another, and the best one is chosen.

##### 6.2.4.1 Distance Based Calculation Methods

The bolt-FRP interface shows extremely large peak stresses, and therefore a large Tsai-Wu value, at loads far below the experimental failure levels. Three methods for calculating failure based on measurement distance have been analyzed; the single point failure, the dual point failure and the

distance average methods. The three methods are graphically presented in Table 13. The measurement distances, X1 and X2, are chosen such that the modeled results have the best correlation with the experimental results.

Failure Calculation Methods	
Graphical Representation of Method	Explanation
<p style="text-align: center;"><b>Single Point</b></p>  <p style="text-align: center;">Distance for Bolt-Laminate Contact Surface [mm]</p>	<p>The single point failure criterion is exceeded when at a predetermined location the Tsai-Wu value exceeds 1.</p>
<p style="text-align: center;"><b>Dual Point</b></p>  <p style="text-align: center;">Distance for Bolt-Laminate Contact Surface [mm]</p>	<p>The dual point failure criteria is exceeded when the linear extrapolation of two Tsai-Wu values at predetermined distances exceeds 1 at the contact surface.</p>

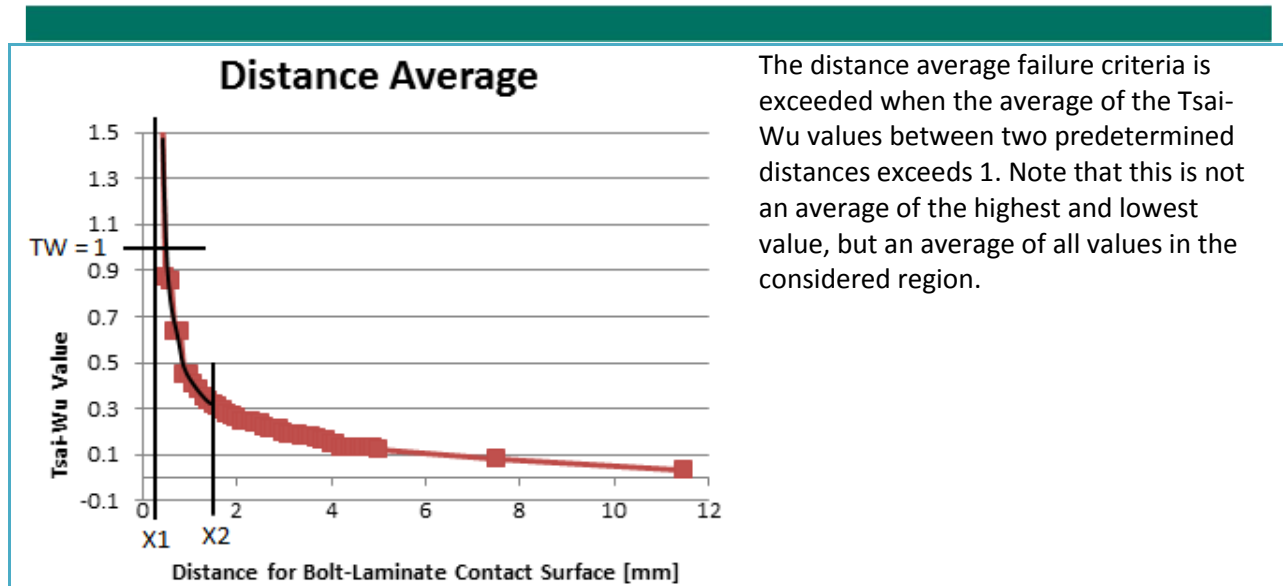


Table 13: Methods For Calculating Model Failure

#### 6.2.4.2 Cross Section Based Measurements

Another variable in determining failure is the method in which the Tsai-Wu value is measured within the cross section. The considered methods were:

1. The top ply of the laminate
2. The maximum value measured within the cross section
3. The average value over all the plies in the laminate.

#### 6.2.4.3 Combination of Distance and Cross Section Based Methods

The distance and cross section based methods can be combined to form 9 trial methods for determining failure. These 9 methods are shown in Table 14.

Combination of Distance and Cross Section Based				
		Height Based		
		Top Ply	Maximum	Height Average
Distance Based	Single Point	Single Point Top Ply	Single Point Maximum	Single Point Height Average
	Dual Point	Dual Point Top Ply	Dual Point Maximum	Dual Point Height Average
	Distance Average	Distance Average Top Ply	Distance Average Maximum	Distance Average Height Average

Table 14: Combination of Distance and Cross Section Based Methods

#### 6.2.4.4 Determination of Measurement Distance

Each of the 9 trial failure methods is dependent on the distance at which the Tsai-Wu value is measured. Therefore, this distance needs to be determined. The process for doing so is outlined below:

1. Choose a distance from the interface
2. Determine the load at which the Tsai-Wu value equals 1 at chosen location, i.e. the modeled failure load
3. Compare the modeled failure load to the experimental failure load
4. Repeat steps 1-3 for multiple distances
5. Determine the distance at which the modeled failure load shows the best correlation to the experimental data.

As an example, this process is made visible for the single point height average method in Figure 31. The measurement distances 0.25mm, 0.375mm, and 0.5mm have been chosen. The loads at which the Tsai-Wu value exceeds 1 at these distances are given on the y-axis. Note that as the measurement distance becomes larger, the modeled failure load becomes larger. This is expected, since the stress peak dissipates at larger distances. The modeled failure loads are compared to the experimental failure loads for each measurement distance, and the relationships are given in the legend. The model should have a good correlation with the experimental values, so that the  $R^2$  value is the criterion on which the appropriate model is selected. In Figure 31, one can see that the highest  $R^2$  value follows from a measurement distance of 0.5mm. Therefore the model is set with this measurement distance. For the remaining trial methods, the same process has been applied. Note that for the dual point, and distance average methods, there are two variable distances which influence the model.



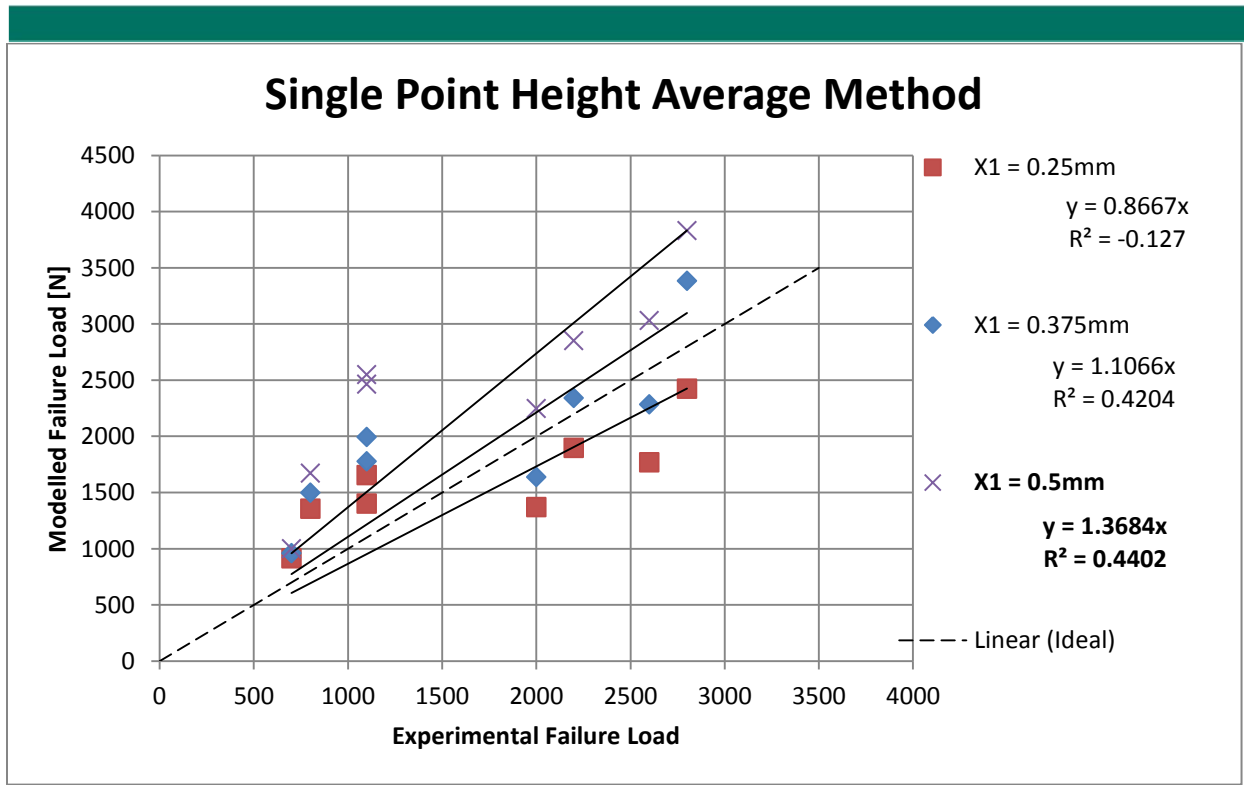


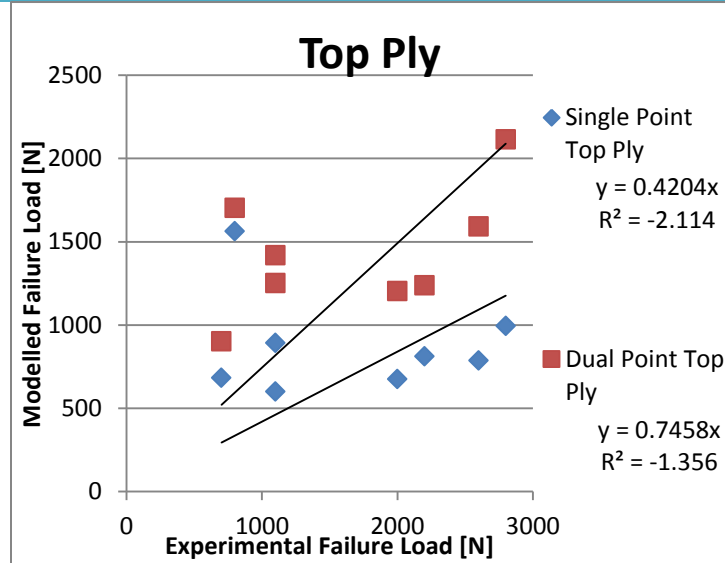
Figure 31: Comparison of Experimental Failure Load and Model Failure Load for the Single Point Height Average Method for Varying Measurement Distances X1

#### 6.2.4.5 Determination of Optimal Failure Criterion

Having determined the distance parameters for all of the trial methods, they can be compared to one another to determine the most suitable failure criterion. The trial methods are shown in Table 15, along with the distances which produce optimal correlation with the data. Two things are worth noting. First, the three trial methods which utilize the top ply show poor correlation with the experimental data, and hence are unusable. Second, the dual point maximum method produces the best correlation with the experimental data. Therefore, the dual point maximum will be applied as the failure criterion for the full scale connection model.

## Failure Calculation Results

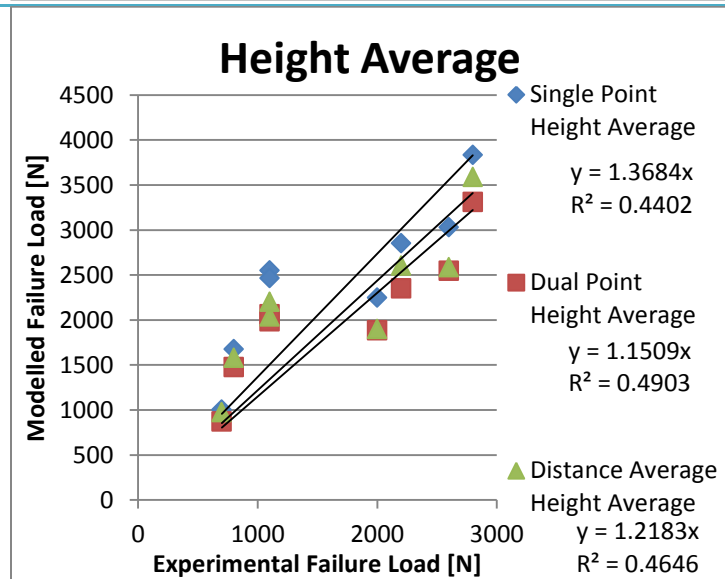
### Plots of Failure Loads for Given Cross-Section Location



### Explanation

When the three failure load calculation methods are applied to the top ply, the results to the left are obtained. Two methods produce results with poor correlation, and the third falls so far outside of the expected range that no value was even obtained. The distances which provide the best possible correlation are given below.

Method	X1 [mm]	X2 [mm]
Single Point	0.125	-
Dual Point	0.5	3.25



Averaging the Tsai-Wu values over the laminate height produces the plot to the left. The correlation with experimental data is decent, and the clustering of the three calculation methods adds some assurance of accuracy. The distances which produced the best correlation are given below.

Method	X1 [mm]	X2 [mm]
Single Point	0.5	-
Dual Point	0.5	1.5
Distance Average	0.375	0.5

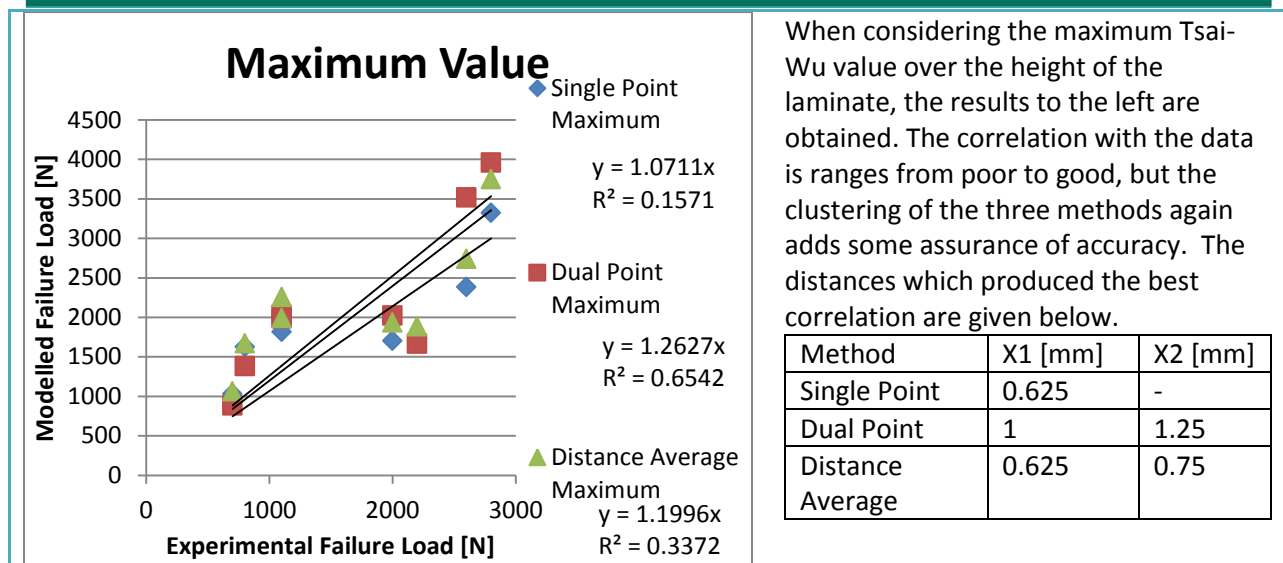


Table 15: Failure Loads for Relevant Failure Criteria

### 6.2.5 Verification of Hand Calculations

To verify the validity of the hand calculations, they have been compared to the results of the experiments and the ANSYS models of the small scale laminates. The results are shown in Figure 32. The hand calculations show good correlation with the experimental data, although a slight overestimation of the strength is present. The results are accurate enough to indicate that the hand calculations are a decent estimator for the strength of a bolted connection. When comparing the hand calculations to the model results, one can see outstanding correlation. For this relationship, one can see that the modelled strength is greater than the hand calculated strength, however, this is not cause for concern, since the comparison between the experimental failure load and the modelled failure load also shows that the model overestimates the strength. This will be compensated for after modelling the full-scale joint.

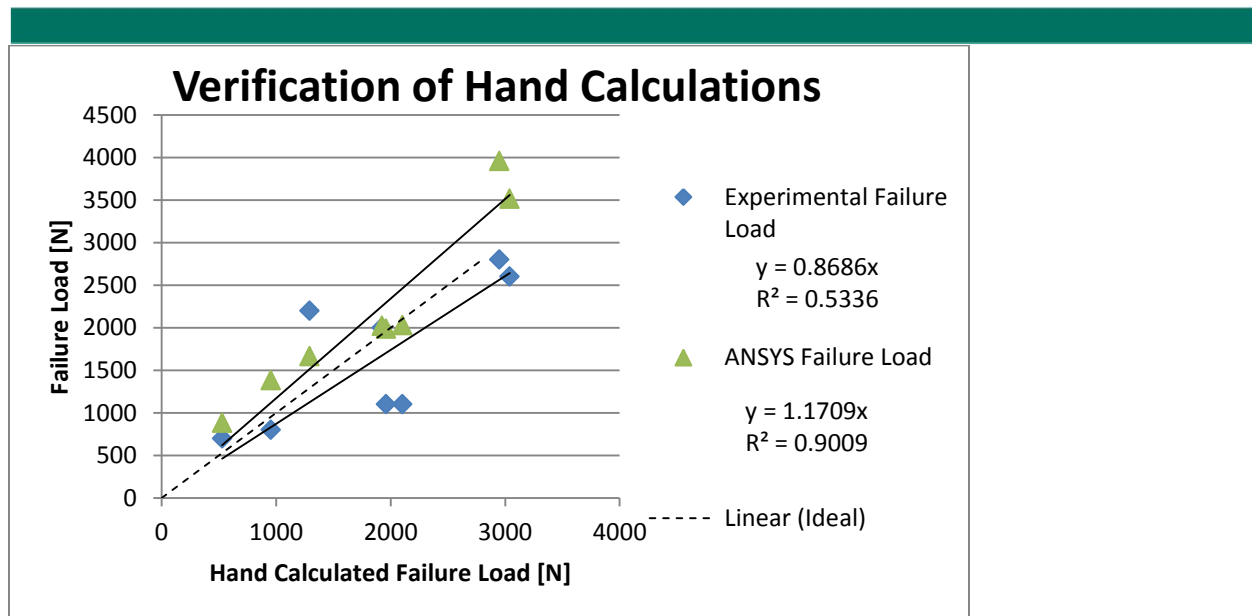


Figure 32: Verification of Hand Calculations Through Comparison to Experimental and Model Results

### 6.2.6 Conclusion of Calibration Study

In the contact region between the bolt and the laminate, huge peak stresses arise. The peak stresses are partially physical and partially numerical. Large peak stresses will show some redistribution in real situations so that they lose some correspondence with modelled values. Therefore, simply pointing to the maximum Tsai-Wu value which arises in the model will lead to an extreme underestimation of the connection strength.

To establish a better failure criterion, measurements have been done at certain distances from the contact interface and at several locations in the cross section. The optimal distances for measurements to take place were determined by comparing the resulting model failure load, to a known experimental failure load. The result is that a dual point measurement of the maximum Tsai-Wu value in a cross section showed the best correlation to the experimental data, and hence will be used as a failure criterion for the full scale model.

## 6.3 Full Scale Joint Model

The next step in designing the connection is to scale the model to the expected required size according to the hand calculations. This will give a better insight into the strength and stiffness of the Full Scale connection.

### 6.3.1 Materials Applied in Full Scale Model

The materials used in this analysis will be steel and FRP. The material properties utilized for the full scale model are listed below, and correspond to those list in 4.3.3 Determination of Lamella Properties. The values listed for FRP are based on lamella properties since in the analysis, the lamellas will be individually modeled. The lamellas will be individually modelled, since their properties and the

stress development over the height of the laminate will play a significant role in the behavior of the system. Typical steel properties will be applied, such as are given in Table 55.

Full Scale FRP Material Properties		
Property	Value	Units
Young's Modulus X	43100	MPa
Young's Modulus Y	12800	MPa
Young's Modulus Z	12800	MPa
Shear Modulus	4400	MPa
Poisson's Ratio XY	0.26	-
Longitudinal Tensile Strength	1036	MPa
Longitudinal Compressive Strength	846	MPa
Transverse Tensile Strength	48	MPa
Transverse Compressive Strength	69	MPa
Shear Strength	55	MPa

Table 16: FRP Material Properties for Full-scale Model

### 6.3.2 Supports and Loading of Full Scale Model

For the full-scale model, the supports and loads will be included through applied displacements. These are visible as blue and green triangles in Figure 33, where 6 locations have been numbered. The numbered values correspond to the displacements described in Table 17.

Displacements Assigned to Model			
Location	Ux [mm]	Uy [mm]	Uz [mm]
1	Fixed	Free	Free
2	Variable	Free	Free
3	Free	Free	Fixed
4	Free	Fixed	Free
5	Constant over Area	Free	Free
6	Constant over Area	Free	Free
7	Variable	Fixed	Fixed
8	Variable	Fixed	Fixed

Table 17: Assigned Displacements in Full Scale Model. Location Numbers Correspond to Figure 33.

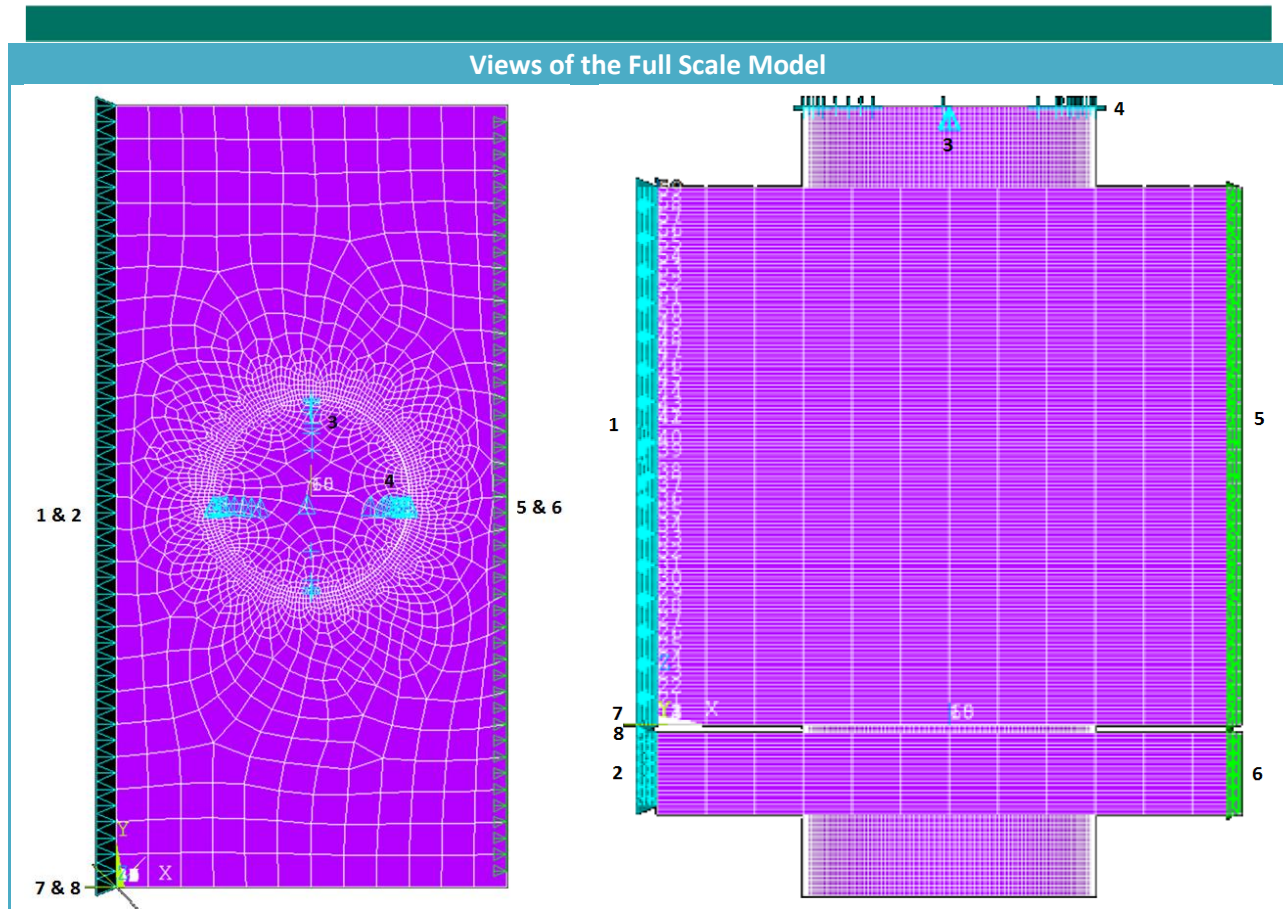


Figure 33: (Left): Top View of the Full Scale Model. (Right) Side View of the Full Scale Model.

### 6.3.3 Visualization of Full Scale Results

This section is devoted to presenting visualizations of the results of the model. This section treats displacements, stress and Tsai-Wu Values.

#### 6.3.3.1 Visualization of Full Scale Displacements

The displacements of the full scale model in x-direction are presented in Figure 34. The assigned displacements are verified by these results. Additionally, one can see that there is slippage between the laminate and the steel flange. To gauge the effect of slippage, the stiffness of the joint is analyzed in 6.3.7 Determination of Stiffness of Full Scale Joint.

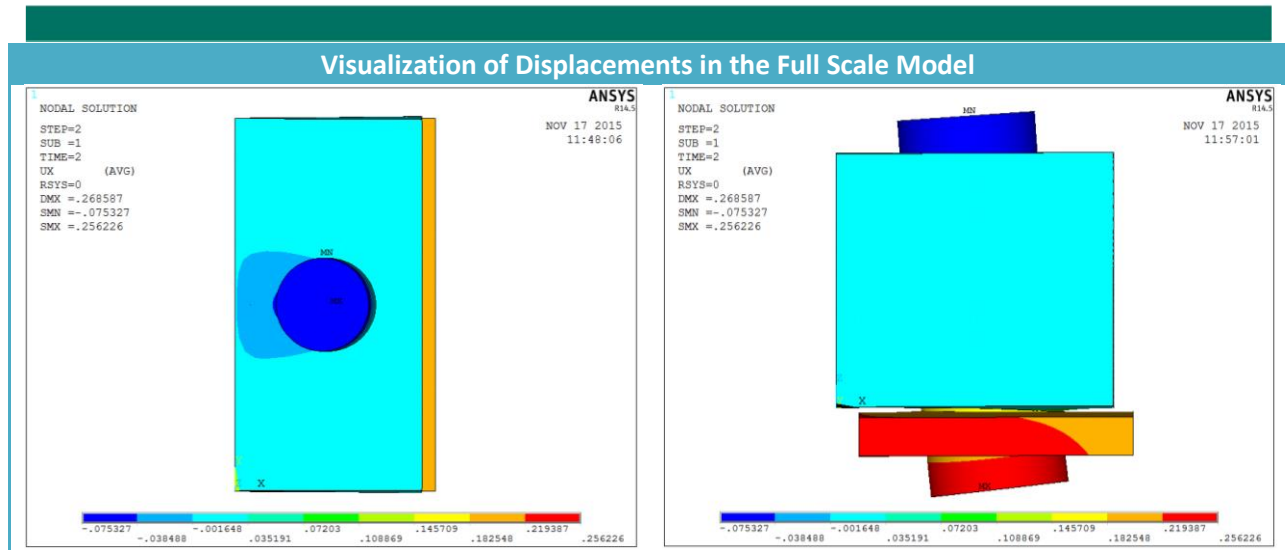
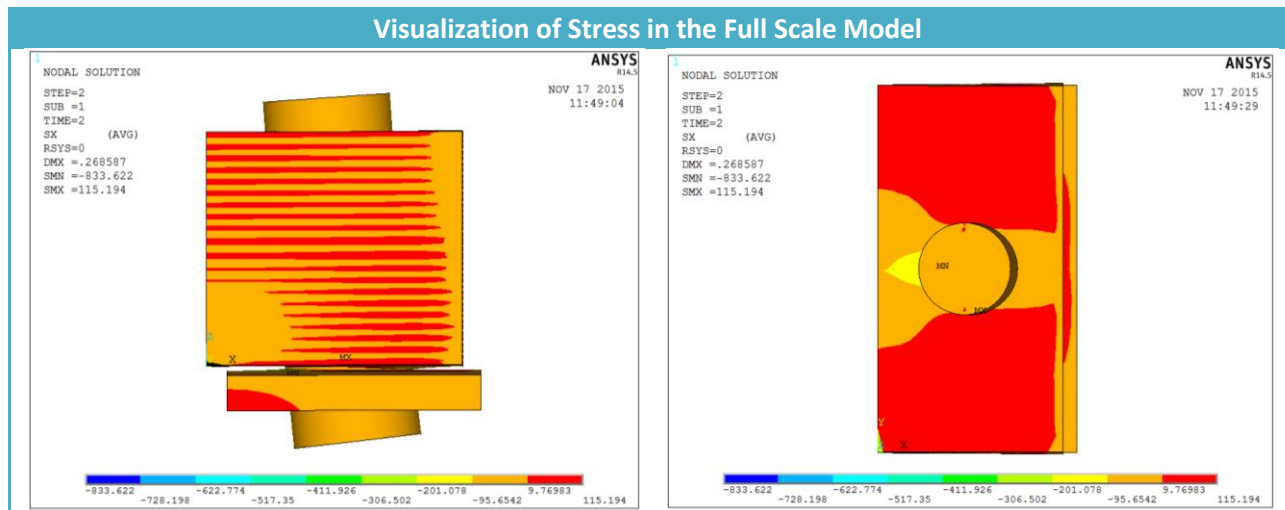


Figure 34: (Left):Top View of Displacements in x-Direction of the Full Scale Model. (Right): Side View of Displacements in x-Direction of the Full Scale Model.

### 6.3.3.2 Visualization of Full Scale Stress

The stress in x-direction is presented in Figure 35. As expected, differently oriented plies show different stress levels. The highest stresses are found at the contact interface of the bolt. Note that the contact region is on opposite sides of the hole when comparing the top of the laminate and the bottom of the laminate. This indicates that the internal moment plays a large role in the stress development.



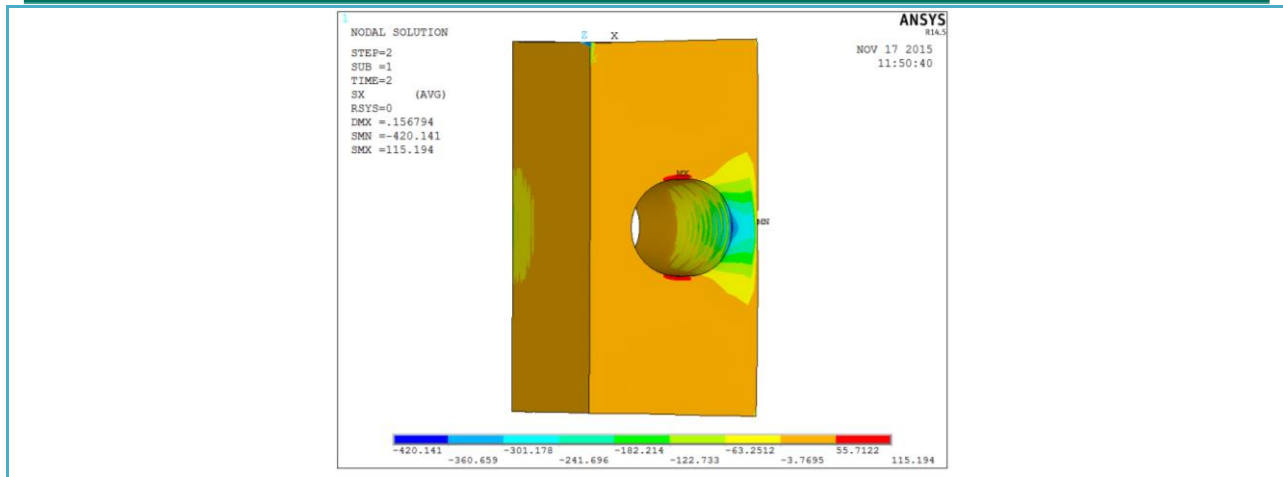


Figure 35: Visualizations of Stress in x-Direction in the Full Scale Model. (Top Left): Side View. (Top Right): Top-Down View. (Bottom Center): Bottom-Up View Where the Bolt and Steel Flange are Invisible to Allow a View Inside the Hole.

### 6.3.3.3 Visualization of Full Scale Tsai-Wu Value

The Tsai-Wu values of the full scale model are presented in Figure 36. The region of high peak stress is relatively small when compared to the small scale models. The effect of this on the failure load is assumed to be accounted for through scaling of the measurement distances. For more information see 6.3.5 Scaling Measurement and N.7 Scaling.

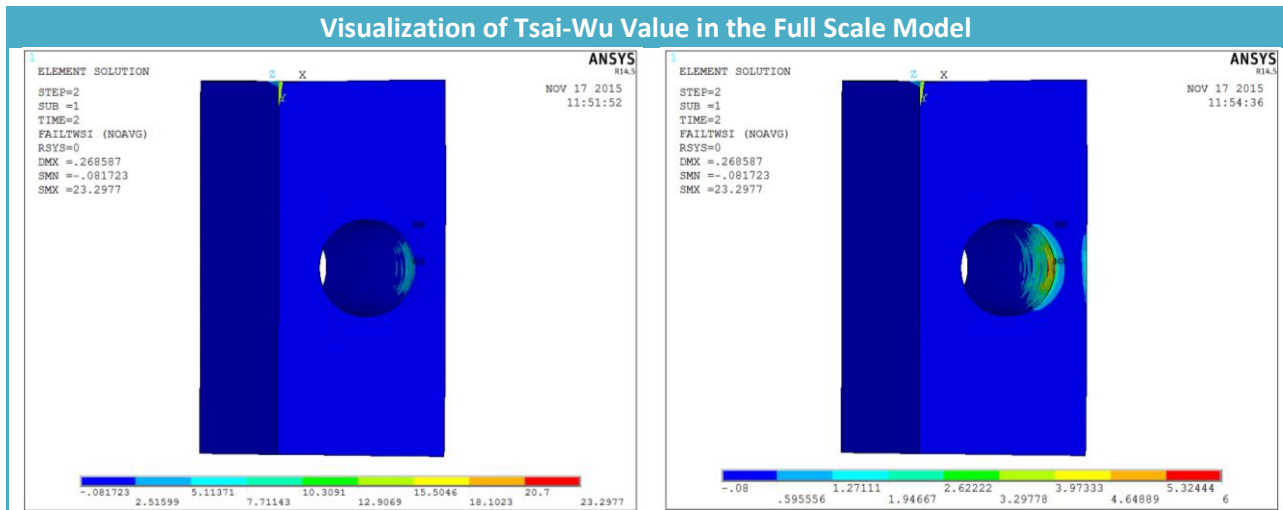


Figure 36: Tsai-Wu Values in Full Scale Model. Steel Flange and Bolt are Invisible to Allow a View Inside the Hole. (Left): Program Define Contours. (Right): Manually Defined Contours to Improve Visual.

### 6.3.4 Convergence Study of Full Scale Model

To determine when the model mesh size is sufficiently fine, a convergence study has been performed. At the contact interface, both physical and numerical peak stresses arise. This makes obtaining convergence close to the contact interface difficult. However, convergence at a large distance is obtained with very few elements. This is visible in Figure 37. The Tsai-Wu value at 3.5mm and 10 mm



from the contact interface show less than 10% difference in value when quadrupling the number of elements. The Tsai-Wu value at 1 and 1.25 mm continues to show instability for all element sizes which were calculable. Therefore, values obtained inside this region remain unconverged and can therefore show large deviations from reality.

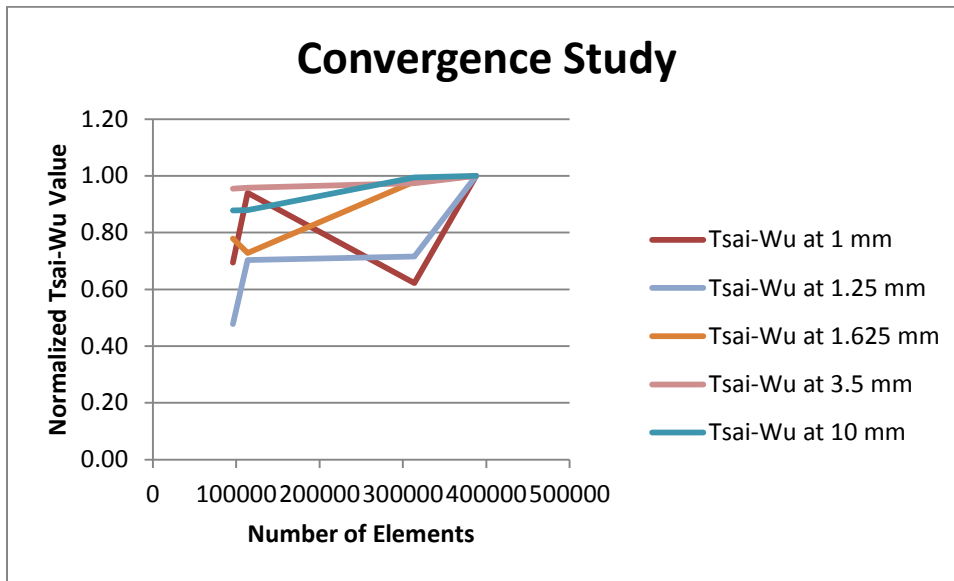


Figure 37: Convergence Study Determining the Tsai-Wu Value at Various Distances from the Contact Interface

### 6.3.5 Scaling Measurement Distances to Bolt Size

The distances at which to determine failure in the calibration model were determined based on thin laminates and small bolts. For the full-scale model, the bolt will be scaled from 5mm to 36mm. The distances from the contact interface which are relevant have been proven to scale linearly for bolt diameters between 6 and 10mm.<sup>42</sup> Linear scaling is unproven to 36 mm so that it may produce results which are much stronger than reality. However, to fully ignore this effect seems overly cautious. Therefore, some insight is required into the effect of scaling linearly on the strength of the connection.

In order to determine the effect of scaling, the failure strength has been calculated with the measurement distances scaled up to the level required for various bolt diameters. Scaling to larger bolt diameters leads to larger measurement distances and hence larger failure loads. This is shown in Figure 38. The manner in which the distances are scaled according to bolt diameter is described in more detail in N.7 Scaling.

<sup>42</sup> (Camanho & Lambert, 2006)

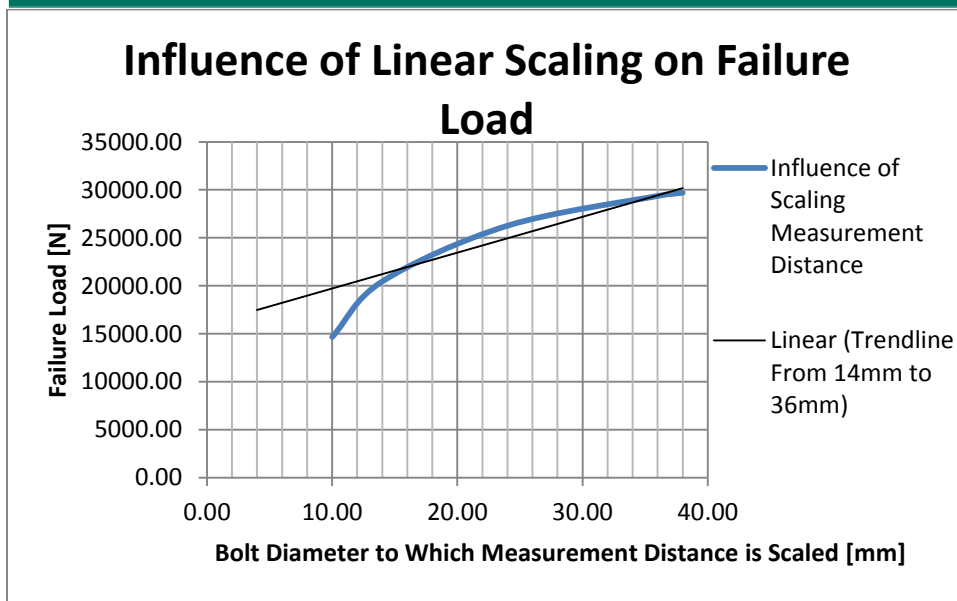


Figure 38: The Relationship Between Scaling the Measurement Distances for Failure Linearly with Bolt Diameter and the Resulting Failure Load

In Figure 38 one can see the relationship between the modeled failure load, and the diameter to which the measurement distances are scaled. This relationship can be approached reasonably well with a line between diameters ranging from 14 to 36 mm. However, below this diameter, the strength of the connection drops unreasonably fast. The 14 to 36 mm diameter range is considered realistic. An average strength shall be determined based on the scaling to 14mm bolts and 36mm bolts, balancing the conservative and expected values. The relevant distances are given in Table 18. Note that the distances are all larger than the convergence distance mentioned in 6.3.3 Visualization of Full Scale Results. This means that the values obtained at these locations are converged.

Scaled Distances for Model Failure				
Scaled to Bolt Size	14 mm		36 mm	
"X" Considered	$X_{1,14}$	$X_{2,14}$	$X_{1,36}$	$X_{2,36}$
Distance [mm]	3.14	3.92	8.37	10.46

Table 18: Scaled Distances for Model Failure

### 6.3.6 Determination of Strength of Full Scale Joint

Based on the distances given above the various methods produce failure loads according to Table 19. These strengths have been calculated using ULS safety factors. As mentioned in 6.3.5 Scaling Measurement, using the 14mm scaled values is too conservative, but applying the 36mm scaled values is unproven. Hence the average of the two has been taken as a design value. The green highlighted value represent the design failure load calculated in this manner.

The calculated failure load between the two dual point maximum failure loads show a large difference. *Proving validity of scaling to larger bolt sizes, such as M36 bolts, would represent a significant step in the design of bolted connection in FRP* due to the following reasons:

- An increased scaling distance corresponds to a higher failure load
- An increased scaling distance reduces computational demands
  - The measurement distances become larger so that a coarser mesh will suffice

Modelled Failure Load		
Scaled to Bolt Size	14 mm	36 mm
Dual Point Maximum [N]	20450	29363
Design Value [N]	24906	

Table 19: Failure Loads as Determined by All Calculation Methods, with Measurement Distances Scaled to 14mm bolts and 36mm bolts.

### 6.3.7 Determination of Stiffness of Full Scale Joint

In addition to the strength, the stiffness is also important, especially for developing composite action. To determine the stiffness, the connection will be approached as a linear spring, for which the spring coefficient is easily determined according to Equation 13. Note that for this calculation, again the average values for 14mm and 36mm scaled bolts has been taken, but the safety factors have been excluded.

$$k = \frac{F_{char}}{u_{char}} = \frac{44416}{0.184} = 241 \frac{kN}{mm}$$

Equation 13: Determination of the Spring Constant Representing the Connection Stiffness

With:

$F_{char}$ : Characteristic Failure Load

$u_{char}$ : Displacement under Characteristic Failure Load

To know the stiffness is one thing, but to know the influence which this has on the development of composite action is much more beneficial. To this end a study has been performed in Q.4.3 Influence of Connection Stiffness relating the influence of connection stiffness to the global displacement of the structure, in order to determine the degree of composite action. While this study was performed on smaller elements, the results indicated that a stiffness of 100kN/mm or greater will lead to nearly full composite action.

## 6.4 Redesign of Girder-Deck System

The model of the full scale connection has shown that the failure load of the full scale connection as currently designed is low compared to the previously performed hand calculations. The modelled failure load of 25kN falls well short of the expected 46kN capacity. This has significant

consequences for the global design as well. As currently designed, the connection is not feasible. The capacity of the bolts is too low to transfer the required shear force. To adapt the design by adding rows of bolts until the required capacity is obtained would lead to a connection with 8 rows of bolts, and a minimum width of 1152mm (when adhering to 4 times diameter spacing). Such a connection is rejected because it has several problems:

- Fabrication become impractical and expensive
- The beam would suffer significantly from shear lag, thereby reducing stiffness and strength
- The bolts would not work in tandem; some would be loaded significantly more than others

#### 6.4.1 Redesign with Reduced Deck Height

With the connection lacking in strength, the force which must be transferred across it should be reduced. This can be done by reducing the static moment of the deck with respect to the neutral axis of the girder-deck composite cross section, or by increasing the stiffness of the bridge cross section. A combination of these two methods will be applied. A new geometry is presented in Figure 39, Figure 40, and Figure 41.

This new design has a much smaller shear flow to transfer between the deck and girder, so that the strength of the bolted connection suffices. The smaller shear flow is realized by applying 3 methods.

1. Part of the deck is removed to reduce the static moment.
2. The height of the steel profile is increased which leads to a greater global stiffness.
3. The top flange of the steel girder is thickened to raise the neutral axis, thereby reducing the static moment of the deck.

Several drawbacks to this design are listed below:

- More steel is required compared to the previous design
  - Heavier Construction
  - More Expensive
- The top of the deck must be lowered at the connection
  - Bolts may not protrude beyond the upper layer of the deck
- The effect of composite action is lowered
  - Increased steel height gives steel greater role and FRP smaller role
- Design is built around connection
  - Poor material efficiency
  - Top flange of girder thickened solely to reduce shear flow.

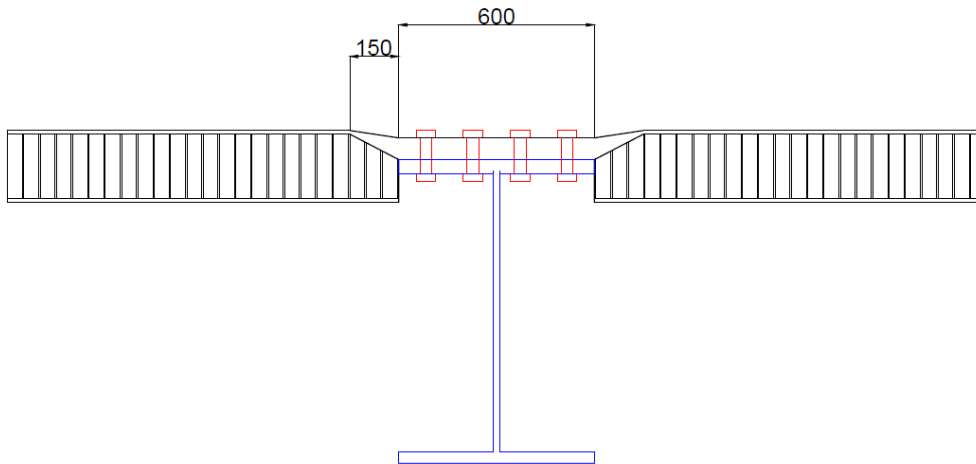


Figure 39: Front view of New Connection Design

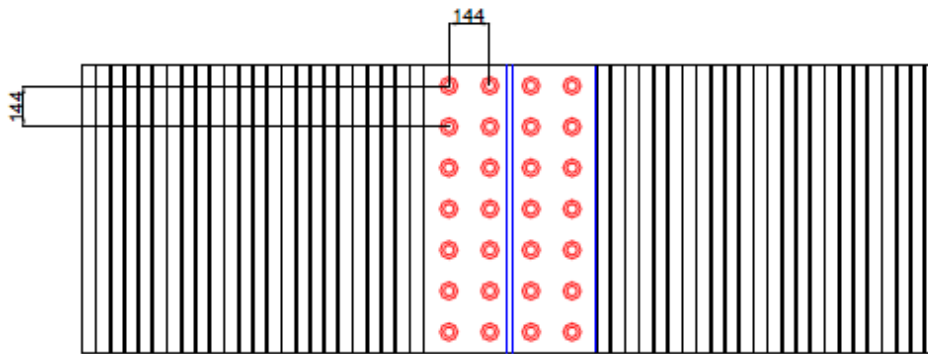


Figure 40: Top View of New Connection Design

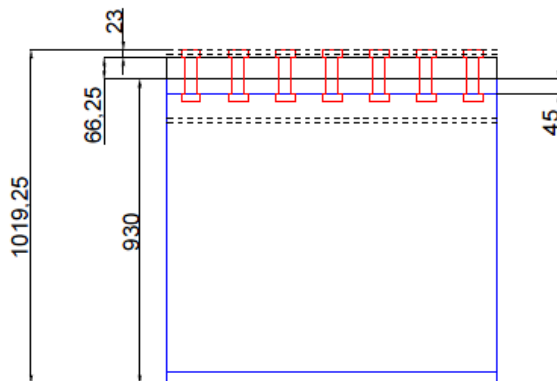


Figure 41: Side View of New Connection Design

### 6.4.2 Redesign with No Composite Action

With all of the drawbacks listed for the previous design, the question arises: does the composite action in a cross section, justify the expenses resulting from this difficult connection. With this in mind, a redesigned version of the deck was made, in which no connection was realized between the deck and girders. Constructing the bridge without such a connection should reduce the manufacturing costs of the bridge. The new design is shown in Figure 42, Figure 43, and Figure 44. A critical location in this design is the FRP layer draped over the main girder. This will be analyzed in more detail in 8 Evaluation of Main Girder to Deck Detail

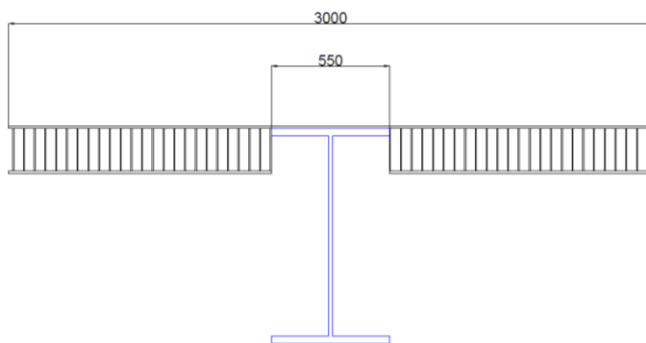


Figure 42: Front View of Design Without Composite Action

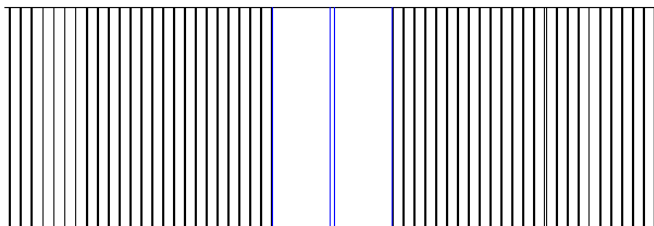


Figure 43: Top View of Design Without Composite Action

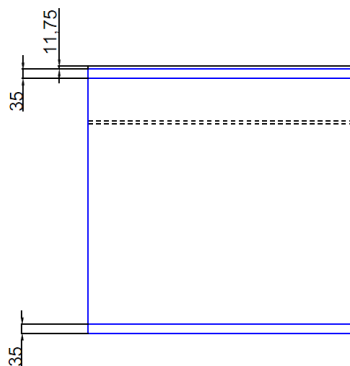


Figure 44: Side View of Design Without Composite Action

In this variant, composite action is neglected, and the stiffness and strength is almost entirely due to the steel girder. The effects of not including a connection in the FRP are as follows:

- The FRP has practically no effect on global strength and stiffness
  - The function of the FRP becomes limited to transferring load to the crossbeams
- The FRP layer can be executed much thinner at the connection
- The height of the steel profile can be increased
- The deck will remain flush
  - Bolts will not protrude above top FRP layer
- Top flange of girder can be executed thinner
  - Shear flow not critical

### 6.4.3 Comparison between Redesign Variants

To determine whether or not the benefits of composite action between the deck and girder outweigh the drawbacks, a comparison between the two must be made. The comparison is done in a manner similar to 5 Laminate Orientation, where the section modulus and the moment of inertia must stay larger than in the original design. The results are shown in Table 20. These results appear counter intuitive, since one would expect a design with composite action to be more efficient. However, by not including composite action all efforts to reduce the shear flow through the interface can be discarded. This means that weight can be saved on the top flange of the steel girder, as well as on the flange of the FRP deck used in the connection. One can see that for the composite action design, that the section modulus and especially the stiffness are not critical, indicating inefficient use of material. For the loose connection, the section modulus becomes critical.

Composite Action vs Loose Connection Design Comparison		
	Composite Action	Loose Connection
<b>Stiffness EI [kNmm<sup>2</sup>]</b>	2.70E+12	2.17E+12
<b>Stiffness Due to Composite Action [%]</b>	22.91%	0
<b>Stiffness Change [%]</b>	45.63%	16.99%
<b>Section Modulus [kNmm]</b>	4.59E+09	4.34E+09
<b>Section Modulus Change [%]</b>	6.53%	1.12%
<b>Mass [kg]</b>	10513	8687
<b>Mass Change [%]</b>	4.21%	20.85%

Table 20: Comparison Between Design of the Main Girders Including and Excluding Composite Action. Mass and Mass Changed Include Effective Width of Deck. Changes are Measured Against the Current Design of the Deck.

## 6.5 Connection Conclusion

The strength of bolted connections in FRP materials is lower according to finite element models than according to hand calculation. The modeled failure load falls below a practicable limit. The result of which is that the design of cross section which shows composite action is centered around the design of

the connection, as opposed to the global behavior. The theoretical mass savings for several variants were determined, and are summarized in Table 21. The mass includes the effective width of the deck to account for the changes in deck geometry.

Summary of Mass of Main Girders for Considered Variants			
Variant	Description	Mass [kg]	Mass Change [%]
<b>1. Current Design</b>	The geometry and FRP properties as applied in the current design of the bridge.	10975	0
<b>2. Lengthwise Laminated</b>	The variant which resulted from 5 Laminate Orientation. This variant uses the geometry of the current design with material properties corresponding to a lengthwise laminate orientation, but does not account for joint strength. This variant only becomes feasible if the joint strength is shown to be significantly stronger.	8119	26%
<b>3. Reduced Deck Height</b>	The variant from 6.4.1 Redesign with Reduced Deck Height, where the steel profile is raised as much as possible. The connection strength is critical.	10513	4.2%
<b>4. Excluding Connection Strength<sup>43</sup></b>	The same geometry as above, but connection strength has been excluded as a limiting parameter and the connection width has been reduced. This variant only becomes feasible if the joint strength is shown to be significantly stronger.	8011	27%
<b>5. No Composite Action</b>	The variant from 6.4.2 Redesign with No Composite Action. The steel profile is raised as much as possible, reducing the height of the deck above the girder	8362	21%

Table 21: A Description of Considered Variants, their Corresponding Mass, and their Mass Savings compared to the current design.

In Table 21 the second and fourth variants are not feasible, unless the strength of a connection is proven much larger than determined in this thesis. These two solutions offer the largest mass savings on the design of the bridge, so that additional studies towards the strength of connections in fiber reinforced polymers could prove to be worthwhile investments. However, until such studies prove higher joint strengths, these variants must be excluded from consideration.

The reduced deck height with and without composite action both show that the mass of the main girder system can be reduced by maximizing the height of the steel girder. Effectively, this means

<sup>43</sup> This variant follows from O.6 Influence of Connection Strength on Mass, where the connection strength is considered variable to see the influence it has on potential mass savings.



that for structures with constrained construction heights, maximizing the steel height should be prioritized over having a continuous deck. For variant 3, the added measures required to enable composite action add more weight than the actual composite action can compensate for. Hence, maximizing the height of the steel profiles while excluding composite action results in the best solution.

Considering both the mass savings and the complexity of the variants realizing composite action between an FRP deck and steel girders is not a competitive solution. For the considered case study, excluding composite action in favor of a loose connection where the girder height is maximized provides a significantly lighter and simpler structure.

## 6.6 Caveats to the Connection Design

The connection which has been designed and modelled in this chapter shows failure below practicable strength limits. However, there is room for improvement of the strength of such connections. Influence studies, found in Appendix O: Joint Influence Studies, have shown that there is quite some variability in the joint strength. The topics considered there, along with several other options which may lead to different results are listed below.

- Tight fit holes were assumed for this connection. However, clearance will typically be required. This would lead to larger stress concentration factors. Injection bolts may solve this problem, see O.1 Bolt Clearance.
- The bolt head was modelled as free to rotate. Modelling it as rotationally fixed, or with rotational resistance may lead to a stronger connection. See O.2 Bolt Head.
- The amount of splitting tension in a bolt hole is uncertain. More tension in the bolt hole would lead to a lower resistance. See O.3 Tension Effect.
- A consistent glass fiber polyester mixture has been assumed in this case study. Local reinforcement with other fiber types may lead to improved performance. See O.4 Alternative Materials For Connection.
- In concrete, doweled connections can exceed the plastic capacity of concrete at the interface. If such a phenomenon is also present in FRP, this could lead to vast increases in design strength. See O.5 Comparison to Connections in Concrete for more detail.
- The first ply failure criterion has been used throughout this model. Last ply failure would lead to higher design resistance.
- For bridges with lower design loads, the shear flow may not be governing in a design with composite action.
- For this case study, the maximum construction height was a stringent criteria. Perhaps if the construction height is free to choose (or at least larger), the connections may not be governing in the design.
- The Tsai-Wu Failure criterion has been applied in this study. However, there are other failure criteria which may produce more accurate results.

- The measurement distances for the failure models have been scaled to 14mm bolt diameters and 36mm bolts diameters and then averaged. If linear scaling remains valid until 36mm bolts, the failure load will increase.
- Full scale experiments can be performed to determine whether the model is accurate and if not, what the actual resistance would be.
- The calculations have been performed elastically. Plastic calculations may be more accurate and give higher failure loads. Validity of plastic calculations would need to be proven through experiments.
- The calibration models were based on a symmetric experiment configuration. However, the large scale model was an asymmetric design. The influence of this eccentricity has not been analyzed further in this thesis.

## 7 Analysis of FRP Decks

The calculations done in this thesis have been based mainly on the Delft Infra Composites (DIC) deck as utilized in the current design of the Julianabrug. This chapter will analyze a few deck shapes so that the optimal deck can be utilized. While there are many different shapes of decks available, only a few will be discussed here. First the considered decks will be presented. Following this, they will be modelled and analyzed to determine the optimal deck. The criteria for the optimal deck are stiffness in longitudinal direction and mass.

### 7.1 Basic Information of Deck Types

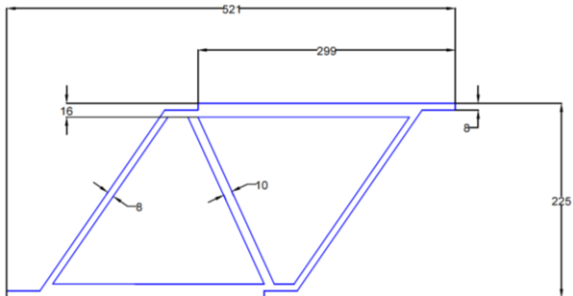
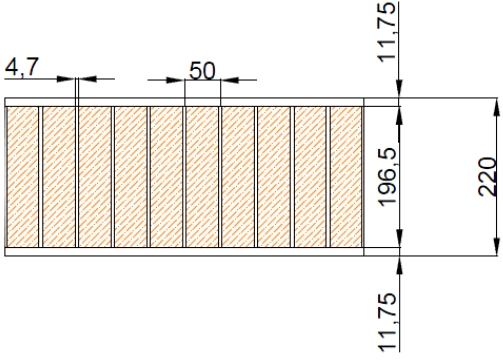
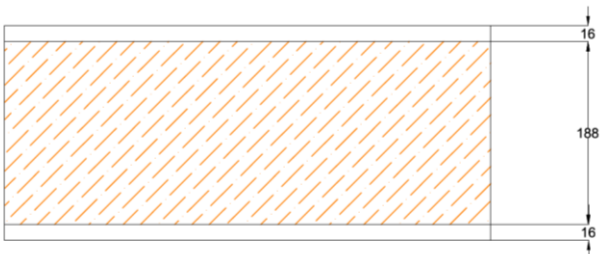
Basic Information of Deck Types	
Visualization	Properties
	<p>1. Asset Deck:</p> <ul style="list-style-type: none"> <li>Produced by Fiberline, Denmark</li> <li>Triangular shape benefits transverse load bearing capability</li> <li>No foam filling</li> <li>Modular Production and Installation</li> <li>Triangular shape makes connections into the deck difficult</li> </ul>
	<p>2. DIC Deck:</p> <ul style="list-style-type: none"> <li>Produced by Delft Infra Composites, Breukelen</li> <li>Two face plates</li> <li>Vertical webbing</li> <li>Foam between webs to enhance stability, but is not intended to contribute to strength</li> <li>Vertical webs allow for easier access to interior of deck prior to foam application</li> <li>Low Transverse Strength</li> </ul>
	<p>3. Sandwich Deck:</p> <ul style="list-style-type: none"> <li>Production by many companies</li> <li>Foam filling with no webs leads to low weight</li> <li>Easy modeling with plate elements</li> <li>Cheap Production</li> <li>Typically applied for low load and low span situations</li> </ul>

Table 22: Basic Information of Deck Types Considered in This Analysis<sup>44</sup>

<sup>44</sup> ASSET Deck Information: (Scholze, 2015), (Knippers & Gabler, New Design Concepts for Advanced Composite Bridges - The Friedberg Bridge in Germany, 2006)

## 7.2 Setup of FRP Deck Models

The three deck types are modelled in ANSYS. The geometries presented in Table 22 are used. The laminate has been modelled using layered shell elements, which allow for the input of each lamella separately, including varying material properties and orientation angles. For the sandwich deck, i.e. variant 3, the foam core has been included as a layer in the element. This means that the entire deck is a single element thick, greatly simplifying the model geometry. The lamella properties used follow from Table 7, in 4.3.3 Determination of Lamella Properties. The assumed properties of the foam filling is presented in Table 23. Note that the foam is only applied in the sandwich deck. It has been neglected in the DIC deck, since the foam there is used to enhance stability, and is not intended to play a role in global load bearing.

Assumed Properties of Structural Foam		
Property	Value	Units
Young's Modulus	143	MPa
Shear Modulus	52	MPa
Poisson's Ratio	0.375	[-]
Density	115	kg/m <sup>3</sup>

Table 23: Properties of Structural Foam Utilized for the Modelling of the Sandwich Deck<sup>45</sup>

The models have a span of 3070mm, in accordance with the distance between crossbeams in the bridge. The decks are simply supported at the ends, and a unity load of 100kN/m<sup>2</sup> has been applied to the top of the deck.

## 7.3 Displacements of Decks Resulting From Models

The displacement fields of the ASSET, DIC, and Sandwich decks are presented in Figure 45, along with a graph containing the displacements along the lengths of the spans. Here one can see that the sandwich deck more than doubles the displacements of the other decks. The foam core does not have enough shear stiffness to properly transfer the stress between the two flanges. The other two decks show similar stiffness to one another in lengthwise direction. The ASSET deck shows variability in displacement in y-direction. This is due to the fact that the deck is asymmetric. This effect will dampen out as the width of the deck grows, but will remain present near the edges of the deck. Additionally, since the segments of the asset deck are larger, one can also see a much larger local displacements.

DIC Deck Information: (Hattink, 2014)

<sup>45</sup> (Gurit, 2015)

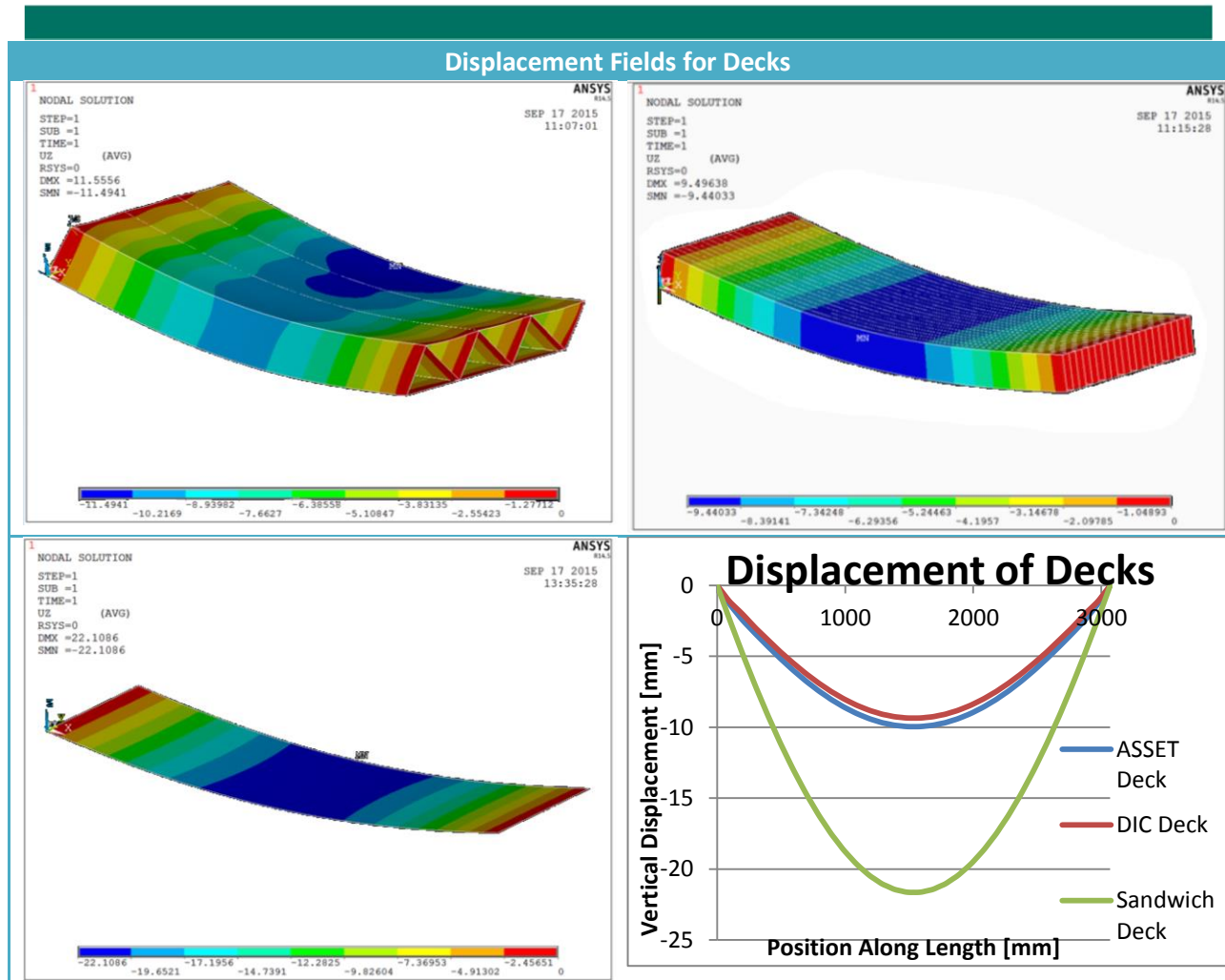


Figure 45: (Left to Right, Then Top to Bottom): (1) Displacement Field of ASSET Deck, (2) Displacement Field of DIC Deck, (3) Displacement Field of Foam Core Sandwich Deck, (4) Individual Displacement Lines over the Length of the Spans

The displacements at mid-span have been determined, and the masses of the decks have been calculated in terms of weight per unit area covered. The results are given in Table 24. Note that the foam core is not only lighter than the other two, but also severely less stiff. The differences between the ASSET and the DIC decks are small. The DIC deck is slightly heavier but also slightly stiffer.

Deck Masses			
Deck	Mass [kg/m <sup>2</sup> ]	Displacement [mm]	Span-to-Displacement Ratio [-]
ASSET	96	-10.0	307
DIC	99	-9.4	327
Foam Core	82	-21.6	142

Table 24: Masses and Displacements for the 3 Models Described Above<sup>46</sup>

## 7.4 Conclusion Regarding FRP Deck Study

Of the three deck types considered here the DIC deck performs best. The foam core deck shows significantly more displacement under the same loading situation, thereby eliminating it from contention. The other two decks show similar mass and stiffness properties, but the design of the webs leads to significant differences.

The ASSET deck is expected to behave better under transverse loading, due to the diagonal placement of the webs. In the design of the Julianabrug the deck is design to carry load only in the longitudinal direction so that the benefit of a higher transverse stiffness is limited to an increased activated width. However, the diagonal webs lead to a design with larger spacing between each segment of the deck, which in turn leads to larger local displacements. Additionally, the modules of the ASSET deck are asymmetric which leads to large displacements along the boundaries of the deck. For designs where part of the deck is removed to heighten the steel profile, this will lead to significant displacements in the middle of the bridge.

The DIC deck, has vertical webs spaced closely together. This leads to local displacements between the webs which are much smaller. Additionally, since the segments are all symmetric the load is more evenly spread amongst the segments. Therefore, the large effect near the boundary of the deck seen for the ASSET deck is not present in the DIC deck. Hence, on both small and medium scale, the DIC deck shows less displacement than the ASSET Deck. Based on these criteria, the DIC deck is considered the best deck for the Julianabrug.

<sup>46</sup> Note: DIC specifies that their deck weighs 100kg/m<sup>2</sup>. For the remainder of this thesis the specified value of 100kg/m<sup>2</sup> will be used.

## 8 Evaluation of Main Girder to Deck Detail

A critical point in the bridge design is the region where the deck covers the main girders. This region is shown in Figure 46 inside the red circle. The intended primary load carrying direction for the deck is towards the crossbeams. However, if a load is placed near this interface, most of the load will actually be transferred directly to the main girders. Hence this detail must be able to withstand the associated forces. This detail will be further analyzed in this section.

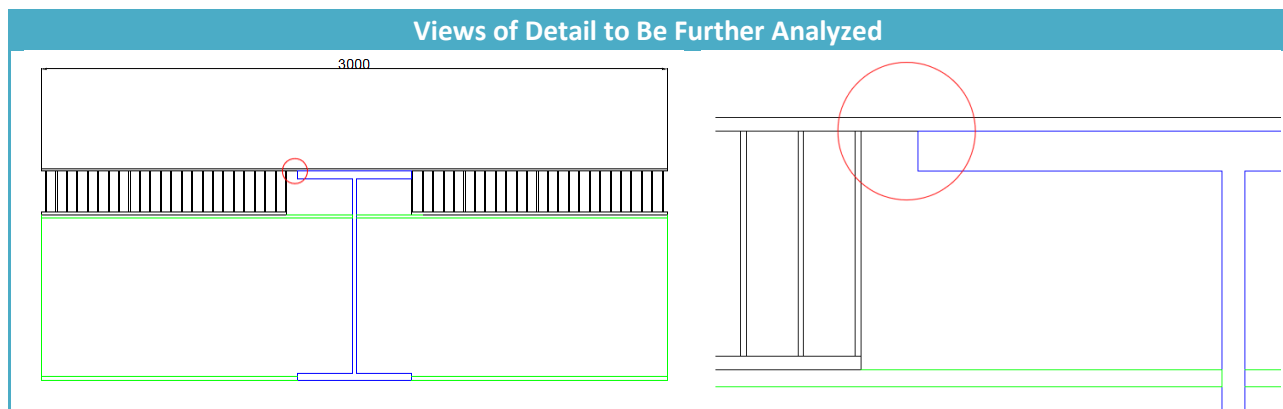


Figure 46: (Left) View of Deck Laid Over Girder, (Right) Close-up View of Detail to be Considered. Red Circle Marks Detail in Both

### 8.1 Hand Calculations of Girder to Deck Detail

The detail will be analyzed for both ultimate limit state and the fatigue limit state. The loads which make up this situation are considered in Table 25. The number of cycles are based on norms, with all traffic in one direction considered.<sup>47</sup>

Loads for Detail Calculations				
	Axle Load [kN]	Axle Type	$S_{max,i}$ [kN]	Cycles
<b>ULS</b>	300	TS		1
<b>FLS</b>	70	A	80.5	14400000
	80	C	92	2880000
	90	B	103.5	4320000
	90	C	103.5	10080000
	120	B	138	1440000
	130	B	149.5	8640000
	140	B	161	2160000
	150	B	172.5	2880000

Table 25: Loads Considered for the Calculations of the Detail.  $S_{max,i}$  is the Axle Load Multiplied by a Dynamic Amplification Factor of 1.15.

<sup>47</sup> (NEN-EN 1991-2: National Annex Steel Bridges, 2011)

The calculations are performed in such a manner as to determine the required FRP laminate thickness for the detail. In order to do this, the following steps have been applied:

1. Obtain an S-N curve for GFRP from literature
2. Determine the cycles until failure per load as a function of the ultimate resistance
3. Utilize Miner's rule to sum the fatigue damage
4. Determine ultimate resistance required to satisfy fatigue loading.
  - a. Compare ULS and FLS resistances
5. Calculate the height at which the laminate obtains this resistance
  - a. An iterative procedure is applied because the thickness of the laminate relates to the portion of the load carried through mechanism one.

### 8.1.1 S-N Curve for FRP

In order to calculate the fatigue resistance of the detail, an S-N curve should be used. For FRP, the curves are typically set up based on force rather than stress. Essentially, the ratio between the applied fatigue load and the ultimate resistance are related to the number of cycles until failure. Such a relationship has been found in literature and is presented graphically in Figure 47 and numerically in Equation 14. There are some caveats to the use of this relationship which are listed below.

- This equation is valid for continuous fiber material only, since short fiber material has much poorer fatigue properties.
- The equation is based on tensile fatigue experiments. They have been applied here for a bending dominant mechanism.
  - A more accurate S-N curve could be obtained by performing fatigue experiments which load the specimens in bending.
- The data presented for E-glass does not show a difference between [0/90] and [ $\pm$ 45] oriented laminates. For carbon fibers, this relationship is presented, and [0/90] oriented laminates perform significantly better under fatigue loading. Note that in the considered laminate in the considered direction, the 90 and 0 degrees are the primary and secondary orientations respectively.
- The S-N curve in Figure 47 is a combination of multiple FRP compositions. A more relevant S-N curve could be obtained by performing fatigue experiments of the specific FRP composition which will be used for the detail.



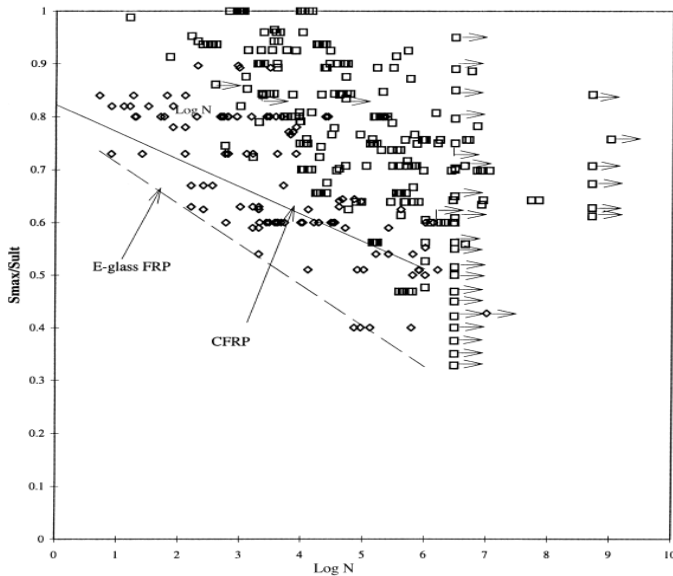


Figure 47: Relationship Between Fraction of Ultimate Load and Number of Cycles until Failure for E-glass and Carbon Fiber Materials. Arrows pointing right indicate that relevant specimen was still intact when experiment was ended.<sup>48</sup>

$$\frac{S_{max}}{S_{ult}} = 0.7902 - 0.0775 \log N_i$$

Equation 14: Equation for Maximum Fatigue Load of Glass Fiber Reinforced Polymers with Continuous Fibers as Obtained from Literature<sup>49</sup>

With:

$S_{max}$ : Maximum Force Applied During Load Cycle

$S_{ult}$ : Ultimate Resistance

$N_i$ : Cycles Until Failure For Considered Loading

Comparing the S-N curve obtained here to guidelines gives a few points worth noting:<sup>50</sup>

- Guidelines specify that logarithmic equations such as Equation 14, can be used to model alternating stress symmetric about a mean stress of zero. The literature from which this equation is obtained is based on asymmetric experiments.
- Guidelines specify a dual logarithmic formula when the S-N curve is obtained from experimental results.
  - This does not correspond to the data found in literature. For the double logarithmic formula, the point at which the maximum force applied equals the

<sup>48</sup> (Demers, 1997)

<sup>49</sup> (Demers, 1997)

<sup>50</sup> (Civieltechnisch Centrum Uitvoering Research en Regelgeving-onderzoekcommissie C 124, 2003-6)

ultimate resistance would need to correspond to 1 load cycle. However, this is not the case for either the GFRP or the CFRP data.

- Guidelines specify that when the mean stress is not zero, this can be corrected for using a Goodman diagram. However, since the experiments upon which Equation 14 is based were asymmetric, which more closely resembles the actual situation, this step was excluded.

### 8.1.2 Cycles until Failure

Equation 14 can be rewritten to determine the cycles until failure as a function of the force.  $S_{max}$  represents the fatigue axle loads, i.e. 8 known values listed in Table 25. Hence the number of cycles until failure is only dependent on the ultimate resistance  $S_{ult}$ . The cycles until failure are given in Equation 15.

$$N_i = 10^{\left(\frac{0.7902}{0.0775} - \frac{S_{max,i}}{0.0775 \cdot S_{ult}}\right)}$$

**Equation 15: Cycles Until Failure of Glass Fiber Reinforced Polymer Material, Dependent on a Known Applied Load and the to be Determined Ultimate Resistance**

### 8.1.3 Miner's Rule

Since there are multiple loads applied, the cumulative damage should be considered. This is calculated according to the Palmgren-Miner rule as given in Equation 16.  $N_i$  is calculated according to Equation 15, and  $n_i$  corresponds to the number of cycles listed in Table 25. The damage "D," should not exceed 1.

$$D = \sum_{i=1}^k \frac{n_i}{N_i}$$

**Equation 16: The Palmgren-Miner Rule for Cumulative Damage, with k the Number of Loading Levels Considered**

With:

$n_i$ : Applied Cycles for Loading Condition "i"

$N_i$ : Cycles Until Failure for Loading Condition "i"

### 8.1.4 Determination of Governing Failure Criterion

When  $S_{max,i}$  and  $n_i$  are substituted into Equation 17, the only remaining variable is  $S_{ult}$ . Solving the equation results in a value of  $S_{ult} = 685 \text{ kN}$ . Since this is bigger than the ultimate limit state load<sup>51</sup>, the fatigue limit state is the governing failure criterion.

$$D = \sum_{i=1}^k \frac{n_i}{N_i}$$

<sup>51</sup> (NEN-EN 1991-2 (en): Traffic Loads on Bridges, 2003)

$$1 = \sum_{i=1}^k \frac{n_i}{10^{\left(\frac{0.7902}{0.0775} \frac{S_{max,i}}{0.0775 * S_{ult}}\right)}}$$

Equation 17: Determination of the Ultimate Resistance Required to Resist Fatigue Damage. The terms  $S_{max,i}$  and  $n_i$  are known values.

### 8.1.5 Schematization of Detail For Determination of Stresses

To analyze the detail it has been schematized according to Figure 48. Load  $F$  represents a wheel load, which has been concentrated to simplify the calculations. Below the wheel load, a vertical spring has been applied with a stiffness corresponding to the stiffness of the deck-to-crossbeam load carrying mechanism. The point where the laminate detail overlays the girder is modelled as a fixed support.

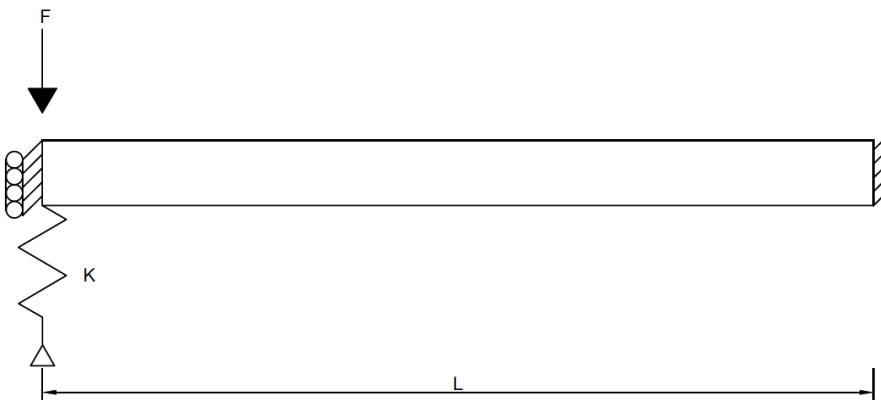


Figure 48: Schematization of Loading Scenario For Detail

The schematization according to Figure 48 makes several conservative assumptions. These are listed below:

- There are two relevant load carrying mechanisms. The first is through the considered detail to the main girder. The second is through the deck to the crossbeams, which is represented in the model as a spring.
- As  $L$  becomes larger, less load will be transferred through mechanism one. However, a larger moment will arise per unit load transferred. Therefore, a maximum value is expected.
- There is some load spreading in length direction. The assumed width for mechanism one is 600mm. This is 1.5 times the width of the ULS tire load.
- There is some load spreading in the width direction. The assumed width for mechanism two is 600mm.
- For fatigue loading, every wheel passes over the same region of the deck, this being the location where the maximum moment arises.
- The load  $F$  is equal to a single concentrated wheel load.

### 8.1.6 Determination of Laminate Height Required

Fatigue calculations have shown that the fatigue limit state is governing. The ultimate limit required to resist the fatigue damage is applied to the schematization in Figure 48. This results in a moment and shear force in the critical cross section, which can be tested against the Tsai-Wu criterion. The thickness required to resist the shear and moment without exceeding the Tsai-Wu criterion is then calculated. This process is repeated several times since a thicker laminate will draw more load to itself, leading to larger shear and bending stresses. To illustrate this effect the bending moment, as a function of length at which the load is applied, is presented in Figure 49 for several laminate thicknesses.

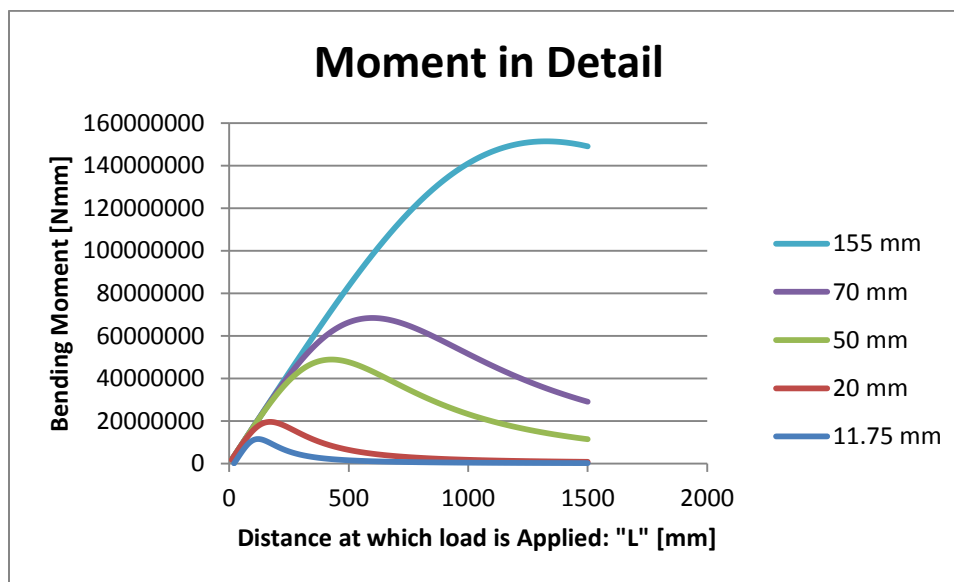


Figure 49: The Moment in the Critical Cross Section, as a Function of Location at which the Load “ $S_{ult}$ ” is Applied, for Several Differing Laminate Thicknesses.

The laminate has sufficient resistance to the applied load when it reaches a thickness of 155mm. This is much larger than originally anticipated and actually falls outside the range of producible thicknesses. Beyond issues arising during the making of the laminate, such a thickness will also invalidate the schematization. Therefore, to obtain more accurate results, the detail will be modelled in ANSYS.

## 8.2 Finite Element Model of Girder to Deck Detail

The hand calculations of the girder to deck detail indicate dimensions of unfeasible proportions are necessary. Several assumptions were made to simplify the calculation. Several points which will influence the results are listed below.

- The girder flange will bend under the load, so that the assumption of a fixed end is unreasonable. The boundary of the detail will show both displacement and rotation, thereby reducing the load carried directly to the girder.

- The load was schematized as a point load in the hand calculation. However, the load has a significant width for the considered dimensions.
- For the fatigue calculation, there are three different wheel geometries which should be accounted for.
- In the hand calculations, for the load carrying mechanism towards the girder (mechanism 1) the laminate is considered constant thickness. However, in reality the “laminade” will acquire the shape of the deck.
- The main girder will displace under the applied load.
- The crossbeams will displace under the applied load.
- The widths of both load carrying mechanisms were estimated. These will likely be different in a more detailed calculation.
- Mechanism two was estimated as a simply supported beam, while in reality it more closely resembles a continuous beam

### 8.2.1 Geometry of Model for Main Girder to Deck Detail Calculation

The model used for the calculation of the main girder to deck detail has been set up to match the geometry according to Figure 50. The behavior of individual beams, the deck, and the interaction between these has been verified in Appendix Q: Model Validation.

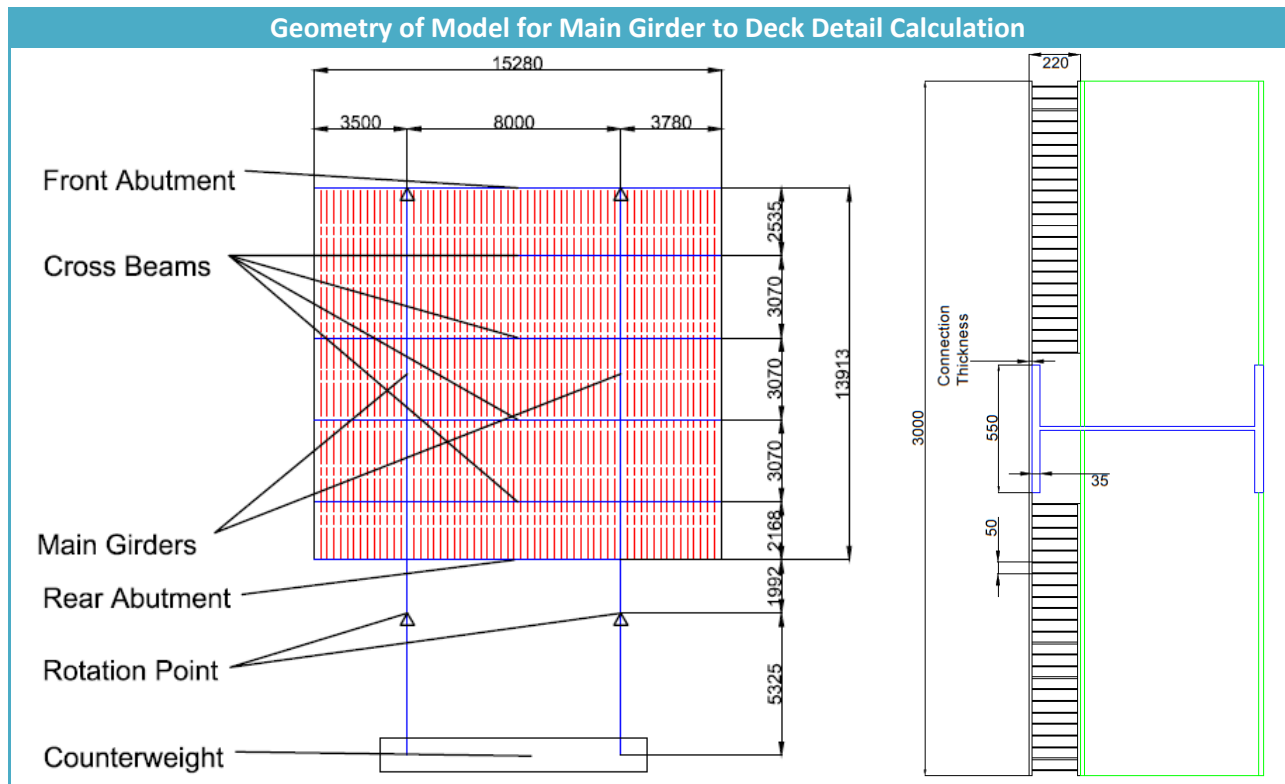


Figure 50: (Left) Global Geometry used for Model. (Right) Geometry of the Main Girder. Note that the Connection Thickness is Still to be Determined at this Point.

### 8.2.2 Simplifications Applied in Model of Detail

The model of the bridge has been simplified when compared to real life in order to ease the creation of the model and to reduce computation time.

- The parts of the deck outside of the main girders have been modelled as a single plate with the same properties as the deck. This saves computation time by allowing the removal of one of the deck plates, as well as all of the webs over a large portion of the width of the bridge. The behavior of the single plate has been verified in Q.5 Validation of Plate Approximation.
- The counterweight has been excluded from the model. This has little influence on the global behavior, since typically a hydraulic cylinder pushes against the counterweight to ensure closure of the bridge.
- The hydraulic cylinder attached to the counterweight is replaced by supports at the end of the main girders where the counterweight would be attached. The supports will show a larger stiffness than the hydraulic cylinder. The influence of this near the detail is expected to be minimal. Additionally, this effect will be partially compensated by the following point.
- In the current design the main girders of the model are enlarged and lowered behind the rear abutment. Since this region falls outside the scope of this study, the girders have been extended behind the abutment at the same height and with the same dimensions. This means that the girders will behave less stiffly than they do in the current design. This will be partially compensated by the previous point.
- The front and rear abutments have been excluded in the model. These are complexly shaped girders which are quite some distance removed from the considered detail. Therefore they are not expected to have a significant impact on the local stress development.
- The location at which the heart of the first wheel load is applied is a distance “L” from the edge of the girder. Here “L” corresponds to the distance at which the bending moment was maximized according to the hand calculations for each individual laminate thickness; see Figure 49. See Appendix R: Verification of Loading Distance in Model for validation of this assumption.

### 8.2.3 Visualization of Model of Girder to Deck Detail

The model is shown in Figure 51. Note that the mesh has been refined in the region around the detail. This results in the nodal forces being more distributed in this region, visible through the different arrow sizes in the model. Also note the boundary conditions which are located at the point of rotation, the front abutment, and the counterweight.

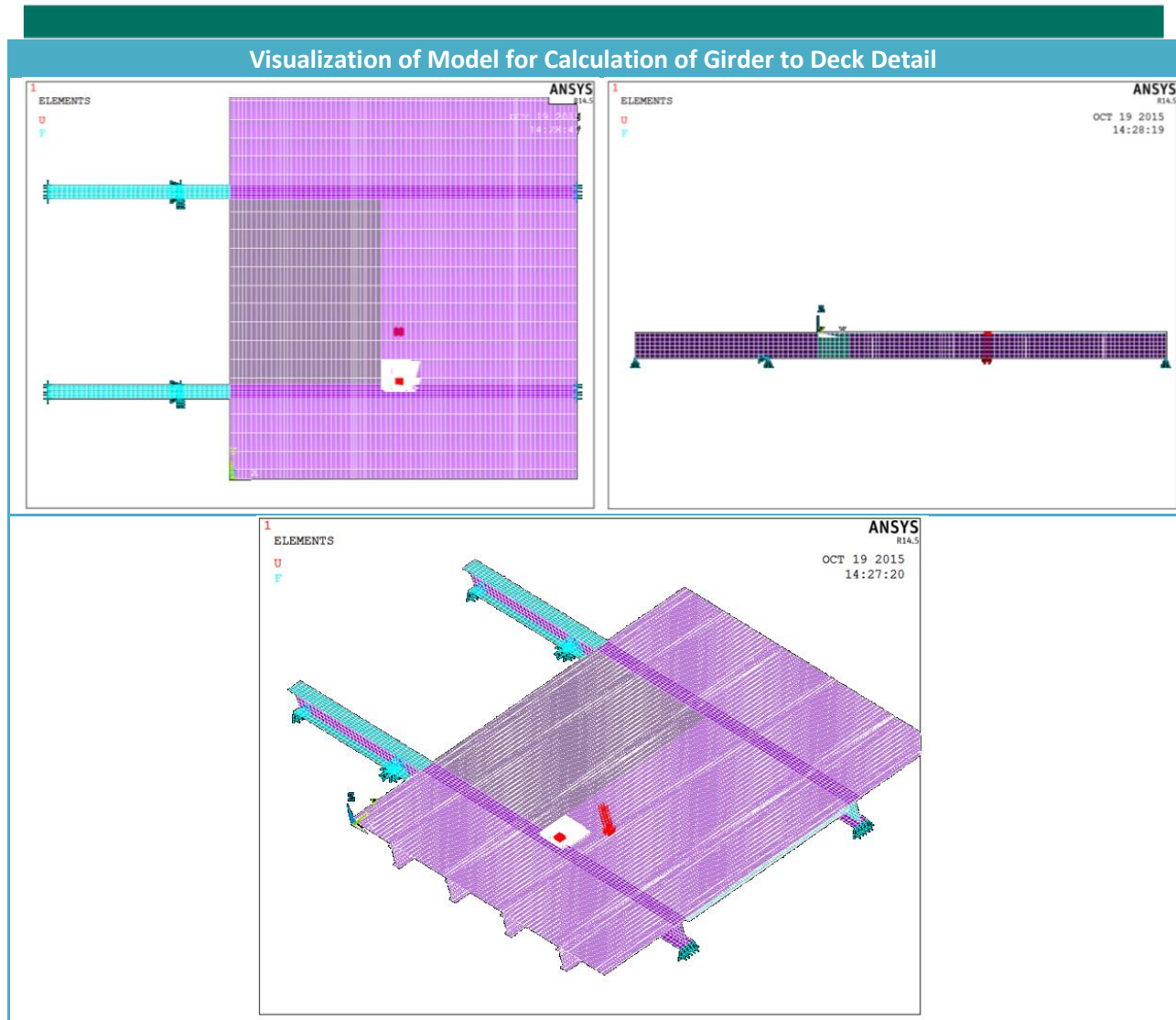


Figure 51: (Top Left) Top View of the Model. (Top Right) Side view of the Model. (Bottom) 3D View of the Model. Note in all Three Views that the Mesh has been Refined Near the Considered Detail.

## 8.2.4 Results of Girder to Deck Detail Calculations

The model has been calculated to determine the ultimate failure load for each of the different axle types according to Table 25. The results for the calculations presented below are a obtained with a laminate thickness of 40mm, and a C-class axle loaded to 600kN.

### 8.2.4.1 Displacements Girder to Deck Detail Model

The vertical displacement of the bridge under traffic loading is presented in Figure 52. The situation shown is one where a 600 kN axle load is applied to a model with a connection thickness of 40 mm. This load approaches the ultimate strength required to prevent fatigue failure.

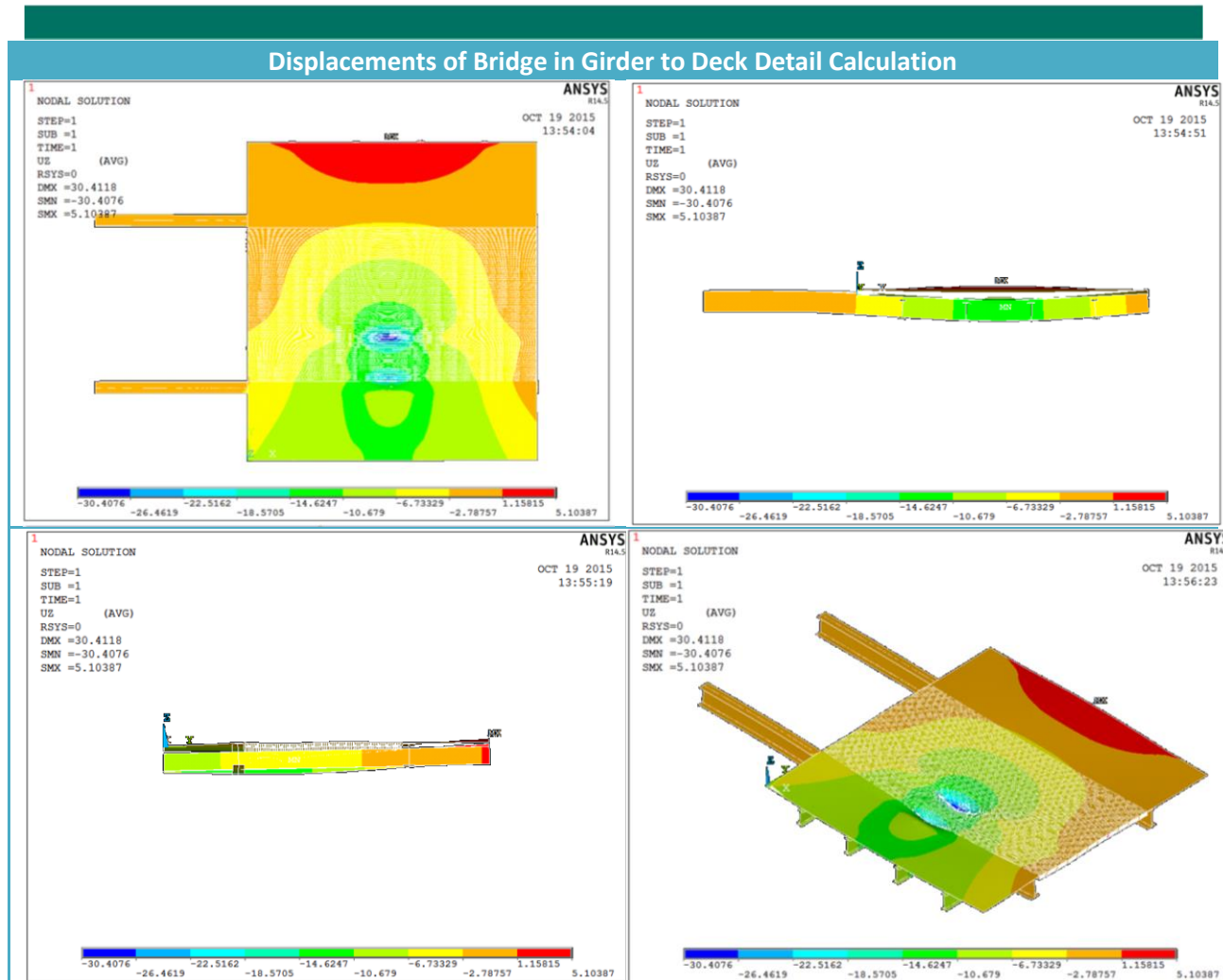


Figure 52: (Top Left) Top View of Vertical Displacement. (Top Right) Side View of Vertical Displacement. (Bottom Left) Front View of Vertical Displacement. (Bottom Right) 3D View of Vertical Displacement. The Results Presented Here Are Obtained With a Laminate Thickness of 40 mm and a C-Class Axle Loaded to 600kN. All displacements in mm.

#### 8.2.4.2 Tsai-Wu Values of Girder to Deck Detail

The Tsai-Wu values resulting from the same loading scenario as above are presented in Figure 53. Interesting to note is that the maximum Tsai-Wu value occurs at a small distance inward from the girder edge.



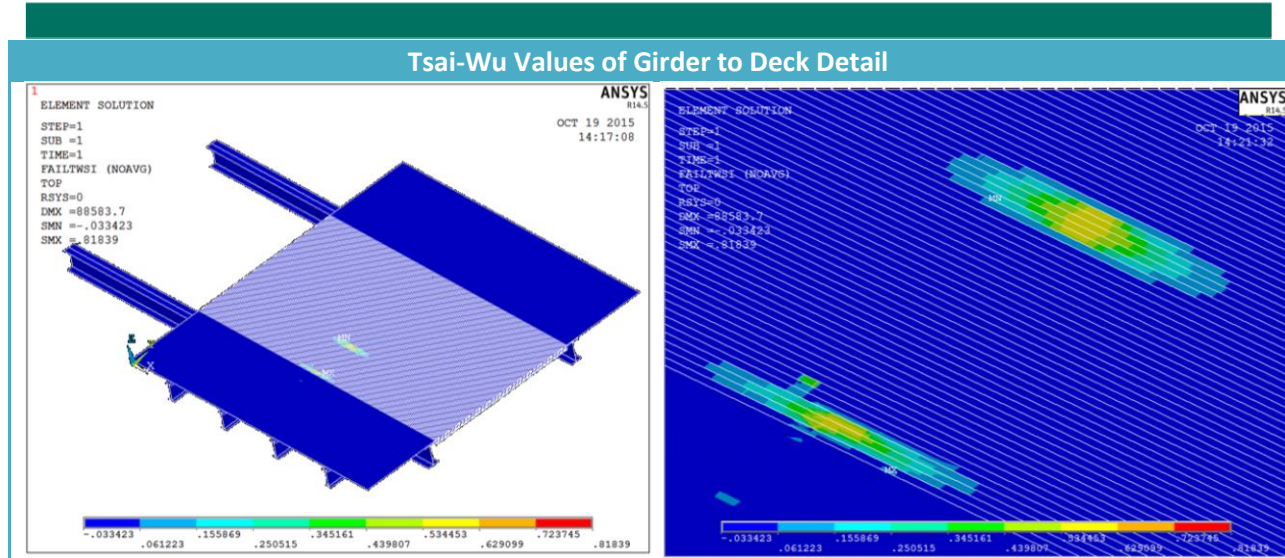


Figure 53: (Left) 3D View of Tsai-Wu Failure Criterion. (Right) Zoomed View of Tsai-Wu Failure Criterion. The Results Presented Here Are Obtained With a Laminate Thickness of 40 mm and a C-Class Axle Loaded to 600kN.

### 8.2.5 Cumulative Fatigue Damage Utilizing Finite Element Model

The purpose of applying a finite element analysis to the main girder to deck detail is to determine the thickness of the laminate required to resist fatigue loading. This has been done in the same manner as in 8.1 Hand Calculations of Girder to Deck Detail. However, it has been expanded with the different wheel loads for the considered axles. This also means that  $S_{ult}$  should be determined for each axle type. Figure 54 graphically represents this process for a C-class axle. The loads at which the lines cross the critical Tsai-Wu value (i.e. including safety factors), marks the ultimate design resistance.

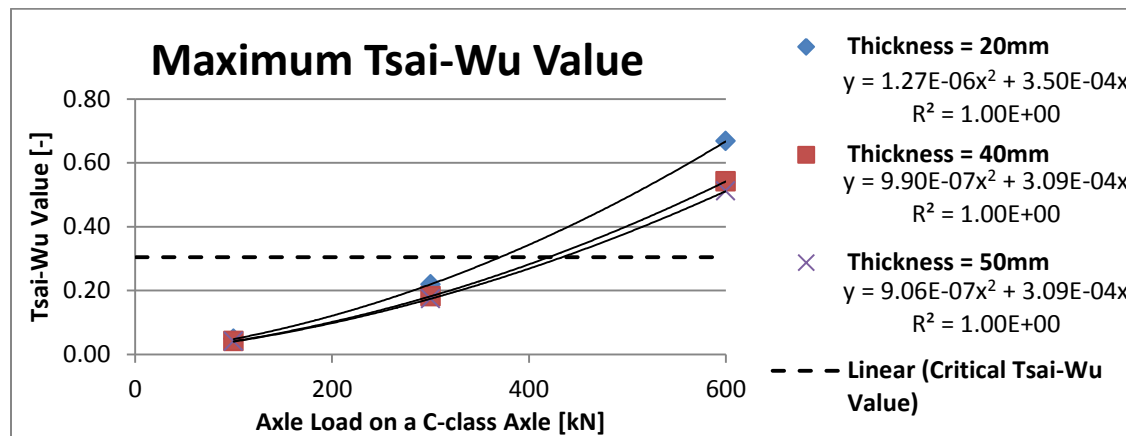


Figure 54: Tsai-Wu Value for a C-class Axle as a Function of Axle Load for Several Laminate Thicknesses

With the design resistances, axle loads, and number of cycles known, the cumulative damage can be calculated according to Equation 18. Calculating the cumulative damage for varying laminate thicknesses produces Figure 55. Note that the damage always exceeds 1 for the given material thicknesses, thereby invalidating this solution.

$$D = \sum_{i=1}^k \frac{n_i}{N_i}$$

$$D = \sum_{i=1}^k \frac{n_i}{10^{\left(\frac{0.7902}{0.0775} \frac{S_{max,i}}{0.0775 * S_{ult,axle}}\right)}}$$

Equation 18: Calculation of Cumulative Damage in Main Girder to Deck Connection Detail.

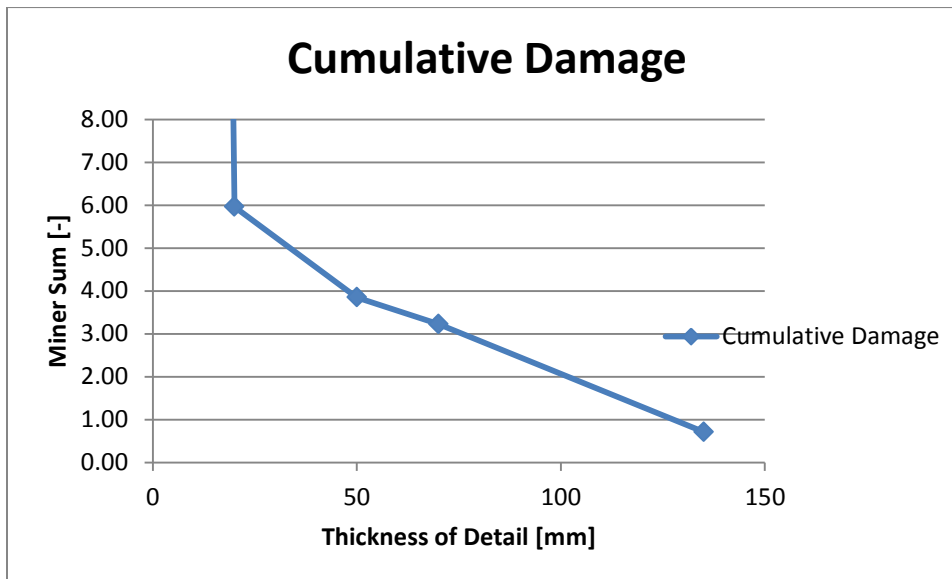


Figure 55: The Cumulative Damage Sustained in the Critical Cross Section of the Detail for Various Thicknesses of the Laminate.

### 8.2.6 Alternative Solution to Fatigue Loading

The detail as described above is not a viable solution. Hence an alternative consisting of carbon fiber reinforced polymer has been analyzed. Carbon fiber, while several times more expensive, offers significantly better material properties. Three important points are listed below.

- CFRP is stronger than GFRP. This should increase the ultimate resistance.
- CFRP has better fatigue resistance than GFRP. Recall Figure 47, where one can see that at the same fraction of the ultimate load, CFRP is capable of resisting 10-1000 times as many cycles.
- CFRP has a much higher stiffness than CFRP. Therefore, a detail containing carbon fibers will draw a larger percentage of the load towards itself.

For the design of the detail HS (high strength) carbon fibers have been applied. These have the high strength to increase the ultimate resistance, and the relatively low modulus to add flexibility to the

detail. The cumulative damage is calculated in the same manner as for GFRP, with the exception that Equation 19 has been applied to determine the number of cycles until failure.

$$\frac{S_{max}}{S_{ult}} = 0.8227 - 0.0519 \log N_i$$

Equation 19: Equation for Maximum Fatigue Load of Carbon Fiber Reinforced Polymers with Continuous Fibers as Obtained from Literature.<sup>52</sup>

The cumulative fatigue damage is given in Figure 56. Adding CFRP to the design creates an additional area of importance, namely the region where the transition from carbon fiber to glass fiber occurs. One can see in Figure 56, that as the carbon fiber layer gets thicker, the material transition point becomes governing over the geometry transition. If the CFRP layer is executed as a flexible layer, the CFRP cross section near the girder and the GFRP towards the other wheel load become governing. In this situation the cumulative damage is far lower than for a more rigid detail, especially for the GFRP.

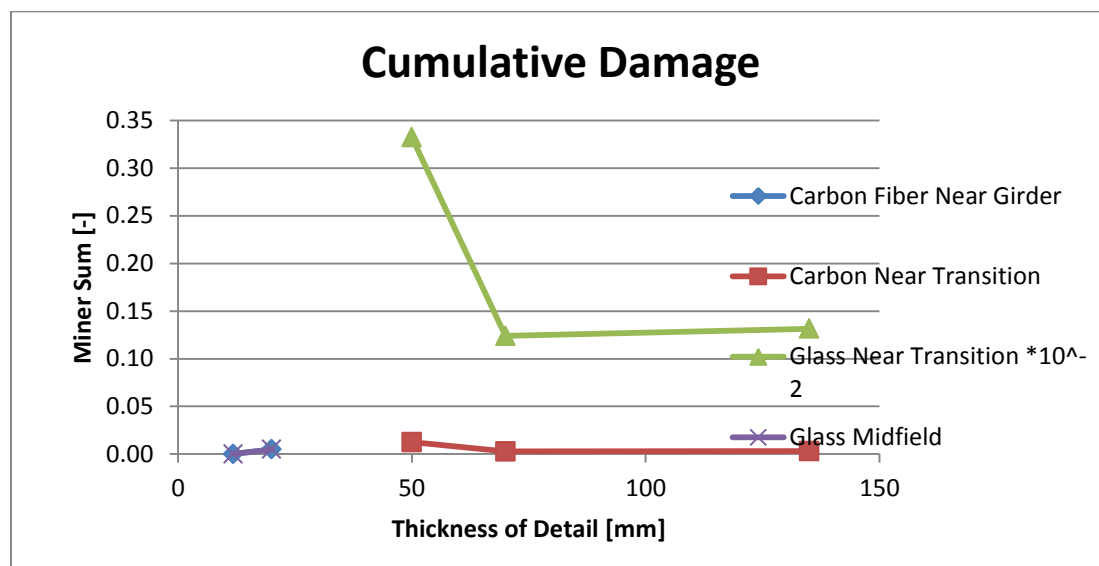


Figure 56: Cumulative Damage In Glass and Carbon Fiber Materials For Fatigue Loading. Note That there are Four Distinct Mechanisms: (1) Fatigue of Carbon Fiber Near the Main Girder, (2) Fatigue of Carbon Fiber near the Glass-Carbon Transition, (3) Glass Fiber near the Glass-Carbon transition, (4) Glass Fiber not Located Near the Detail. Note that the Cumulative Damage of the Glass Fiber near the Glass-Carbon Transition has been scaled down by a factor 100, to Improve Visibility of the Mechanisms.

### 8.3 Conclusion Regarding Girder to Deck Detail

To execute the main girder to deck connection detail in glass fiber is not a satisfactory solution in the case of the Julianabrug. The connection will fail due to fatigue damage, for any producible thickness. The solution is to execute this detail in a carbon fiber reinforced polymer. Carbon fiber shows

<sup>52</sup> (Demers, 1997)

---

significantly better fatigue properties so that the connection can be executed as a thinner layer. According to fatigue calculations a thickness of 11.75 mm will easily suffice with regards to fatigue loading.

Executing the detail in CFRP has several benefits. First, the transition back to the glass fiber deck is not loaded as heavily. Secondly, the CFRP layer which is needed is of a thickness which is easily produced. Thirdly, with this design, the carbon fiber layer can be made to seamlessly connect to the upper flange of the deck. These factors all indicate that a CFRP detail is significantly better than a GFRP detail.

## 9 Case Study

This thesis has focused on an FRP-steel hybrid structure. Several variants have already been analyzed in previous chapters. These include designs with and without composite action, the original design, and designs with elevated steel profiles. However, the standard method for executing a moveable bridge deck is based on an orthotropic steel deck, as shown in Figure 57. Therefore, an orthotropic bridge deck should also be considered when determining an optimal solution. To this end an orthotropic deck will be globally dimensioned, and compared to the optimal FRP-hybrid solution. The grounds for comparison will be mass and production cost.



Figure 57: View of the Bottom of an Orthotropic Bridge Deck<sup>53</sup>

### 9.1 Design of Orthotropic Bridge Deck

The orthotropic bridge deck will be designed on the basis of stiffness and strength. For each considered element, the stiffness and strength must be greater than or equal to that of the current bridge design. The exceptions are the deck plate and longitudinal stiffeners, which have been based on the design guidelines found in norms.<sup>54</sup>

<sup>53</sup> (Yuan, 2011)

<sup>54</sup> (NEN-EN 1993-2: Design of Steel Structures - Part 2: Steel Bridges, 2007), (NEN-EN 1993-2+C1/NB: Design of Steel Structures - Part 2: Steel Bridges, 2011)

### 9.1.1 Design of the Deck Plate and Stiffeners

The deck plate and the longitudinal stiffeners are based on norms.<sup>55</sup> Table 26 shows the values specified by the norms and the values assumed for this case study, where several of the listed properties are shown in Figure 58.

Properties of Deck Plate and Longitudinal Stiffeners		
Property	Norm	Assumed Value
Deck Plate Thickness	18mm	18mm
Spacing Between Stiffeners	$600\text{mm} \leq e_{LS} \leq 900\text{mm}$	650mm
Edge Distance First Stiffener	$e_E \geq e_{LS}$	750mm
Height of Stiffener	$h_{stiff} \leq 0.4h_{crossb}$	300mm
Thickness Stiffener Web	$6\text{mm} \leq t_{stiff,w} \leq 10\text{mm}$	8mm
Thickness Stiffener Flange	$6\text{mm} \leq t_{stiff,f} \leq 10\text{mm}$	8mm
Width Stiffener at Deck	[-]	250
Width Stiffener Flange	[-]	200

Table 26: Properties of Deck Plate and Longitudinal Stiffeners for Orthotropic Deck as Specified by Norms and as Assumed for this Case Study.<sup>56</sup>

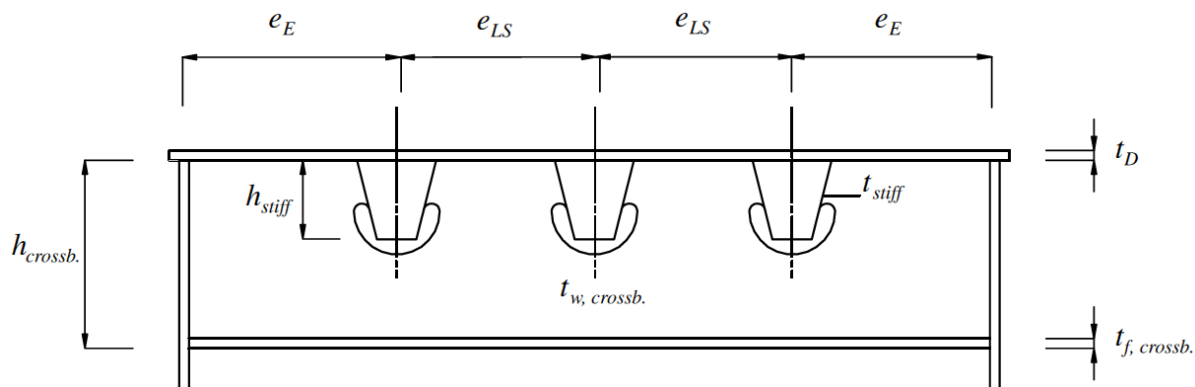


Figure 58: Cross Section of Orthotropic Deck with Relevant Properties Labeled<sup>57</sup>

### 9.1.2 Effective Width

When considering an orthotropic deck, the deck plate will act as the top flange of the girders and crossbeams. For the main girders, the stiffeners will also contribute. However, stress dissipates as one gets further away from the body of the girders, so that a portion of the total width is assumed as the effective width which acts as the top flange of the girders. The effective width of the deck is given by Equation 20.

<sup>55</sup> (NEN-EN 1993-2: Design of Steel Structures - Part 2: Steel Bridges, 2007), (NEN-EN 1993-2+C1/NB: Design of Steel Structures - Part 2: Steel Bridges, 2011)

<sup>56</sup> Deck Plate Thickness: (NEN-EN 1993-2+C1/NB: Design of Steel Structures - Part 2: Steel Bridges, 2011); Other Dimensions: (NEN-EN 1993-2: Design of Steel Structures - Part 2: Steel Bridges, 2007)

<sup>57</sup> (NEN-EN 1993-2: Design of Steel Structures - Part 2: Steel Bridges, 2007)

$$b_{eff} = \beta b_0$$

$$\beta = \frac{1}{5.9\kappa}$$

$$\kappa = \frac{\alpha_0 b_0}{L_e}$$

$$\alpha_0 = \sqrt{1 + \frac{A_{st}}{b_0 t_D}}$$

Equation 20: Effective Width of a Steel Deck<sup>58</sup>

With:

$b_0$ : "taken as the flange outstand or half the width of an internal element"<sup>59</sup>

$L_e$ : Effective Length. Follows from Figure 59.

$A_{st}$ : "Area of all longitudinal stiffeners within the width  $b_0$ "<sup>60</sup>

$t_D$ : Thickness of the Deck Plate

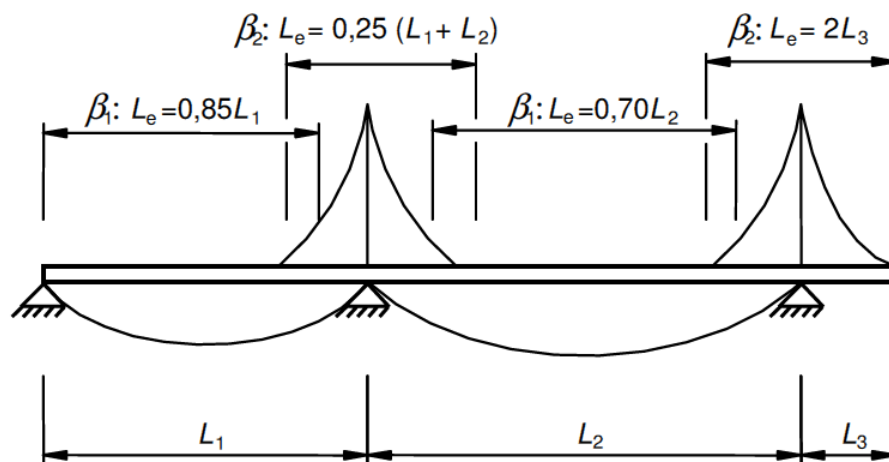


Figure 59: Effective Length for a Beam Based on Span and Support Type<sup>61</sup>

Using Equation 20, the effective widths of the deck can be determined for each girder. The results are given Table 27, along with values for steel and FRP as a reference. Note that the effective width of steel is larger than that of FRP, and falls in the same order size as concrete (See also 5.3 Effective Width of FRP Deck).

<sup>58</sup> (NEN-EN 1993-2: Design of Steel Structures - Part 2: Steel Bridges, 2007)

<sup>59</sup> (NEN-EN 1993-2: Design of Steel Structures - Part 2: Steel Bridges, 2007)

<sup>60</sup> (NEN-EN 1993-2: Design of Steel Structures - Part 2: Steel Bridges, 2007)

<sup>61</sup> (NEN-EN 1993-2: Design of Steel Structures - Part 2: Steel Bridges, 2007)

Effective Width of Deck			
Material	Steel [m]	FRP Lengthwise Laminated [m]	Concrete [m]
Rear Abutment	1.35	0.47	1.11
Main Girders	4.33	2.12	4.05
Front Abutment	1.19	0.47	1.00
Crossbeams	2.07	0.95	1.70

Table 27: Effective Widths for Each Girder Calculated for Steel, FRP, and Concrete.

The effective width of the deck above the main girders includes several longitudinal stiffeners. For calculations of stiffness and strength the area of the longitudinal stiffeners within the effective width has been spread out over the deck plate.

### 9.1.3 Stiffness of Orthotropic Deck Girders

One of the criteria for designing the girders of the orthotropic deck is stiffness. The stiffness of the orthotropic deck may not fall below that of the current design as described in 5.1 Basis of Laminate Orientation Determination for any of the girders. The method for determining stiffness is identical to the manner described in 5.4 Composite Stiffness of Girders. The results are presented in Table 28. The following points are worth noting:

- The rear abutment is required to show an increase in stiffness of at least 30% with respect to the current design
- The front abutment has a relatively small increase in stiffness, due mainly to rounding dimensions to standard sizes
- The main girder and crossbeams show large increases in stiffness, which indicates that stiffness is not the critical criteria for these elements.

Stiffness of Girders [EI]			
Girder	Current [kNmm <sup>2</sup> ]	Orthotropic [kNmm <sup>2</sup> ]	Change
Main	1.86E+12	3.70E+12	99%
Rear Abutment	2.20E+12	2.93E+12	33%
Front Abutment	8.26E+11	9.24E+11	12%
Crossbeams	4.31E+11	6.61E+11	53%

Table 28: Stiffness of the Considered Girders for the Current and Orthotropic Deck Designs

### 9.1.4 Section Modulus of Orthotropic Deck Girders

The second criterion which is applied during the design of the girders is that the section modulus of the girders is not allowed to fall below that of the original design, in order to maintain structural integrity. The manner in which the section moduli have been determined is identical to the manner



described 5.5 Section Modulus. The results are presented in Table 29. The following points are worth noting:

- The rear abutment shows the largest increase in section modulus, indicating that this criterion is not critical
- The main and crossbeams show a limited increase in section modulus, indicating that this is the governing criterion
- The front abutment shows a slight increase in section modulus. However, recall that the increase in stiffness was also limited. Therefore both criteria are critical.

Section Moduli of Girders			
Girder	Current [mm <sup>3</sup> ]	Orthotropic [mm <sup>3</sup> ]	Change
Main	2.04E+07	2.11E+07	3.3%
Rear Abutment	1.73E+07	2.62E+07	51.1%
Front Abutment	7.35E+06	8.04E+06	9.4%
Crossbeams	4.80E+06	4.96E+06	3.4%

Table 29: Section Moduli of the Considered Girders for the Current and Orthotropic Deck Designs

### 9.1.5 Mass of Orthotropic Deck Compared to FRP Deck

The goal of the design is to minimize the mass of the bridge. The stiffness and section modulus have been used as design criteria, which must be maintained while a minimization procedure is applied to the girder elements. The method in which the mass of the girder are determined is described in 5.6 Mass Change. The results are given in Table 30. The following points are worth noting:

- The mass of the deck increases greatly. The deck plate and longitudinal stiffeners together weigh more than twice as much as the current deck design.
- The girders are all much lighter than in the current design.
  - The deck plate acts as the top flange, so that only the bottom “T” is considered.
  - The main girders and rear abutment have an increased construction height.
- The optimized FRP variant can reduce the weight compared to the current design
- The orthotropic variant will be heavier than the deck in current situation
- Recall that one design requirement is that the rear abutment is 30% stiffer in the new variants.
  - The influence of neglecting this design requirement is given in Appendix S: Influence of Reduced Stiffness of Rear Abutment.

Mass of Girder Elements and Deck For Variants					
Location	Current	Optimized FRP		Orthotropic	
	Mass [tonnes]	Mass [tonnes]	Change	Mass [tonnes]	Change
Deck	22.4	20.7	-8%	31.6	109%
Stiffeners	N/A	N/A		15.2	
Main	16.7	13.1	-22%	8.2	-51%
Crossbeams	9.4	10.1	8%	5.7	-40%
Rear Abutment	10.5	10.0	-4%	5.6	-47%
Front Abutment	3.9	3.6	-10%	2.3	-42%
<b>Total</b>	<b>63.0</b>	<b>57.5</b>	<b>-9%</b>	<b>68.5</b>	<b>9%</b>

Table 30: Mass of Girder Elements and Deck for Current, Optimized FRP, and Orthotropic Designs

The mass calculated here represents the structural mass from the point of rotation forwards, meaning that the weight of the rear part of the construction and the ballast have been excluded. An indication of the total mass which can be saved is given in Table 31. The manner in which these indicative values have been determined is outlined below:

- The mass of the construction behind the point rotation will not show a significant change in mass as a result of the reduction in deck mass
  - This mass has been kept equal to the mass in the current design<sup>62</sup>
- The mass of the ballast will change significantly if the deck mass changes.
  - The ballast outweighs the front part of the bridge construction by 13% in the current design<sup>63</sup>
  - The change in ballast has been included proportionally to the change in mass of the front construction.

Indicative Values of Bridge Mass				
Location	Original [tonnes]	Current [tonnes]	Optimized FRP [tonnes]	Orthotropic [tonnes]
Front Construction		63.0	57.5	68.5
Rear Construction	57	32.5	32.5	32.5
Ballast	80	70.8	64.7	77.1
<b>Total</b>	<b>137</b>	<b>166.3</b>	<b>154.7</b>	<b>178.1</b>
<b>Change</b>	<b>0.0</b>	<b>29.3</b>	<b>17.7</b>	<b>41.1</b>

Table 31: Indicative Values of the Bridge Mass Including the Rear Construction and the Ballast

An indication of the mass of the rear construction and the ballast is given in Table 31. There is a significant change in the mass of the structure. Especially when comparing the optimized FRP variant to the orthotropic deck variant, one can see that the expected change in mass is well over 20 tons. This

<sup>62</sup> (Hattink, 2014)

<sup>63</sup> (Hattink, 2014)

indicates that a properly applied FRP deck has a significant advantage over a traditional steel orthotropic deck.

The division of mass when considering the construction and the ballast changes between the original and the current designs. For the current design the construction becomes heavier but the ballast becomes lighter, which is counterintuitive. This is possible because the current design includes more powerful machinery responsible for the opening and closing of the bridge.

## 9.2 Orthotropic Deck Model

The orthotropic deck has been based on design guidelines. However, it does differ significantly from the FRP deck, so that comparing the two is difficult. This difficulty arises from the following points:

- The different material applied in the decks
- Determination the effective width of the load carrying mechanisms of the two deck types under an applied load
- Different local effects present in the decks
  - Below the applied load
  - Interaction with the girders

In order to analyze these influences, a finite element model has been made of the orthotropic bridge deck, so it can be compared to the FRP deck.

### 9.2.1 Loading and Supports

The boundary conditions and applied loads are shown in Figure 60. The following things are worth noting:

- The boundary conditions are located in the place of the counterweight, the point of rotation, and the front abutment. This is identical to the model with the FRP deck.
- The applied load is a single SLS wheel load applied in the middle between the two main girders in y-direction, and in the middle between the two central crossbeams in x-direction.
- The FRP deck has been replaced with steel troughs.

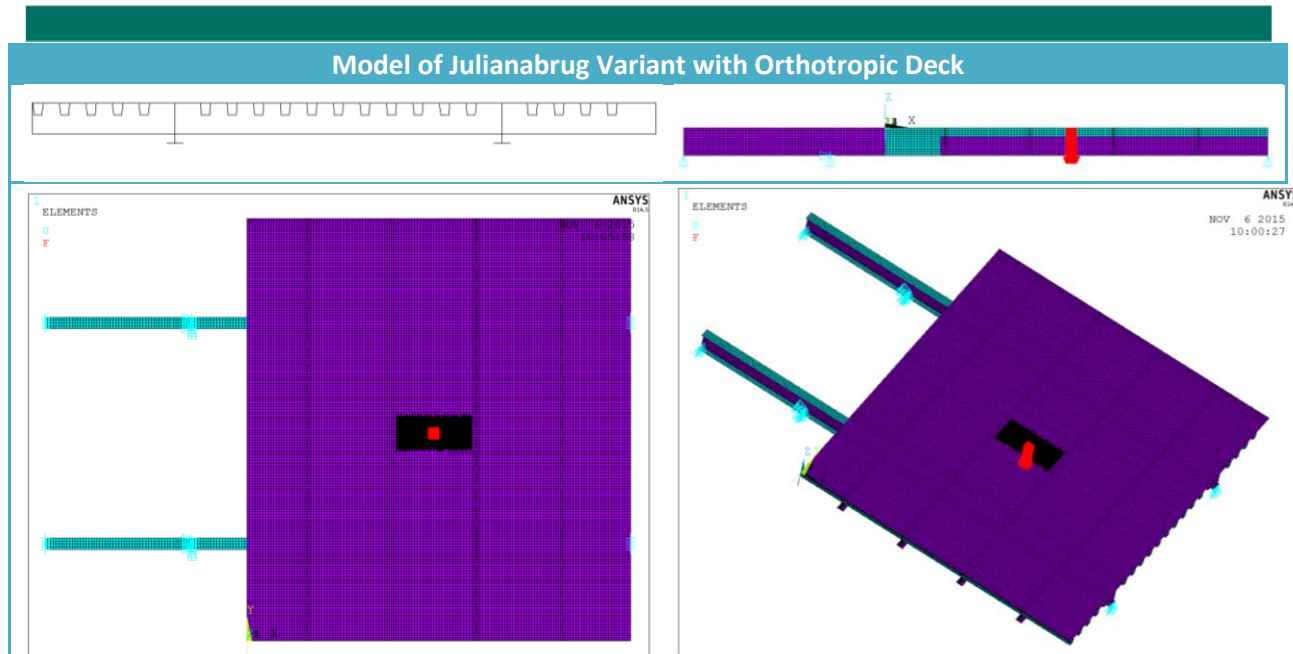


Figure 60: (Top Left): Cross Section of the Model Viewed from the Front. (Top Right): Side View of the Model. (Bottom Left): Top View of the Model. (Bottom Right): 3-Dimensional View of the Model.

### 9.3 Orthotropic Deck Results

The stress and displacement results are extracted from the model. Visualizations of the global behavior of these results are extracted. Additionally, the stress is analyzed along two paths: the lengthwise path and the crosswise path, which are shown in Figure 61.

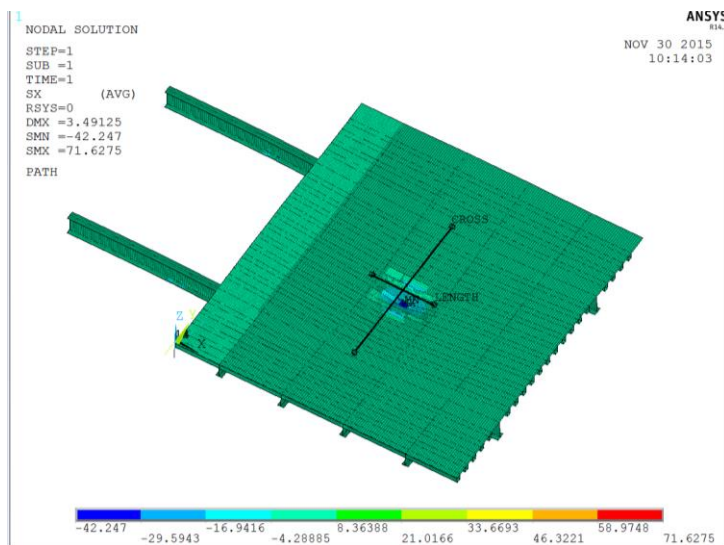
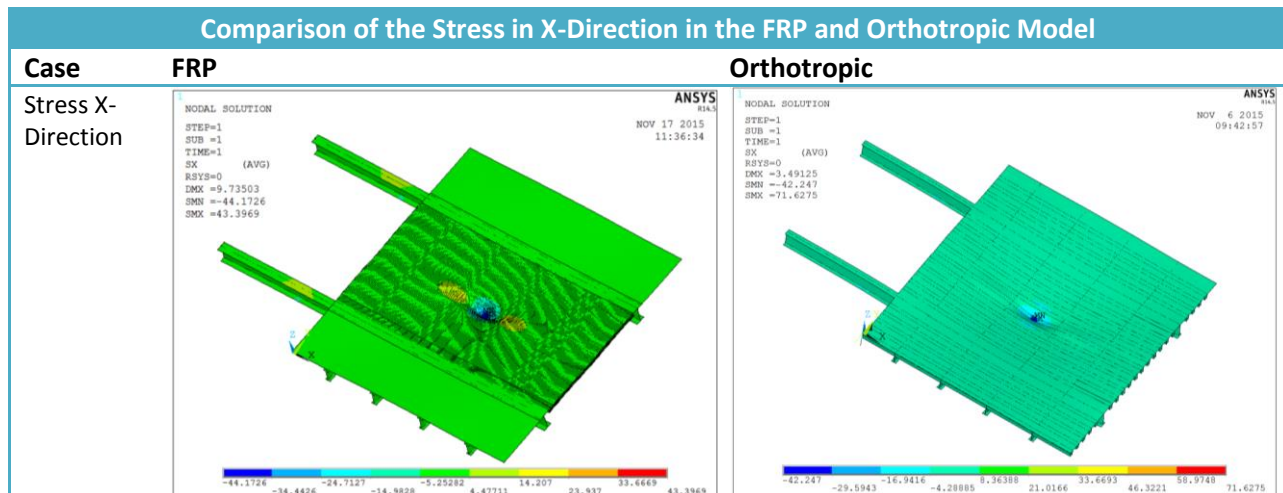


Figure 61: The Paths Along Which the Behavior of the Deck Will be Analyzed. The Lengthwise Path Runs Between The Two Middle Crossbeams and the Crosswise Path Runs Between the Two Main Girders. The Middle of both Paths is the Location Where the Load is Applied.

### 9.3.1 Stresses in FRP and Orthotropic Variants

The stress in x-direction is presented in parallel for the FRP and orthotropic variants in Figure 62. The following points are worth noting:

- The stresses in the deck arise in different materials in the two variants
  - The FRP has a lower stress in x-direction than the steel deck.
  - Since different materials are considered, the higher stress in steel is not necessarily detrimental.
  - The presented stress in the FRP is the maximum value in the laminate. In addition to the membrane and bending stresses, the different directional properties of the plies are taken into account.
- Along the crosswise path
  - The width which is activated in order to carry the load is larger for the FRP deck
  - The development of stress is smoother in the FRP variant. This is due to the small spacing between deck webs.
  - The steel deck develops stresses slower from the edge of the activated width inwards, but then shows a significant peak development between the edges of the trough.
- Along the lengthwise path
  - The FRP deck shows a relatively uniform stress development towards the middle of the span
  - The steel deck shows a significant increase in stress due to local behavior



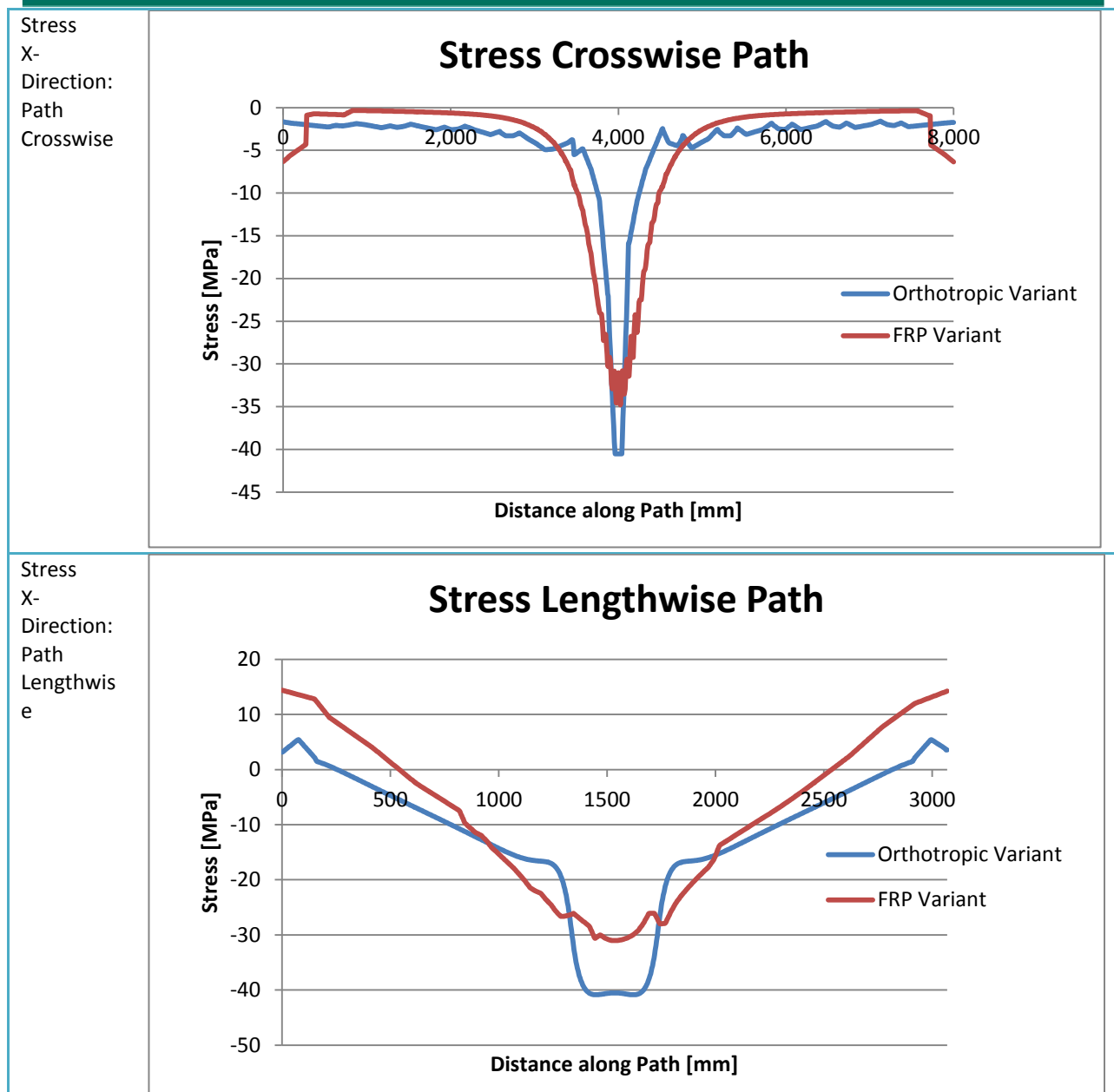


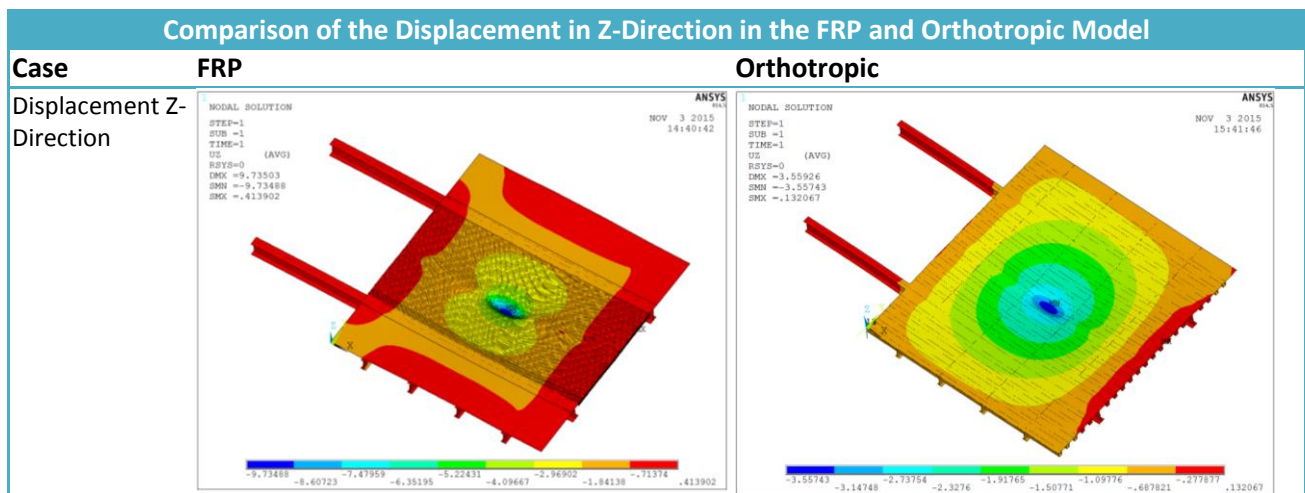
Figure 62: A comparison of the Stress in X-Direction Between the FRP and Orthotropic Models. Stresses in MPa.

Figure 62 shows the development of stresses in the FRP and the steel deck. The stress levels are higher in the steel deck. This is not troublesome, since steel is able to resist higher stresses than the FRP deck. The important thing to take away from the comparison is that the FRP has a more uniform load distribution. The effective width carrying the wheel load is larger, and local load carrying mechanisms play a smaller role in the development of stresses.

### 9.3.2 Displacements in FRP and Orthotropic Variants

The displacement in z-direction is presented in parallel for the FRP and orthotropic variants in Figure 63. The following points are worth noting:

- The displacements are significantly higher when an FRP deck is applied
  - This is because FRP has a significantly lower modulus of elasticity
- For the crosswise path,
  - The kink in the displacement profile occurs at similar locations for the two variants indicating a similar activated width. This corresponds well with the stress development in this region, as indicated above.
  - The steel deck is stiffer than the FRP deck. This is visible in the magnitude of the trough.
  - The displacement along the path, excluding the central trough, is larger for the FRP variant. This follows from the crossbeams being significantly stiffer in the orthotropic variant.
- The displacements along the lengthwise path show similar behavior, except that the steel displaces proportionally less.



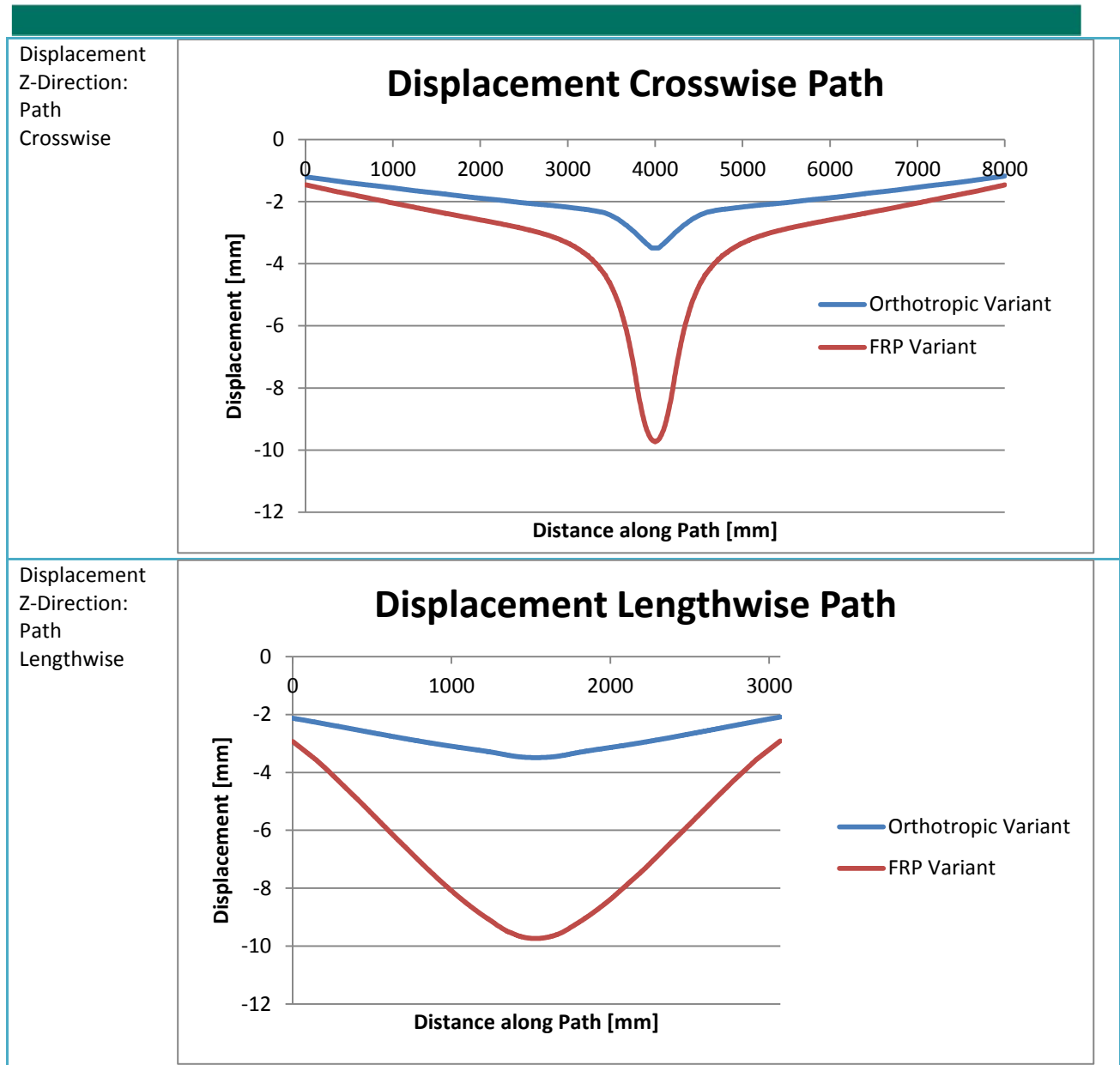


Figure 63: A Comparison of the Displacement in Z-Direction Between the FRP and Orthotropic Models. Displacements in mm.

Figure 63 compares the displacements between the orthotropic and FRP variants. The FRP displaces significantly more than the steel deck. This is mainly due to the large difference in material stiffness, but does not constitute a problem. Even if the girder displacements are not taken into account, the maximum displacement would constitute a 1-to-300 displacement to span ratio. This is an acceptable displacement ratio.



## 9.4 Conclusions Regarding Case Study

A steel orthotropic deck is the current standard for executing moveable bridges. In order to discover if applying an FRP deck is beneficial, the FRP variant needs to be compared to the steel orthotropic variant. This chapter has therefore focused on comparing an orthotropic design with the FRP variant.

The steel orthotropic deck outperforms the FRP deck when considering displacements. Both locally as well as globally, the displacement of the steel deck are smaller. This is due to the following reasons:

- The Young's Modulus of steel is significantly larger than that of an FRP laminate
- The height of the various construction elements is larger for the orthotropic variant.
  - For the FRP variant, the available construction height for the crossbeams and abutments is reduced by the height needed for the deck. Therefore a balance is reached between the height given to the deck and that given to the girders.
  - In the steel variant, the longitudinal stiffeners do not influence the available construction height for the girders, so that the full construction height can be used.
- For the orthotropic variant, the deck acts as the top flange of the girders. This raises the neutral axis, and leads to a relatively large moment of inertia.

A comparison of the stresses has limited value, since they occur in different materials. However, looking at the stress development, one can see that the local effects have a much larger influence on the maximum stresses in the orthotropic deck variant. This is an acknowledged problem in steel orthotropic decks. Large peak stresses can occur in around the longitudinal stiffeners and these can lead to fatigue damage. This is why norms<sup>64</sup> recommend a deck thickness which is larger than one would initially expect if this were not taken into account. The FRP deck is built up with elements which have a much smaller width, so that the response is much more of a result of global behavior than local behavior. This should result in maximum stresses which are lower than those in steel.

The mass of an FRP deck is much lower than a comparable deck in steel. However, the light weight FRP deck needs to be supported with heavier girders. Taken altogether, a bridge with an FRP deck can be executed significantly lighter than a bridge executed with an orthotropic steel deck. This is especially true for moveable bridges, since any mass reduction of the deck will also be felt as a reduction in the ballast. Since the ballast is typically closer to the point of rotation than the centerline of the bridge, the total reduction in mass of the entire structure, will be more than twice what can be saved on the front end of the bridge.

---

<sup>64</sup> (NEN-EN 1993-2+C1/NB: Design of Steel Structures - Part 2: Steel Bridges, 2011)

## 10 Conclusion

The work presented here has analyzed the influence of attempting to realize composite action between steel and FRP. While during this analysis as many issues as possible have been considered, it is impossible to include everything. As such, below a conclusion is given regarding what has been considered in this thesis, followed by several topics which are recommended for future study.

### 10.1 Conclusions of Considered Topics

Fiber reinforced polymers are increasing in popularity in civil engineering. This is largely due to the high strength-to-weight ratio. The low weight is especially helpful in the design of moveable bridges, where any weight savings will also be felt in the counterweight. When renovating the superstructure of old bridges, if the mass of the new bridge is lower than that of the old bridge the foundations can be saved. This is the current motivation for applying FRP.

The influence of laminate layup on potential mass savings has been analyzed in chapter 5 Laminate Orientation. The conclusion is that laminating the bridge in the direction of the main span leads to the lightest construction, when compared to quasi-isotropic, or crosswise lamination. Limitations to this conclusions are that the analysis was done with the dimensions of the Julianabrug only and that for this analysis composite action between steel and FRP was assumed, i.e. a full strength connection between FRP and steel.

The benefits of realizing composite action between the two materials appeared to be significant. A mass reduction of nearly 8 tonnes was expected on the bridge leaf alone. However, this was determined prior to considering the method for joining the two materials together.

Connecting steel and FRP using a bolted connection is problematic according to calculations performed in this thesis. Finite element models, which were calibrated against small scale experiments, indicate that a bolted FRP connection will fail under a relatively small load. This result meant that the construction needed to be redesigned according to 6.4.1 Redesign with Reduced Deck Height. The low connection strength meant that the joints became governing in the design. This resulted in an inefficient use of material, where significant quantities of steel were added to reduce the shear flow between the deck and the girder.

Designing the steel girders such that they occupy nearly the entire available construction height, and are not compositely connected to the deck leads to a more efficient design. This is a result of the design no longer being governed by the connection. Limitations to this statement include that the calculations were based solely on the geometry of the Julianabrug, the connection strength was based on finite element models, and only a bolted connection was considered.

Details in which high stresses or considerable fatigue damage are expected can be executed in carbon fiber reinforced polymers. CFRP has the benefit of being stronger and showing significantly

better behavior under fatigue loading. FRP can be designed such that fibers can be locally adapted. This allows for more expensive materials such as CFRP to be applied in detail designs without the need to apply them across the entire construction.

A comparison between the design with an FRP deck and a steel orthotropic deck shows that the application of an FRP deck can lead to significant weight savings. The difference in mass between a bridge with an FRP deck and one with a steel deck was estimated to exceed 20 tonnes. However, even with this large reduction in mass, the design still significantly outweighs the original bridge which is being replaced.

A bridge with an FRP deck displaces more than its steel counterpart, however the displacements fall well within acceptable ranges. The difference in stiffness is mainly due to the increased height of elements, the functioning of the deck plate as the top flange of the profile, and the higher material stiffness.

Due to its design as a more uniform deck comprised of repeated thin segments, the FRP deck shows less dependency on local load carrying mechanisms. Loads spread to global load carrying mechanisms faster, so that peak stresses are smaller.

Designing a bridge with an FRP deck can lead to large reductions in mass at the cost of a reduced stiffness. However, do not anticipate that the reductions in mass will be so large that one can design a bridge according to modern codes that will be lighter than its counterpart designed according to the codes pertinent 60 years ago.

## 10.2 Recommended Future Areas of Study

This thesis handles many topics centered around the design of the Julianabrug. However, there are still many subjects left untreated or only partially treated worthy of further research regarding the use of FRP bridge decks.

### 10.2.1 Experimental Verification of Joint Strength

A large portion of this thesis has focused on the design of bolted connection in FRP. This included hand calculations and modeling. While the modeling was calibrated to small scale experiments, there is no verification of accuracy for large scale joints. In order to prove accuracy for large scale connections, experiments should be performed.

Experiments may also prove that the modeled failure load is inaccurate. When considering concrete, the experimental joint strength tends to far exceed both elastic and plastic calculations. There is no evidence that the same would be valid for FRP, but it would be remiss to assume accuracy of the model without experimental verification.

### 10.2.2 Local Application of Different Materials

In this thesis, the properties of the FRP have been treated as specifiable. During the design of the joints, several hand calculations were made to determine the influence of the constituent materials of FRP on the strength of bolted connections. As one can see in O.4 Alternative Materials For Connection, the application of carbon or aramid fibers appear to significantly improve the strength of the joint. Additionally in 8.2.6 Alternative Solution to Fatigue Loading, carbon fiber has been applied at the connection between the main girder and the FRP deck to help prevent fatigue damage. Local material deviations are to the author's knowledge untested and unproven. However, manufacturers have stated that such deviations are producible. Subjects which could be studied under this topic include:

- The strength increase resulting from the application of different materials
- The minimum size of the region with different constituent materials
- The strength of the interface between the two materials
- The optimal manner of transitioning between the two situations

### 10.2.3 Verification of Scaling of the Measurement Distances for the Failure Criterion

The failure criterion for the bolted connection contained a measurement distance from the interface. For small scale bolts, from 6-10mm, this distance has been proven to scale linearly with the diameter. In this thesis, a short analysis has been made of the influence of scaling the measurement distance. The influence appears to be significant. Verification of the ability to scale the measurement distance to the bolt diameter would lead to significant improvements in the design strength of connections.

### 10.2.4 Application of Alternate Failure Criterion

This thesis has assumed that the Tsai-Wu failure criterion was relevant to the design of a bolted joint. There are a multitude of failure criteria which have been left untreated in this thesis. These include, but are not limited to:

- Maximum Stress
- Maximum Strain
- Tsai-Hill
- Marin
- Stassi D'Alia
- Norris
- Hashin<sup>65</sup>

The Tsai-Wu criterion along with the first three listed above are by far the most common failure criteria applied in the industry, but at least a dozen alternatives are available.<sup>66</sup> However, all criteria

---

<sup>65</sup> (U.S. Department of Transportation: Federal Aviation Administration, 1996)

have been tested for behavior of lamellas and laminates. No data has been found comparing the performance of these failure criteria to locally induced peak stresses such as arise in a bolted connection. An entire study could be made of calibrating these failure criteria against experimental data with the purpose of determining the optimal failure criteria of bolted connections.

### 10.2.5 Calibration against Last Ply Failure

The first ply failure refers to the moment that a single ply within a laminate reaches its ultimate resistance and fails. However, since a laminate is typically made up of a multitude of plies, there is generally a significant amount of residual strength left. Activation of this residual strength comes paired with damage to the material and potentially expensive structural repairs, but is worth considering for ultimate limit state analyses.

### 10.2.6 Flexural Fatigue Behavior of FRP

The main girder to deck detail has been analyzed under bending dominant fatigue loading. However, the data used for this analysis is based on tensile fatigue tests. Studies towards the behavior of FRP under flexural fatigue are limited, although some have shown that FRP behaves poorer under flexural fatigue than under tensile fatigue loading.<sup>67</sup>

### 10.2.7 Optimization of Deck Geometry

The analyzed deck shapes were all previously used or readily available profiles. An optimization procedure might greatly enhance the performance of a deck. For instance, analysis of sandwich panels in steel have shown that T-core decks outperform the web-core type deck used in this thesis. See Figure 64 for the geometry of such decks. The dimensions in the analysis of steel decks are not practicable for FRP decks. However, further research could be done towards optimizing the shape of deck to minimize weight while optimizing performance.

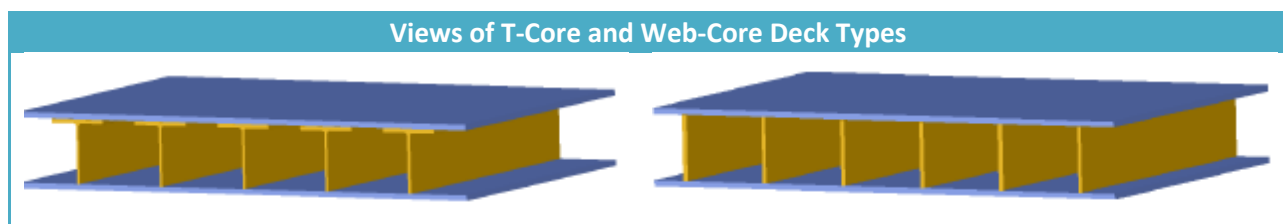


Figure 64: (Left) T-Core Deck. (Right): Web-Core Deck.<sup>68</sup>

### 10.2.8 Influence of Moment in Bolted Joint

The influence of a moment in the bolted connection comes into question in two different manners. First, during the transition from small scale to full scale, an eccentricity moment is added. Second, the

<sup>66</sup> (U.S. Department of Transportation: Federal Aviation Administration, 1996)

<sup>67</sup> (Solvay: Asking More From Chemistry, 2015). It should be noted that while both tensile and flexural fatigue are visually presented for the same composite, no quantitative data is given. Additionally, no information regarding the method of testing is available. Therefore these results should only be treated skeptically.

<sup>68</sup> (Gondar, 2013)

influence of the bolt head and the nut is excluded, both of which would limit rotation at the ends of the bolt.

The moment increases with laminate thickness. This follows from an increased eccentricity between the steel plate and the laminate. The experiments against which the failure criteria were calibrated did not include an eccentricity since they were symmetric experiments. Therefore, a large moment was introduced when going full scale which was never included in any calibration. Therefore, the influence of this moment on failure remains unknown and should be studied.

The second instance where moment plays a role is at the ends of the bolt. In reality, the bolt head and bolt nut will resist rotation due to their contact with the laminate or steel. This resisted rotation introduces a moment in the bolt which will reduce the rotation of the bolt and hence reduce the peak stress at the boundary of the laminate. Preliminary calculations have indicated that including this effect could theoretically increase the failure load by up to a factor 2.

#### 10.2.9 Influence of Consecutive Bolts on One Another

A spacing of 4 times the bolt diameter has been applied in order minimize the influence of consecutive rows of bolts. These 4 diameters should lead to a significant limitation of stress. However, residual stress will still be present at the location of the next bolt, which will influence the capacity of the next bolt. The degree to which the remaining stresses influence consecutive bolts should be determined.

An uniform distribution of force among bolts has been assumed. This is an ideal but unlikely scenario. Experiments have shown that for connections with two bolt rows and two bolt columns, one row is loaded 30% more than the other.<sup>69</sup> For more bolt rows and columns, this distribution will likely vary. Deviations in force distribution will lead to higher strength requirements in joints, so that they become more governing.

#### 10.2.10 Eurocomp

The Eurocomp<sup>70</sup> is the guideline currently used in industry when determining the strength of bolted connections. However, it appears that this guideline underestimates the strength of connections severely. While the guidelines for design strength should naturally be lower than experimental strengths, the difference between these two appears significantly larger than necessary. While caution is advised, reviewing the Eurocomp to reduce the discrepancy between the guidelines and laboratory experiments would result in significant advantages for the FRP industry.

---

<sup>69</sup> (The European Structural Polymeric Composites Group, 1996)

<sup>70</sup> (The European Structural Polymeric Composites Group, 1996)

### 10.2.11 Injection Bolts

The application of bolts without clearance is a difficult prospect within civil engineering. Fitted bolts are typically significantly more expensive due to the additional precision with which the construction must be built. However, adding clearance leads to a much smaller contact surface between a bolt and the laminate, so that higher stresses arise. This will lead to a lower failure load.

A proposed solution, is the application of injection bolts. These are bolts specially constructed to allow for a resin to be injected between the bolt and the laminate. This means that there is not clearance after injection. Tests performed with injection bolts produce promising results as shown in O.1.1 Injection Bolts. Because the force is transferred to the laminate through the injected resin, the peak stress is reduced so that the reduction in failure load is minimized. Additionally, prior to injection, a clearance can be included, so that expensive fitted holes can be avoided. Injection bolts appear to be a promising solution to minimize the influence of applying a clearance in bolted connection.

## Appendix A: Codes and Guidelines

There are codes and guidelines which specify the actions which work on a structure. All loading conditions will not be accounted for in this thesis due to time constraints. However, key loading forms will be regarded. These include thermal loading, vertical traffic loading, and fatigue loading.

There are many important variable loads which must be accounted for in the design of bridges. Due to the scope of this thesis and the time allotted for it, it is not possible to consider all possible loading situations. The first loads which are included in the design are those resulting from thermal expansion. In steel-concrete hybrid structures, thermal expansion typically does not present a problem, since the coefficients of thermal expansion are so close. However, for FRP-steel hybrid structures the thermal expansion may cause a problem, due to the different coefficients of expansion for FRP and Steel. The next load case taken into account is traffic loading. Traffic is typically the dominant form of loading for the type of bridge under consideration. It is often key for local strength and is especially relevant to the determination of fatigue life.

This leaves several loading situations which have not been taken into consideration. The most important one is wind loading. Wind can act as a load in both the vertical and horizontal directions. The horizontal wind loading is considered irrelevant to this thesis. This load acts in the plane of the deck, and hence will only result in small stresses. The horizontal force is relevant for determining the horizontal reaction forces in the points of rotation. However, since the design of the supports falls outside of the scope of this study, this force may be neglected. The vertical wind load is neglected because it works in the opposite direction of the traffic load. Therefore it is considered a favorable action, so that not taking it into account is conservative. Finally, the unique loading situations are neglected. This is because these events are supposed to occur so rarely, that the added value of their analysis is not sufficient to warrant the time required.

### A.1 Thermal Load

For the determination of the thermal load, three temperature situations are required. These are the uniform minimum temperature, the uniform maximum temperature, and the installation temperature. These values have been obtained from norms.<sup>71</sup> Note that the maximum and minimum temperatures are not of import because the temperature changes over the assumed installation temperature are what causes internal forces. Hence, the temperature changes will be the ones used for calculations.

- $T_{e,max} = 46^{\circ}\text{C}$
- $T_{e,min} = -28^{\circ}\text{C}$
- $T_0 = 10^{\circ}\text{C}$

---

<sup>71</sup> (NEN-EN 1991-1-5+C1/NB: National Annex Thermal Actions, 2011)



- $\Delta T_{max} = 36^{\circ}\text{C}$
- $\Delta T_{min} = -38^{\circ}\text{C}$

The norms do not specify temperature gradients for steel-composite deck systems, hence, those for concrete-steel bridges have been applied. This is believed to be a conservative approach, since the thermal conductivity of composite materials tends to be much lower than that of concrete.<sup>72</sup> The temperature gradient applied to the structure corresponds to the simplified procedure given in Figure 65.<sup>73</sup>

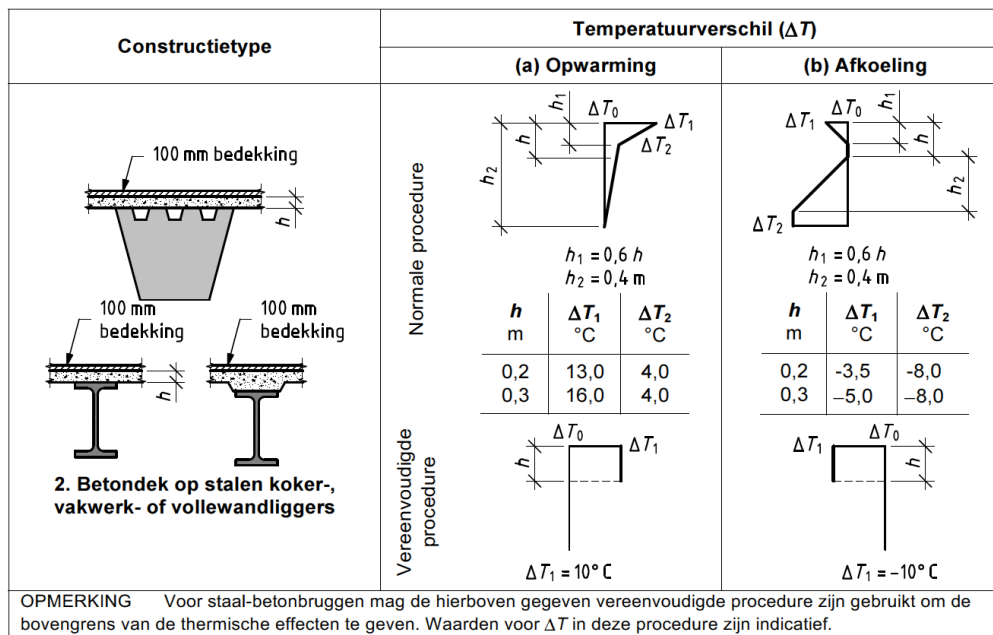


Figure 65: Temperature Gradient Concrete-Steel Bridges<sup>74</sup>

## A.2 Vertical Traffic Load

Traffic loading is one of the more expansive loading situations acting on the structure. It needs to take into account different weights of different vehicles traveling on different lanes, as well as the horizontal forces resulting from braking. In this thesis, ULS and Fatigue loading will be accounted for explicitly, while SLS loads will be accounted for through comparison of main structural components to the current design of the Julianabrug.

<sup>72</sup> (Hattink, 2014)

<sup>73</sup> Simplified Procedure is Labeled “Vereenvoudigde procedure” in Dutch, and is represented by the bottom sketches in Figure 65.

<sup>74</sup> (NEN-EN 1991-1-5+C1/NB: National Annex Thermal Actions, 2011)

### A.2.1 Ultimate Limit State Load

The ultimate limit state loads represent the highest loads that a structure must be able to resist. For the vertical loading, Load Model 1<sup>75</sup> is applied in accordance with demands set during project specification. Load Model 1 specifies a tandem system of axle loads as well as a uniformly distributed load per lane for while the values are given in Table 23. The distribution of these loads is given in Figure 66. Since the global behavior of the bridge has already been checked in the current design of the Julianabrug, several ULS values will be taken from that calculation report.<sup>76</sup> Additional considerations in effect for Load Model 1 are:

- The adjustment factor is set as  $\alpha = 1$  according to project specification
- The contact surface of each wheel is  $0.40 \times 0.40 \text{ m}^2$

Location	Tandem system <i>TS</i>	<i>UDL</i> system
	Axle loads $Q_{ik}$ (kN)	$q_{ik}$ (or $q_{ik}$ ) (kN/m <sup>2</sup> )
Lane Number 1	300	9
Lane Number 2	200	2,5
Lane Number 3	100	2,5
Other lanes	0	2,5
Remaining area ( $q_{rk}$ )	0	2,5

Table 32: Characteristic Load Values for Load Model 1<sup>77</sup>

<sup>75</sup> (NEN-EN 1991-2 (en): Traffic Loads on Bridges, 2003)

<sup>76</sup> (Hattink, 2014)

<sup>77</sup> (NEN-EN 1991-2 (en): Traffic Loads on Bridges, 2003)

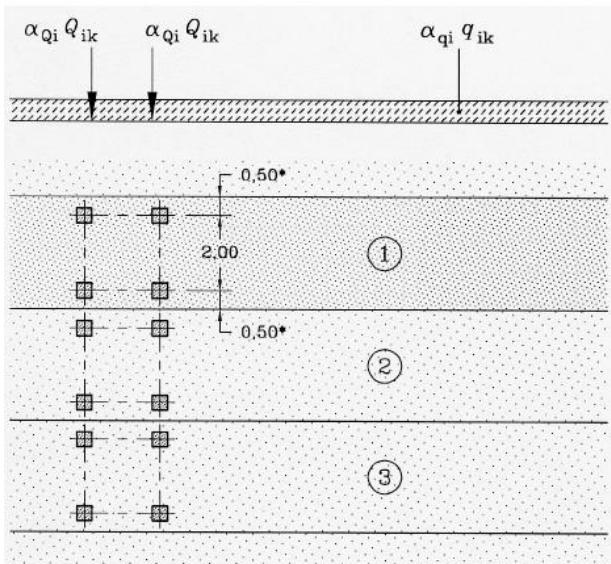
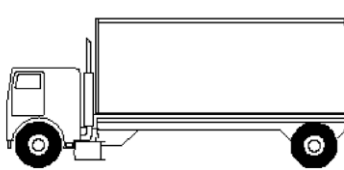


Figure 66: Distribution of Load Model 1<sup>78</sup>

### A.2.2 Fatigue Loading

One of the key reasons an ever increasing number of bridges are becoming structurally deficient is the accumulation of fatigue damage. Hence, to verify the structural integrity of the bridge, an analysis for fatigue damage needs to be performed. The fatigue calculation is dominated by the traffic loading, but the opening/closing cycle of the bridge should also be accounted for. However, due to time constraints, this will be excluded.

The fatigue loading has been schematized according to *Fatigue Load Model 4*.<sup>79</sup> This models the traffic as a combination of 5 trucks with varying masses and axles. The five lorries are shown in Table 33. The wheel types referred to in this table are given in Table 34.

Equivalent Lorries				
Lorry	Axle Spacing [m]	Equivalent Axle Load [kN]	Lorry Percentage	Wheel Type
	4.5	70	50	A
		130		B

<sup>78</sup> (NEN-EN 1991-2 (en): Traffic Loads on Bridges, 2003)

<sup>79</sup> (NEN-EN 1991-2 (en): Traffic Loads on Bridges, 2003)

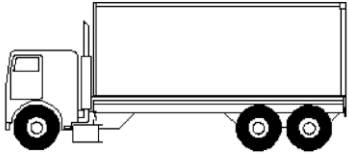
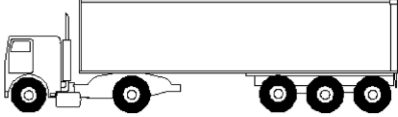
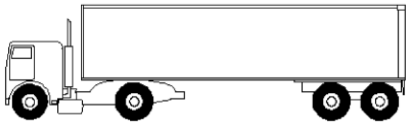
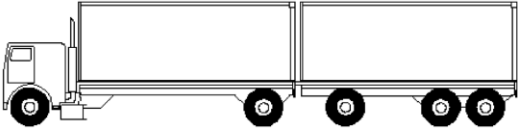
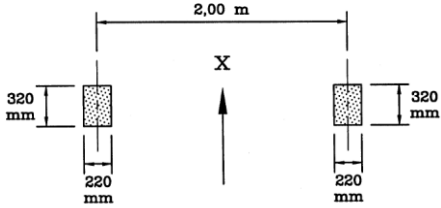
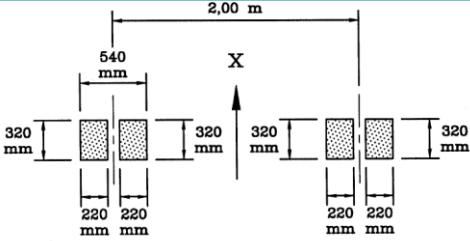
	4.2 1.3	70 120 120	5	A B B
	3.2 5.2 1.3 1.3	70 150 90 90 90	20	A B C C C
	3.4 6.0 1.8	70 140 90 90	15	A B B B
	4.8 3.6 4.4 1.3	70 130 90 80 80	10	A B C C C

Table 33: Equivalent Lorry Information<sup>80</sup>

Wheels and Axles	
Type	Geometrical Definition
A	
B	

<sup>80</sup> (NEN-EN 1991-2 (en): Traffic Loads on Bridges, 2003)

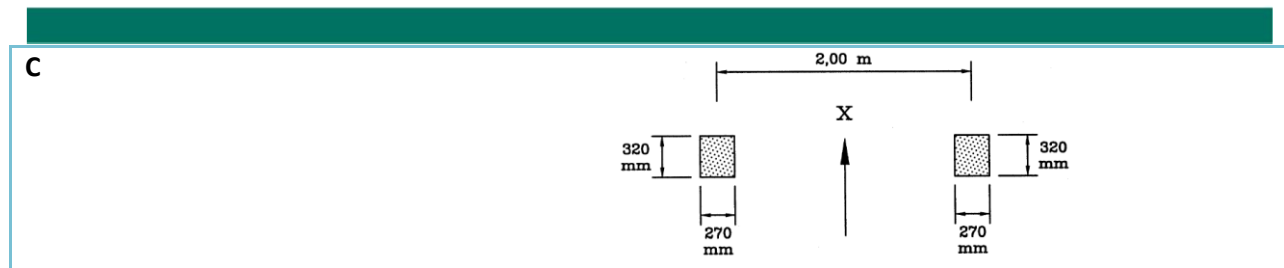


Table 34: Geometrical Information of Wheel Types<sup>81</sup>

In total,  $2.88 \cdot 10^7$  trucks are expected to pass over the bridge during its lifetime. Naturally, these will not all pass over the bridge on the same lane in the same direction. Therefore the trucks are distributed by lane according to Table 35. Note that the distributions of truck types according to Table 33, will be applied on top of the lane-based distribution.

Traffic Lane Distribution		
Direction	Percentage	Number
Passes in direction 1	40	11 520 000
Passes in direction 2	40	11 520 000
Passes in directions 1 and 2	20	5 760 000
<b>Total Passes</b>	<b>100</b>	<b>28 800 000</b>

Table 35: Lane Distribution for Traffic<sup>82</sup>

According to the norms, a dynamic amplification factor needs to be applied. This factor accounts for vibrations resulting in increases in stresses due to the dynamic nature of traffic. The factor needs to be applied on any the bridge in the case that any axle of the crossing truck is with 6 meters of the edge joint of the structure. Considering the length of the bridge and the length of the lorries, an axle will always be within 6 meters of an edge of the bridge. Therefore the factor must be applied to all lorries. The value of the dynamic amplification factor is set as  $\Delta\phi_{fat} = 1.15$ .

### A.3 Serviceability Limit State (SLS)

The serviceability limit state is a set of design criteria based on the maximum deformations a structure may experience while in use. The maximum vertical deflection criteria have been established for the centers of the main beams, the front abutment and the rear abutment. The maximum horizontal displacement is defined for the front abutment. An additional SLS requirement is that the front of the bridge must maintain contact pressure with the support at all times excluding lifting. The maximum deflection criteria have been given in Table 36, along with the displacement obtained from the current design. Note that the rear abutment still exceeds the vertical displacement design criterion. This was accepted since the costs reaching the criterion were deemed disproportional to the consequences of exceedance. For the new design, the rear abutment will be expected to satisfy the criterion.

<sup>81</sup> (NEN-EN 1991-2 (en): Traffic Loads on Bridges, 2003)

<sup>82</sup> (NEN-EN 1991-2: National Annex Steel Bridges, 2011)

Maximum Displacement Criteria		
Location	Design Criteria [mm]	Current Design Results [mm]
Main Steel Girder	32.2	29.5
Front Abutment (Vertical)	5	4
Rear Abutment (Vertical)	5	6.5
Front Abutment (Horizontal)	20	5.8

Table 36: Maximum Displacement Criteria<sup>83</sup>

---

<sup>83</sup> (Hattink, 2014)

## Appendix B: Movable Bridge Types

An elaboration of the different bridge types specified in 3.1.1 Types of Movable Bridges is given below.

### *Trunnion Bascule*

Trunnion bascule bridges rotate around one or two fixed transverse axes. Generally bascule bridges are counterweighted to allow for easier rotation around this axis. A visual of this bridge is given in Figure 67.



Figure 67: Double Trunnion Bascule Bridge<sup>84</sup>

### *Rolling Bascule*

Rolling bascule bridges rotate around one or two moving transverse axes. These are also typically counterweighted for easier rotation. A rolling bascule bridge is shown in Figure 68.



Figure 68: Rolling Bascule Bridge<sup>85</sup>

### *Swing Bridge*

Swing bridges rotate around a fixed vertical axis. This axis can be either on shore for a single sided swing bridge, or in the middle for a two sided swing bridge. A two sided version is shown in Figure 69.

<sup>84</sup> (Wikipedia, 2015)

<sup>85</sup> (Wikipedia, 2015)



Figure 69: Swing Bridge<sup>86</sup>

### *Vertical Lift Bridge*

Vertical lift bridges translate upward along a fixed vertical axis. These bridges still limit the free vertical space when opened. A vertical lift bridge is shown in Figure 70.



Figure 70: Vertical Lift Bridge<sup>87</sup>

### *Submersible Bridge*

Submersible bridges translate downward along a fixed vertical axis. These bridges end up under water when opened. A submersible bridge is shown in Figure 71.

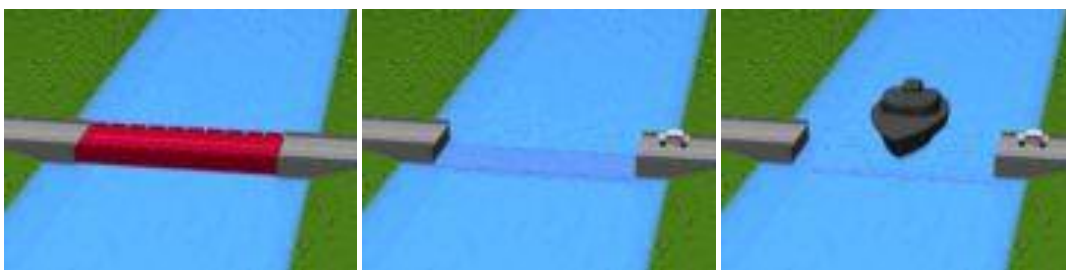


Figure 71: Submersible Bridge<sup>88</sup>

<sup>86</sup> (Wikipedia, 2015)

<sup>87</sup> (Wikipedia, 2015)

<sup>88</sup> (Wikipedia, 2015)



### *Retractable Bridge*

Retractable bridges translate along a longitudinal axis. The bridge connects to both ends of the roadway when closed. A retractile bridge is shown in Figure 72.



Figure 72: Retractable Bridge<sup>89</sup>

### *Transporter Bridge*

Transporter bridges also translate along a longitudinal axis. However, they never connect to both ends of the roadway simultaneously. They ferry passengers across. A transporter bridge is shown in Figure 73.



Figure 73: Transporter Bridge<sup>90</sup>

### *Gyratory*

Gyratory bridges rotate around a fixed longitudinal axis. When open, they still limit the free vertical space. A gyratory bridge is shown in Figure 74.

<sup>89</sup> (Wikipedia, 2015)

<sup>90</sup> (Wikipedia, 2015)



Figure 74: Gyrotory Bridge<sup>91</sup>

### *Folding*

Folding bridges rotate around multiple moving transverse axes. Where each consecutive rotating component rotates in the opposite direction. A folding bridge is shown in Figure 75.



Figure 75: Folding Bridge<sup>92</sup>

### *Curling*

Curling bridges rotate around multiple moving transverse axes. Where each consecutive rotating component rotates in the equivalent direction. A folding bridge is shown in Figure 76.



Figure 76: Curling Bridge<sup>93</sup>

<sup>91</sup> (Wikipedia, 2015)

<sup>92</sup> (Wikipedia, 2015)

<sup>93</sup> (Wikipedia, 2015)

Appendix C: Current Bridge Design

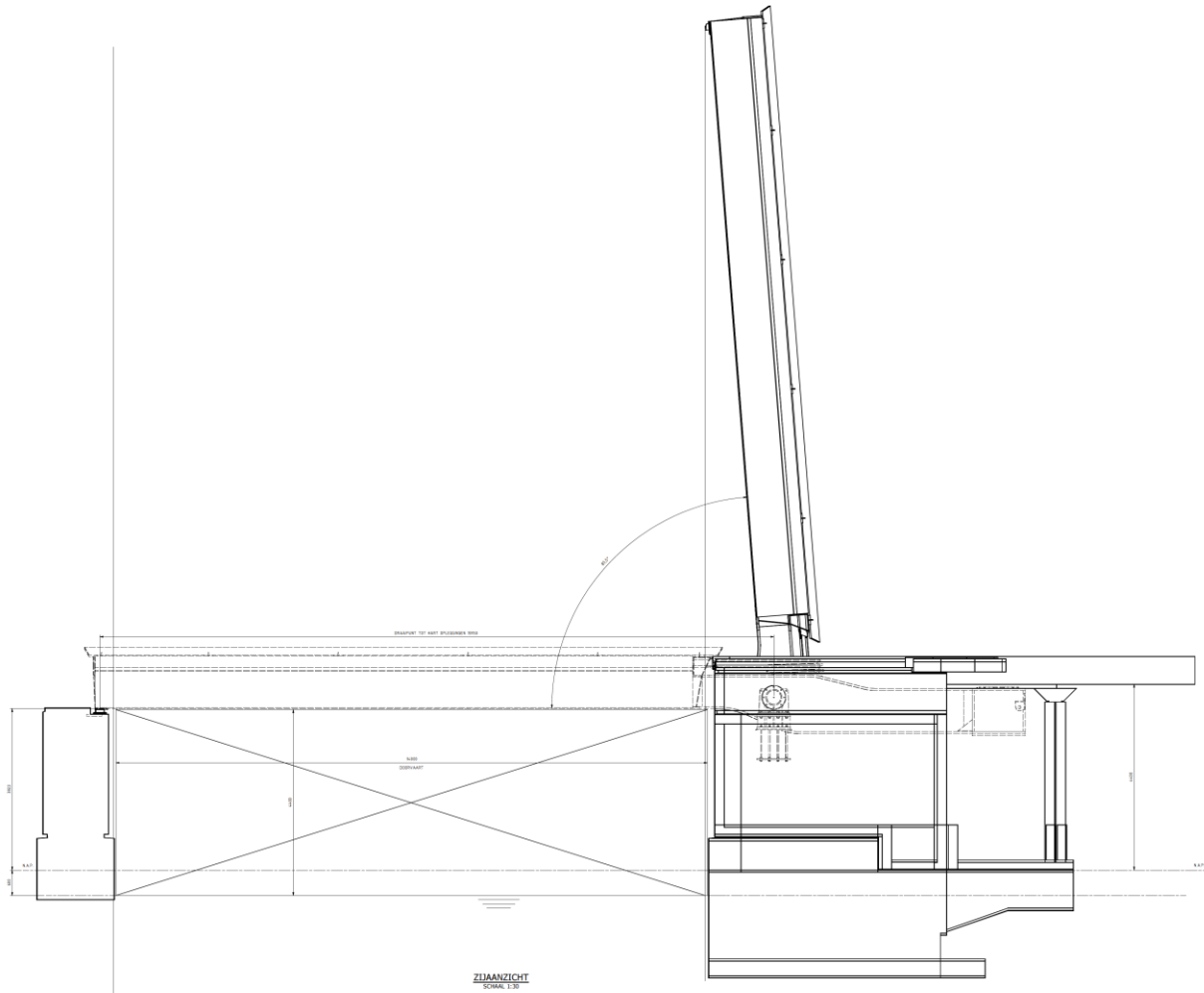


Figure 77: Side View of Bridge<sup>94</sup>

<sup>94</sup> (Offereins)

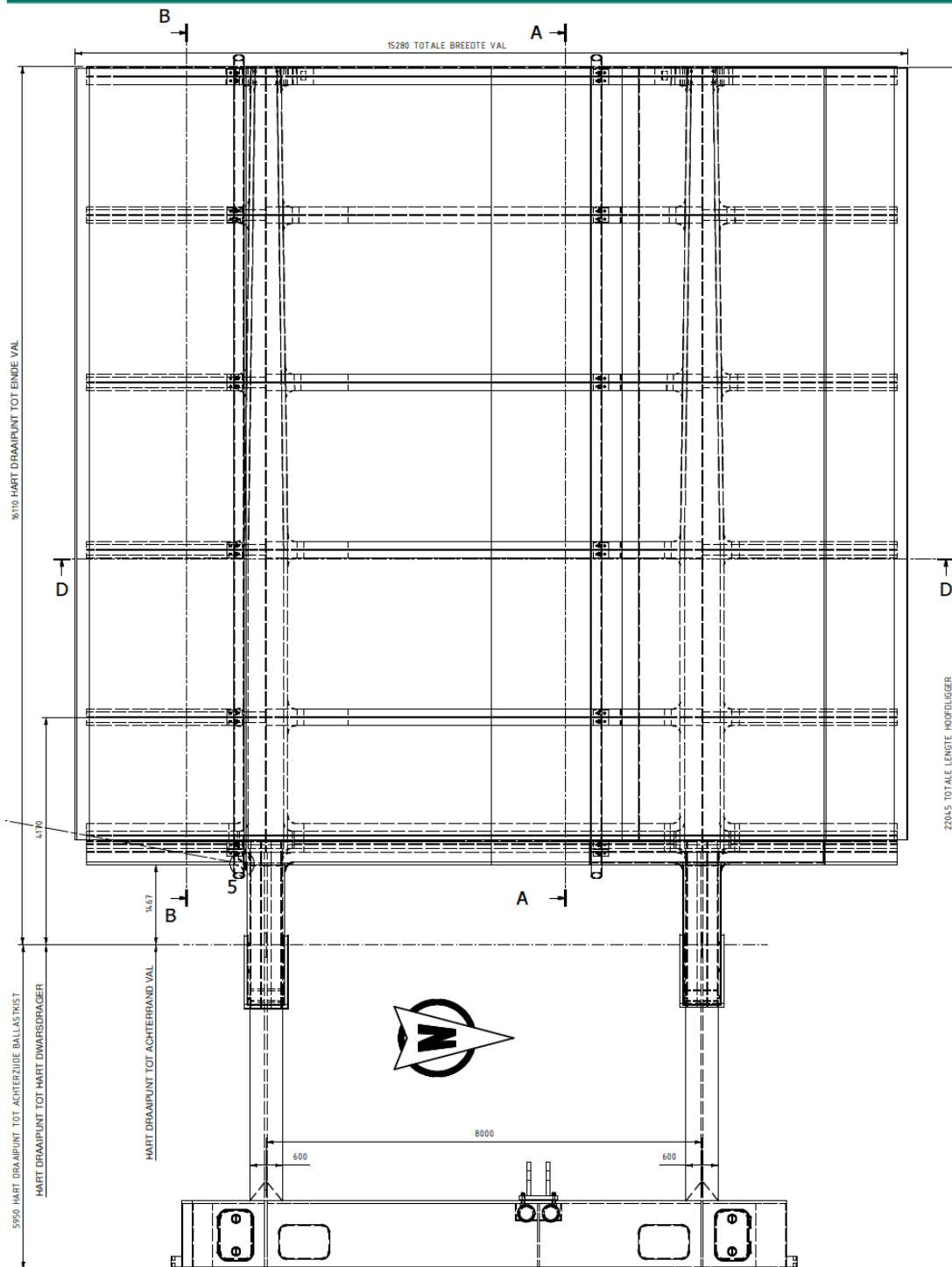


Figure 78: Top View of Bridge Leaf<sup>95</sup>

<sup>95</sup> (Offereins)

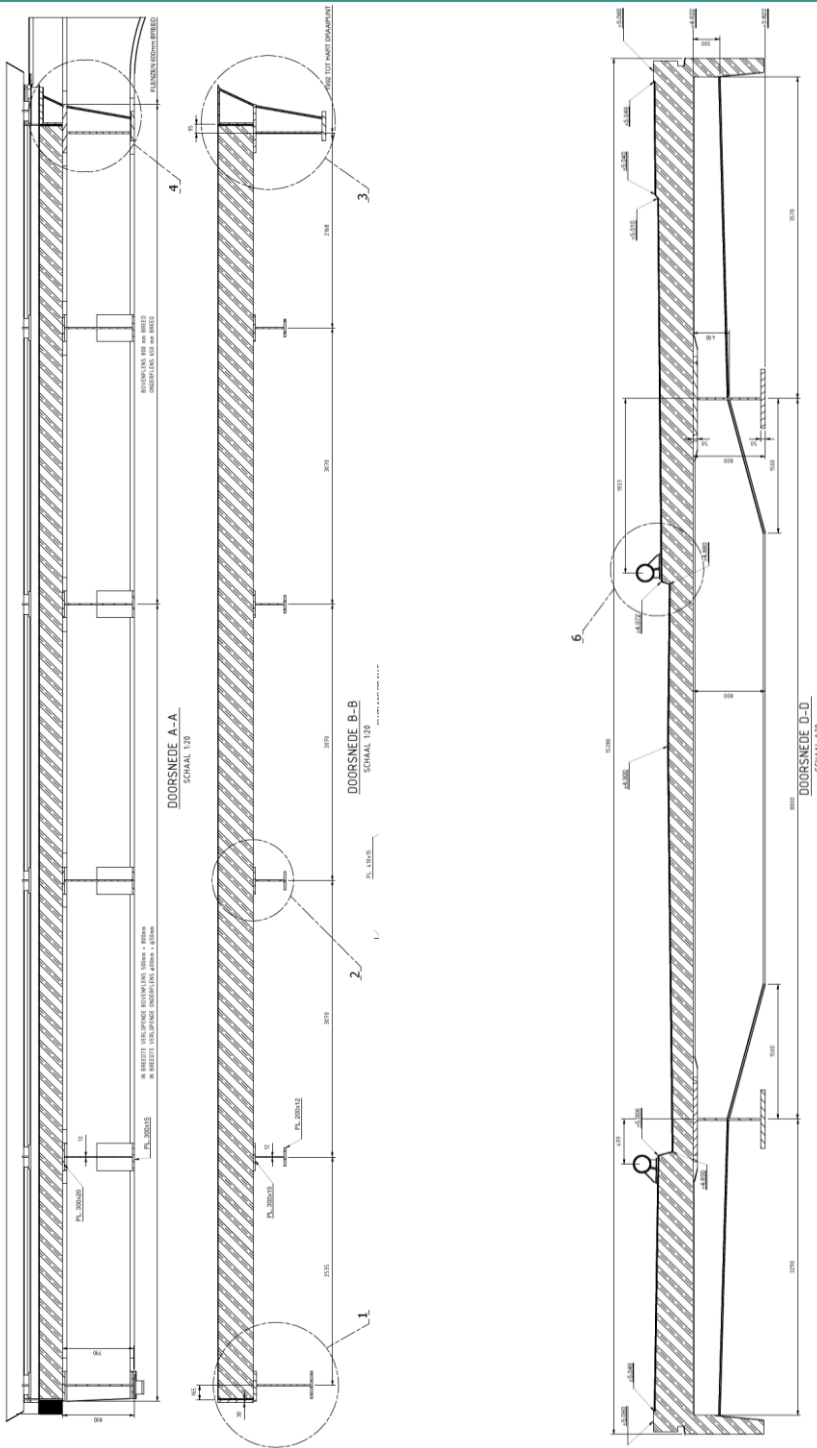


Figure 79: Cross Sections A-A, B-B, and D-D (Left to Right) as Labeled in Figure 78<sup>96</sup>

<sup>96</sup> (Offereins)

## Appendix D: Design Requirements of the Case Study

As part of any design, the design requirements must be listed. These include the locations and types of supports, predetermined dimensions, and design restrictions.

### D.1 Girders and Supports

A reference design was made available, specifying the locations of the supports, as well as preliminary dimensions for the girder locations. These are visible in Figure 80. The main girder locations are set to match with the rotational supports present in the bascule basement.

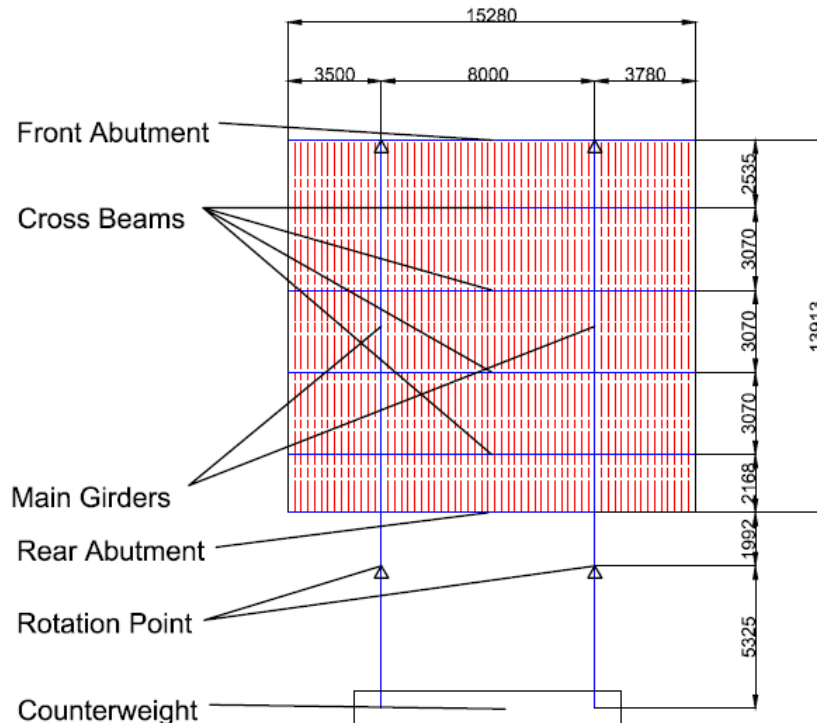


Figure 80: Global Geometry and Support Locations of Julianabrug.

The counterweight is supported by a spring buffer, visible in Figure 81. This spring buffer has the following properties:

- Designed to ensure contact pressure at the front supports
- Spring constant of 27 kN/mm
- Attached to the counterweight at 41 degrees in the x-z plane

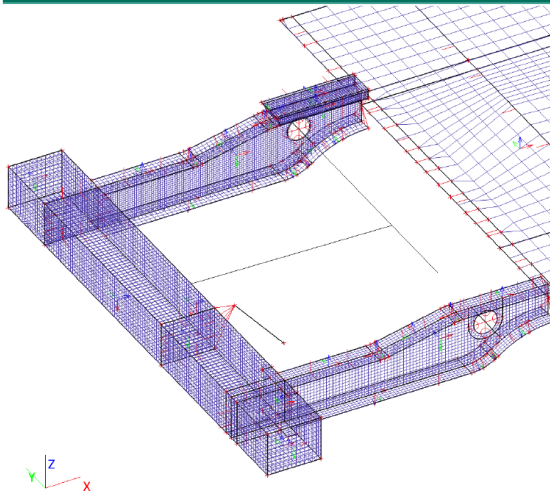


Figure 81: Deployment Spring Buffer<sup>97</sup>

For the finite element models, the counterweight and spring supports will be simplified to regular supports at the ends of the main girders. Such a schematic is presented in Figure 82. Note that the flexibility associated with the spring support as opposed to the fixed support will partially be compensated by not taking into account the increased height of the main girders behind the points of rotation. The functions of the supports are presented in

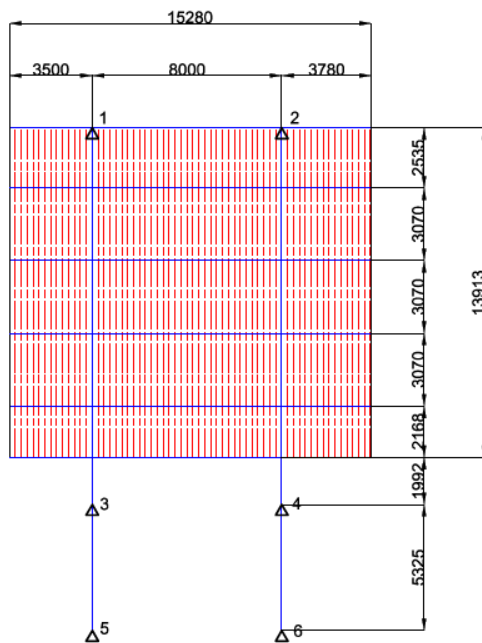


Figure 82: Geometry of Julianabrug With Simplified Rear Supports

<sup>97</sup> (Hattink, 2014)

Functions of Modelled Supports			
Support Number	$U_x$	$U_y$	$U_z$
1	Free	Free	Fixed
2	Free	Free	Fixed
3	Fixed	Fixed	Fixed
4	Fixed	Fixed	Fixed
5	Free	Free	Fixed
6	Free	Free	Fixed

Table 37: Functions of the Supports In Models, Numbers Correspond to Figure 82

## D.2 Height Requirements

There are strict height requirements which must be satisfied in the design of the Julianabrug. These are presented in Figure 83. The bottom of the bridge is limited by the free space requirement for the waterway below. The top of the bridge is limited because the surface of the bridge must connect smoothly to the approaching roadway. For the main structural components (i.e. excluding the wearing surface and sidewalks), this limits the height to 1020mm.

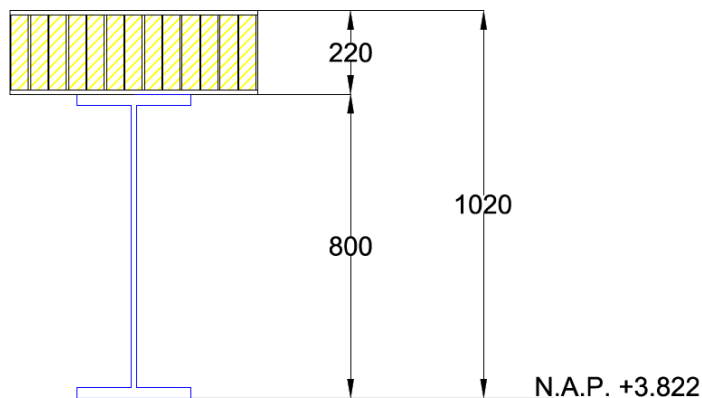


Figure 83: Height Restrictions in The Design of the Julianabrug



## Appendix E: Basics of Fiber Reinforced Polymers

Fiber reinforced polymers (sometimes: fiber reinforced plastics, or simply FRP), are a synthetic composite consisting of fibers and a resin matrix. In general, the fibers provide the strength while the resin is used to bond the fibers together. This section is dedicated to literature review of FRPs, treating the configuration of FRPs, the history of FRPs, the matrix materials, the fibrous materials, and the production processes.

### E.1 Fiber Reinforced Polymer Configuration

Before diving into the detail of composite materials, a short global description is given of the production sequence of FRPs. This sequence is shown in Figure 84. The component materials of FRPs are the fibers and the polymer. These two components are mixed in order to create a lamella, which has distinctly different properties from the two component materials. The lamellas are then stacked to create a laminate, where the lamellas are stacked at varying angles to create strength and stiffness in all directions.

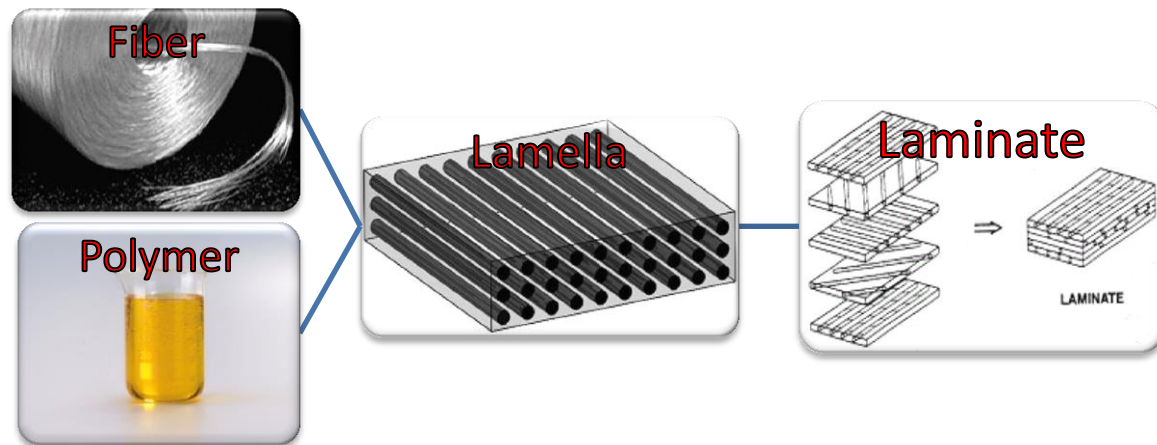


Figure 84 Laminate Build Up<sup>98</sup>

### E.2 History Of Fiber Reinforced Polymers

Evidence of fiber reinforced polymers has been dated as far back as 3000 years ago, when the Ancient Egyptians used glass fibers in resins to create artwork.<sup>99</sup> However, this was a far cry from the

<sup>98</sup> Pictures from: (Direct Industry, 2015), (Core Systems), (Allred & Associates Inc., 2015), (Rijswijk, Brouwer, & Beukers, 2003)

<sup>99</sup> (Kolstein, 2008)

FRP materials we think of today. It took until the 20<sup>th</sup> century for FRPs to start resembling what is used now.

### E.2.1 Polymer History

Polymers are found throughout nature. One of the more well-known polymers is called cellulose, a key component of wood. In 1870 cellulose was first modified into celluloid, a moldable material that took after ivory as it cooled, and would be used in the production of billiard balls. However, cellulose was a natural product, and celluloid was an adaptation of it. The first synthetic (manmade) polymer, Bakelite, was announced in 1909. Bakelite was a phenol-formaldehyde resin, that was initially moldable, but after cooling would not melt again.<sup>100</sup>

Many developments were made with regard to thermoplastics during the 1930s. This development extended into the 1940s when due to World War II, the demand for alternatives to natural materials skyrocketed. Much later, following the invention of linear low density polyethylene in 1978, large scale production of polymeric materials reduced material costs. Thereby making plastics a much more competitive replacement for traditional materials.<sup>101</sup> A Short overview of the inventions of some important plastics is given in Table 38.

Year	Material
1868	Cellulose Nitrate
1900	Viscose Rayon
1909	Phenol-Formaldehyde
1927	Cellulose Acetate
1927	Polyvinyl Chloride
1936	Acrylic
1938	Polystyrene
1939	Nylon
1942	Low Density Polyethylene
1942	Unsaturated Polyester
1952	Polyethylene Terephthalate
1957	Polypropylene
1964	Polyimide
1970	Thermoplastic Polyester
1978	Linear Low Density Polyethylene
1985	Liquid Crystal Polymers

Table 38: Plastic Resin Invention Timeline<sup>102</sup>

<sup>100</sup> (American Chemical Society, 1993)

<sup>101</sup> (U.S. Environmental Protection Agency, 1997)

<sup>102</sup> (U.S. Environmental Protection Agency, 1997)

## E.2.2 Fiber History

Naturally FRPs rely not only on the resin, but also on the fibers. Some fibers occur naturally, such as cellulose fibers, or even glass fibers.<sup>103</sup> As stated, human use of glass fibers has been dated to over 3000 years ago. The creation of synthetic fibers started in the 1880s, when chemical modification of cellulose produced filaments for incandescent light bulbs.<sup>104</sup> Yet the greater application of these fibers lay in the textile industry, where synthetic fibers were used as a replacement for silk.<sup>105</sup> The textile industry continues to dominate fiber production even today, with estimates as high as 59% of all manmade fibers being utilized in textile products.<sup>106</sup> For this thesis, the relevant fibers are those used in FRP construction materials. This specialized use of fibers is dominated by three types of fibers; carbon, glass and aramid.

As mentioned, glass fiber is the oldest of these fibers, as it is naturally occurring, and found as a manmade product over 3000 years ago. Therefore, little is known of how man first started producing glass fibers. What is known however is that the modern method for creating glass fibers was invented in 1933, when it was used to make glass wool as a thermal insulator.<sup>107</sup> Glass fibers nowadays are available in many different forms by altering the glass composition or the coating, and are used in a variety of applications.

Carbon fiber is another well-known type of fiber. In fact, the light bulb filament mentioned above was a primitive carbon fiber. The production of modern carbon fibers started in 1958, when rayon was used as a base, and carbonization through heating yielded fibers. The use of different base materials and newer processes increased the strength and stiffness of carbon fibers. Carbon fibers are mainly used in aerospace and military applications.<sup>108</sup>

Aramid fibers are based on nylon fibers. In the 1950s and 1960s, nylon fibers were chemically altered to produce a compound called Nomex. Later, a different form of aramid was marketed as the relatively well-known Kevlar. Aramid is used in products such as bulletproof vests, aircraft panels, flame-resistant materials and as a replacement for asbestos in some applications.<sup>109</sup>

---

<sup>103</sup> (Macdonald, Abbot, & Peterson, 1983)

<sup>104</sup> (The Editors of Encyclopaedia Britannica, 2013)

<sup>105</sup> (Marshall Cavendish Corporation Staff, 2003)

<sup>106</sup> (U.S. Environmental Protection Agency, 1997)

<sup>107</sup> (Slayter, 1933)

<sup>108</sup> (American Chemical Society, 2003)

<sup>109</sup> (The Editors of Encyclopaedia Britannica, 2015)

### E.2.3 Fiber Reinforced Polymer History

The age of fiber reinforced polymers is said to coincide with the invention of the first synthetic polymer resin; Bakelite. Bakelite itself was brittle and needed to be reinforced.<sup>110</sup> Bakelite was reinforced with cellulose, in the form of sawdust, or asbestos (Where the reinforced form of Bakelite is generally also referred to simply as Bakelite).<sup>111</sup>

The next stage in the history of FRP materials is the creation of glass fiber composites. A few years after the invention of glass wool, it was combined with a polymer resin. This created a composite with good strength properties, so that it seemed a suitable structural material.<sup>112</sup> Glass fiber reinforced polymers (GFRPs), were used mainly in transportation (cars, boats, and airplanes).

The last step into what we view as modern-day FRPs was the introduction of carbon fiber reinforced polymers (CFRPs) and aramid fiber reinforced polymers (AFRPs) in the late 1950s. Since GFRPs had proven their usefulness as a structural material, the invention of carbon and aramid fibers led quite quickly to their being assimilated into the FRP scene. CFRP and AFRP industrial production began in the early 1960s. Their main use continues to be high specification industries where material costs are of secondary importance.<sup>113</sup>

### E.2.4 Previous Applications

In order to have a basis from which to design anything with FRP, it is useful to research in what manner it has been previously applied. In this case, since the goal of this thesis is to design an FRP solution for an old damaged bridge, it seems appropriate to narrow the field of study to the use of FRPs in bridges. Three bridges made partially or entirely out of FRP are highlighted below.

#### *Aberfeldy Footbridge*

The Aberfeldy footbridge is located across the river Tay in Perthshire, Scotland. It is a footbridge commissioned by a golf club to connect two parts of the course. The river is 60m wide at the crossing, and the bridge is 113m long, 2.23m wide and 17.5m tall. The bridge was constructed in 1992, and remains one of the longest span composite bridges to this day.<sup>114</sup>

The Aberfeldy bridge is a cable stayed bridge consisting entirely of FRP, mainly GFRP but the cables of AFRP. The deck was constructed out of 3 different types of modular parts which fit together, known as the advanced composite construction system (ACCS). This system is shown in Figure 85. Three of the “plank” elements shown in Figure 85 were connected across the bridge deck to create the

<sup>110</sup> (American Chemical Society, 1993)

<sup>111</sup> (Meikle, 1997)

<sup>112</sup> (Marsh, 2006)

<sup>113</sup> (Erhard, 2006)

<sup>114</sup> (Stratford, 2012)

walkway. They were connected with the “3-way connectors” and “toggle connectors” to hold them in place prior to the glue setting. The “3-way connectors” were used as transverse supports over the length of the bridge. They were also used to anchor the cables. A schematic representation of the construction is given in Figure 86. Note the Plank components visible in section A-A and the 3-way connector-cable connection visible in detail 1. Figure 87 shows the bridge after completion.

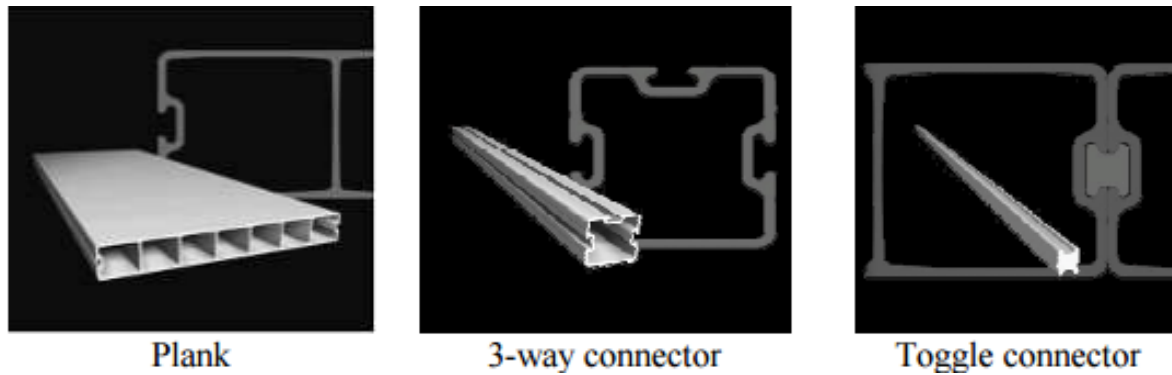


Figure 85: ACCS Components<sup>115</sup>

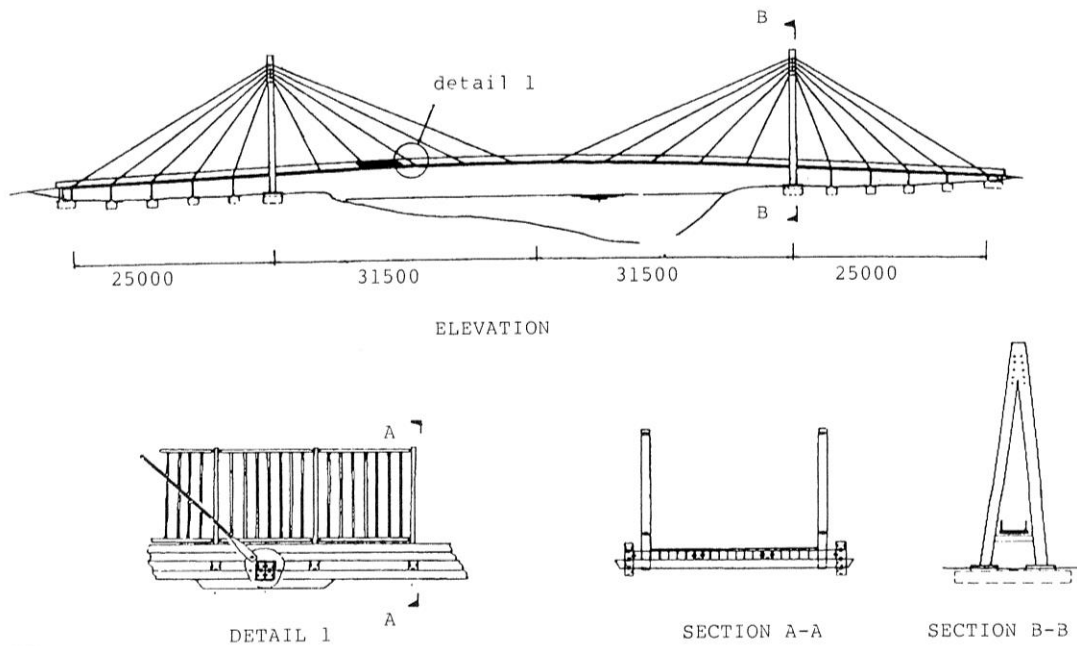


Figure 86: Schematic of Aberfeldy Footbridge Construction<sup>116</sup>

<sup>115</sup> (Stratford, 2012)

<sup>116</sup> (Burgoyne & Head, 1993)



Figure 87: (Left) Deck and Tower of the Aberfeldy Footbridge, (Right) Bottom of Bridge Deck<sup>117</sup>

Due to the low weight of the construction, the bridge was installed very quickly. It took only 8 weeks for a group of students to construct the bridge. The towers were prefabricated and connected to the foundation, while the ACCS components for the deck structure were assembled on location.<sup>118</sup>

The Aberfeldy Footbridge suffered damage in 1997, when a tractor towing a trailer of sand crossed the bridge. Since the bridge was only designed to carry people, this resulted in cracks in several deck components. The bridge was subsequently strengthened to also allow for small traffic to also cross the bridge.<sup>119</sup>

Since this is one of the oldest FRP bridges built, it is the best place to examine the durability of FRP structures. The design lifetime of FRP structures can exceed 100 years, so that the examinations between 2004 and 2011 are not representative of end-of-life scenarios. However, the examination after nearly 20 years was promising. The bridge appeared to have suffered no structural deterioration following a visual inspection. Moss and Lichens have grown over the bridge, yet this is not expected to influence structural properties. However, there are some causes for concern. First, the protective layer over the cables has degraded, which means that the cables are now exposed to the elements. Secondly, there has been impact damage to the bridge. This has caused local damage and local weakening, but does not have a large impact on the strength of the overall structure. Secondly, there has been a slight

<sup>117</sup> (Stratford, 2012)

<sup>118</sup> (Burgoyne & Head, 1993)

<sup>119</sup> (Stratford, 2012)

decrease in the Eigenfrequencies of the structure. This has partially been caused by the added mass due to the repairs in 1997, but another reduction was measured after the repairs. This is believed to be largely caused by moisture content of the GFRP, since these measurements were taken following a wet period.<sup>120</sup>

### *Bonds Mill Roadbridge*

The Bonds Mill Bridge was built in 1994 and crosses the Stroudwater Canal in Gloucestershire, UK. The bridge is a single lift bascule bridge made almost entirely out of FRP, and has span measurements of 8.2m in length and 4.3m in width. The construction of this bridge utilized the same ACCS system as described in 0 Aberfeldy Footbridge. However, in this case, to achieve the necessary height, the components were combined to form a box girder. The components of the ACCS were combined into a 3 box girder as shown in Figure 88. To obtain the necessary width, two of these girders were laid next to each other and glued together. The ACCS components were, like before, manufactured out of glass fiber reinforced polymers. Foaming epoxy was used to fill the compressive flanges and webs to provide stability and help with load transfer. The Bonds Mill Bridge is shown in Figure 89.<sup>121</sup> Note the uncommonly large height to span ratio which has been applied in order to stiffen the structure. Steel-Concrete bridges can have height to span ratios easily exceeding 1:30<sup>122</sup>, where the Bonds Mill Bridge fails to reach 1:11. In urban areas where a bridge must connect to an incoming road, while minimizing the limits placed on the free space below, this increased structural height is a major disadvantage.

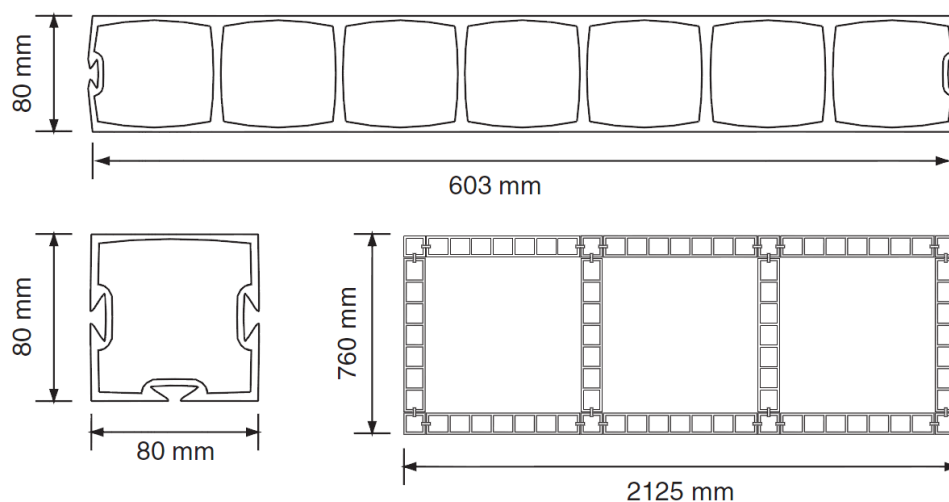


Figure 88: Cross Section of ACCS components and load bearing structure of half of Bonds Mill Bridge<sup>123</sup>

<sup>120</sup> (Stratford, 2012)

<sup>121</sup> (Network Group for Composites in Construction, 2013)

<sup>122</sup> (JFE Engineering Corporation, 2014)

<sup>123</sup> (Hewson & Parke, 2008)



Figure 89: Bonds Mill Bridge<sup>124</sup>

The use of FRP in this bridge was motivated by some external factors. The original plan called for a steel bridge, but the steel supplier tripled the price of their original estimate prior to construction. Therefore, the decision was made to proceed with an FRP structure. The Bonds Mill Bridge weighed 4.5 tonnes, but could carry a truck up to 38 tonnes.<sup>125</sup> The low self-weight of the bridge meant that the original abutments could be reused (after repairs and modifications), and no counterweights were required. This combination of factor meant the FRP option became a competitive economic option compared to the steel option. Many problems have plagued the bridge since its opening in 1994. However, none of the problems were of a structural nature, and none related to the FRP. Most problems were associated with the hydraulics, but problems were also present for some secondary construction elements. The problems are listed below:

- The Hydraulics
  - Were designed with insufficient strength,
  - Showed imbalance during lifting causing twisting of the deck
  - Contained air pockets leading to vibrations.
- Edging along the bridge came loose
- The wearing surface deteriorated very quickly<sup>126</sup>

<sup>124</sup> (Network Group for Composites in Construction, 2013)

<sup>125</sup> (Hollaway, 2001)

<sup>126</sup> (Company of Proprietors of the Stroudwater Navigation, 2010)



The Bonds Mill Bridge was the first moveable FRP bridge. Two major theoretical advantages in reducing the weight of a bridge came to fruition in this project. Namely, the abutments could be reused and the counterweight was removed. This construction has proven that the use of FRPs is possible in moveable bridges.

### *Friedberg Bridge*

The Friedberg Bridge was built across the B3 Highway in Friedberg, Germany in 2008. It is 27m long in total with a span of 21.5m and a width of 5m. The road across the bridge is a small country road, but should therefore be able to withstand the load of vehicles. The superstructure consists of the ASSET deck system glued onto two parallel steel girders. The ASSET deck (Advanced Structural Systems for Tomorrow's Infrastructure), is a modular sandwich panel system with triangular cross sections, as shown in Figure 90. A second layer of the deck was added along the longitudinal edges to create a curb. Similarly to the other two bridges, this deck was also manufactured out of glass fiber reinforced polymer.<sup>127</sup> A schematic of the bridge is visible in Figure 91.

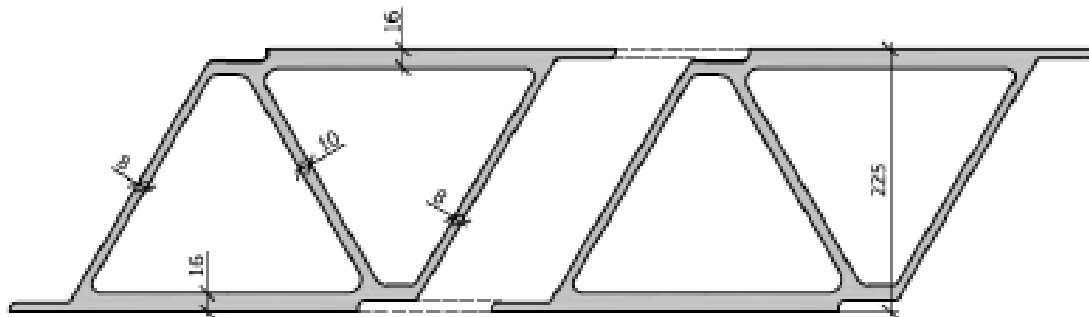


Figure 90: ASSET Deck System<sup>128</sup>

<sup>127</sup> (Knippers & Gabler, The FRP road bridge in Friedberg Germany - new approaches to a holistic and aesthetic design, 2008)

<sup>128</sup> (Knippers & Gabler, New Design Concepts for Advanced Composite Bridges - The Friedberg Bridge in Germany, 2006)

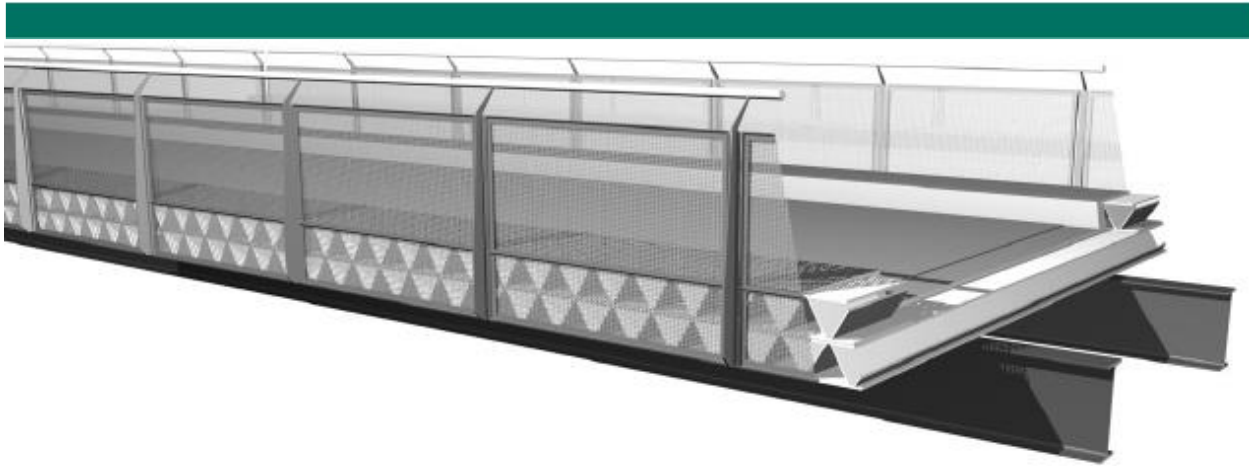


Figure 91: Schematic of the Friedberg Bridge<sup>129</sup>

While the bridge itself was meant for a small country road, it crossed a much larger road: the B3 Highway. It was desired that this road should be closed for a minimal duration. This was achieved since the installation of the Friedberg bridge took only one day. This was possible because a majority of construction took place in a factory, so that the main span was complete upon arrival. The light weight meant it could be hoisted into position relatively quickly, and only the connections were still necessary.<sup>130</sup> The installation of the bridge is shown in Figure 92.

<sup>129</sup> (Knippers & Gabler, The FRP road bridge in Friedberg Germany - new approaches to a holistic and aesthetic design, 2008)

<sup>130</sup> (Knippers & Gabler, The FRP road bridge in Friedberg Germany - new approaches to a holistic and aesthetic design, 2008)



Figure 92: Installation of Friedberg Bridge<sup>131</sup>

This bridge is believed to be the first bridge in which composite action between steel and FRP materials is utilized. This is achieved by creating an adhesive bond between the steel and the FRP Deck. Introducing composite action should stiffen and strengthen the bridge, so that the steel-FRP composite is expected to displace 20% less under loading than the steel girders alone would have.<sup>132</sup>

<sup>131</sup> (Kable)

<sup>132</sup> (Knippers & Gabler, The FRP road bridge in Friedberg Germany - new approaches to a holistic and aesthetic design, 2008)

## Appendix F: Components of Fiber Reinforced Polymers

The composite materials described above are naturally very dependent on its constituents. Therefore, it is necessary to give a description of both the fibers and the resin materials which are typically applied in synthetic composites. Using the background information regarding the different available constituents will allow for a choice to be made regarding which ones to apply to this thesis. In addition the production processes used to combine the fibers and the resin will be described.

### F.1 Fibers

Fiber Reinforced Polymers derives most of their strength properties from the fibers embedded in the matrix. These fibers tend to have much better mechanical properties than the matrix, so that in general fiber contents of FRPs will be as high as possible. There are three relevant types of fibers, namely: glass, carbon and aramid.

- Glass fibers
  - Most commonly used fibers in structural engineering
  - Produced by drawing thin filaments of glass from a molten reservoir
  - Filaments
    - Vary in diameter from 3 to 24  $\mu\text{m}$
    - Clustered into groups of 200
    - Undergo a surface treatment
    - Wound onto a drum
  - Adaptable chemical composition
    - Alters its properties
    - Multiple types
  - E-glass
    - High Electrical Resistance
    - Cheap
  - S-glass
    - Stronger
    - Better resistance to environmental factors.<sup>133</sup>
- Carbon fibers
  - Carbon in crystalline form
  - Created from
    - Polyacrylonitrile (PAN)
    - Pitch fibers
  - Created by

---

<sup>133</sup> (Hewson & Parke, 2008)

- Spinning into fibers
  - Heating to temperatures exceeding 1200°C (Up to 3000°C)
  - As the fibers are heated:
    - First oxygen is absorbed
    - Secondly, carbon crystals are formed
    - Finally, crystallites become oriented
  - Commonly, 12000 filaments combined into strand
  - Increasing orientation of crystallites increases modulus of elasticity
    - Results from increasing production temperature
  - Categorized by their modulus
    - High Modulus
    - Ultra-High Modulus.<sup>134</sup>
- Aramid fibers
  - Polymer strands consisting of:
    - Benzene rings
    - Amide groups
  - Created by
    - Cooling to -50°C to -80°C
    - Dissolving
    - Spinning solution
    - Draw filaments into a cylinder
      - Temperature around 200°C
      - Evaporate the solvent
      - Leaving a fiber
  - Large variation in stiffness
    - Stiffer fibers used in construction composites
    - Flexible fibers used in cables and body armor.<sup>135</sup>

The mechanical properties of each of these fibers is different. In fact, each fiber material has multiple types of fibers due to different chemical compositions or production processes. To give an idea of the properties one may expect from these fibers, typical values are given in Table 39 and stress strain curves for various materials are given in Figure 93.

---

<sup>134</sup> (Hewson & Parke, 2008)

<sup>135</sup> (Hewson & Parke, 2008)

Fiber Properties				
Material	Fiber Type	Elastic Modulus [GPa]	Tensile Strength [MPa]	Ultimate Strain [%]
Glass	E	72	2400	3.50
	A	72	3030	3.50
	S2	88	4600	5.70
Carbon Fiber (PAN Based)	IM	300	5200	1.73
	HM	450	3500	0.77
	HS	260	5020	2.00
Carbon Fiber (Pitch Based)	T300	228	2758	1.76
	T500	241	3448	1.79
	T600	241	4137	1.80
	T700	248	4551	1.81
Aramid Fiber	49	125	2760	2.40
	29	83	2750	4.00

Table 39: Typical Properties of Fibers<sup>136</sup>

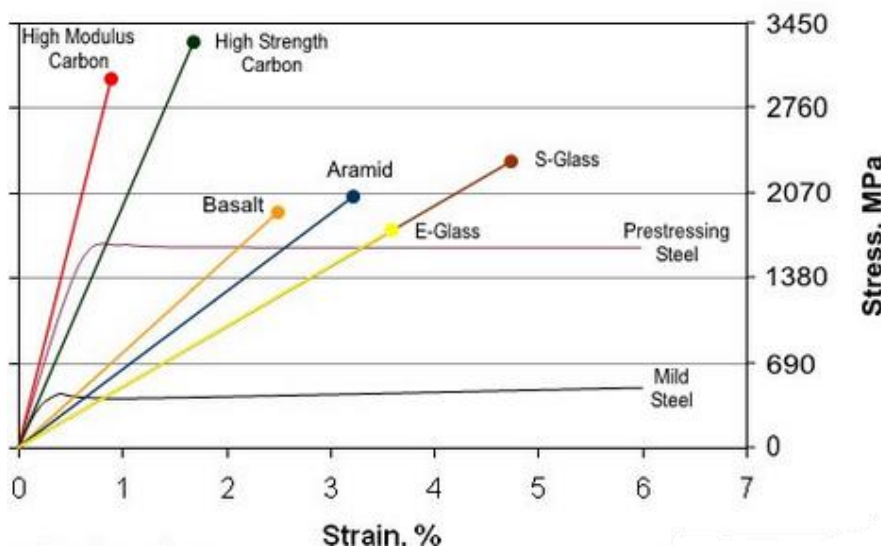


Figure 93: Stress-Strain Curve Various Fiber Materials and Steels<sup>137</sup>

<sup>136</sup> (Hewson & Parke, 2008)

<sup>137</sup> (Prince Engineering, 2015)

### F.1.1 Fiber Products

A single fiber, be it of any of the materials mentioned in Table 39, is generally of little use. Therefore, so called fabrics are created. Fabrics are defined as “a manufactured assembly of long fibres of carbon, aramid or glass, or a combination of these, to produce a flat sheet of one or more layers of fibres. These layers are held together either by mechanical interlocking of the fibres themselves or with a secondary material to bind these fibres together and hold them in place, giving the assembly sufficient integrity to be handled.”<sup>138</sup> Fabrics come in several forms, including Unidirectional, Woven, Continuous Filament Mats (CFM) and Chopped Strand Mats (CSM). A fiber product which is not classified as a fabric, but is still relevant is the continuous filament roving.

The unidirectional (UD) fabric is a fabric with the majority of the fibers oriented in one direction. This gives it anisotropic mechanical properties, being much stronger and stiffer in the direction of the fibers. To give some stability perpendicular to the main fiber orientation, a small fraction may be laid down perpendicularly. Typically the fibers are oriented in the lengthwise direction of the fabric, but occasionally may be perpendicular to the length of the fabric.<sup>139</sup>

Woven fabrics come in many different types. They consist of fibers running in the 0° direction and the 90° direction. By weaving the fibers together, more stability is generated compared to UD fabrics. Also, mechanical properties in the transverse direction can be greatly enhanced.<sup>140</sup> Some typical types of weaves are shown in Figure 94.

---

<sup>138</sup> (Cripps, 2015)

<sup>139</sup> (Cripps, 2015)

<sup>140</sup> (Cripps, 2015)

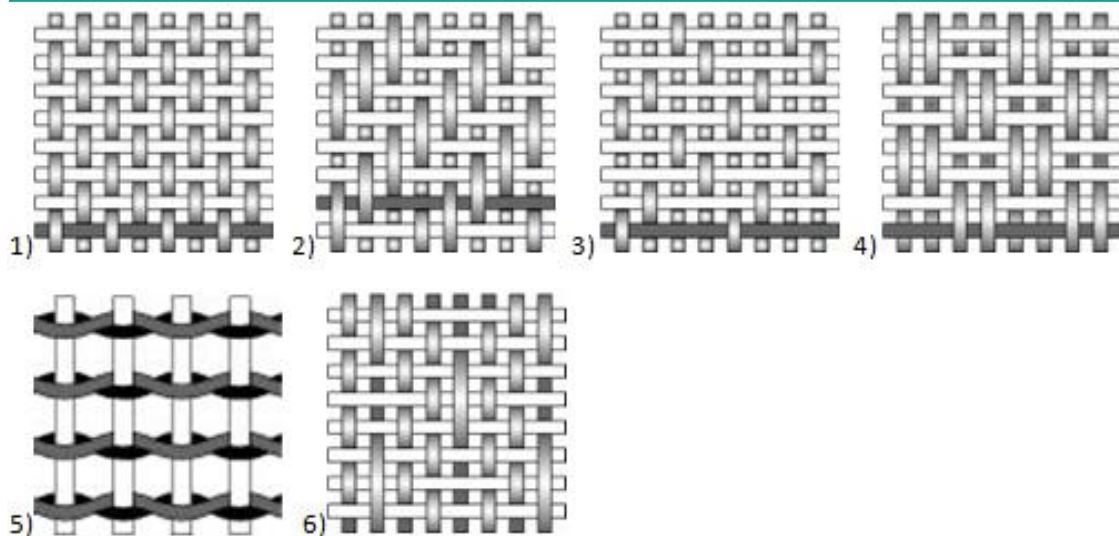


Figure 94: Various Types of Weaves. In order: 1) Plain, 2) Twill, 3) Satin, 4) Basket, 5) Leno, 6) Mock Leno<sup>141</sup>

Continuous filament mats (CFM) and chopped strand mats are mats in which the fibers are randomly laid out onto on another. This creates a convoluted network of fibers which has transversal isotropic properties. In CFMs the fibers used are continuous while in CSMs, the fibers are first chopped into relatively short strands. The interlocking is not enough to provide the mat with stability, so that a binding agent<sup>142</sup> is applied to hold the mat together.<sup>143</sup> A schematic for direction strength of the fabrics and mats is given in Figure 95.

<sup>141</sup> (Cripps, 2015)

<sup>142</sup> Note that this binding agent is not the same as the matrix which will be discussed later.

<sup>143</sup> (Kolstein, 2008)



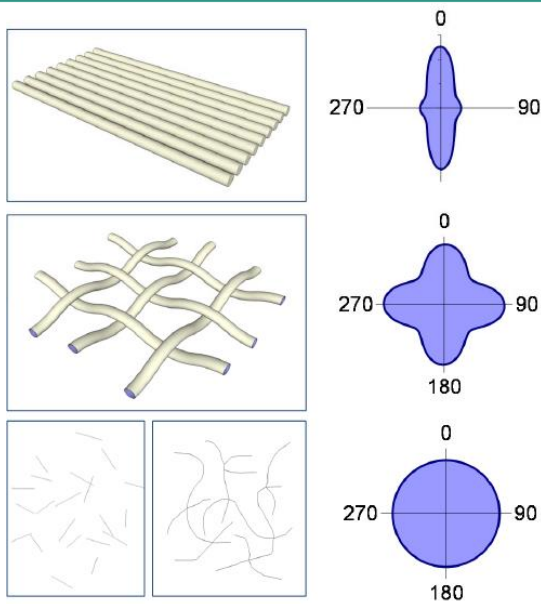


Figure 95: Schematic of Directional Strength (Top: UD Fabric; Middle: Woven Fabric; Bottom Left: CSM; Bottom Right: CFM)<sup>144</sup>

Finally, the continuous filament roving is worth mentioning. This consists of unwoven and untangled fibers which are wound onto a spool. These can feed out the fibers during a later stage of FRP production. Several spools feeding out glass fiber can be seen in Figure 96.



Figure 96: Glass Fiber Spools<sup>145</sup>

<sup>144</sup> (Nijssen, 2013)

## F.1.2 Fiber Prices

For many FRP applications nowadays, cost is generally considered a secondary factor. Carbon fiber tends to be heavily used in the aerospace industry and the specialized sporting industry. Aramid fibers are used in manufacture of body armor. These are typical industries in which higher costs can be compensated by either weight savings or enhanced performance. But for civil engineering applications, when large quantities of the materials are required, the costs must be considered. Therefore the price ranges of the fibers are given in Table 40. Note that the prices are in pounds Sterling per kg. Based on the prices shown here, and comparing these to the mechanical properties in Table 39, we can see that the E-glass fibers represent the best performance to price ratio.

Typical Fiber Costs		
Fiber Type	Lower Cost Estimate	Upper Cost Estimate
	[£/kg]	[£/kg]
<b>E-glass</b>	1	2
<b>S-Glass</b>	12	20
<b>Aramid</b>	15	25
<b>Carbon Fiber</b>	15	40

Table 40: Fiber Prices<sup>146</sup>

## F.2 Matrix Phase

The Matrix Phase refers to the polymer aspect of FRPs. The matrix has several critical tasks, including:

- locking the fibers in place,
- coating the fibers so as to protect against corrosion and erosion,
- to transfer stresses between fibers
- to prevent fibers from buckling

There are three main types of polymers which are currently used for composites. These are the thermoplastic polymers, the elastomers, and the thermosetting polymers. All three are organic molecules, but they have different properties.

- Thermoplastic Polymers
  - Long chained organic molecules
  - Held together by local magnetic forces, known as Van der Waals forces
    - Forces are dependent on molecular weight
    - Longer chains show better mechanical properties

<sup>145</sup> (Composites World Staff, 2014)

<sup>146</sup> (Cripps, 2015)

- Weak compared to ionic, or covalent bonding
    - Some types show visco-elastic behavior
    - Better alternatives available for structural components
      - Thermoplastic polymers mainly used in geotextiles.<sup>147</sup>
  - Elastomers
    - Chemically similar to thermoplastics
    - Consist of long chained organic molecules
      - Arbitrarily wound about each other
        - Elastomers show a large degree of flexibility.
      - Matrix is vulcanized
        - Creates covalent bonds between the molecules
          - Stronger than the Van der Waals forces
          - Stiffer than thermoplastics
    - Mainly used for bearings.<sup>148</sup>
  - Thermosetting Polymers
    - Curing reaction
      - Covalent bonds created
      - Mechanical properties affected by
        - Quantity of the covalent bonds
        - Network of covalent bonds
    - Three types utilized
      - Epoxies
      - Vinylesters
      - Unsaturated polyesters
    - Most used matrix material for structural components.<sup>149</sup>

### F.2.1 Thermosetting Polymers

Thermosetting polymers are by far the most commonly used in FRP materials used in civil engineering applications. Yet, thermosetting polymers also come in several different variants. Therefore, the three most common types of thermosetting polymers will be discussed in more detail. These are unsaturated polyester, vinylester, and epoxy.

- Unsaturated polyesters
  - Three groups
    - Orthophthalic

---

<sup>147</sup> (Hewson & Parke, 2008)

<sup>148</sup> (Hewson & Parke, 2008)

<sup>149</sup> (Hewson & Parke, 2008)

- Isophthalic
  - Bisphenol A
  - As listed above they are ordered in terms of increasing quality
    - Strength
    - Thermal properties
    - Chemical resistance
  - Used in pultrusion components (see F.3 Production Process)
  - Low costs.<sup>150</sup>
- Vinylesters
  - Similar to polyester resins
  - Toughened by mixing with epoxy
  - Compared to polyesters
    - Less susceptible to hydraulic degradation
    - Less susceptible to chemical degradation
    - Similar mechanical properties.<sup>151</sup>
- Epoxies
  - Best quality
    - Better mechanical properties
    - Better thermal properties
    - Better shrinkage properties
    - Better corrosion resistance
  - Preferred as a matrix material
  - Used as adhesive between different FRP surfaces
  - Curing agent required
    - Resin and curing agent must be mixed in exact proportions
      - Improper mixing leaves pockets of unreacted material
  - More expensive than other matrix materials.<sup>152</sup>

Similarly to the fibers, the mechanical properties of each type of thermoset is different. Therefore typical values for resin properties are given in Table 41.

---

<sup>150</sup> (Hewson & Parke, 2008)

<sup>151</sup> (Hewson & Parke, 2008)

<sup>152</sup> (Hewson & Parke, 2008)

Resin Properties			
Material	Ultimate Tensile Strength	Modulus of Elasticity in Tension	Coefficient of Thermal Expansion
	MPa	GPa	10 <sup>-6</sup> /K
<b>Polyester</b>	45-90	2.5-4.0	100-110
<b>Vinylester</b>	90	4	80
<b>Epoxy</b>	90-110	3.5	45-65

Table 41: Typical Properties of Matrix Materials<sup>153</sup>

### F.2.2 Resin Costs

The costs of the different resins is important when selecting which type to apply to a given structure. There are many different forms of each type of thermosetting polymer, and the price will vary depending on the specific type chosen. The typical price ranges for each of these thermosets is given in Table 42.

Typical Resin Costs		
Resin Type	Lower Cost Estimate	Upper Cost Estimate
	[£/kg]	[£/kg]
<b>Polyester</b>	1	2
<b>Vinylester</b>	2	4
<b>Epoxy</b>	3	15

Table 42: Typical Resin Costs<sup>154</sup>

### F.3 Production Process

The fibers and the matrix need to be combined into a useful product. However, there are many ways in which this can be achieved. Several of these will shortly be described below.

#### *Spray Lay-up*

Continuous fiber is fed into a gun where it is chopped and mixed with resin. The mixture is sprayed from the gun directly onto a mold. This is a cheap manufacturing process, but produces FRP with low quality.<sup>155</sup>

<sup>153</sup> (Hewson & Parke, 2008)

<sup>154</sup> (Cripps, 2015)

<sup>155</sup> (Cripps, 2015)

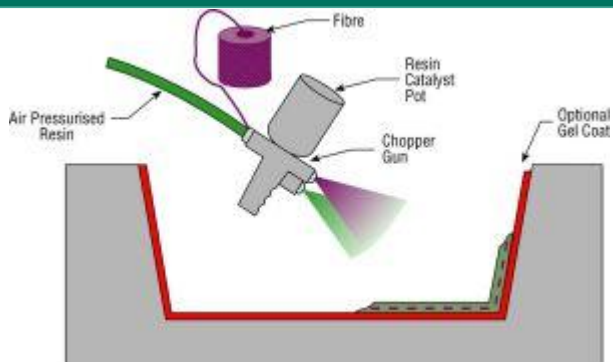


Figure 97: Spray Lay-up Method<sup>156</sup>

### Wet Lay-up

A fabric is laid down onto a mold. The resin is then poured onto and spread over the fabric. This is another relatively cheap production process, but also produces a relatively weak FRP.<sup>157</sup>

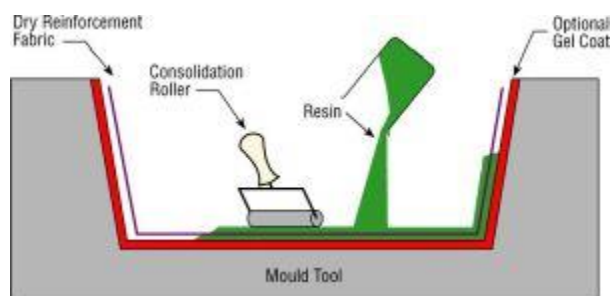


Figure 98: Wet Lay-up Method<sup>158</sup>

### Vacuum Bagging

Vacuum Bagging builds on the wet lay-up process. After the fabric has been impregnated, a bag is placed over the mold and drawn to a (near) vacuum. The pressure this applies to the material helps consolidate it producing a lower resin content fiber.<sup>159</sup>

<sup>156</sup> (Cripps, 2015)

<sup>157</sup> (Cripps, 2015)

<sup>158</sup> (Cripps, 2015)

<sup>159</sup> (Cripps, 2015)

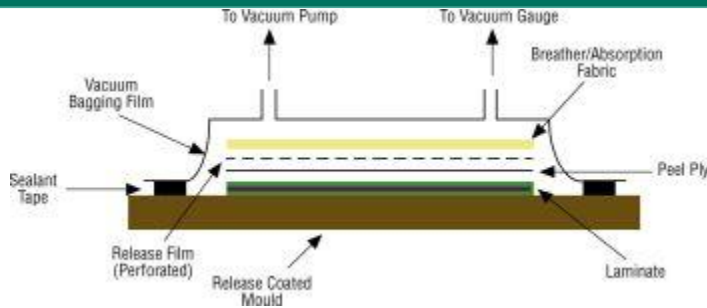


Figure 99: Vacuum Bagging Method<sup>160</sup>

### Filament Winding

Filament winding is a method by which continuous fibers are passed through a resin bath after which they are wound onto a convex mold. This method is particularly suited to creating tanks and pipes.<sup>161</sup>

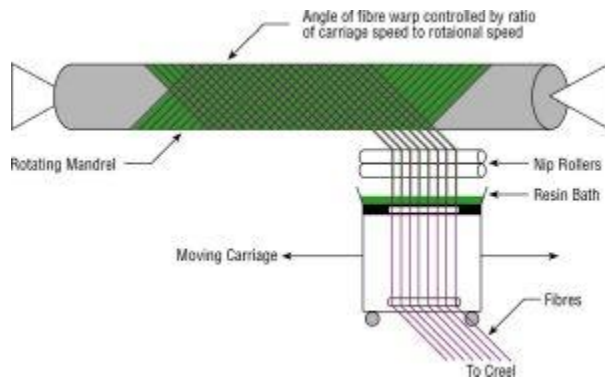


Figure 100: Filament Winding Method<sup>162</sup>

### Pultrusion

During pultrusion continuous profiles are made. Fibers or fabrics are pulled through a forming die, which determines the shape of the cross section. Resin may be introduced prior to the die, or injected into the die. After leaving the die the profiles can be cut to the desired length.<sup>163</sup>

<sup>160</sup> (Cripps, 2015)

<sup>161</sup> (Cripps, 2015)

<sup>162</sup> (Cripps, 2015)

<sup>163</sup> (Cripps, 2015)

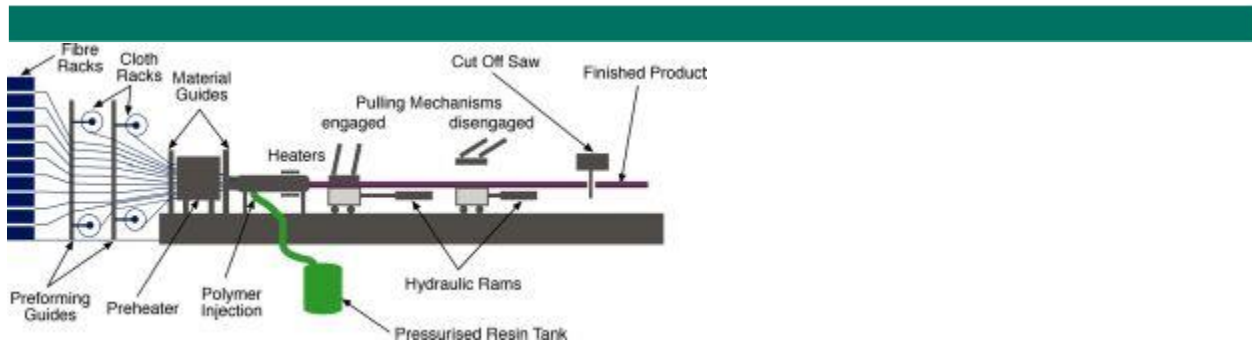


Figure 101: Pultrusion Method<sup>164</sup>

### Resin Transfer

During resin transfer, fabrics are placed onto a mold. A negative mold then closed over the first mold, after which the resin is injected into the mold.<sup>165</sup>

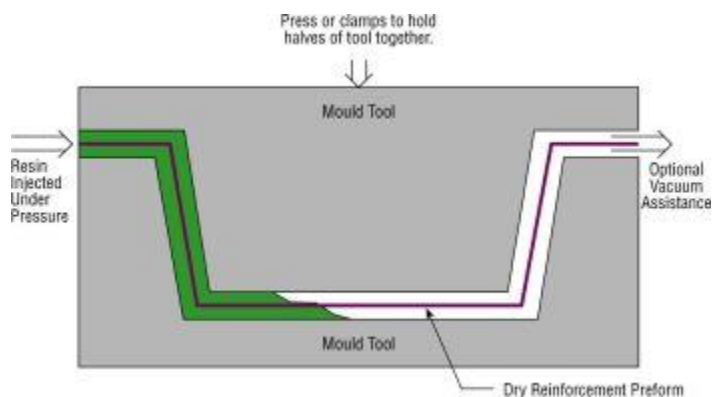


Figure 102: Resin Transfer Method<sup>166</sup>

### Infusion Processes

There are multiple types of infusion processes, but the basis is described here. Fabrics are laid over a mold and covered with a highly permeable extra layer. The fabrics are drawn to a vacuum, after which the resin is allowed to flow into the mold. The extra layer of fabric provides an easy path of flow for the resin to impregnate the entire mold.<sup>167</sup>

<sup>164</sup> (Cripps, 2015)

<sup>165</sup> (Cripps, 2015)

<sup>166</sup> (Cripps, 2015)

<sup>167</sup> (Cripps, 2015)



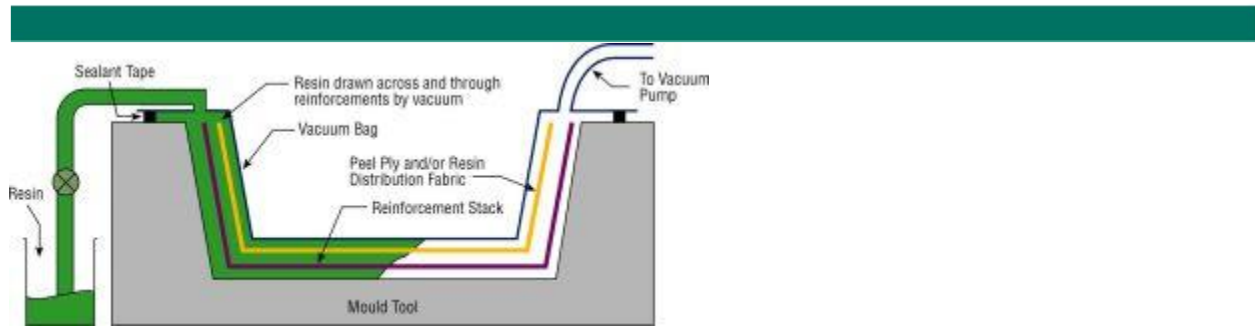


Figure 103: Infusion Process Method<sup>168</sup>

### Prepreg Molding

Pre-impregnated molding begins during the manufacture of the fibers and fabrics. The manufacturer includes a pre-catalyzed resin into their fabric, which is inactive for several weeks. These fabrics can be stored until needed (Storage is typically limited to several months), after which they can be placed onto a mold. To cure the resin, heat is applied, typically combined with extra pressure from an autoclave. There are low temperature low pressure variants available.<sup>169</sup>

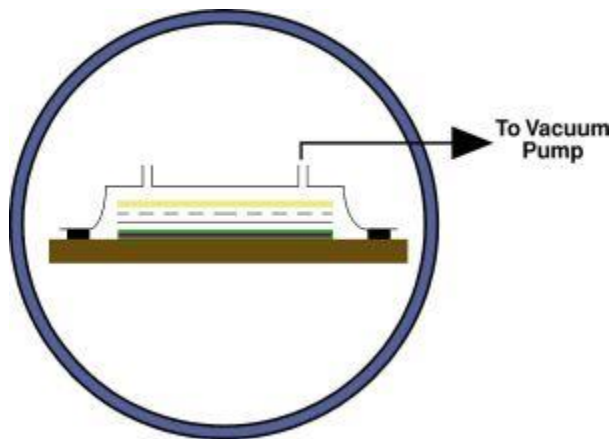


Figure 104: Prepreg Molding Method<sup>170</sup>

### Resin Film Infusion

During resin film infusion fabrics and films resin on release paper are laid over a mold. The fabric stack is vacuum bagged and heated to melt the resin. The resin can then impregnate the fabrics.<sup>171</sup>

<sup>168</sup> (Cripps, 2015)

<sup>169</sup> (Cripps, 2015)

<sup>170</sup> (Cripps, 2015)

<sup>171</sup> (Cripps, 2015)

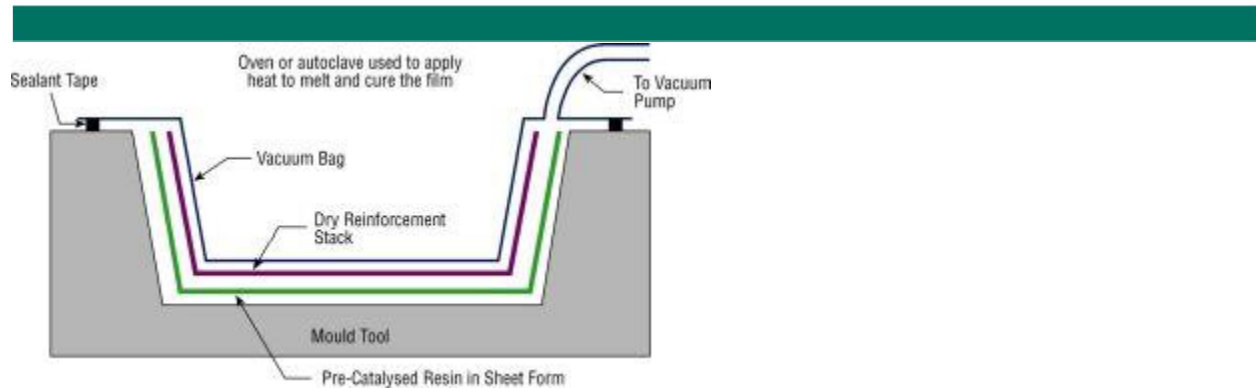


Figure 105: Resin Film Infusion Method<sup>172</sup>

Not all of the production processes named above are suitable for civil engineering applications. For instance, prepreg molding in an autoclave will naturally produce elements which are of a limited size. Resin transfer or infusion methods, require time for the resin to permeate the entire fabric. Since the resin sets after a short time, these methods would need many injection sites to produce the desired product. This is possible, but not always equally practical.

The pultrusion, the wet lay-up, and the vacuum bag methods are most common in civil engineering. Filament winding may also be used if pipe elements are required. The pultrusion process is used when profiles are needed. These can be typical I- or H-profiles as is common, but also triangular, double I, or rectangular may be produced. For instance, the ACCS deck system (Figure 85) and the ASSET deck system (Figure 90), were produced using the pultrusion method. The wet lay-up and vacuum bagging techniques will be applied in the case of inconsistent cross sections and large, typically planar, components.

<sup>172</sup> (Cripps, 2015)

## Appendix G: Lamella Properties

Combining the fiber and resin according to the processes described above will create either a lamella or a laminate. Where a laminate is a stack of lamellas. A lamella consists of one layer of composite material, with a layer being defined as a section with identical fiber and matrix properties. The fiber properties are defined by the type of mat applied (chopped strand, continuous filament, or woven fabric), the direction in which this is oriented, and the fiber material. The resin properties are typically determined by the resin material. Additionally the proportion of each of the two constituents is important.

The properties which a lamella obtains from these influences are parametrically calculated in this chapter. They are determined in accordance with the following outline:

- Fiber Volume Fraction
- Stiffness
  - Axial
  - Transverse
  - Halpin-Tsai Correction
    - Valid for axial, transverse, shear and poisson's ratio.
- Strength
  - Axial Tensile
  - Axial Compressive
  - Transverse Tensile
  - Transverse Compressive
  - Shear
- Failure Criteria
  - Tsai-Hill
  - Tsai-Wu
- Correction Factors
  - Material Factor
  - Conversion Factor
  - Stiffness Reduction Factor
- Thermal Expansion
  - Axial Expansion
  - Transverse Expansion

Note that many of these calculations assume a unidirectional fiber mat. If a multidirectional mat is applied, this can be modelled as a laminate according to chapter Appendix H: Laminate Properties.

## G.1 Fiber Volume Fraction

The differences between the fibers and the matrix have been explained above. Clearly, the fibers have much better mechanical properties than the resin. Therefore it is beneficial to reduce the amount of resin as much as possible, without compromising the composite nature of the material. In general, this limits the fiber volume fraction to approximately 70% in optimal situations.

The fiber volume fraction (FVF) is defined according to Equation 21.

$$FVF = \frac{V_f}{V_f + V_r} = \frac{W_f}{\frac{\rho_f}{\rho_r} * (1 - W_f) + W_f}$$

Equation 21: Fiber Volume Fraction

With:

$V_f$  = Total Fiber Volume [ $m^3$ ]

$V_r$  = Total Resin Volume [ $m^3$ ]

$\rho_f$  = Fiber Density [ $kg/m^3$ ]

$\rho_r$  = Resin Density [ $kg/m^3$ ]

$W_f$  = Weight Fraction of Fibers [-]

Since it is typical to specify production through weight, but to calculate with the volume fractions, a typical relation between the two is plotted in Figure 106. For the following calculations, several assumptions were made:

- $\rho_r = 1200 \text{ kg/m}^3$
- $\rho_f = 2550 \text{ kg/m}^3$  (A typical value for glass fiber).

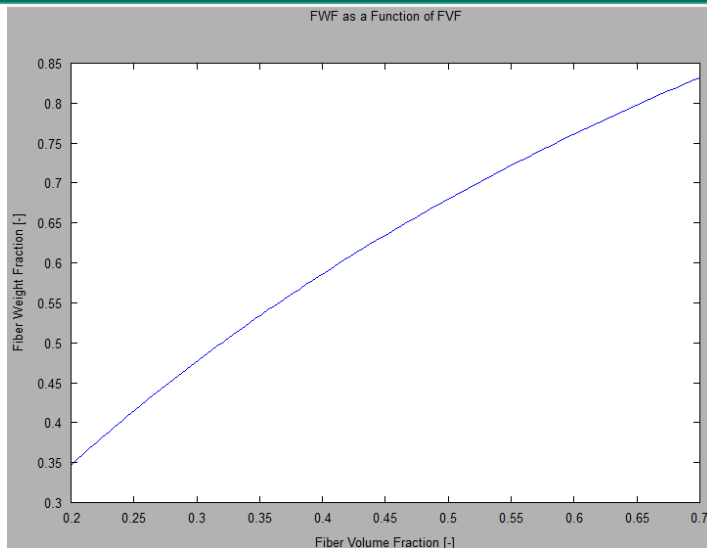


Figure 106: Fiber Weight Fraction vs Fiber Volume Fraction

The FVF has quite some influence on the mechanical properties of the composite. To illustrate this, the equations created by Halpin and Tsai (see: G.2.3 Halpin-Tsai Stiffness Correction) have been used to determine the effect FVF has on the stiffness in both longitudinal and transversal direction of a unidirectional lamella,<sup>173</sup> which has been plotted in Figure 107.<sup>174</sup> The technique used for calculating the stiffness of UD-lamellas can also be expanded for multidirectional fabrics if needed.

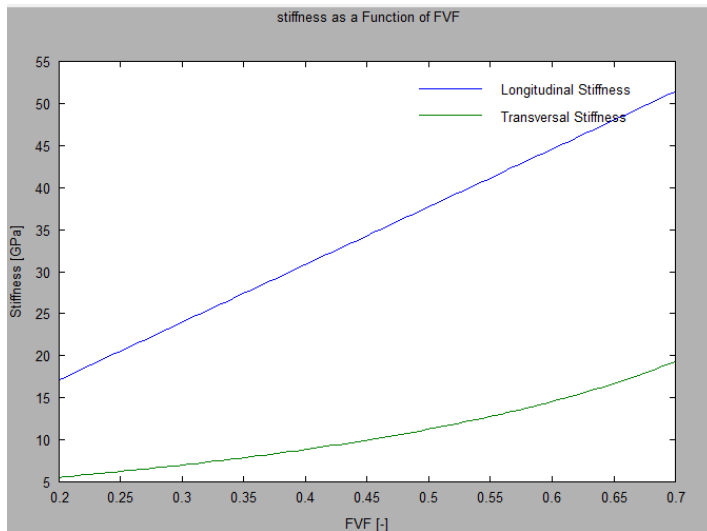


Figure 107: UD Lamella Stiffness as a Function of FVF

<sup>173</sup> (Civieltechnisch Centrum Uitvoering Research en Regelgeving-onderzoekcommissie C 124, 2003-6)

<sup>174</sup> Note that for this comparison, some typical values for the material properties of glass fibers and epoxy resin have been used.

## G.2 Stiffness

The importance of the fiber orientation when discussing stiffness is already visible in Figure 107. The stiffness perpendicular to the fibers is much less than the stiffness in the direction of the fibers. The reasoning behind this is visible in the parallel and series simplifications of the composite material. These can be seen in Figure 108. For both models the composite nature is simplified to a two layer system, with volumes equal to the fibers and matrix of the composite. In the case of the parallel model, the loading is applied in the plane of the layers, while for the series model the load is applied perpendicular to that plane.

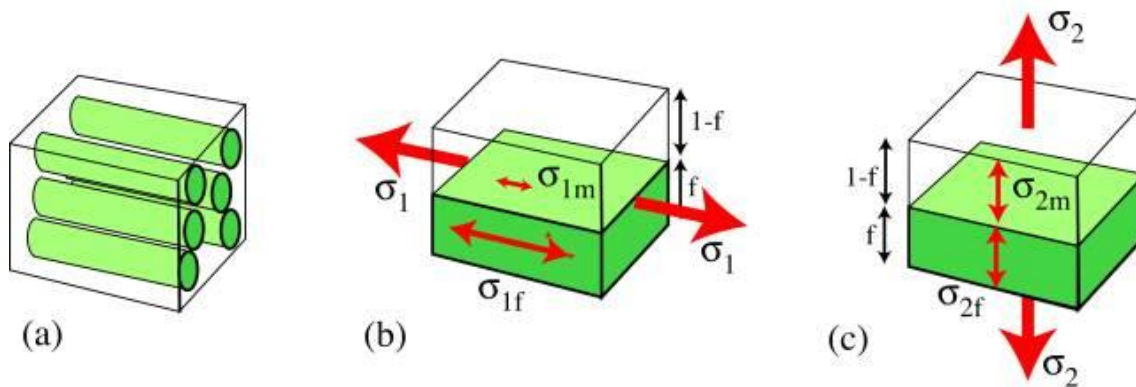


Figure 108: Parallel Model (b) and Series Model (c) for Composites (a) Under Loading<sup>175</sup>

### G.2.1 Parallel Model Stiffness

For the parallel model, where loading is assumed in the longitudinal direction, the assumption is that the strain is constant across the cross section and hence equal for the fibers and the matrix. This leads to Equation 22. Notice that since the modulus of elasticity of the fiber is much larger than that of the resin, the composite stiffness is governed by the fiber stiffness and the FVF.

$$\varepsilon_f = \varepsilon_r = \varepsilon_1 = \frac{\sigma_f}{E_f} = \frac{\sigma_r}{E_r} = \frac{\sigma_1}{E_1}$$

$$\sigma_1 = FVF * \sigma_f + (1 - FVF) * \sigma_r$$

$$\begin{aligned} E_1 = \frac{\sigma_1}{\varepsilon_1} &= \frac{FVF * \sigma_f + (1 - FVF) * \sigma_r}{\frac{\sigma_f}{E_f}} = FVF * E_f + (1 - FVF) * \frac{\sigma_r}{\sigma_f} * E_f \\ &= FVF * E_f + (1 - FVF) * E_r \end{aligned}$$

Equation 22: Composite Stiffness for Parallel Model

<sup>175</sup> (University of Cambridge, 2008)

With:

- $\varepsilon_f$ : Fiber Strain [-]
- $\varepsilon_r$ : Resin Strain [-]
- $\varepsilon_1$ : Composite Strain in Longitudinal Direction [-]
- $\sigma_f$ : Fiber Stress [MPa]
- $\sigma_r$ : Resin Stress [MPa]
- $\sigma_1$ : Composite Stress in Longitudinal Direction [MPa]
- $E_f$ : Fiber Young's Modulus [MPa]
- $E_r$ : Resin Young's Modulus [MPa]
- $E_1$ : Composite Young's Modulus [MPa]
- $FVF$ : Fiber Volume Fraction According to Equation 21

### G.2.2 Series Model Stiffness

The series model, where loading is assumed in the transverse direction, the assumption is that stress is equal throughout the thickness of the specimen. So that the materials are free to have different strains. This model leads to Equation 23. Notice that the stiffness is now largely dominated by the matrix material and the FVF.

$$\sigma_2 = \sigma_f = \sigma_r = \varepsilon_2 E_2 = \varepsilon_f E_f = \varepsilon_r E_r$$

$$\varepsilon_2 = FVF * \varepsilon_f + (1 - FVF) * \varepsilon_r$$

$$E_2 = \frac{\sigma_2}{\varepsilon_2} = \frac{\sigma_2}{FVF * \varepsilon_f + (1 - FVF) * \varepsilon_r}$$

$$\frac{1}{E_2} = \frac{FVF * \varepsilon_f + (1 - FVF) * \varepsilon_r}{\sigma_2} = \frac{FVF}{E_f} + \frac{1 - FVF}{E_r}$$

**Equation 23: Composite Stiffness for Series Model**

With:

- $\varepsilon_2$ : Composite Strain in Transverse Direction [-]
- $\sigma_2$ : Composite Stress in Transverse Direction [MPa]
- $E_2$ : Composite Young's Modulus in Transverse Direction [MPa]

### G.2.3 Halpin-Tsai Stiffness Correction

The models described above were semi-empirically expanded by Halpin and Tsai. They determined that stiffness properties of a composite could be written according to Equation 24. Here  $\zeta$  represents the nature of the fibers. It accounts for the shape, distribution and orientation.<sup>176</sup>

$$\frac{P_c}{P_r} = \frac{1 + \zeta * \eta * FVF}{1 - \eta * FVF}$$

$$\eta = \frac{\frac{P_f}{P_r} - 1}{\frac{P_f}{P_r} + \zeta}$$

Equation 24: Halpin-Tsai Empirical Formulas<sup>177</sup>

With:

$P_c$ : Value of Considered Property of Composite

$P_r$ : Value of Considered Property of Resin

$P_f$ : Value of Considered Property of Fiber

Note that as  $\zeta$  becomes zero, the equation simplifies to the idealized series model described above. As it approaches  $\infty$ , the equation simplifies to the parallel model. Typical values which will also be utilized here are<sup>178, 179</sup>:

- $\zeta = \infty$  for longitudinal stiffness and Poisson's ratio
- $\zeta = 2$  for transverse stiffness
- $\zeta = 1$  for shear stiffness

The influence of the Halpin-Tsai model is illustrated in Figure 109.

<sup>176</sup> (Indian Institute of Technology, 2014)

<sup>177</sup> (Indian Institute of Technology, 2014)

<sup>178</sup> (Indian Institute of Technology, 2014)

<sup>179</sup> (Pilling, 2005)



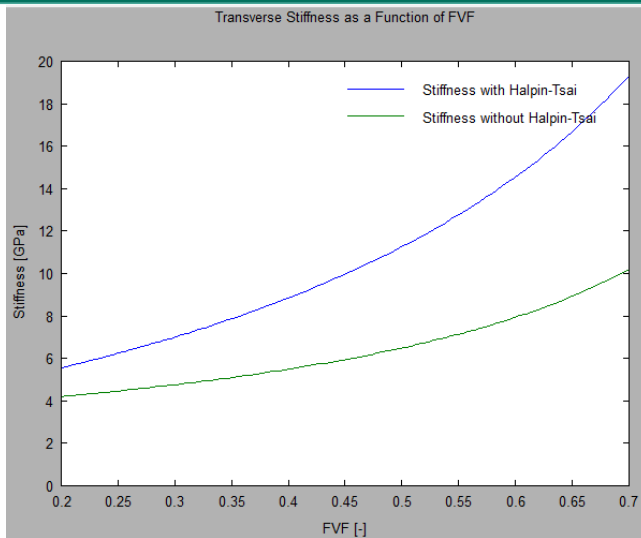


Figure 109: Transverse Stiffness with and without the Halpin-Tsai Correction

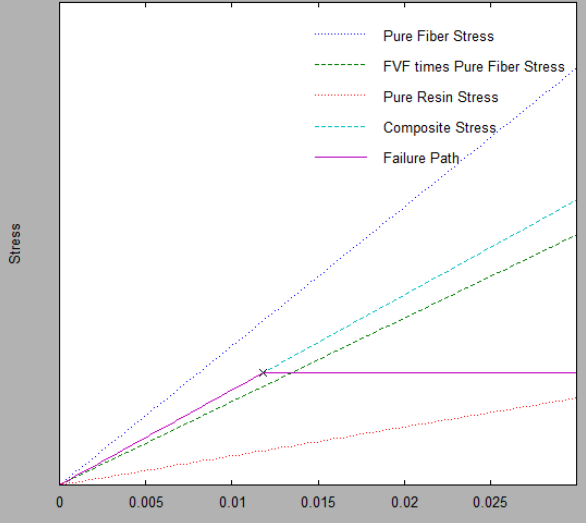
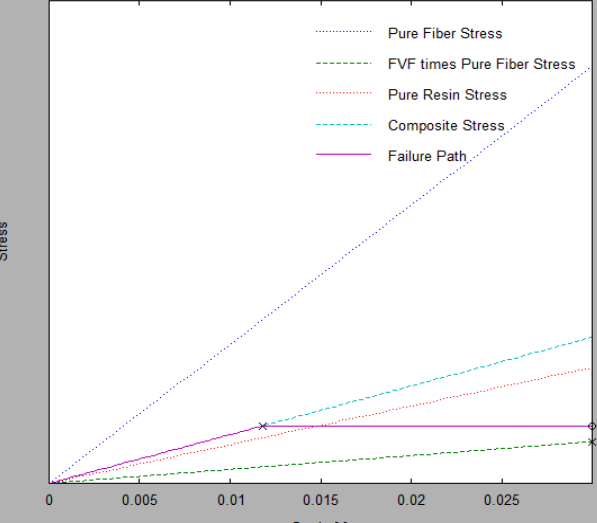
### G.3 Strength

Naturally, the strength of a material is important when it is utilized as a construction material. Composites are no exception. However, due to their orthotropic nature their strength must be analyzed in multiple direction. Here, the longitudinal, transverse, and shear strength will be discussed.

#### G.3.1 Longitudinal Tensile Strength

The method for determining the longitudinal strength of the composite is based on the parallel model discussed above. The strain of the fibers and of the resin is considered equal during the loading process. There are two situation which may occur during failure. Either the failure strain of the fibers is reached first, or that of the resin is reached first. These situation are compared in Table 43.

Comparison Longitudinal Failure Mechanisms	
Fiber Failure Strain Lower	Resin Failure Strain Lower
$\epsilon_f = \epsilon_r = \epsilon_1 = \frac{\sigma_f}{E_f} = \frac{\sigma_r}{E_r} = \frac{\sigma_1}{E_1}$	
$\epsilon_{f,u} < \epsilon_{r,u}$	$\epsilon_{f,u} > \epsilon_{r,u}$
$\sigma_1 = FVF * \sigma_f + (1 - FVF) * \sigma_r$	
$\sigma_{1,u,t} = FVF * \sigma_{f,u} + (1 - FVF) * E_r * \epsilon_{f,u}$	$\sigma_{1,u,t} = FVF * E_f * \epsilon_{r,u} + (1 - FVF) * \sigma_{r,u}$

<p style="text-align: center;">Failure Mechanism: Low Fiber Failure Strain, High FVF</p> 	<p style="text-align: center;">Failure Mechanism: High Fiber Failure Strain, Low FVF</p> 
<p>The resin material has residual strength left. If the residual strength is more than the force acting on the fibers at this point, the actual point of failure will coincide with resin failure. This is a rare occurrence since fibers are typically much stronger.</p>	<p>The fibers have residual strength left. If the residual strength is larger than the force acting on the matrix at this point, the actual point of failure will coincide with fiber failure. This is only possible in continuous fiber composites. This situation occurs frequently, since fibers are typically much stronger than resins.</p>
$FVF_{crit} = \frac{\sigma_{r,u} + E_r * \epsilon_{f,u}}{\sigma_{f,u} - E_r * \epsilon_{f,u} + \sigma_{r,u}}$	$FVF_{crit} = \frac{\sigma_{r,u}}{\sigma_{f,u} + E_f * \epsilon_{r,u} + \sigma_{r,u}}$
<p>If FVF falls below the critical value described above, the composite failure stress is given by the equation below.</p>	<p>If FVF rises above the critical value described above, the composite failure stress is given by the equation below.</p>
$\sigma_{1,u,t} = (1 - FVF) * \sigma_{r,u}$	$\sigma_{1,u,t} = FVF * \sigma_{f,u}$

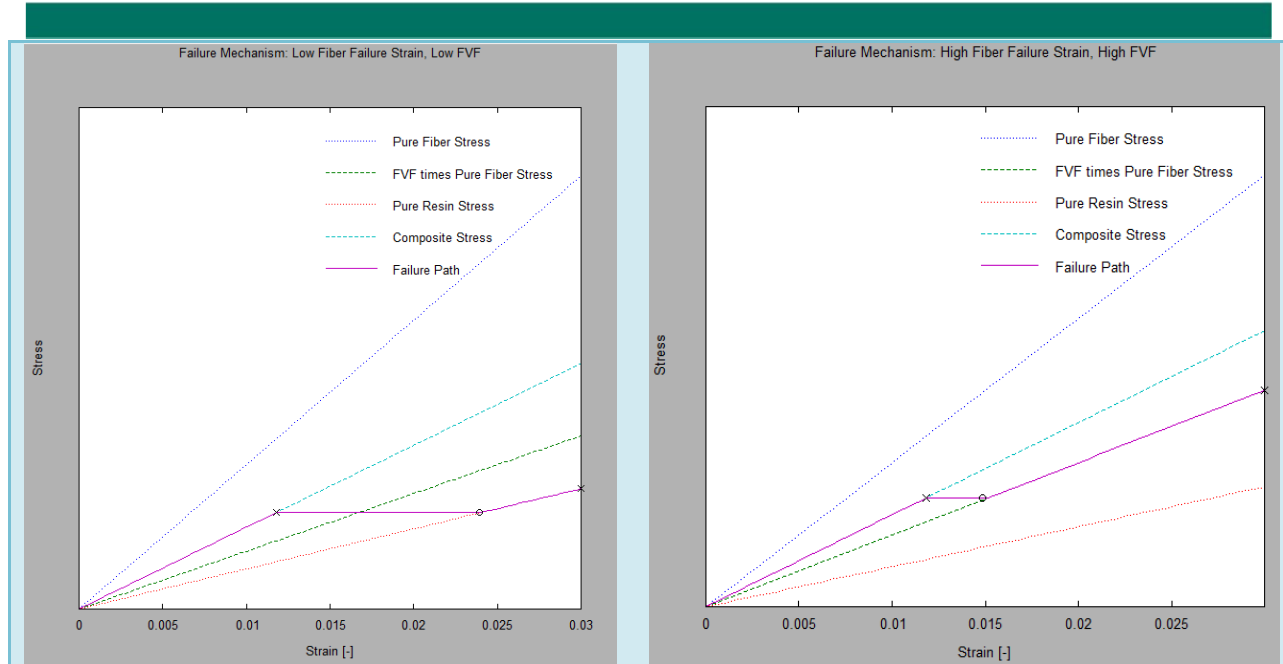


Table 43: Comparison Longitudinal Failure Mechanisms<sup>180</sup>

With:

$\varepsilon_{f,u}$ : Ultimate Strain of the Fiber Material [-]

$\varepsilon_{r,u}$ : Ultimate Strain of the Resin Material [-]

$\sigma_{1,u,t}$ : Ultimate Tensile Stress of the Composite in Longitudinal Direction [MPa]

$\sigma_{f,u}$ : Ultimate Stress of the Fiber Material [MPa]

$\sigma_{r,u}$ : Ultimate Stress of the Resin Material [MPa]

$FVF_{crit}$ : Critical Fiber Volume Fraction at Which the Failure Mechanism Changes [-]

The table above gives four different longitudinal failure mechanisms, depending on the fiber content and the relative failure strains of the materials. The calculations for composite failure given above are simplifications of reality. The load is never carried fully by the fibers or the matrix. Typically the failure mechanism resulting from a low fiber failure strain and a high FVF are most common. This is because the resins are typically chosen so that the fibers can strain to their full potential, and the FVF is kept as high as possible.

### G.3.2 Longitudinal Compressive Strength

Longitudinal Compressive Strength is not just a dependent on the material properties of the parent materials. They are also dependent on the stability of the fibers inside the matrix. The phenomenon wherein the fibers become unstable is termed microbuckling. The Rosen model stipulated that there were two modes in which fibers could buckle: the extension mode and the shear mode, as

<sup>180</sup> Equations obtained from (University of Cambridge, 2008).

shown in . The shear mode predicted lower strength than the extension mode, but still predicted much higher than experimental values. As such, Rosen's work was adapted by many, and several predictive models were made. Here Xu and Reifsnider's Model will be used.

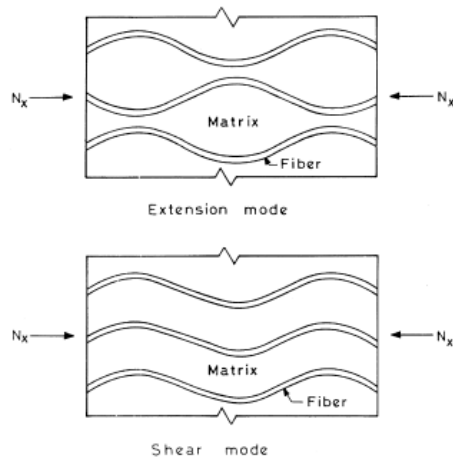


Figure 110: Microbuckling Failure Modes<sup>181</sup>

Xu and Reifsnider modeled the fibers as elastically supported beams, and included terms for the condition of matrix-fiber bonding, matrix slippage and fiber radius. These three terms are represented by the factors  $\xi$ ,  $\eta$ , and  $r_f$  respectively. Typically, the first two terms should be determined experimentally, and the last term depends on the fibers used. Since this it is not possible to determine the coefficients experimentally, typical values from literature have been applied:  $\xi = 0.02$  and  $\eta = 1.98$ .  $r_f$  Has been chosen as  $6\mu\text{m}$  in accordance with typical values. The Xu-Reifsnider model has been chosen because it corresponds reasonable well to experimental data.<sup>182</sup> The Xu-Reifsnider equation is given in Equation 25, and is plotted against FVF in Figure 111.

<sup>181</sup> (Naik)

<sup>182</sup> (Naik)

$$\sigma_{1,u,c} = G_r * \left[ FVF + \frac{E_r}{E_f} (1 - FVF) \right] * \left[ 2 * (1 + \nu_r) * \sqrt{\frac{\pi \sqrt{\pi} \eta_{1,c} r_f}{3 * \left(\frac{E_r}{E_f}\right) \left(FVF \frac{E_r}{E_f} + 1 - FVF\right) (1 + FVF \nu_f + \nu_r (1 - FVF))}} + 1 - \xi \right] - \frac{\sin(\pi \xi)}{2\pi}$$

Equation 25: Xu-Reifsnider Equation for Longitudinal Compressive Strength<sup>183</sup>

With:

$\sigma_{1,u,c}$ : Ultimate Compressive Stress of the Composite in Longitudinal Direction [MPa]

$G_r$ : Shear Modulus of the Resin [MPa]

$\nu_r$ : Poisson's Ratio of the Resin [-]

$\eta_{1,c}$ : Matrix Slippage Factor. Assumed as 1.98

$r_f$ : Radius of Fibers. Assumed as 6 $\mu$ m

$\nu_f$ : Poisson's Ratio of the Fibers [-]

$\xi$ : Matrix-Fiber Bonding Factor. Assumed as 0.02

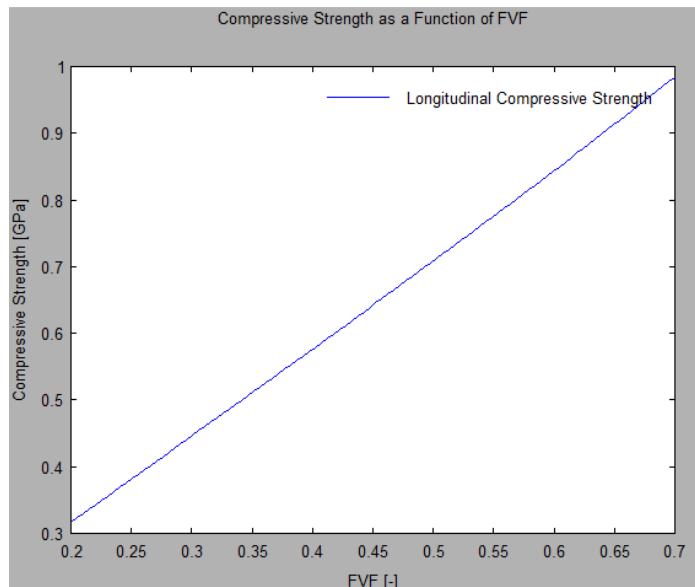


Figure 111: Longitudinal Compressive Strength

<sup>183</sup> (Naik)

### G.3.3 Transverse Tensile Strength

The orthotropic nature of composites visible in the stiffness is also present in the strength. When a stress acts on a lamella the lamella will fail at its weakest cross section. Since the resin is weaker than the fibers, the weakest cross section will be the one which consists entirely out of resin. This negates the strength of the fibers. However, this schematization does not represent reality very well. The goal is typically to have a high FVF, so that there will not be cross sections without fibers. In addition there will be interaction effects between the fibers and the resin, so that a constant stress distribution cannot be assumed. The fibers actually weaken the composite because the stiffnesses of the resin and fibers differ so much that it induces peak stresses locally.

This effect is difficult to quantify. One method which is used is to model the fibers as holes in the composite. With this method, the maximum expected cross sectional area of the resin is calculated. This fraction of the whole area is then utilized as a reduction factor. The reduction factor is shown between brackets in Equation 26, and plotted in Figure 112.

$$\varepsilon_{2,u,t} = \left[ \frac{d}{s} \frac{E_r}{E_f} + \left( 1 - \frac{d}{s} \right) \right] \varepsilon_{r,u,t}$$

$$\frac{d}{s} = 2 * \left( \frac{FVF}{\pi} \right)^{\frac{1}{2}}$$

Equation 26: Reduction Factor for Transverse Strength<sup>184</sup>

With:

$\varepsilon_{2,u,t}$ : Ultimate Tensile Strain of Composite in Transverse Direction [-]

$d$ : Diameter of Fibers [ $\mu\text{m}$ ]

$s$ : Heart-to-Heart Spacing of Fibers [ $\mu\text{m}$ ]

Which when multiplied by the transverse Young's Modulus can be rewritten as Equation 27.

$$\sigma_{2,u,t} = \sigma_{r,u,t} * \left[ \frac{E_2}{E_r} + \left( \frac{E_2}{E_f} - \frac{E_2}{E_r} \right) * 2 * \left( \frac{FVF}{\pi} \right)^{\frac{1}{2}} \right]$$

Equation 27: Equivalent Transverse Tensile Strength Equation

With:

$\sigma_{2,u,t}$ : Ultimate Tensile Stress of Composite in Transverse Direction [MPa]

$\sigma_{r,u,t}$ : Ultimate Tensile Stress of Resin [MPa]

<sup>184</sup> (University of Cambridge, 2008)

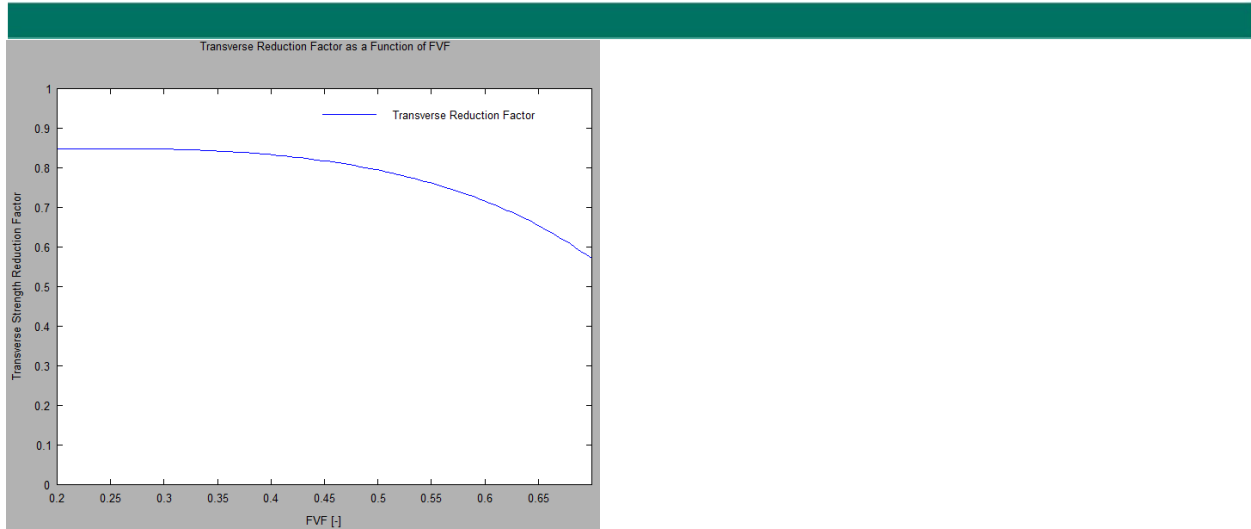


Figure 112: Transverse Strength Reduction Factor

### G.3.4 Transverse Compressive Strength

Transverse compressive strength works in a similar way to transverse tensile stresses. The strength of the composite is largely due to the compressive strength of the resin. However, the fibers in the matrix introduce a weakness into the composite material. The equation is given in Equation 28. note that it is analogous with Equation 27.

$$\sigma_{2,u,c} = \sigma_{r,u,c} * \left[ \frac{E_2}{E_r} + \left( \frac{E_2}{E_f} - \frac{E_2}{E_r} \right) * 2 * \left( \frac{FVF}{\pi} \right)^{\frac{1}{2}} \right]$$

Equation 28: Equivalent Transverse Compressive Strength Equation<sup>185</sup>

With:

$\sigma_{2,u,c}$ : Ultimate Compressive Stress of Composite in Transverse Direction [MPa]

$\sigma_{r,u,c}$ : Ultimate Compressive Stress of Resin [MPa]

Comparison with Equation 26 shows a very similar concept. The difference is that the reduction factor is dependent on the resin compression strength rather than tensile strength. Recall that the reduction factor is seen in Figure 112.

### G.3.5 Shear Strength

The theory for determining the shear strength is similar to that for the transverse tensile and compressive strength: the fibers cause stress concentrations in the matrix, so that the strength is

<sup>185</sup> (Kaw, 2006)

reduced. For shear strength this is usually done by dividing the matrix strength by a stress concentration factor. Several theories for this reduction factor have been established and one is given in Equation 29. The resulting stress concentration factor, as a function of the FVF is plotted in Figure 113. Unfortunately, this theory does not correlate with experimental results: experimental results have shown that the method above is a gross underestimate of reality. Typically, the shear strength of lamellas will exceed that of pure resin. Some experiments have shown a factor 9 difference in theoretical and experimental values<sup>186</sup>; clearly worth adjusting for. Since there is no known method for accurately predicting the shear strength, the value used in this thesis will be conservatively estimated based on values found in literature. See 4.3.3 Determination of Lamella Properties for more information.

$$k_{\tau} = \frac{1 - FVF \left(1 - \frac{G_r}{G_f}\right)}{1 - 2 \left(\frac{FVF}{\pi}\right)^{\frac{1}{2}} * \left(1 - \frac{G_r}{G_f}\right)}$$

Equation 29: Shear Concentration Factor<sup>187</sup>

With:

$k_{\tau}$ : Shear Stress Concentration Factor [-]

$G_r$ : Shear Modulus of the Resin [MPa]

$G_f$ : Shear Modulus of the Fiber Material [MPa]

---

<sup>186</sup> (Kaw, 2006)

<sup>187</sup> (Tiwari)



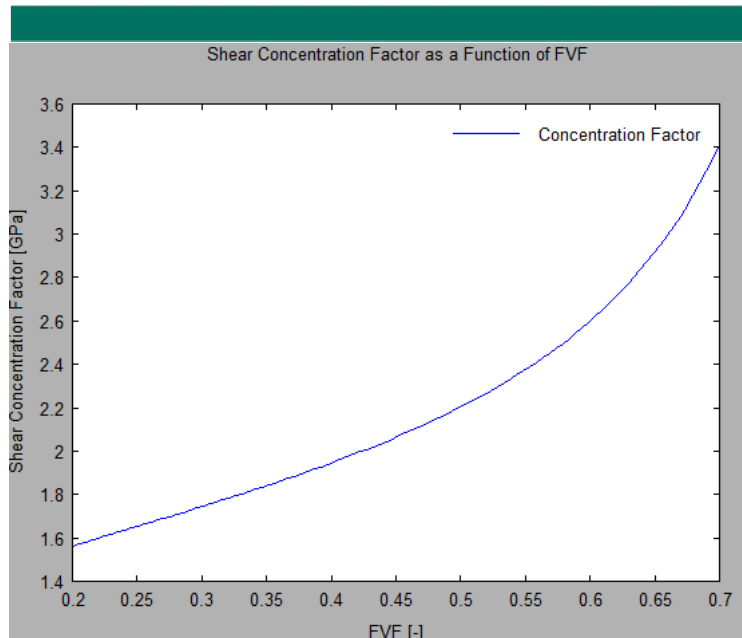


Figure 113: Shear Concentration Factor

## G.4 Failure Criteria

The strength of the lamellas in each direction is relevant information. However, it is unlikely that uniaxial loading will occur, so that a combined failure criterion needs to be established. A failure criterion established for composites is the Tsai-Hill criterion. This criterion is limited when considering compression. Since compression is expected, this criterion is considered inadequate for this case. However, an expansion of this criterion called the Tsai-Wu failure criterion, accounted for the difference in tensile and compressive strength, and will therefore be applied. First, Tsai-Hill is briefly explained, followed by a more detailed analysis of the Tsai-Wu criterion.

### G.4.1 Tsai-Hill Criterion

The axial, transverse, and shear failure criteria can be used to describe the failure of composites. However, as presented above, no interaction has been taken into account. Interaction does play a role in the failure of composite materials. Therefore, Tsai and Hill created a combined failure criterion: the Tsai-Hill Criterion.

The Tsai-Hill Criterion is based upon the von Mises yield criterion for metals. Von Mises states that the onset of metal yielding takes place when the following limit state is reached:

$$(\sigma_{1,m} - \sigma_{2,m})^2 + (\sigma_{2,m} - \sigma_{3,m})^2 + (\sigma_{3,m} - \sigma_{1,m})^2 = 2 * f_y^2$$

For materials under plane-stress conditions:  $\sigma_3 = 0$ , so that the equation above reduces to:

$$\left(\frac{\sigma_{1,m}}{f_y}\right)^2 + \left(\frac{\sigma_{2,m}}{f_y}\right)^2 - \left(\frac{\sigma_{1,m}\sigma_{2,m}}{f_y^2}\right) = 1$$

Tsai and Hill expanded this criterion to account for the orthotropic nature of composites. One can see that this is done by adding several terms for the different failure mechanisms which arise. The result is given below:

$$\left(\frac{\sigma_1}{\sigma_{1,u}}\right)^2 + \left(\frac{\sigma_2}{\sigma_{2,u}}\right)^2 - \left(\frac{\sigma_1\sigma_2}{\sigma_{1,u}^2}\right) - \left(\frac{\sigma_1\sigma_2}{\sigma_{2,u}^2}\right) + \left(\frac{\sigma_1\sigma_2}{\sigma_{3,u}^2}\right) + \left(\frac{\tau_{12}}{\tau_{12,u}^2}\right) = 1$$

This equation accounts for orthotropic properties in all directions. However, composite properties tend to be considered transversely isotropic, i.e. properties in the two directions perpendicular to the fibers (the y- and z-directions or 2- and 3-directions), are considered equal. Therefore the 4<sup>th</sup> and 5<sup>th</sup> terms in the equation above are equal, so that the criterion reduces to Equation 30.

$$\left(\frac{\sigma_1}{\sigma_{1,u}}\right)^2 + \left(\frac{\sigma_2}{\sigma_{2,u}}\right)^2 - \left(\frac{\sigma_1\sigma_2}{\sigma_{1,u}^2}\right) + \left(\frac{\tau_{12}}{\tau_{12,u}^2}\right) = 1$$

Equation 30: Tsai-Hill Criterion for Composite Failure<sup>188</sup>

With:

- $\sigma_{i,m}$ : Stress in “i” Direction in Metals [MPa]
- $f_y$ : Yield Stress in Metal [MPa]
- $\tau_{12}$ : Shear Stress [MPa]
- $\tau_{12,u}$ : Ultimate Shear Stress [MPa]
- $\sigma_{i,u}$ : Ultimate Stress in “i” Direction.

### G.4.2 Tsai-Wu Criterion

For Tsai-Hill, the calculations regarding strength did not differentiate between tensile and compressive stresses. However, considering that FRP behaves differently in tension and compression, it is prudent to include this when establishing strength criteria. Therefore, the Tsai-Hill criterion was expanded to the Tsai-Wu criterion, which accounts for the differences in tensile and compressive behavior of the material.

The failure criterion described here assumes composite failure due to stresses and stress interactions. The starting point is partially based on the von Mises and Tsai-Hill criteria, but it assumes that stress components of the first and second order need to be accounted for. Since not all of these

<sup>188</sup> (University of Cambridge, 2008)

terms derive from von Mises, they were simply added to the equation. The plane stress condition used for Tsai-Hill is maintained in this calculation. The following equation was set up, where  $F_{ij} = \text{constant}$ .

$$F(\sigma_1, \sigma_2, \tau_{12}) = F_1\sigma_1 + F_2\sigma_2 + F_6\tau_{12} + F_{11}\sigma_1^2 + F_{22}\sigma_2^2 + F_{66}\tau_{12}^2 + 2F_{12}\sigma_1\sigma_2 + 2F_{16}\sigma_1\tau_{12} + 2F_{26}\sigma_2\tau_{12}$$

Equation 31: Preliminary Tsai-Wu Criterion<sup>189</sup>

This equation is much more expansive than Tsai-Hill. It makes allotments for the same 4 terms, but also includes 5 new ones. Including the first order axial stresses, the second order shear stress, and the axial-shear stress interaction terms. However, at this point the values of the 9 constants  $F_{ij}$ , are still unknown. If the value of  $F(\sigma_1, \sigma_2, \tau_{12})$  exceeds 1 it is assumed the material fails. In order to determine the constants, several loading conditions are applied, such as uniaxial tension, uniaxial compression,

Determination of Tsai-Wu Constants			
Loading Type	Assumptions	Equations	Results
Uniaxial Tension (1)	$\sigma_1 = \sigma_{1,u,t}$ $\sigma_2 = 0$ $\tau_{12} = 0$	$1 = F_1\sigma_{1,u,t} + F_{11}\sigma_{1,u,t}^2$	$F_1 = \frac{1}{\sigma_{1,u,t}} + \frac{1}{\sigma_{1,u,c}}$
Uniaxial Compression (1)	$\sigma_1 = \sigma_{1,u,c}$ $\sigma_2 = 0$ $\tau_{12} = 0$	$1 = F_1\sigma_{1,u,c} + F_{11}\sigma_{1,u,c}^2$	$F_{11} = -\frac{1}{\sigma_{1,u,t}\sigma_{1,u,c}}$
The hypothetical conditions of uniaxial tension and compression are assumed on the specimen, where the specimen is loaded to failure. This leaves only the terms $F_1$ and $F_{11}$ from the original equation. Solving the two equations for the two unknowns gives the results on the right.			
Uniaxial Tension (2)	$\sigma_1 = 0$ $\sigma_2 = \sigma_{2,u,t}$ $\tau_{12} = 0$	$1 = F_2\sigma_{2,u,t} + F_{22}\sigma_{2,u,t}^2$	$F_2 = \frac{1}{\sigma_{2,u,t}} + \frac{1}{\sigma_{2,u,c}}$
Uniaxial Compression (2)	$\sigma_1 = 0$ $\sigma_2 = \sigma_{2,u,c}$ $\tau_{12} = 0$	$1 = F_2\sigma_{2,u,c} + F_{22}\sigma_{2,u,c}^2$	$F_{22} = -\frac{1}{\sigma_{2,u,t}\sigma_{2,u,c}}$
Uniaxial loading in direction 2 gives results which are analogous to those for direction 1. However, note that while the terms are analogous, the values of the terms will be different.			
Pure Shear (+)	$\sigma_1 = 0$ $\sigma_2 = 0$ $\tau_{12} = \tau_{12,u}$	$1 = F_6\tau_{12,u} + F_{66}\tau_{12,u}^2$	$F_6 = 0$
Pure Shear (-)	$\sigma_1 = 0$ $\sigma_2 = 0$ $\tau_{12} = -\tau_{12,u}$	$1 = -F_6\tau_{12,u} + F_{66}\tau_{12,u}^2$	$F_{66} = \left(\frac{1}{\tau_{12,u}}\right)^2$
The situation consisting of pure shear loading is analyzed next. Again, filling in the assumed values leaves only two constants in the equation. Since shear can be applied in positive and negative direction,			

<sup>189</sup> (Indian Institute of Technology)

this loading scenario also gives two equations. Note that constant  $F_6$  is zero. This is because there is no physical difference in which direction the shear stress is applied.

Combined Uniaxial Stress and Shear (+)	$\begin{aligned} \sigma_1 &= \sigma_1' \\ \sigma_2 &= 0 \\ \tau_{12} &= \tau_{12}' \end{aligned}$	$1 = F_1\sigma_1' + F_6\tau_{12}' + F_{11}\sigma_1'^2 + F_{66}\tau_{12}'^2 + 2F_{16}\sigma_1'\tau_{12}'$	$\begin{aligned} F_{16} &= 0 \\ F_{26} &= 0 \end{aligned}$
Combined Uniaxial Stress and Shear (-)	$\begin{aligned} \sigma_1 &= \sigma_1' \\ \sigma_2 &= 0 \\ \tau_{12} &= -\tau_{12}' \end{aligned}$	$1 = F_1\sigma_1' - F_6\tau_{12}' + F_{11}\sigma_1'^2 + F_{66}\tau_{12}'^2 - 2F_{16}\sigma_1'\tau_{12}'$	

Applying a combined axial stress and shear stress leaves more terms from the original equation. However, by applying the same axial stress in both cases, the terms relating to  $F_1$ ,  $F_{11}$  are equal between the two equations. By applying the shear strain in positive and negative direction, the term relating to  $F_{66}$  is also equal between the two equations, and the  $F_{16}$  term has the opposite sign. Note that the term  $F_6$  in this equation is zero according to the previous step. Therefore, subtracting the equations leaves only the term relating to  $F_{16}$ . Hence, this term equals zero. For brevity, the derivation of  $F_{26}$  has not been shown, but the method and result is the same.

Biaxial Loading in principal stress directions compared with von Mises	$\begin{aligned} \sigma_1 &= \sigma_1' \\ \sigma_2 &= \sigma_2' \\ \tau_{12} &= 0 \\ \sigma_{1,u,t} &= f_y \\ \sigma_{1,u,c} &= -f_y \\ \sigma_{2,u,t} &= f_y \\ \sigma_{2,u,c} &= -f_y \end{aligned}$	$1 = F_1\sigma_1' + F_2\sigma_2' + F_{11}\sigma_1'^2 + F_{22}\sigma_2'^2 + 2F_{12}\sigma_1'\sigma_2'$	$2F_{12} = -\left(\frac{1}{f_y}\right)^2$
		$1 = \left(\frac{\sigma_1'}{f_y}\right)^2 + \left(\frac{\sigma_2'}{f_y}\right)^2 - \left(\frac{\sigma_1'\sigma_2'}{f_y^2}\right)$	$\begin{aligned} \ni F_{12} &= -\frac{1}{2}\sqrt{F_{11}F_{22}} \\ &= -\frac{1}{2}\sqrt{\frac{1}{\sigma_{1,T}\sigma_{1,C}\sigma_{2,T}\sigma_{2,C}}} \end{aligned}$
		$\begin{aligned} F_1 &= 0 \\ F_2 &= 0 \\ F_{11} &= F_{22} = \left(\frac{1}{f_y}\right)^2 \end{aligned}$	

The constant  $F_{12}$  is generally considered the most difficult to determine, since there is no manner to determine this with hypothetical situations as for other constants. In general, the recommendation is to determine  $F_{12}$  through experiments. However, since this may not always be possible, another method has been suggested. This method makes several invalid assumptions and the solution obtained is simply one of many that satisfy the equations.

The calculation equates the von Mises and the Tsai-Wu criteria. The assumptions are (1) that the tensile and compressive strengths are equal and (2) that the material is isotropic. Under these assumption, the terms  $F_1$  and  $F_2$  are zero, and the terms  $F_{11}$  and  $F_{22}$  are equal to their corresponding terms in the von Mises criterion. So that the combined stress terms in the two equations should also be equal.

The calculated value of  $F_{12}$  has many solutions due to assumptions (1) and (2). To account for the different strengths in different directions the term is approximated as a joint function of ALL axial strengths. The chosen solution is just one of many which satisfy the equation.

Table 44: Determination of Tsai-Wu Constants<sup>190</sup>

<sup>190</sup> Equations and methods in table obtained from (Indian Institute of Technology)

With the constants determined according to Table 38, the Tsai-Wu criterion can be rewritten according to Equation 32, with an overview of the constants in Equation 33.

$$F(\sigma_1, \sigma_2, \tau_{12}) = F_1\sigma_1 + F_2\sigma_2 + F_{11}\sigma_1^2 + F_{22}\sigma_2^2 + F_{66}\tau_{12}^2 - \sqrt{F_{11}F_{22}}\sigma_1\sigma_2$$

#### Equation 32: Tsai-Wu Criterion

$$F_1 = \frac{1}{\sigma_{1,u,t}} + \frac{1}{\sigma_{1,u,c}}$$

$$F_{11} = -\frac{1}{\sigma_{1,u,t}\sigma_{1,u,c}}$$

$$F_2 = \frac{1}{\sigma_{2,u,t}} + \frac{1}{\sigma_{2,u,c}}$$

$$F_{22} = -\frac{1}{\sigma_{2,u,t}\sigma_{2,u,c}}$$

$$F_{66} = \left(\frac{1}{\tau_{12,u}}\right)^2$$

#### Equation 33: Tsai-Wu Constants

The surface plot of the Tsai-Wu Criterion is shown in Figure 114, and a contour plot is shown in Figure 115. Note the oblong shape and the asymmetry across the x- and y-axes. The oblong shape is a result of anisotropy, where the material is much stronger in x-direction than in y- and z-direction. The asymmetry indicates strengthening of the material under bidirectional compression, and weakening under bidirectional tension. Note that there is symmetry across the zero shear plane (indicated by the blue plane). This is because the maximum shear stress is independent of direction, a concept used to determine coefficients  $F_6$  and  $F_{66}$ . For the contour plot, each contour represents failure criteria for different levels of constant shear stress. Note that the graph is shifted towards the biaxial compression quadrant, and that the maximum shear strength under biaxial compression exceeds the value for pure shear.

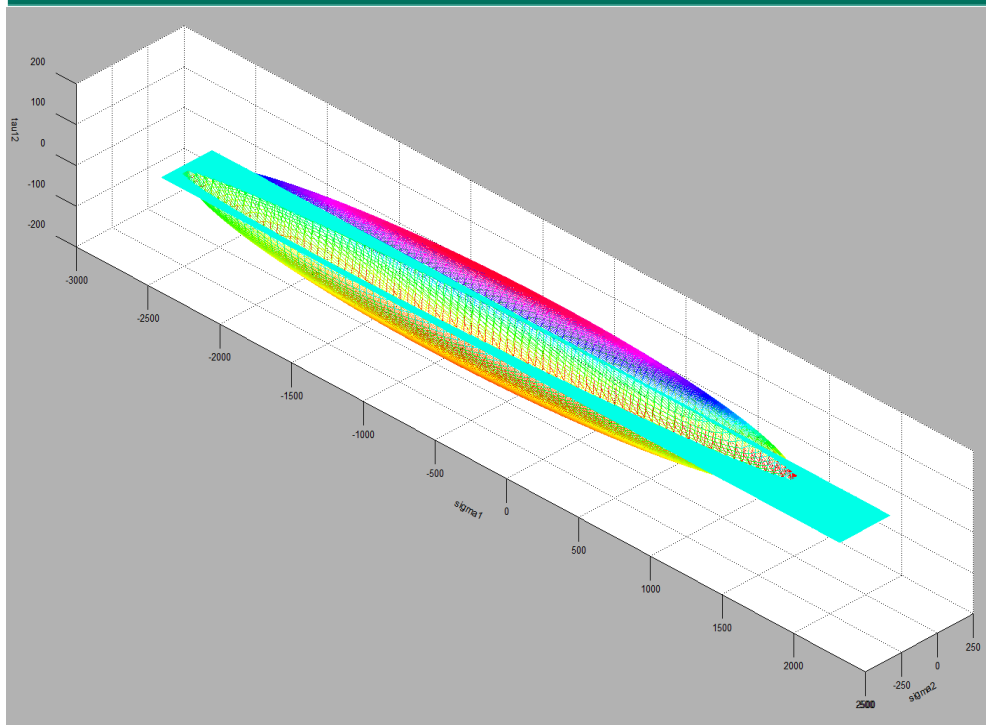


Figure 114: Tsai-Wu Failure Surface<sup>191</sup>

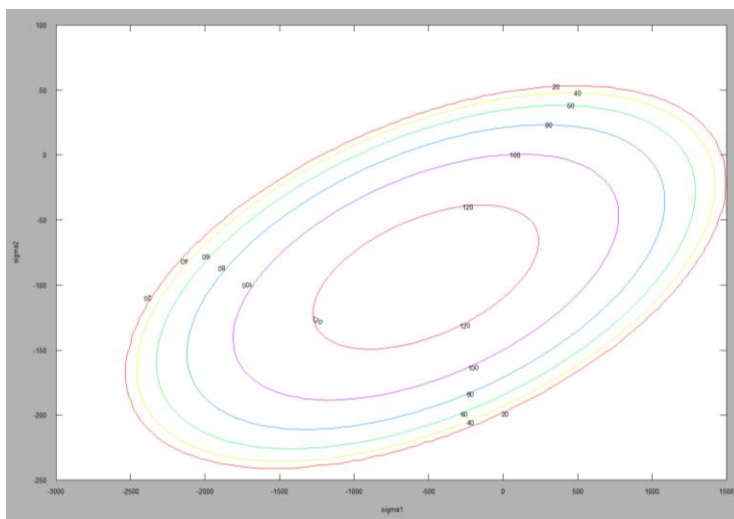


Figure 115: Contour Plot of Tsai-Wu Failure Criterion

For the Tsai-Wu failure criterion, it is interesting to see how the terms of the equation relate to one another under loading. To that end, the values of each term, and their sum, are shown in Figure 116.

<sup>191</sup> The values assumed for calculating this figure are:  $\sigma_{1,T} = 1500\text{MPa}$ ,  $\sigma_{1,C} = -1250\text{MPa}$ ,  $\sigma_{2,T} = 50\text{MPa}$ ,  $\sigma_{2,C} = -200\text{MPa}$ ,  $\tau_{12,F} = 100\text{MPa}$

The terms are numbered according to their order of appearance in Equation 32. The values shown in this figure are based on a ply from a laminate loaded in a direction 45 degrees to its axial direction. Note that in this situation one term, the shear term, is dominant, and that the total Tsai-Wu value is nonlinear. The Tsai-Wu value even becomes negative at low loading conditions.

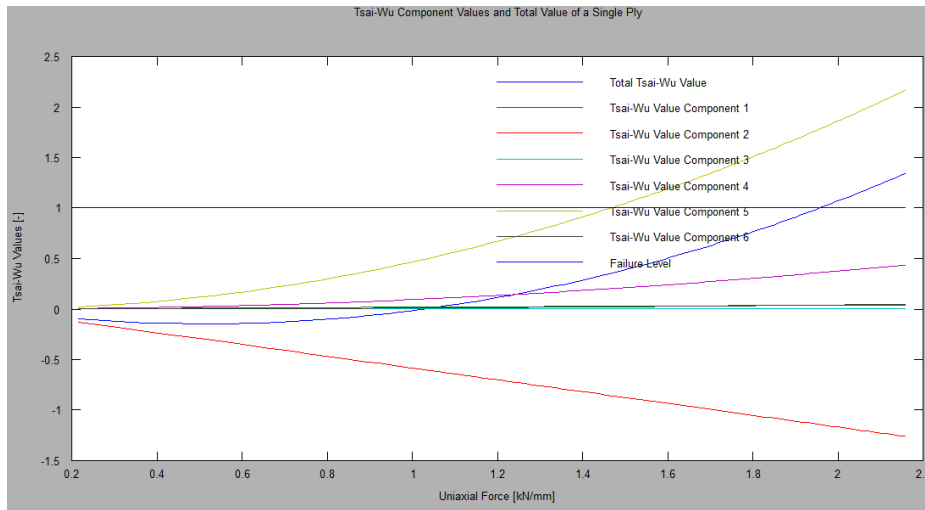


Figure 116: Tsai-Wu Total Value and Component Values

## G.5 Correction Factors

The sections above describe the mechanical properties of lamella specimens, yet not all specimens are created equal. There is a distribution in the strength and stiffness of specimens. This can be caused during manufacture, through inconstant fiber volume fractions, improper resin bonding, improper resin mixing, resin voids, discontinuous fibers, damaged fibers, etc. In addition there are things that the specimen can be subjected to throughout its life which can weaken (or strengthen) it. The variability in the strength following production is accounted for with the material factor, while the weakening which occurs over the life of the material is accounted for with a conversion factor. The variability in stiffness is accounted for with a similar conversion factor and a stiffness reduction factor.

### G.5.1 Material Factor

The material factor for composites is determined slightly similarly to those for other materials, where a reliability index  $\beta$  needs to be reached. This reliability is required from two partial material factors. The first is determined from the manner in which the characteristic material properties have been statistically determined. The second partial factor accounts for the variability in material properties caused by the production method and the curing. The product of these two gives the material factor, as

shown in Equation 34. The value of the second partial factor can be found in Table 45. The combined material factor can then be applied in the same manner as those for more traditional materials.<sup>192</sup>

$$\gamma_M = \gamma_{M,1} * \gamma_{M,2}$$

$$\gamma_{M,1} = 1.35$$

Equation 34: Material Factor<sup>193</sup>

Production Method	Partial Material Factor $\gamma_{M,2}$	
	Post-Cured	Not Post-Cured
Spray-up	1.6	1.9
Wet Lay-up	1.4	1.7
Vacuum or Pressure Injection	1.2	1.4
Filament Winding	1.1	1.3
Prepreg	1.1	1.3
Pultrusion	1.1	1.3

Table 45: Partial Material Factor  $\gamma_{M,2}$ <sup>194</sup>

There are two additional restrictions placed on the material factor. First, for the ULS calculation, the combined factor may not be smaller than 1.5. This is only relevant where the lowest second partial factor is applied. A more relevant restriction regards the stability criterion. When this is being tested, the combined material factor must exceed 2.5.<sup>195</sup>

### G.5.2 Conversion Factors

Fiber reinforced polymers can be weakened by things they are subjected to throughout their lifetime. While there are many factors which can affect the properties of the material, the 4 largest influences are regarded here. These 4 effects are temperature, moisture, creep, and fatigue. Each of these is responsible for a partial conversion factor, and the product of the partial conversion factors is the total conversion factor, as shown in Equation 35. Depending on the limit state regarded, not all of these conversion factors need be applied, see Table 47.

$$\gamma_c = \gamma_{ct} * \gamma_{cv} * \gamma_{ck} * \gamma_{cf}$$

Equation 35: Combined Conversion Factor<sup>196 197</sup>

<sup>192</sup> (Civieltechnisch Centrum Uitvoering Research en Regelgeving-onderzoekcommissie C 124, 2003-6)

<sup>193</sup> (Civieltechnisch Centrum Uitvoering Research en Regelgeving-onderzoekcommissie C 124, 2003-6)

<sup>194</sup> (Civieltechnisch Centrum Uitvoering Research en Regelgeving-onderzoekcommissie C 124, 2003-6)

<sup>195</sup> (Civieltechnisch Centrum Uitvoering Research en Regelgeving-onderzoekcommissie C 124, 2003-6)

<sup>196</sup> (Civieltechnisch Centrum Uitvoering Research en Regelgeving-onderzoekcommissie C 124, 2003-6)

<sup>197</sup> Note that the first three subscripts are derived from Dutch. With “v” referring to moisture (“vocht”), “k” referring to creep (“kruip”), and “t” referring to temperature (“temperatuur”). “f” Refers to fatigue.



## Temperature

The temperature affects the strength and stiffness of materials. In the case of composites, the resin is affected significantly more than the fibers. Thermosetting polymers have a glass transition temperature. This is a temperature at which a steep decrease in stiffness (and strength) occurs, as shown in Figure 117, but this temperature will not be reached under normal conditions. What is relevant in Figure 117, is that there is still a negative slope in the region not affected by the glass transition temperature. This indicates that the material properties degrade at increasing temperature prior to reaching the glass transition temperature. To account for this, the temperature conversion factor is applied. The value of this factor is given in Equation 36.

$$\gamma_{ct} = 1.1$$

Equation 36: Temperature Conversion Factor<sup>198</sup>

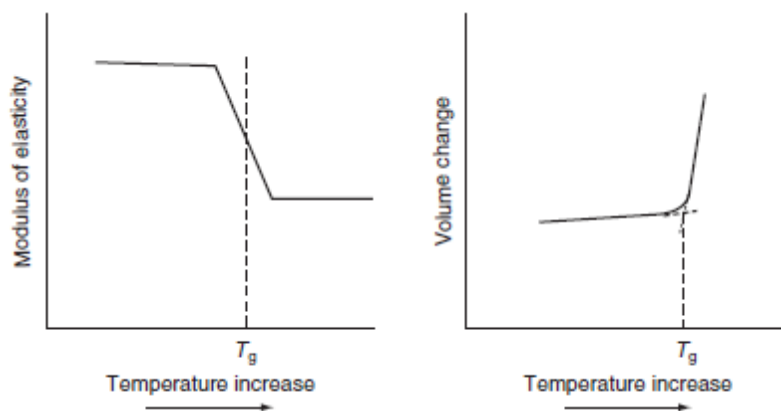


Figure 117: Effect of Temperature on Thermosetting Polymers<sup>199</sup>

## Moisture

The second partial conversion factor which must be applied is the one regarding moisture. Moisture ingress negatively affects the material properties, as shown in Figure 118<sup>200</sup>. The degree of degradation is dependent on the relative humidity of the specimen, which is in turn dependent on the moisture situation in which it is placed. The situations are subdivided into three groups, constant exposure, intermittent exposure, no exposure. The corresponding conversion factors are given in Table 46. For this case study, intermittent exposure is expected.

<sup>198</sup> (Civieltechnisch Centrum Uitvoering Research en Regelgeving-onderzoekcommissie C 124, 2003-6)

<sup>199</sup> (Hewson & Parke, 2008)

<sup>200</sup> Note that the negative influence of temperature is also visible in this figure.

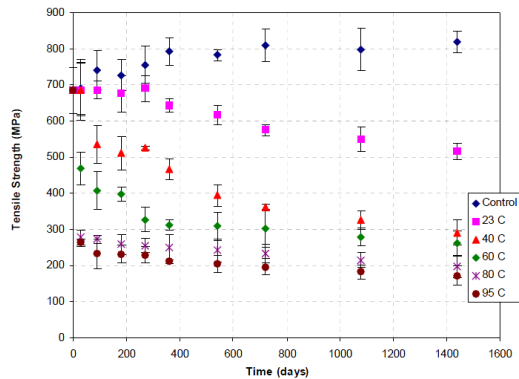


Figure 118: Tensile Strength of FRP Specimens Submersed in Water<sup>201</sup>

Moisture Conversion Factor	
Constant Exposure	1.25
Intermittent Exposure	1.1
No Exposure	1

Table 46: Moisture Conversion Factor<sup>202</sup>

### Creep

The third conversion factor which must be accounted for is the creep conversion factor. Creep is a phenomenon whereby over time, a material will continue to deform under loading. Typical creep behavior of thermoset polymers is shown in Figure 119. The creep factor consists of two partial factors for composite laminates. The first is, as expected, a time dependent factor. The second, accounts for the different orientations of the lamellas, expecting the lamellas with fibers in loading to take a larger percentage of the load since the other lamellas will creep more. The time dependent factor is determined according to Equation 37. In which time is measured in hours, and n is dependent for on the fiber product used. For UD lamellas  $n = 0.01$ .<sup>203</sup>

$$\gamma_{ck,1} = t_{life}^n$$

$$\gamma_{ck,1} = 1.14$$

Equation 37: Time dependent creep conversion factor<sup>204</sup>

With:

$t_{life}$ : Design Lifetime of the Structure [hours]

n: Factor Dependent on Type of Fiber Product Used. For UD lamellas  $n=0.01$

<sup>201</sup> (Surathi & Karbhari, 2006)

<sup>202</sup> (Civieltechnisch Centrum Uitvoering Research en Regelgeving-onderzoekcommissie C 124, 2003-6)

<sup>203</sup> (Civieltechnisch Centrum Uitvoering Research en Regelgeving-onderzoekcommissie C 124, 2003-6)

<sup>204</sup> (Civieltechnisch Centrum Uitvoering Research en Regelgeving-onderzoekcommissie C 124, 2003-6)

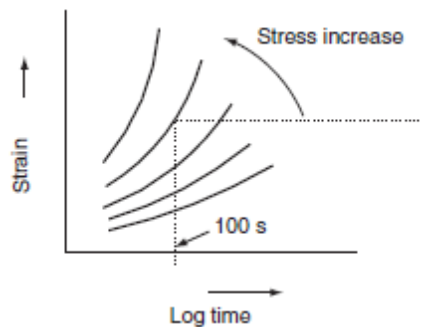


Figure 119: Effect of Creep on FRP Strain<sup>205</sup>

The second creep effect which must be taken into consideration for laminates, regards lamella orientation. Lamellas whose fibers are in the direction of the load show less creep deformation than lamellas with other orientations. Therefore, as the material undergoes creep, these lamellas will begin to carry a larger portion of the load, so that they will also creep more. The method for calculating the partial conversion factor responsible for this effect is to establish the quotient of the strain when only the lamellas oriented in the loading direction carry the load and the strain when the entire laminate contributes. This method is shown in Equation 38. An important note, is that the creep conversion factor is only applied when considering permanent or long-term loading.<sup>206</sup> The method for determining the Young's Modulus of a laminate is outlined H.2 Classical Laminate Theory in followed by H.3 Engineering Constants of Laminate

$$\varepsilon_{1,laminate} = \frac{F_1}{E_{1,laminate} * A_{laminate}}$$

$$\varepsilon_1 = \frac{F_1}{E_1 * A_{lamella}}$$

$$\gamma_{ck,2} = \frac{\varepsilon_1}{\varepsilon_{1,laminate}} = \frac{E_1 * h_{lamella}}{E_{1,laminate} * h_{laminate}}$$

Equation 38: Second Partial Creep Conversion Factor

With:

- $\varepsilon_{1,laminate}$ : Strain in Primary Direction of the Laminate [-]
- $F_1$ : Hypothetical Force Acting on the Laminate [N]
- $E_{1,laminate}$ : Young's Modulus of the Laminate in Primary Direction [MPa]
- $A_{laminate}$ : Cross sectional Area of the Laminate [mm<sup>2</sup>]
- $\varepsilon_1$ : Strain in Longitudinal Direction of Lamella [-]
- $E_1$ : Young's Modulus in Longitudinal Direction of Lamella [MPa]

<sup>205</sup> (Hewson & Parke, 2008)

<sup>206</sup> (Civieltechnisch Centrum Uitvoering Research en Regelgeving-onderzoekcommissie C 124, 2003-6)

$h_{lamella}$ : Total Height of Lamellas Oriented in Primary Direction [mm]  
 $h_{laminat}$ : Total Height of the Laminat [mm]

### Fatigue

Fatigue damage is accumulated over the lifetime of a structure. In composites, the fatigue damage accumulation is divided into three segments, compliant with the stiffness-load cycles curve presented in Figure 120. During the first phase of the life of the structure, a quick decrease in material stiffness is expected, amounting to between 10% and 20% of the original value. The second phase shows a slow decline of the Young's Modulus over time. The third phase shows an very fast drop in stiffness and typically represent failure. Since the design goal is that this third stage is never reached, the reduction will be limited to the 10% to 20% accumulated during the first stage. The conversion factor applied accounts for 10% damage, as shown in Equation 39.<sup>207</sup>

$$\gamma_{cf} = 1.1$$

Equation 39: Fatigue Conversion Factor<sup>208</sup>

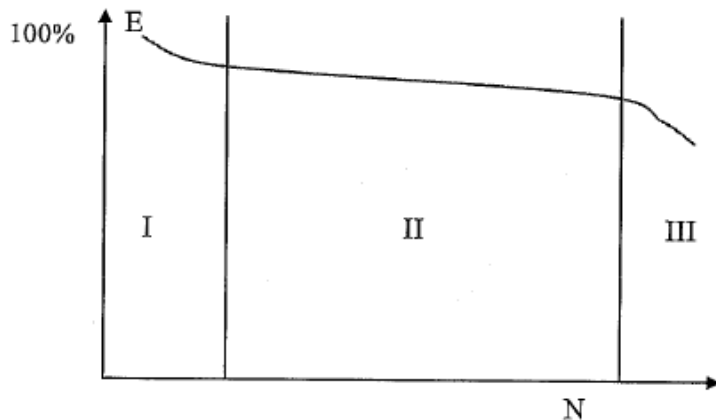


Figure 120: Stiffness Reduction Due to Fatigue<sup>209</sup>

### Application of Conversion Factors

Not all conversion factors need to be applied in all situations. For instance, when performing an ultimate limit state analysis, the fatigue conversion factor is not relevant. This is because the fatigue

<sup>207</sup> (Civieltechnisch Centrum Uitvoering Research en Regelgeving-onderzoekcommissie C 124, 2003-6)

<sup>208</sup> (Civieltechnisch Centrum Uitvoering Research en Regelgeving-onderzoekcommissie C 124, 2003-6)

<sup>209</sup> (Civieltechnisch Centrum Uitvoering Research en Regelgeving-onderzoekcommissie C 124, 2003-6)

conversion factor presented here only applies to material stiffness. The relevance of each of the conversion factors for the various limit states is presented in Table 47.<sup>210</sup>

Application of Conversion Factors			
	ULS Strength	Fatigue	SLS Deformations
Temperature	x	x	x
Moisture	x	x	x
Creep	x		x
Fatigue			x
<b>Total</b>	<b>1.8175</b>	<b>1.21</b>	<b>1.9992</b>

Table 47: Application of Conversion Factors<sup>211</sup>

### G.5.3 Stiffness Reduction Factor

The stiffness reduction factor is specified by norms. It needs to be applied to the stiffnesses in axial, transverse and shear direction. It is not applied to the Poisson's Ratio. The value of the reduction factor is given in Equation 40, under the assumption that UD-lamellas will be applied.

$$\gamma_{reduction} = 0.97$$

Equation 40: Stiffness Reduction Factor<sup>212</sup>

## G.6 Thermal Expansion

The thermal expansion must be calculated in the axial and transverse direction. To this end, the parallel and series model will be used respectively. In both cases, the assumption is made that a cross section of the material will remain flat and show uniform contraction/expansion. Since the material consists of two materials with very different thermal expansion coefficients, this may not be entirely accurate, but the difference is considered negligible.

### G.6.1 Axial Thermal Expansion

The axial thermal expansion is calculated in based on the parallel model stiffness. The fibers typically expand less than the resin, but the assumption is made that the cross-section expands uniformly. Therefore, stresses will arise in the fibers and resin. A balance will be reached at a certain stress level, where the strains due to thermal expansion and stress are equal. This is expansion will give the combined thermal expansion.

First the thermal strain for each material is given in Equation 41. Next the linear strains due to force on a specimen are given in Equation 42. First, note that due to the requirement of force equilibrium, the

<sup>210</sup> (Civieltechnisch Centrum Uitvoering Research en Regelgeving-onderzoekcommissie C 124, 2003-6)

<sup>211</sup> (Civieltechnisch Centrum Uitvoering Research en Regelgeving-onderzoekcommissie C 124, 2003-6)

<sup>212</sup> (Civieltechnisch Centrum Uitvoering Research en Regelgeving-onderzoekcommissie C 124, 2003-6)

two forces regarded are equal and opposite, i.e.  $F_r = -F_f$ . Secondly, note that the areas under consideration are directly proportional to the fiber volume fraction under the assumption of a continuous fiber, UD-lamella.

$$\varepsilon_{f,T} = \alpha_f * \Delta T$$

$$\varepsilon_{r,T} = \alpha_r * \Delta T$$

**Equation 41: Thermal Expansion of Pure Fibers and Pure Resin<sup>213</sup>**

With:

$\varepsilon_{f,T}$ : Strain in Fibers Due to Thermal Expansion [-]

$\alpha_f$ : Thermal Expansion Coefficient of Fiber Material [1/K]

$\Delta T$ : Change in Temperature [K]

$\varepsilon_{r,T}$ : Strain in Resin Due to Thermal Expansion [-]

$\alpha_r$ : Thermal Expansion Coefficient of Resin [1/K]

$$\varepsilon_{f,F} = \frac{F_f}{E_f A_f}$$

$$\varepsilon_{r,F} = \frac{F_r}{E_r A_r}$$

**Equation 42: Linear Strain Due to Force.**

With:

$\varepsilon_{f,F}$ : Strain in Fibers Due to Force [-]

$F_f$ : Force Acting on Fibers [N]

$E_f$ : Young's Modulus of Fibers [MPa]

$A_f$ : Cross Sectional Area of Fibers [mm<sup>2</sup>]

$\varepsilon_{r,F}$ : Strain in Resin Due to Force [-]

$F_r$ : Force in Resin [N]

$E_r$ : Young's Modulus of Resin [MPa]

$A_r$ : Cross Sectional Area of Resin [mm<sup>2</sup>]

Combining the two equations yields Equation 43, which can be rewritten into Equation 44, to find the equalization force. This for using this force, the combined expansion under thermal loading can be found according to Equation 45.

$$\varepsilon_{f,T} + \varepsilon_{f,F} = \varepsilon_{r,T} + \varepsilon_{r,F}$$

---

<sup>213</sup> (Roylance, 2000)

$$\alpha_f * \Delta T + \frac{F_f}{E_f A_f} = \alpha_r * \Delta T + \frac{F_r}{E_r A_r}$$

Equation 43: Expansion Considering Thermal Expansion and an Equalizing Force Component

$$F_f = \frac{(\alpha_r - \alpha_f) * \Delta T}{\left(\frac{1}{E_f A_f} + \frac{1}{E_r A_r}\right)}$$

Equation 44: Equalization Force

$$\alpha_1 = \frac{\varepsilon_{1,T}}{\Delta T} = \alpha_f + \left(\frac{1}{E_f A_f}\right) * \frac{(\alpha_r - \alpha_f)}{\left(\frac{1}{E_f A_f} + \frac{1}{E_r A_r}\right)}$$

Equation 45: Axial Coefficient of Thermal Expansion of Composite

With:

$\alpha_1$ : Thermal Expansion Coefficient of Composite in Longitudinal Direction [1/K]

$\varepsilon_{1,T}$ : Thermal Strain in Longitudinal Direction of Composite [-]

The values of the varying types of strain are given in Figure 121. Note here the large difference in strains between the resin and the fibers. And also that the thermal expansion of the composite material is mainly governed by the fibers.

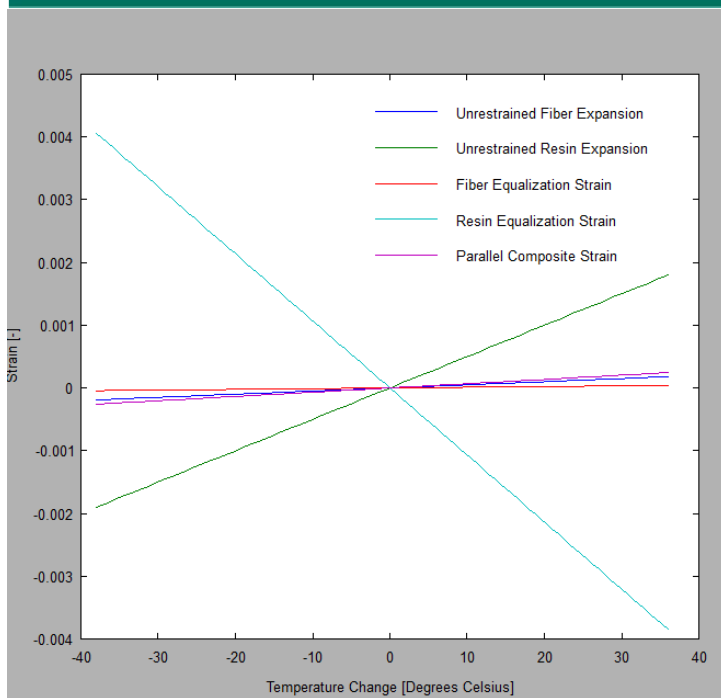


Figure 121: Various Axial Strains for Thermal Expansion

## G.6.2 Transverse Thermal Expansion

The transverse thermal expansion is accordance with the series model. Again, it will be calculated by combining the expansion of each material and adding these together, similar to G.2.1 Parallel Model Stiffness. The expected thermal strain is given in Equation 46. Rewriting this gives the coefficient of thermal expansion, as done in Equation 47.

$$\varepsilon_{2,T} = A_f * \alpha_f * \Delta T + A_r * \alpha_r * \Delta T$$

Equation 46: Transverse Thermal Strain

With:

$\varepsilon_{2,T}$ : Thermal Strain in Transverse Direction [-]

$$\alpha_2 = \frac{\varepsilon_{2,T}}{\Delta T} = A_f * \alpha_f + A_r * \alpha_r$$

Equation 47: Transverse Coefficient of Thermal Expansion



With:

$\alpha_2$ : Thermal Expansion Coefficient of Composite in Transverse Direction

## G.7 Summary of Lamella Properties

A short summary of the lamella properties determined above is given here.

1. Fiber Volume Fraction: The percentage of fibers in a lamella by volume. Influences all strength and stiffness values.
2. Stiffness
  - a. Axial Stiffness: Theoretical value for the stiffness in axial direction
  - b. Transverse Stiffness: Theoretical value for the stiffness in transverse direction
  - c. Tsai-Halpin: Empirical relationship between the constituent properties and the stiffnesses in axial, transverse, and shear directions.
3. Strength
  - a. Axial Tensile Strength
  - b. Axial Compressive Strength
  - c. Transverse Tensile Strength
  - d. Transverse Compressive Strength
  - e. Shear Strength
4. Failure Criteria
  - a. Tsai-Hill: A failure criteria which does not take into account the difference in tensile and compressive properties.
  - b. Tsai-Wu: An expansion of Tsai-Hill to account for differences in tensile and compressive behavior.
5. Correction Factors
  - a. Material Factor: A safety factor accounting for material strength variability and production process variability.
  - b. Conversion Factor: A safety factor dependent on loading condition which takes into account (any of): Temperature, creep, fatigue and moisture.
  - c. Stiffness Reduction Factor: A reduction in axial, transverse and shear stiffness.
6. Thermal Expansion: The expansion behavior of a lamella under changing temperature.
  - a. Axial Expansion Coefficient
  - b. Transverse Expansion Coefficient

## Appendix H: Laminate Properties

Due to the minimal strength of the resin, guidelines have been created for the fiber orientation. To ensure unforeseen forces, impact forces, creep and fatigue are never solely resisted by the resin, a minimum of 15% of the fiber volume is required in each direction. Each direction refers to four specific angles:  $0^\circ$ ,  $+45^\circ$ ,  $90^\circ$  and  $-45^\circ$ , although an allowance has been made for the  $0^\circ$ ,  $60^\circ$ , and  $-60^\circ$  orientation.<sup>214</sup>

The required minimum percentage of FVF in each direction can be achieved in several ways. Chopped strand mats or continuous filament mats can be applied. Although these are not allowed to be used without other fabrics. Therefore woven or UD fabrics or multiple layers of thereof stitched together should be applied.<sup>215</sup> Applying several of these layers together is commonly called a laminate. Generally, a laminate will consist of layers of UD lamellas rather than woven fabrics, since the FVF will be higher for UD lamella based composites.

Note that for this chapter, the x,y,z-coordinate system will apply to lamellas, and the 1,2,3-coordinate system corresponds to the global laminate coordinate system.

### H.1 Classic Plate Theory

The method by which the different properties of laminates are accounted for is called Classical Laminate Theory (CLT). CLT is based on classic plate theory (CPT), but adapted for use with a layered material. Classic plate theory establishes an analytical method for calculating stresses, moments, and displacements of a thin plate. The plate theory is based on Kirchhoff's hypotheses; a series of assumptions upon which these derivations are based:

1. *"The material of the plate is elastic, homogenous, and isotropic"*
2. *The plate is Initially flat*
3. *The deflection (the normal component of the displacement vector) of the midplane is small compared with the thickness of the plate. The slope of the deflected surface is therefore very small and the square of the slope is a negligible quantity in comparison with unity.*
4. *The straight lines, initially normal to the middle plane before bending, remain straight and normal to the middle surface during the deformation, and the length of such elements is not altered. This means that the shear strains  $\gamma_{xz}$  and  $\gamma_{yz}$  are negligible and the normal strain  $\varepsilon_z$  may also be omitted. This assumption is referred to as the "hypothesis of straight normals"*
5. *The stress normal to the middle plane,  $\sigma_z$ , is small compared with the other stress components and may be neglected in the stress-strain relations.*

<sup>214</sup> (Civieltechnisch Centrum Uitvoering Research en Regelgeving-onderzoekcommissie C 124, 2003-6)

<sup>215</sup> (Civieltechnisch Centrum Uitvoering Research en Regelgeving-onderzoekcommissie C 124, 2003-6)

6. *Since the displacements of a plate are small, it is assumed that the middle surface remains unstrained after bending.*<sup>216</sup>

### H.1.1 Kinematic Equations

The kinematic equations are based on the assumed displacement fields given below. In the equations below, the first term on the right hand side represents the displacement of the neutral line, while the second term represents the displacement due to rotation of the neutral line. Note that due to the assumption of a thin plate the equation in vertical direction is missing the bending term.

$$u = u(x, y, z) = u_0(x, y) - z \frac{\partial w}{\partial x}$$

$$v = v(x, y, z) = v_0(x, y) - z \frac{\partial w}{\partial y}$$

$$w = w(x, y, z) = w_0(x, y)$$

Equation 48: Displacement Fields<sup>217</sup>

With:

$x$ : Coordinate Along the x-Axis [mm]

$y$ : Coordinate Along the y-Axis [mm]

$z$ : Coordinate Along the z-Axis [mm]

$u$ : Displacement in x-Direction [mm]

$v$ : Displacement in y-Direction [mm]

$w$ : Displacement in z-Direction [mm]

$u_0$ : Displacement in x-Direction of the Neutral Axis at the Considered Coordinates [mm]

$v_0$ : Displacement in y-Direction of the Neutral Axis at the Considered Coordinates [mm]

$w_0$ : Displacement in z-Direction of the Neutral Axis at the Considered Coordinates [mm]

The displacement field is converted to the strain field by taking the derivative with respect to the desired direction. Note here that the normal strain in z-direction, as well as both shear strains containing a z-component, are set to zero. This is due to the hypothesis of straight normal; assumption 4 above.

$$\varepsilon_x = \frac{d(u(x, y, z))}{dx} = \frac{du_0}{dx} - z \frac{\partial^2 w}{\partial x^2}$$

$$\varepsilon_y = \frac{d(v(x, y, z))}{dy} = \frac{dv_0}{dy} - z \frac{\partial^2 w}{\partial y^2}$$

<sup>216</sup> (Ventsel & Krauthammer, 2001)

<sup>217</sup> (Ventsel & Krauthammer, 2001)

$$\varepsilon_z = \frac{d(w(x, y, z))}{dz} = 0$$

Equation 49: Kinematic Equations Normal Strain<sup>218</sup>

With:

$\varepsilon_x$ : Normal Strain in x-Direction [-]

$\varepsilon_y$ : Normal Strain in x-Direction [-]

$\varepsilon_z$ : Normal Strain in x-Direction [-]

$$\gamma_{xy} = \frac{d(v(x, y, z))}{dx} + \frac{d(u(x, y, z))}{dy} = \frac{dv_0}{dx} + \frac{du_0}{dy} - 2z \frac{\partial w}{\partial x \partial y}$$

$$\gamma_{yz} = 0$$

$$\gamma_{xz} = 0$$

Equation 50: Kinematic Equations Shear Strain<sup>219</sup>

With:

$\gamma_{xy}$ : Shear Strain in the xy-Plane

$\gamma_{yz}$ : Shear Strain in the yz-Plane

$\gamma_{xz}$ : Shear Strain in the xz-Plane

Writing the kinematic equations in vector form and eliminating the null terms, we obtain Equation 51. Note that the strains are split into a normal strain component and a curvature component dependent on vertical coordinate z.

$$[\varepsilon] = \begin{bmatrix} \varepsilon_x \\ \varepsilon_y \\ \gamma_{xy} \end{bmatrix} = \begin{bmatrix} \frac{du_0}{dx} \\ \frac{dv_0}{dy} \\ \frac{du_0}{dx} + \frac{dv_0}{dy} \end{bmatrix} + z \begin{bmatrix} -\frac{\partial^2 w}{\partial x^2} \\ -\frac{\partial^2 w}{\partial y^2} \\ -2\frac{\partial w}{\partial x \partial y} \end{bmatrix} = [\varepsilon_0] + z[\kappa]$$

Equation 51: Kinematic Equations in Vector Form<sup>220</sup>

With:

$[\kappa]$ : Curvature Tensor [1/mm]

<sup>218</sup> (Ventsel & Krauthammer, 2001)

<sup>219</sup> (Ventsel & Krauthammer, 2001)

<sup>220</sup> (Ventsel & Krauthammer, 2001)

## H.1.2 Constitutive Equations

The constitutive equations are based on Hooke's law. Hooke's law is shown here for materials with orthotropic properties. This means that different Young's moduli, Poisson's ratios and shear moduli have been included.

$$\varepsilon_x = \frac{\sigma_x}{E_x} - \frac{\nu_{yx}\sigma_y}{E_y} - \frac{\nu_{xz}\sigma_z}{E_z}$$

$$\varepsilon_y = \frac{\sigma_y}{E_y} - \frac{\nu_{xy}\sigma_x}{E_x} - \frac{\nu_{yz}\sigma_z}{E_z}$$

$$\varepsilon_z = \frac{\sigma_z}{E_z} - \frac{\nu_{xz}\sigma_x}{E_x} - \frac{\nu_{zy}\sigma_y}{E_y}$$

Equation 52: Constitutive Equations for Axial Strain<sup>221</sup>

With:

$\sigma_i$ : Axial Stress in "i-Direction" [MPa]

$E_i$ : Young's Modulus in "i-Direction" [MPa]

$\nu_{ij}$ : Poisson's Ratio in the "ij-plane" [-]

$$\gamma_{xy} = \frac{1}{G_{xy}} \tau_{xy}$$

$$\gamma_{yz} = \frac{1}{G_{yz}} \tau_{yz}$$

$$\gamma_{xz} = \frac{1}{G_{xz}} \tau_{xz}$$

Equation 53: Constitutive Equations for Shear Strain<sup>222</sup>

With:

$G_{ij}$ : Shear Modulus in the "ij-plane" [MPa]

$\tau_{ij}$ : Shear Stress in the "ij-plane" [MPa]

The relationships between the stresses and strains is given in Equation 54. Note that the components in z-direction are not shown. This is again based on the assumption that they are negligible. The relationship in Equation 54 is inverted in Equation 55, to produce the form which will be used later.

<sup>221</sup> (Ventsel & Krauthammer, 2001)

<sup>222</sup> (Ventsel & Krauthammer, 2001)

$$[\varepsilon] = \begin{bmatrix} \frac{1}{E_x} & -\frac{\nu_{yx}}{E_y} & 0 \\ -\frac{\nu_{xy}}{E_x} & \frac{1}{E_y} & 0 \\ 0 & 0 & \frac{1}{G} \end{bmatrix} * \begin{bmatrix} \sigma_x \\ \sigma_y \\ \tau_{xy} \end{bmatrix} = [S][\sigma]$$

Equation 54: 2-Dimensional Constitutive Equations in Matrix Form<sup>223</sup>

With:

[S]: Compliance Matrix [MPa<sup>-1</sup>]

$$[\sigma] = [S]^{-1}[\sigma] = [Q][\varepsilon] = \begin{bmatrix} \frac{E_x}{1 - \nu_{yx}\nu_{xy}} & \frac{\nu_{xy}E_y}{1 - \nu_{yx}\nu_{xy}} & 0 \\ \frac{\nu_{yx}E_x}{1 - \nu_{yx}\nu_{xy}} & \frac{E_y}{1 - \nu_{yx}\nu_{xy}} & 0 \\ 0 & 0 & G \end{bmatrix} [\varepsilon]$$

Equation 55: Inverse Constitutive Equation<sup>224</sup>

With:

[Q]: Stiffness Matrix. Sometimes denoted as [C]. [MPa]

### H.1.3 Equilibrium Equations

The equilibrium equations set the relationship between the forces and moments acting on a cross section, and the stresses present in that cross section. For normal stresses this amounts to the straight integral of stresses over the height of the cross section. While for moments, the integrand is first multiplied by z. Note that for both forces and moments, the values are per unit width. After that the definition of the stresses found in Equation 55 substituted into the equation. Combining the results leads to Equation 58.

$$[N] = \begin{bmatrix} N_x \\ N_y \\ N_{xy} \end{bmatrix} = \int_{z_{bottom}}^{z_{top}} \begin{bmatrix} \sigma_x \\ \sigma_y \\ \tau_{xy} \end{bmatrix} dz = \int_{z_{bottom}}^{z_{top}} [Q][\varepsilon] dz = [Q] \left( \int_{z_{bottom}}^{z_{top}} [\varepsilon_0] dz + \int_{z_{bottom}}^{z_{top}} z[\kappa] dz \right)$$

<sup>223</sup> (Ventsel & Krauthammer, 2001)

<sup>224</sup> (Ventsel & Krauthammer, 2001)

$$[N] = [Q] \left( [\varepsilon_0] * z \Big|_{z_{bottom}}^{z_{top}} + [\kappa] * \frac{z^2}{2} \Big|_{z_{bottom}}^{z_{top}} \right)$$

Equation 56: Equilibrium Equation for Normal Force<sup>225</sup>

With:

- $N_x$ : Normal Force in x-direction per unit width [N/mm]
- $N_y$ : Normal Force in y-direction per unit length [N/mm]
- $N_{xy}$ : Shear Force in the xy-plane per unit width [N/mm]
- $z_{top}$ : Highest z-coordinate of Layer
- $z_{bottom}$ : Lowest z-coordinate of Layer

$$[M] = \begin{bmatrix} M_x \\ M_y \\ M_{xy} \end{bmatrix} = \int_{z_{bottom}}^{z_{top}} \begin{bmatrix} \sigma_x \\ \sigma_y \\ \tau_{xy} \end{bmatrix} z dz = \int_{z_{bottom}}^{z_{top}} [Q][\varepsilon] z dz = [Q] \left( \int_{z_{bottom}}^{z_{top}} [\varepsilon_0] z dz + \int_{z_{bottom}}^{z_{top}} z^2 [\kappa] dz \right)$$

$$[M] = [Q] \left( [\varepsilon_0] * \frac{z^2}{2} \Big|_{z_{bottom}}^{z_{top}} + [\kappa] * \frac{z^3}{3} \Big|_{z_{bottom}}^{z_{top}} \right)$$

Equation 57: Equilibrium Equation for Moments<sup>226</sup>

With:

- $M_x$ : Bending Moment in x-Direction per unit width [Nmm/mm]
- $M_y$ : Bending Moment in y-direction per unit length [Nmm/mm]
- $M_{xy}$ : Bending Moment in the xy-plane per unit width [Nmm/mm]

$$\begin{bmatrix} [N] \\ [M] \end{bmatrix} = \begin{bmatrix} [Q] * z \Big|_{z_{bottom}}^{z_{top}} & [Q] * \frac{z^2}{2} \Big|_{z_{bottom}}^{z_{top}} \\ [Q] * \frac{z^2}{2} \Big|_{z_{bottom}}^{z_{top}} & [Q] * \frac{z^3}{3} \Big|_{z_{bottom}}^{z_{top}} \end{bmatrix} \begin{bmatrix} [\varepsilon] \\ [\kappa] \end{bmatrix} = \begin{bmatrix} A & B \\ B & D \end{bmatrix} \begin{bmatrix} [\varepsilon] \\ [\kappa] \end{bmatrix}$$

Equation 58: Combined Equations for Normal Forces and Moments<sup>227</sup>

With:

- $\begin{bmatrix} A & B \\ B & D \end{bmatrix}$ : The ABD Matrix. Variable Units Per Quadrant. [A : N/mm]; [B : N]; [D : Nmm]

<sup>225</sup> (Ventsel & Krauthammer, 2001)

<sup>226</sup> (Ventsel & Krauthammer, 2001)

<sup>227</sup> (Ventsel & Krauthammer, 2001)

Equation 58 gives the relationships between forces per unit width, and strains. Note that the quadrants of the matrix denoted by [B] are zero in case of a symmetric cross section (assumption 1). The terms have been included here as they will be useful later.

## H.2 Classical Laminate Theory

The assumption of a homogenous, isotropic material is not valid for laminates. Therefore, the theory needs to be adapted to fit to laminates. The first step in doing so is to realize that laminates consist of layers of material with different properties. The properties may be different because different materials have been used in each ply, but will generally be due to the rotations of the plies with respect to each other. For different material lamellas, different [Q] matrices must be established. However, for rotated plies, the properties can be rotated according to Equation 59.

$$[\bar{Q}] = [T]^{-1}[Q][R][T][R]^{-1}$$

$$[T] = \begin{bmatrix} \cos^2(\theta) & \sin^2(\theta) & 2 \cos(\theta) \sin(\theta) \\ \sin^2(\theta) & \cos^2(\theta) & -2 \cos(\theta) \sin(\theta) \\ -\cos(\theta) \sin(\theta) & \cos(\theta) \sin(\theta) & \cos^2(\theta) - \sin^2(\theta) \end{bmatrix}$$

$$[R] = \begin{bmatrix} 1 & 0 & 0 \\ 0 & 1 & 0 \\ 0 & 0 & 2 \end{bmatrix}$$

Equation 59: Rotation Function for [Q] Matrix<sup>228</sup>

With:

[ $\bar{Q}$ ]: Stiffness Matrix for a Rotated Ply [MPa]

[T]: Transformation Matrix [-]

[R]: Reuter's Matrix [-]

$\theta$ : Rotation of the Considered Ply [Radians]

A second problem consists of how to add the plies together. The theory of Equation 58, remains valid, however, since there are separate distinct layers, the terms must be calculated per layer according to Equation 60. Note here that k denotes the layer under consideration.

$$[A]^k = [\bar{Q}]^k (z_{k,top} - z_{k,bottom})$$

$$[B]^k = \frac{1}{2} [\bar{Q}]^k (z_{k,top}^2 - z_{k,bottom}^2)$$

<sup>228</sup> (Roylance, 2000)



$$[D]^k = \frac{1}{3}[\bar{Q}]^k(z_{k,top}^3 - z_{k,bottom}^3)$$

Equation 60: Definitions of [A],[B], and [D] per layer<sup>229</sup>

With:

$[A]^k$ : The Quadrant of the ABD Matrix in Equation 58 Labelled A, for Ply k.

$[B]^k$ : The Quadrant of the ABD Matrix in Equation 58 Labelled B, for Ply k.

$[D]^k$ : The Quadrant of the ABD Matrix in Equation 58 Labelled D, for Ply k.

$[\bar{Q}]^k$ : The Stiffness Matrix, Rotated in the Direction of Ply k

When the three matrices are determined for each layer, the matrices for the laminate becomes the summation over the lamellas. This is shown in Equation 61. Where the indices i and j range from 1 to 3.

$$A_{ij} = \sum_{k=1}^n A_{ij}^k$$

$$B_{ij} = \sum_{k=1}^n B_{ij}^k$$

$$D_{ij} = \sum_{k=1}^n D_{ij}^k$$

Equation 61: Terms of Total [A],[B],and [D] Matrices<sup>230</sup>

With:

$A_{ij}$ : Term in row "i," column "j" of A Matrix for Entire Laminate [N/mm]

$B_{ij}$ : Term in row "i," column "j" of B Matrix for Entire Laminate [N]

$D_{ij}$ : Term in row "i," column "j" of D Matrix for Entire Laminate [Nmm]

$A_{ij}^k$ : Term in row "i," column "j" of A Matrix for Lamella k [N/mm]

$B_{ij}^k$ : Term in row "i," column "j" of B Matrix for Lamella k [N]

$D_{ij}^k$ : Term in row "i," column "j" of D Matrix for Lamella k [Nmm]

## H.2.1 Thermal Stresses inside Laminates

Thermal effects are expected to play a significant part in the case study, due to the application of different materials. Therefore, the laminate theory should be augmented to include thermal expansion.

<sup>229</sup> (Calard, 2011)

<sup>230</sup> (Calard, 2011)

To this end recall Equation 51. This equation defined the strains as a function of neutral line extension and curvature. However, now the thermal strain will also be taken into account, as shown in Equation 62. Note that the thermal strain is subtracted from the mechanical strain. This is done because thermal expansion does not directly lead to stresses. A material which has a set strain, will see the mechanical component of said strain decrease as temperature increases (for most materials). Hence, for determining stresses in the laminate, thermal expansion should be subtracted.

$$[\varepsilon_M] = [\varepsilon] - [\varepsilon_T] = \begin{bmatrix} \varepsilon_x \\ \varepsilon_y \\ \gamma_{xy} \end{bmatrix}_M = \begin{bmatrix} \frac{du_0}{dx} \\ \frac{dv_0}{dy} \\ \frac{du_0}{dx} + \frac{dv_0}{dy} \end{bmatrix} + z \begin{bmatrix} -\frac{\partial^2 w}{\partial x^2} \\ -\frac{\partial^2 w}{\partial y^2} \\ -2\frac{\partial w}{\partial x \partial y} \end{bmatrix} - \begin{bmatrix} \alpha_x \\ \alpha_y \\ 0 \end{bmatrix} \Delta T = [\varepsilon_0] + z[\kappa] - \Delta T[\alpha]$$

Equation 62: Strains Including Thermal Expansion<sup>231</sup>

with:

$[\varepsilon_M]$ : Mechanical Strain in the Laminate [-]

$[\varepsilon]$ : Total Strain in the Laminate [-]

$[\varepsilon_T]$ : Thermal Strain in the Laminate [-]

$\alpha_x$ : Thermal Expansion Coefficient of the Lamella in x-Direction [1/K]

$\alpha_y$ : Thermal Expansion Coefficient of the Lamella in y-Direction [1/K]

$\Delta T$ : Change in Temperature [K]

The equation for the strain is plugged into the constitutive equations, repeated in . The same process is then followed to arrive at the equations for force and moments, as shown in Equation 64.

$$[\sigma] = [Q][\varepsilon_M]$$

Equation 63: Constitutive Equation, Repeated

$$[N] = [A \quad B] \begin{bmatrix} [\varepsilon_0] \\ [\kappa] \end{bmatrix} - [Q] \int_{z_{bottom}}^{z_{top}} \Delta T[\alpha] dz$$

$$[M] = [B \quad D] \begin{bmatrix} [\varepsilon_0] \\ [\kappa] \end{bmatrix} - [Q] \int_{z_{bottom}}^{z_{top}} \Delta T[\alpha]z dz$$

Equation 64: Equations for Force and Moment

<sup>231</sup> (Roylance, 2000)

For now, we assume no external forces or moments are applied. This is essentially assuming a free expansion scenario. This, naturally, does not need to be the case, yet any expansion which is restricted will return in the form of an external load on the structure. Therefore, this method will still produce accurate results. The simplification under no external forces is given in Equation 65. Note that while the final results are accurate, the values obtained here do not represent actual forces, but rather fictitious forces.

$$[A \quad B] \begin{bmatrix} [\varepsilon_0] \\ [\kappa] \end{bmatrix} = [Q] \int_{z_{bottom}}^{z_{top}} \Delta T [\alpha] dz = \Delta T [Q] [\alpha] (z_{top} - z_{bottom})$$

$$[B \quad D] \begin{bmatrix} [\varepsilon_0] \\ [\kappa] \end{bmatrix} = [Q] \int_{z_{bottom}}^{z_{top}} \Delta T [\alpha] z dz = \frac{1}{2} \Delta T [Q] [\alpha] (z_{top}^2 - z_{bottom}^2)$$

Equation 65: Stiffness Relation Under Thermal Loading<sup>232</sup>

To expand this from lamella to laminate, the same principle can be applied as in section H.2 Classical Laminate Theory. The main difference is that the thermal expansion coefficients also need to be rotated per lamella. This can be done according to Equation 66. Following this the right hand side of

$$\begin{bmatrix} \alpha_1 \\ \alpha_2 \\ \alpha_{12} \end{bmatrix} = [R][T]^{-1}[R]^{-1} \begin{bmatrix} \alpha_x \\ \alpha_y \\ 0 \end{bmatrix}$$

Equation 66: Rotation of Thermal Expansion Vector<sup>233</sup>

With:

- $\alpha_1$ : Normal Thermal Expansion Coefficient in Primary Direction [1/K]
- $\alpha_2$ : Normal Thermal Expansion Coefficient in Primary Direction [1/K]
- $\alpha_{12}$ : Shear Thermal Expansion Coefficient in Primary Direction [1/K]

Following this the right hand side of Equation 65 can be summed to find the fictitious thermal force, as given in Equation 67.

$$[N_T] = \sum_{k=1}^n \Delta T [\bar{Q}]^k [\alpha]^k (z_{k,top} - z_{k,bottom})$$

<sup>232</sup> (Kaw, 2006)

<sup>233</sup> (Roylance, 2000)

$$[M_T] = \frac{1}{2} \sum_{k=1}^n \Delta T [\bar{Q}]^k [\alpha] (z_{k,top}^2 - z_{k,bottom}^2)$$

Equation 67: Fictitious Thermal Forces and Moments<sup>234</sup>

With:

$[N_T]$ : Thermal Normal Forces [N/mm]

$[M_T]$ : Thermal Moments [Nmm/mm]

The fictitious forces and moments result will give actual mid-plane strains and curvatures which can be calculated according to Equation 68.

$$\begin{bmatrix} N_T \\ M_T \end{bmatrix} = \begin{bmatrix} A & B \\ B & D \end{bmatrix} \begin{bmatrix} [\varepsilon] \\ [\kappa] \end{bmatrix}$$

$$\begin{bmatrix} [\varepsilon_0] \\ [\kappa] \end{bmatrix} = \begin{bmatrix} A & B \\ B & D \end{bmatrix}^{-1} \begin{bmatrix} N_T \\ M_T \end{bmatrix}$$

Equation 68: Fictitious Thermal Strains<sup>235</sup>

Now, recall the definition of mechanical strains including thermal strain; repeated in Equation 69. All three components on the right hand side of the equation have now been determined. Therefore, the mechanical component of the strains is now known. This is the component of the strain which is responsible for actual internal stresses in the laminate. Be aware that the height  $z_k$  and the thermal expansion coefficient,  $\alpha$ , vary per lamella.

$$[\varepsilon_M] = [\varepsilon] - [\varepsilon_T] = [\varepsilon_0] + z_k [\kappa] - \Delta T [\alpha]^k$$

Equation 69: Mechanical Strains Resulting from Thermal Expansion<sup>236</sup>

The mechanical stresses following from this strain can be calculated according to Equation 63. Calculations show that the magnitude of these internal mechanical stresses are of the order  $3 \cdot 10^{-4}$  GPa/K. Therefore, with the maximum temperature change as described in A.1 Thermal Load, the loading should be limited in size to the order of 10 MPa. For illustrative purposes, a profile of the thermal stresses in the  $0^\circ$  direction of a  $[0 / 45 / 90 / -45 / -45 / 90 / 45 / 0]$  laminate with 3mm thick plies is shown in Figure 122.

<sup>234</sup> (Kaw, 2006)

<sup>235</sup> (Kaw, 2006)

<sup>236</sup> (Kaw, 2006)

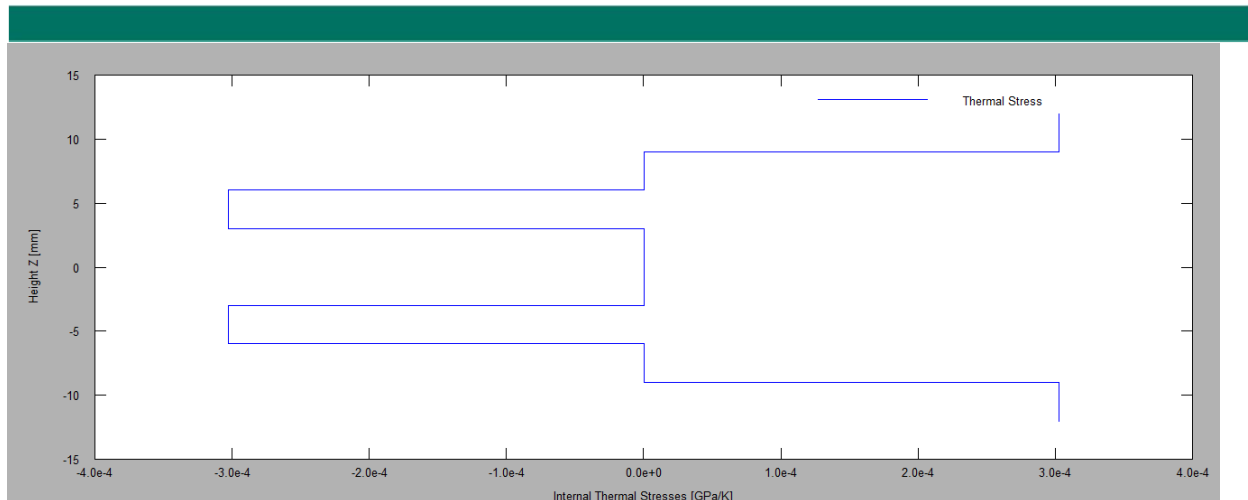


Figure 122: Internal Thermal Stress Profile

## H.2.2 Thermal Expansion of Laminates

Beyond the strains and stresses introduced internally, the global coefficients of thermal expansion of the composite material are also required. Luckily, this does not require a large step from the previous section. Continuing from where the fictitious thermal forces were found, Equation 67, the global thermal expansion coefficients can be found simply according to Equation 70. Here  $[A]$  represents the extensional component of the ABD matrix.

$$\begin{bmatrix} \alpha_1 \\ \alpha_2 \\ \alpha_{12} \end{bmatrix}^{Laminate} = [A]^{-1}[N_T]$$

Equation 70: Global Thermal Expansion Coefficients<sup>237</sup>

<sup>237</sup> (Kaw, 2006)

### H.3 Engineering Constants of Laminate

Following the derivation of the ABD matrix according to H.2 Classical Laminate Theory, it may be useful to obtain the traditional engineering constants from said matrix. The method for doing this is based on the definitions of the engineering constants and some linear algebra. First, the linear algebra principles of Cramer's rule of cofactor expansion will be explained.

#### Cramer's Rule

Cramer's Rule states that to find the solution of a linear system of equations in matrix form, the value of any individual variable can be found by the quotient of two matrix determinants. The denominator being the determinant of the coefficient matrix, and the numerator being the determinant of this same matrix with the answer column replacing the column associated with the desired variable. The process is shown in Table 48.

System of Equations	Coefficient Matrix Determinant	Answer Column	Coefficient Matrix with Answer Column in x-column	Solution
$2x + 1y + 1z = 3$ $1x - 1y - 1z = 0$ $1x + 2y + 1z = 0$	$D = \begin{vmatrix} 2 & 1 & 1 \\ 1 & -1 & -1 \\ 1 & 2 & 1 \end{vmatrix}$	$\begin{bmatrix} 3 \\ 0 \\ 0 \end{bmatrix}$	$D_x = \begin{vmatrix} 3 & 1 & 1 \\ 0 & -1 & -1 \\ 0 & 2 & 1 \end{vmatrix}$	$x = \frac{D_x}{D}$

Table 48: Cramer's Rule<sup>238</sup>

#### Cofactor Expansion

Cofactor expansion is a method for finding the determinant of large matrices. The method is valid for all sizes larger than [2X2]. It will be shown here for a [3X3] matrix, and later applied to a [6X6] matrix. Essentially the method boils down to 5 steps:

1. Choose a row or column
2. For each term in said row or column find the determinant of the matrix that is left over when the row and column of each term is removed from the original matrix.
3. Raise -1 to the power of the summation of the indices of the term it is based on. The result is called the cofactor.
4. Multiply each cofactor by the term which it was based on.
5. Sum the results for each term.<sup>239</sup>

<sup>238</sup> (Stapel, Cramer's Rule, 2012)

<sup>239</sup> (Stapel, Minors and Cofactors, 2012)

$$\det \begin{bmatrix} a_{1,1} & a_{1,2} & a_{1,3} \\ a_{2,1} & a_{2,2} & a_{2,3} \\ a_{3,1} & a_{3,2} & a_{3,3} \end{bmatrix} = a_{1,1} * (-1)^{(1+1)} * \det \begin{bmatrix} a_{2,2} & a_{2,3} \\ a_{3,2} & a_{3,3} \end{bmatrix} \\ + a_{1,2} * (-1)^{(1+2)} * \det \begin{bmatrix} a_{2,1} & a_{2,3} \\ a_{3,1} & a_{3,3} \end{bmatrix} \\ + a_{1,3} * (-1)^{(1+3)} * \det \begin{bmatrix} a_{2,1} & a_{2,2} \\ a_{3,1} & a_{3,2} \end{bmatrix}$$

#### Equation 71: Cofactor Expansion

In Equation 71, the choice has been made to use the first row to calculate the determinant. The three sub-matrices have then been set up deleting the first row and each of the columns one at a time. This process is quite common to see for [3X3] matrices, but the method may be expanded for any size matrix, and is quite useful when a sparse row or column is present.

#### Young's Modulus

The first engineering constant which will be derived is the engineering constant in the 1-direction. First, recall Equation 58, repeated in Equation 72. Next we start with the definition of the Young's Modulus, presented in Equation 73.

$$\begin{bmatrix} N_1 \\ N_2 \\ N_{12} \\ M_1 \\ M_2 \\ M_{12} \end{bmatrix} = \begin{bmatrix} A_{1,1} & A_{1,2} & A_{1,3} & B_{1,1} & B_{1,2} & B_{1,3} \\ A_{2,1} & A_{2,2} & A_{2,3} & B_{2,1} & B_{2,2} & B_{2,3} \\ A_{3,1} & A_{3,2} & A_{3,3} & B_{3,1} & B_{3,2} & B_{3,3} \\ B_{1,1} & B_{1,2} & B_{1,3} & D_{1,1} & D_{1,2} & D_{1,3} \\ B_{2,1} & B_{2,2} & B_{2,3} & D_{2,1} & D_{2,2} & D_{2,3} \\ B_{3,1} & B_{3,2} & B_{3,3} & D_{3,1} & D_{3,2} & D_{3,3} \end{bmatrix} \begin{bmatrix} \varepsilon_1 \\ \varepsilon_2 \\ \gamma_{12} \\ \kappa_1 \\ \kappa_2 \\ \kappa_{12} \end{bmatrix}$$

#### Equation 72: Load-Strain Relationship

With:

N: Normal Forces per Unit Length [N/mm]

M : Moments per Unit Length [Nmm/mm]

$A_{i,j}$ : A Component of the ABD Matrix According to Equation 61. [N/mm]

$B_{i,j}$ : B Component of the ABD Matrix According to Equation 61. [N]

$D_{i,j}$ : D Component of the ABD Matrix According to Equation 61. [Nmm]

$\varepsilon$ : Normal Strain [-]

$\gamma_{12}$ : Shear Strain [-]

$\kappa$ : Curvature [1/mm]

$$E_{1,lam} = \frac{F_1}{A * \epsilon_{1,lam}} = \frac{N_1}{h_{laminate} * \epsilon_{1,lam}}$$

#### Equation 73: Young's Modulus

With:

$E_{1,lam}$ : Young's Modulus of the Laminate in 1-Direction [MPa]

$F_1$ : Fictitiously Applied Force Applied to Laminate [N]

$A$ : Area of Laminate Under Consideration [mm<sup>2</sup>]

$\epsilon_{1,lam}$ : Strain of the Laminate in 1-Direction [-]

$N_1$ : Fictitiously Applied Force per Unit Width [N/mm]

$h_{laminate}$ : Height of Laminate [mm]

In order to solve Equation 73, Equation 72 must be solved to find a relationship between force and strain. This is done by simply applying a force in 1-direction, and setting all other forces and moments to zero. Then, using Cramer's rule the solution for strain in 1-direction may be found.

$$\begin{bmatrix} N_1 \\ 0 \\ 0 \\ 0 \\ 0 \\ 0 \end{bmatrix} = \begin{bmatrix} A_{1,1} & A_{1,2} & A_{1,3} & B_{1,1} & B_{1,2} & B_{1,3} \\ A_{2,1} & A_{2,2} & A_{2,3} & B_{2,1} & B_{2,2} & B_{2,3} \\ A_{3,1} & A_{3,2} & A_{3,3} & B_{3,1} & B_{3,2} & B_{3,3} \\ B_{1,1} & B_{1,2} & B_{1,3} & D_{1,1} & D_{1,2} & D_{1,3} \\ B_{2,1} & B_{2,2} & B_{2,3} & D_{2,1} & D_{2,2} & D_{2,3} \\ B_{3,1} & B_{3,2} & B_{3,3} & D_{3,1} & D_{3,2} & D_{3,3} \end{bmatrix} \begin{bmatrix} \epsilon_1 \\ \epsilon_2 \\ \gamma_{12} \\ \kappa_1 \\ \kappa_2 \\ \kappa_{12} \end{bmatrix}$$

$$\epsilon_{1,lam} = \frac{\det \begin{bmatrix} N_1 & A_{1,2} & A_{1,3} & B_{1,1} & B_{1,2} & B_{1,3} \\ 0 & A_{2,2} & A_{2,3} & B_{2,1} & B_{2,2} & B_{2,3} \\ 0 & A_{3,2} & A_{3,3} & B_{3,1} & B_{3,2} & B_{3,3} \\ 0 & B_{1,2} & B_{1,3} & D_{1,1} & D_{1,2} & D_{1,3} \\ 0 & B_{2,2} & B_{2,3} & D_{2,1} & D_{2,2} & D_{2,3} \\ 0 & B_{3,2} & B_{3,3} & D_{3,1} & D_{3,2} & D_{3,3} \end{bmatrix}}{\det \begin{bmatrix} A_{1,1} & A_{1,2} & A_{1,3} & B_{1,1} & B_{1,2} & B_{1,3} \\ A_{2,1} & A_{2,2} & A_{2,3} & B_{2,1} & B_{2,2} & B_{2,3} \\ A_{3,1} & A_{3,2} & A_{3,3} & B_{3,1} & B_{3,2} & B_{3,3} \\ B_{1,1} & B_{1,2} & B_{1,3} & D_{1,1} & D_{1,2} & D_{1,3} \\ B_{2,1} & B_{2,2} & B_{2,3} & D_{2,1} & D_{2,2} & D_{2,3} \\ B_{3,1} & B_{3,2} & B_{3,3} & D_{3,1} & D_{3,2} & D_{3,3} \end{bmatrix}}$$

#### Equation 74: Solution for Axial Strain under Uniaxial Loading Using Cramer's Rule<sup>240</sup>

<sup>240</sup> (Nettles, 1994)



Next, using one round of cofactor expansion, Equation 74 can be simplified to Equation 75. When this solution is plugged into Equation 73, a relatively easily answer is found for the value of the Young's modulus, given in Equation 76.

$$\epsilon_{1,lam} = \frac{N_1 * \det \begin{bmatrix} A_{2,2} & A_{2,3} & B_{2,1} & B_{2,2} & B_{2,3} \\ A_{3,2} & A_{3,3} & B_{3,1} & B_{3,2} & B_{3,3} \\ B_{1,2} & B_{1,3} & D_{1,1} & D_{1,2} & D_{1,3} \\ B_{2,2} & B_{2,3} & D_{2,1} & D_{2,2} & D_{2,3} \\ B_{3,2} & B_{3,3} & D_{3,1} & D_{3,2} & D_{3,3} \end{bmatrix}}{\det \begin{bmatrix} A_{1,1} & A_{1,2} & A_{1,3} & B_{1,1} & B_{1,2} & B_{1,3} \\ A_{2,1} & A_{2,2} & A_{2,3} & B_{2,1} & B_{2,2} & B_{2,3} \\ A_{3,1} & A_{3,2} & A_{3,3} & B_{3,1} & B_{3,2} & B_{3,3} \\ B_{1,1} & B_{1,2} & B_{1,3} & D_{1,1} & D_{1,2} & D_{1,3} \\ B_{2,1} & B_{2,2} & B_{2,3} & D_{2,1} & D_{2,2} & D_{2,3} \\ B_{3,1} & B_{3,2} & B_{3,3} & D_{3,1} & D_{3,2} & D_{3,3} \end{bmatrix}}$$

Equation 75: Axial Strain Simplified with Cofactor Expansion<sup>241</sup>

$$E_{1,lam} = \frac{\det \begin{bmatrix} A_{1,1} & A_{1,2} & A_{1,3} & B_{1,1} & B_{1,2} & B_{1,3} \\ A_{2,1} & A_{2,2} & A_{2,3} & B_{2,1} & B_{2,2} & B_{2,3} \\ A_{3,1} & A_{3,2} & A_{3,3} & B_{3,1} & B_{3,2} & B_{3,3} \\ B_{1,1} & B_{1,2} & B_{1,3} & D_{1,1} & D_{1,2} & D_{1,3} \\ B_{2,1} & B_{2,2} & B_{2,3} & D_{2,1} & D_{2,2} & D_{2,3} \\ B_{3,1} & B_{3,2} & B_{3,3} & D_{3,1} & D_{3,2} & D_{3,3} \end{bmatrix}}{h_{laminare} * \det \begin{bmatrix} A_{2,2} & A_{2,3} & B_{2,1} & B_{2,2} & B_{2,3} \\ A_{3,2} & A_{3,3} & B_{3,1} & B_{3,2} & B_{3,3} \\ B_{1,2} & B_{1,3} & D_{1,1} & D_{1,2} & D_{1,3} \\ B_{2,2} & B_{2,3} & D_{2,1} & D_{2,2} & D_{2,3} \\ B_{3,2} & B_{3,3} & D_{3,1} & D_{3,2} & D_{3,3} \end{bmatrix}}$$

Equation 76: Solution for Young's Modulus of a Laminate<sup>242</sup>

Naturally, this same method may be applied to finding the Young's Modulus in the 2-direction. The only difference is that now a force in 2-direction is assumed, and the strain in 2-direction is solved for. The process is not repeated here, but the solution is given in Equation 77.

<sup>241</sup> (Nettles, 1994)

<sup>242</sup> (Nettles, 1994)

$$E_{2,lam} = \frac{\det \begin{bmatrix} A_{1,1} & A_{1,2} & A_{1,3} & B_{1,1} & B_{1,2} & B_{1,3} \\ A_{2,1} & A_{2,2} & A_{2,3} & B_{2,1} & B_{2,2} & B_{2,3} \\ A_{3,1} & A_{3,2} & A_{3,3} & B_{3,1} & B_{3,2} & B_{3,3} \\ B_{1,1} & B_{1,2} & B_{1,3} & D_{1,1} & D_{1,2} & D_{1,3} \\ B_{2,1} & B_{2,2} & B_{2,3} & D_{2,1} & D_{2,2} & D_{2,3} \\ B_{3,1} & B_{3,2} & B_{3,3} & D_{3,1} & D_{3,2} & D_{3,3} \end{bmatrix}}{h_{laminare} * \det \begin{bmatrix} A_{1,1} & A_{1,3} & B_{1,1} & B_{1,2} & B_{1,3} \\ A_{3,1} & A_{3,3} & B_{3,1} & B_{3,2} & B_{3,3} \\ B_{1,1} & B_{1,3} & D_{1,1} & D_{1,2} & D_{1,3} \\ B_{2,1} & B_{2,3} & D_{2,1} & D_{2,2} & D_{2,3} \\ B_{3,1} & B_{3,3} & D_{3,1} & D_{3,2} & D_{3,3} \end{bmatrix}}$$

Equation 77: Young's Modulus in 2-direction<sup>243</sup>

With:

$E_{2,lam}$ : Young's Modulus in 2-Direction [MPa]

### Shear Modulus

The method for finding the shear modulus is identical for that of finding the Young's Modulus. The result is given in

$$G_{12,lam} = \frac{\det \begin{bmatrix} A_{1,1} & A_{1,2} & A_{1,3} & B_{1,1} & B_{1,2} & B_{1,3} \\ A_{2,1} & A_{2,2} & A_{2,3} & B_{2,1} & B_{2,2} & B_{2,3} \\ A_{3,1} & A_{3,2} & A_{3,3} & B_{3,1} & B_{3,2} & B_{3,3} \\ B_{1,1} & B_{1,2} & B_{1,3} & D_{1,1} & D_{1,2} & D_{1,3} \\ B_{2,1} & B_{2,2} & B_{2,3} & D_{2,1} & D_{2,2} & D_{2,3} \\ B_{3,1} & B_{3,2} & B_{3,3} & D_{3,1} & D_{3,2} & D_{3,3} \end{bmatrix}}{h_{laminare} * \det \begin{bmatrix} A_{1,1} & A_{1,2} & B_{1,1} & B_{1,2} & B_{1,3} \\ A_{2,1} & A_{2,2} & B_{2,1} & B_{2,2} & B_{2,3} \\ B_{1,1} & B_{1,2} & D_{1,1} & D_{1,2} & D_{1,3} \\ B_{2,1} & B_{2,2} & D_{2,1} & D_{2,2} & D_{2,3} \\ B_{3,1} & B_{3,2} & D_{3,1} & D_{3,2} & D_{3,3} \end{bmatrix}}$$

Equation 78: Shear Modulus of a Laminate<sup>244</sup>

With:

$G_{12,lam}$ : Shear Modulus of the Laminate [MPa]

<sup>243</sup> (Nettles, 1994)

<sup>244</sup> (Nettles, 1994)

## Poisson's Ratio

Poisson's ratio is defined as -1 times the ratio of the strains in y- and x-direction under a load applied in x-direction, as shown in Equation 79. The strain in x-direction under loading in x-direction has been calculated above. The strain in y-direction is calculated by applying Cramer's rule and cofactor expansion to the second column. Note that because the force is still in the x-direction the sub-matrix is established by removing the second column, but the first row. Since the summation of these indices is odd, a negative sign appears during cofactor expansion. This agrees with expectations, since positive axial strain results in negative transverse strain, and a positive Poisson's ratio is expected under normal conditions.<sup>245</sup> The result is given in Equation 80.

$$\nu_{12,lam} = -\frac{\varepsilon_{2,lam}}{\varepsilon_{1,lam}}$$

### Equation 79: Definition of Poisson's Ratio

With:

$\nu_{12,lam}$ : Primary Poisson's Ratio of Laminate [-]

$\varepsilon_{2,lam}$ : Strain in 2-Direction [-]

$\varepsilon_{1,lam}$ : Strain in 1-Direction [-]

$$\varepsilon_{2,lam} = \frac{\det \begin{bmatrix} A_{1,1} & N_1 & A_{1,3} & B_{1,1} & B_{1,2} & B_{1,3} \\ A_{2,1} & 0 & A_{2,3} & B_{2,1} & B_{2,2} & B_{2,3} \\ A_{3,1} & 0 & A_{3,3} & B_{3,1} & B_{3,2} & B_{3,3} \\ B_{1,1} & 0 & B_{1,3} & D_{1,1} & D_{1,2} & D_{1,3} \\ B_{2,1} & 0 & B_{2,3} & D_{2,1} & D_{2,2} & D_{2,3} \\ B_{3,1} & 0 & B_{3,3} & D_{3,1} & D_{3,2} & D_{3,3} \end{bmatrix}}{\det \begin{bmatrix} A_{1,1} & A_{1,2} & A_{1,3} & B_{1,1} & B_{1,2} & B_{1,3} \\ A_{2,1} & A_{2,2} & A_{2,3} & B_{2,1} & B_{2,2} & B_{2,3} \\ A_{3,1} & A_{3,2} & A_{3,3} & B_{3,1} & B_{3,2} & B_{3,3} \\ B_{1,1} & B_{1,2} & B_{1,3} & D_{1,1} & D_{1,2} & D_{1,3} \\ B_{2,1} & B_{2,2} & B_{2,3} & D_{2,1} & D_{2,2} & D_{2,3} \\ B_{3,1} & B_{3,2} & B_{3,3} & D_{3,1} & D_{3,2} & D_{3,3} \end{bmatrix}} = \frac{-N_1 * \det \begin{bmatrix} A_{2,1} & A_{2,3} & B_{2,1} & B_{2,2} & B_{2,3} \\ A_{3,1} & A_{3,3} & B_{3,1} & B_{3,2} & B_{3,3} \\ B_{1,1} & B_{1,3} & D_{1,1} & D_{1,2} & D_{1,3} \\ B_{2,1} & B_{2,3} & D_{2,1} & D_{2,2} & D_{2,3} \\ B_{3,1} & B_{3,3} & D_{3,1} & D_{3,2} & D_{3,3} \end{bmatrix}}{\det \begin{bmatrix} A_{1,1} & A_{1,2} & A_{1,3} & B_{1,1} & B_{1,2} & B_{1,3} \\ A_{2,1} & A_{2,2} & A_{2,3} & B_{2,1} & B_{2,2} & B_{2,3} \\ A_{3,1} & A_{3,2} & A_{3,3} & B_{3,1} & B_{3,2} & B_{3,3} \\ B_{1,1} & B_{1,2} & B_{1,3} & D_{1,1} & D_{1,2} & D_{1,3} \\ B_{2,1} & B_{2,2} & B_{2,3} & D_{2,1} & D_{2,2} & D_{2,3} \\ B_{3,1} & B_{3,2} & B_{3,3} & D_{3,1} & D_{3,2} & D_{3,3} \end{bmatrix}}$$

### Equation 80: Strain in y-direction Under Loading in x-direction<sup>246</sup>

Combining the strains in x- and y-direction according to Equation 79, results in Equation 81.

<sup>245</sup> It is interesting to note that the Poisson's ratio of FRP laminates do not have to fall within the range typically associated with traditional building materials (0-0.5). FRP laminates have been experimentally shown to have Poisson's ratios which range between -2 and 14. Theoretical laminates have shown an even broader range, with values for laminates being predicted between -60 and 100. (Peel, 2005).

<sup>246</sup> (Nettles, 1994)

$$v_{12,lam} = \frac{\det \begin{bmatrix} A_{2,1} & A_{2,3} & B_{2,1} & B_{2,2} & B_{2,3} \\ A_{3,1} & A_{3,3} & B_{3,1} & B_{3,2} & B_{3,3} \\ B_{1,1} & B_{1,3} & D_{1,1} & D_{1,2} & D_{1,3} \\ B_{2,1} & B_{2,3} & D_{2,1} & D_{2,2} & D_{2,3} \\ B_{3,1} & B_{3,3} & D_{3,1} & D_{3,2} & D_{3,3} \end{bmatrix}}{\det \begin{bmatrix} A_{2,2} & A_{2,3} & B_{2,1} & B_{2,2} & B_{2,3} \\ A_{3,2} & A_{3,3} & B_{3,1} & B_{3,2} & B_{3,3} \\ B_{1,2} & B_{1,3} & D_{1,1} & D_{1,2} & D_{1,3} \\ B_{2,2} & B_{2,3} & D_{2,1} & D_{2,2} & D_{2,3} \\ B_{3,2} & B_{3,3} & D_{3,1} & D_{3,2} & D_{3,3} \end{bmatrix}}$$

Equation 81: Poisson's Ratio in Primary Direction<sup>247</sup>

Applying the same steps with a force in y-direction allows for the calculation of Poisson's ratio in the secondary direction. The solution for this is given in Equation 82.

$$v_{21,lam} = \frac{\det \begin{bmatrix} A_{1,2} & A_{1,3} & B_{1,1} & B_{1,2} & B_{1,3} \\ A_{3,2} & A_{3,3} & B_{3,1} & B_{3,2} & B_{3,3} \\ B_{1,2} & B_{1,3} & D_{1,1} & D_{1,2} & D_{1,3} \\ B_{2,2} & B_{2,3} & D_{2,1} & D_{2,2} & D_{2,3} \\ B_{3,2} & B_{3,3} & D_{3,1} & D_{3,2} & D_{3,3} \end{bmatrix}}{\det \begin{bmatrix} A_{1,1} & A_{1,3} & B_{1,1} & B_{1,2} & B_{1,3} \\ A_{3,1} & A_{3,3} & B_{3,1} & B_{3,2} & B_{3,3} \\ B_{1,1} & B_{1,3} & D_{1,1} & D_{1,2} & D_{1,3} \\ B_{2,1} & B_{2,3} & D_{2,1} & D_{2,2} & D_{2,3} \\ B_{3,1} & B_{3,3} & D_{3,1} & D_{3,2} & D_{3,3} \end{bmatrix}}$$

Equation 82: Poisson's ratio in Secondary Direction of a Laminate<sup>248</sup>

With:

$v_{21,lam}$ : Secondary Poisson's Ratio of Laminate

<sup>247</sup> (Nettles, 1994)

<sup>248</sup> (Nettles, 1994)

## Appendix I: Stability of Girders

In Chapter 5 Laminate Orientation, the stability of the girders has been excluded from consideration. However, the flange thicknesses resulting from the analysis raise questions about flange stability. Because the variants in this chapter are later rejected, the system is not fully verified in terms of stability. However, a sample stability analysis is performed for the main girder. To start this the geometry of the main girder is presented in Figure 123. Figure 124 gives the maximum width to thickness ratios for flanges in compression.

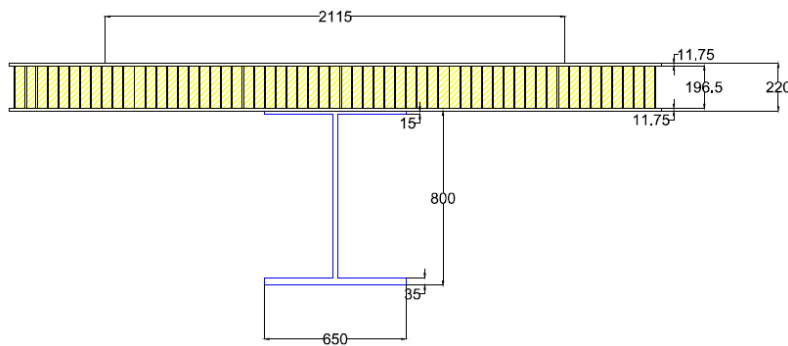


Figure 123: Cross-Section of Main Girder in the Lengthwise Laminated Variant Corresponding to Chapter 5 Laminate Orientation

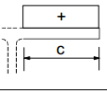
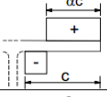
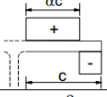



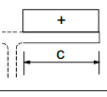
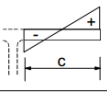
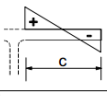



Outstand flanges						
Rolled sections		Welded sections				
Class	Part subject to compression	Part subject to bending and compression				
		Tip in compression		Tip in tension		
Stress distribution in parts (compression positive)						
	1	$c/t \leq 9\epsilon$	$c/t \leq \frac{9\epsilon}{\alpha}$	$c/t \leq \frac{9\epsilon}{\alpha\sqrt{\alpha}}$	$c/t \leq \frac{9\epsilon}{\alpha\sqrt{\alpha}}$	$c/t \leq \frac{9\epsilon}{\alpha\sqrt{\alpha}}$
2	$c/t \leq 10\epsilon$	$c/t \leq \frac{10\epsilon}{\alpha}$	$c/t \leq \frac{10\epsilon}{\alpha\sqrt{\alpha}}$	$c/t \leq \frac{10\epsilon}{\alpha\sqrt{\alpha}}$	$c/t \leq \frac{10\epsilon}{\alpha\sqrt{\alpha}}$	
Stress distribution in parts (compression positive)						
3	$c/t \leq 14\epsilon$	$c/t \leq 21\epsilon\sqrt{k_\sigma}$ For $k_\sigma$ see EN 1993-1-5				
$\epsilon = \sqrt{235/f_y}$	$f_y$	235	275	355	420	460
	$\epsilon$	1,00	0,92	0,81	0,75	0,71

Figure 124: Maximum Width-to-Thickness Ratios for Compression Flanges<sup>249</sup>

<sup>249</sup> (NEN-EN 1993-1-1: Design of Steel Structures, 2006)

The girders are welded profiles for which the top flange is considered to undergo uniform compression. The assumed class is class 4. Where the norm specifies that class 4 cross sections may be treated as class 3 cross sections with a correction factor. Therefore, in accordance with Figure 124, the relevant criterion is given in Equation 83.

$$\frac{c}{t_{flange}} \leq 14\varepsilon$$

$$c = \frac{w_{flange} - t_{web}}{2}$$

$$\varepsilon = \sqrt{\frac{235}{f_y}} \sqrt{\frac{f_y \gamma_{M0}}{\sigma_{com,Ed}}}$$

Equation 83: Maximum Width to Thickness Ratio for Compressive Flanges<sup>250</sup>

With:

$c$ : Flange Outstand [mm]

$t_{flange}$ : Flange Thickness [mm]

$w_{flange}$ : Flange Width [mm]

$t_{web}$ : Web Thickness [mm]

$f_y$ : Yield Stress [MPa]

$\gamma_{M0}$ : Material Factor [-]<sup>251</sup>

$\sigma_{com,Ed}$ : Design Stress in Compression [MPa]<sup>252</sup>

This results in the inequality given Equation 84. Here one can see that the cross section does not suffice. The flange thickness would need to be increased to 20mm in order to satisfy the flange stability criterion. However, since the design which has been considered here is rejected on other grounds, this step has not been taken in the design process. Also note that any stability derived from the deck to which the flange is attached is neglected.

$$\frac{315}{15} \leq 14 * 1.19$$

$$21 \leq 16.66$$

Equation 84: Calculation of Width to Thickness Ratios Applied and Allowed for the Lengthwise Laminated Variant

<sup>250</sup> (NEN-EN 1993-1-1: Design of Steel Structures, 2006)

<sup>251</sup> Value taken as 1 in accordance with (Normcommissie 351 001, 2011)

<sup>252</sup> Value in Main Girder at Midspan = 165MPa, taken from (Hattink, 2014)

The variant presented in 6.4.2 Redesign with No Composite Action has a flange width of 550mm and a flange thickness of 35mm. Plugging these values into Equation 83 yields Equation 85. Here one can see that the flange satisfies the width to thickness requirement.

$$\frac{265}{35} \leq 14 * 1.19$$

$$7.57 \leq 16.66$$

Equation 85: Calculation of Width to Thickness Ratios Applied and Allowed for the Redesign Without Composite Action

## Appendix J: Comparing the Influence of Composite Action to Concrete

Composite action is beneficial for the stiffness and strength of a construction. This principle is very commonly used in the design of hybrid steel-concrete structures. This chapter is aimed at comparing the influence of composite action between FRP-steel and steel-concrete hybrid structures in order to give perspective to the influence composite action has in FRP-steel hybrid structures. Table 49 gives the influence composite action has on steel-concrete systems and Table 50 does the same for FRP-steel systems.

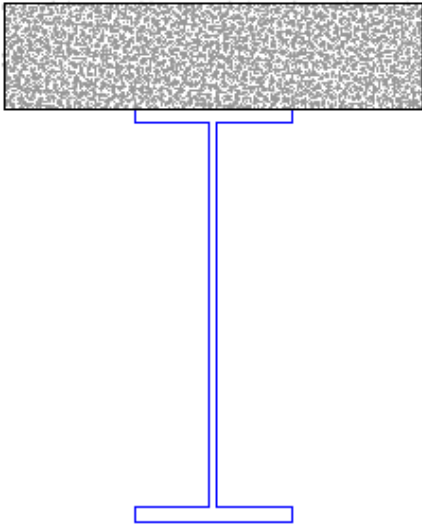
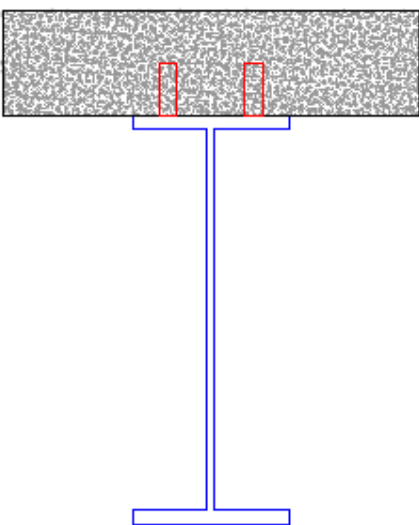
Effect of Composite Action on Steel-Concrete Beam		
	Concrete Without Shear Connection	Concrete With Shear Connection
<b>Image</b>		
<b>Profile</b>	HEA800	HEA800
<b>Concrete Height [mm]</b>	220	220
<b>Stiffness</b>	100%	273%
<b>Capacity</b>	100%	194%

Table 49: Analysis of the Effect Which Composite Action has on the Stiffness and Bending Moment Capacity of a Steel-Concrete Hybrid Beam.<sup>253</sup>

<sup>253</sup> Calculations verified against: (Stark & Stark, 2009)



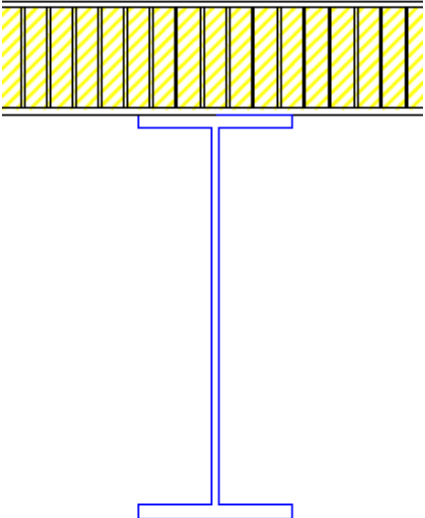
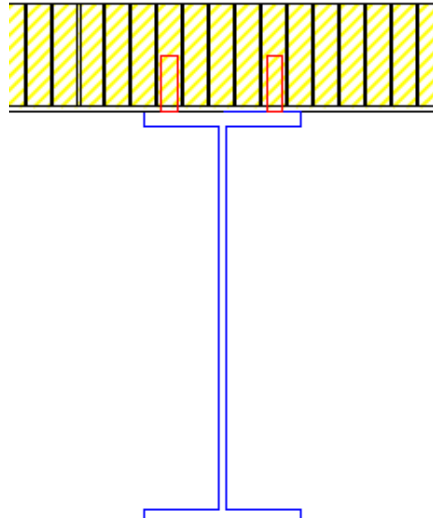
Effect of Composite Action on FRP-Steel Beam		
	FRP Without Shear Connection	FRP With Shear Connection
<b>Image</b>		
<b>Profile</b>	HEA800	HEA800
<b>FRP Height [mm]</b>	220	220
<b>Stiffness</b>	100% (87%)	159% (138%)
<b>Capacity</b>	100% (102%)	121% (124%)

Table 50: Analysis of the Effect Which Composite Action has on the Stiffness and Bending Moment Capacity of an FRP-Steel hybrid Beam. Values in Parentheses Represent Comparisons to the Concrete Without Shear Connection Solution.

One can see in Table 49 that adding a shear connection to steel-concrete system, gives a tremendous benefit stiffness and strength. Table 50 shows that a shear connection will add stiffness and strength to an FRP-steel system as well. However, the benefits of such a connection in with an FRP deck are much smaller. This is largely due to the reduced area of an FRP deck in comparison to a concrete deck, following from both the hollow nature as well as the reduced effective width.

For the case study, the effects of adding a shear connection to the system is even smaller. In this situation, the low height of the steel profile demands that the flanges be extraordinarily wide and thick, so that the profile also has a large cross sectional area. Therefore, the addition of the FRP deck will only cause a slight upward shift of the neutral axis, so that the influence is minimal. Remember that in the case study, a concrete deck is not a viable solution, since the deck alone would weight more than the entire FRP-steel structure according to its current design.

### Assumptions for Calculations

In order to calculate the values above, several values were assumed, which will have an influence on the results. In the interest of reproducibility, these assumptions are given in Table 51. Note the difference in effective widths in accordance with chapter 5.3 Effective Width.

Assumed Values for Calculation of the Influence of Composite Action		
Item	Value	Units
Young's Modulus Concrete	30	GPa
Young's Modulus Steel	210	GPa
Effective Width of Concrete Deck	4050	mm
Effective Width FRP Deck	2115	mm

Table 51: Assumed Values for the Comparison between the Influence of Composite Action on Concrete and FRP decks.

## Appendix K: Possible Connection Method Sketches

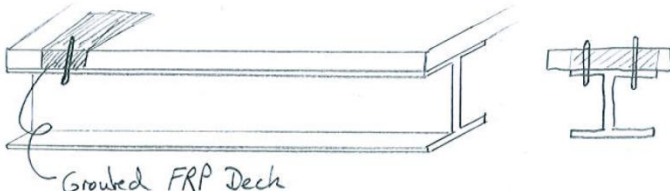
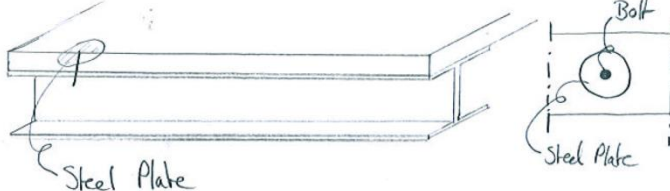
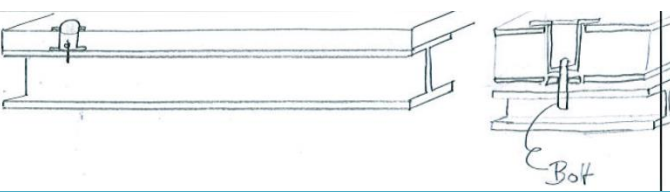
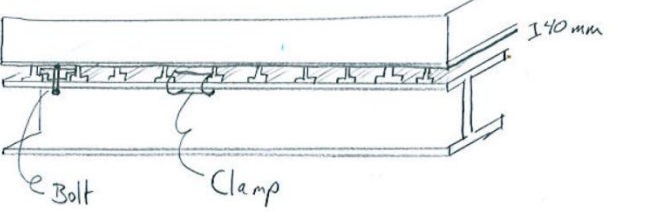
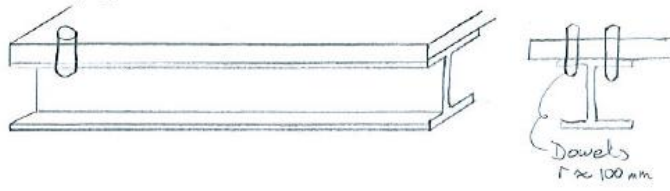
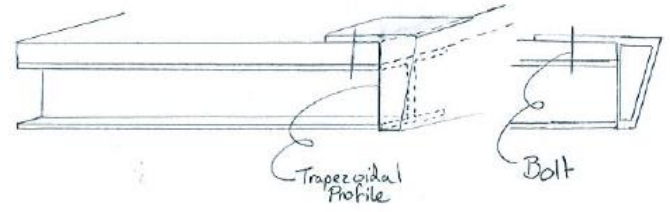
Possible Connection Method Sketches and Properties			
# Sketch		Advantages	Disadvantages
1	 <p>Grouded FRP Deck</p>	<ul style="list-style-type: none"> <li>• Bolts in both FRP Layers</li> <li>• Loading Spread over wide area</li> </ul>	<ul style="list-style-type: none"> <li>• High Weight Concrete</li> <li>• Concrete Curing Time</li> </ul>
2	 <p>Steel Plate</p>	<ul style="list-style-type: none"> <li>• Steel plates spreads loading on FRP surface</li> <li>• Entirely below deck surface</li> </ul>	<ul style="list-style-type: none"> <li>• Single layer loading</li> <li>• Single side inspectability</li> </ul>
3	 <p>Bolt</p>	<ul style="list-style-type: none"> <li>• Loading both FRP layers</li> <li>• Accessible from both sides</li> </ul>	<ul style="list-style-type: none"> <li>• Low Stiffness</li> <li>• Higher loading for bottom layer than top layer</li> </ul>
4	 <p>Bolt</p> <p>Clamp</p> <p>140 mm</p>	<ul style="list-style-type: none"> <li>• Fully visible and inspectable</li> <li>• No post processing of FRP deck required</li> <li>• Entirely below deck surface</li> </ul>	<ul style="list-style-type: none"> <li>• I-profile layer lacks stiffness</li> <li>• Friction based connection: pre-stress unstable</li> </ul>
5	 <p>Dowels</p> <p>~ 100 mm</p>	<ul style="list-style-type: none"> <li>• Dowels Spread Loading</li> <li>• Applies load to both FRP layers</li> </ul>	<ul style="list-style-type: none"> <li>• Moment action on dowels</li> <li>• Large holes in steel profile</li> </ul>
6	 <p>Trapezoidal Profile</p> <p>Bolt</p>	<ul style="list-style-type: none"> <li>• Steel profile on end increases local stiffness</li> <li>• Bolts apply equal load to both FRP Plates</li> <li>• Accessible from both sides</li> </ul>	<ul style="list-style-type: none"> <li>• Applicable only at end of beams</li> <li>• High steel weight</li> </ul>

Table 52: Possible Connection Methods

## Appendix L: Joint Literature

Prior to any modelling, it behooves one to review the literature available regarding the subject. To that end, literature regarding mechanical and adhesive connections has been reviewed. Unfortunately, little literature regarding FRP connections is available. That which is available is typically only valid for specific FRP compositions, making it inapplicable to different compositions. The available literature has been analyzed below, starting with mechanical joints.

### L.1 Mechanical Joints

Mechanical joints typically refer to bolts or shear studs. The use of these connection methods requires a hole in the laminate through which a rod is placed. The creation of a hole in the laminate naturally causes a weak spot, with a stress concentration factor around the hole. This may lead to laminate failure in tension. Additionally, the hole must be able to resist the bearing load the bolt creates on the hole. Shear out failure and cleavage-tension failure should also be resisted. Shear out and cleavage failure occur at the ends of laminates and since a continuous deck is considered, these failure methods are not expected to occur. The other two must be considered. All four failure mechanisms are shown in Figure 125.

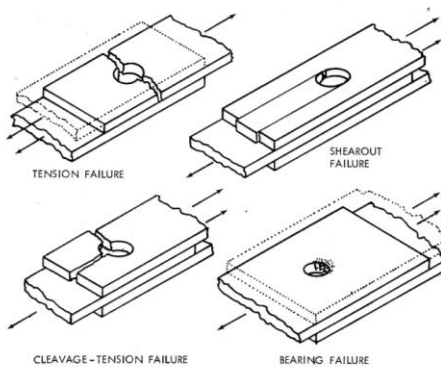


Figure 125: Failure Mechanisms for Composite Laminates. The Expected Failure Method for the Case Study is Bearing.<sup>254</sup>

The net-tension and bearing failure mechanisms of composites vary from that of metals. When considering metals, plastic deformation will occur when locally the maximum stress is exceeded. This allows for the stresses to redistribute, so that the entire cross-section will reach the yield limit, greatly enhancing the ultimate strength. When considering FRP, the stress-strain relationship is nearly linear until failure. This means that no local yielding may occur, so that failure will occur as soon as the elastic limit is reached. This is particularly undesirable when one expects large stress concentration factors.

<sup>254</sup> (Hart-Smith, 1976)

Luckily, some delamination may occur, which also leads to spreading of peak stresses. The effect of delamination is shown in Figure 126. This effect is not nearly as pronounced as yielding is in metals, but still benefits the ultimate strength of the connection.

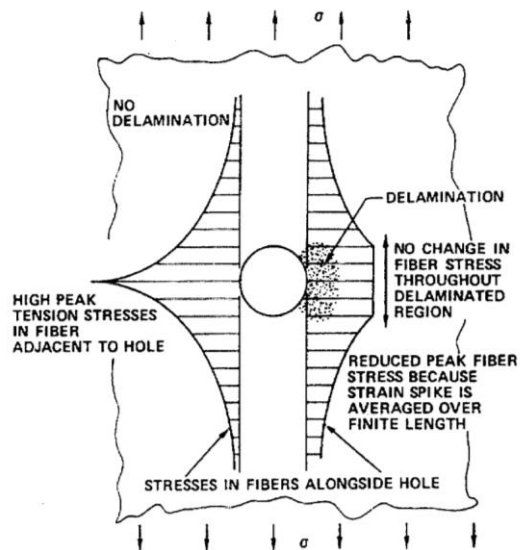


Figure 126: Reduction in Peak Stress Resulting From Delamination<sup>255</sup>

### L.1.1 Net Tension

The net tension criterion requires a stress concentration factor. This stress concentration factor is multiplied by the average stress which is present at the cross section where the hole is present. A problem which arises here is that the mathematics of such a plate assumes a finite width. The ratio of the bridge deck width to bolt hole diameter is sufficiently large, that the theory (Hart-Smith, 1976) becomes nonsensical. To resolve this problem an effective tensile width is proposed. The FRP material should be bolted to the steel girders symmetrically about the girder web. Under this assumption, the fictitious width of the FRP “plate” equals the heart to heart distance of the bolts; half this distance to the middle and the other half to the outside. The recommended bolt spacing is 4 times the diameter in width and length directions, so this will be the assumed plate width and end distance.

The stress concentration factor can be estimated based on an elastic approach. The stress concentration factor can be found according to Equation 86. The values of the concentration factor is shown as a function of bolt diameter, plate width, and end distance in Figure 127. However, as mentioned, laminates can delaminate to slightly relieve stress concentration factors. This effect has been determined through experiment. Since each composite is unique this effect will be different for varying types of composites. Taking this into account, the least favorable of the experimental

<sup>255</sup> (Hart-Smith, 1976)

relationships is presented here. This regards an orthotropic graphite-epoxy mixture, for which the relationship can be seen in Equation 87. Hart-Smith notes that similar specimens with glass partially replacing graphite showed no failure in tension, so that the tensile stress concentration factor may be assumed much lower.<sup>256</sup> Hence the graphite relationship shown below is conservative.

$$k_{te} = 2 + \left(\frac{w}{d} - 1\right) - 1.5 * \frac{\left(\frac{w}{d} - 1\right)}{\left(\frac{w}{d} + 1\right)} * \theta$$

$$\theta_{con} = \begin{cases} 1.5 - \frac{0.5 * w}{e} & \text{for } \frac{w}{e} \geq 1 \\ 1 & \text{for } \frac{w}{e} \leq 1 \end{cases}$$

**Equation 86: Elastic Stress Concentration Factor Tension**<sup>257</sup>

With:

- $k_{te}$ : Elastic Stress Concentration Factor For Net Tension [-]
- $w$ : Width of Specimen [mm]
- $d$ : Diameter of Bolt [mm]
- $e$ : Distance to End of Laminate [mm]

$$k_{tc} = 0.54 + 0.46 * k_{te}$$

**Equation 87: Composite Stress Concentration Factor Tension**<sup>258</sup>

With:

- $k_{tc}$ : Stress Concentration Factor in Composite Material for Net Tension [-]

Using the applied recommended spacing yield elastic and composite concentration factors according to equations Equation 88 and Equation 89, respectively.

$$k_{te} = 2 + \left(\frac{w}{d} - 1\right) - 1.5 * \frac{\left(\frac{w}{d} - 1\right)}{\left(\frac{w}{d} + 1\right)} * \theta = 2 + (4 - 1) - 1.5 * \frac{4 - 1}{(4 + 1)} * 1 = 4.1$$

**Equation 88: Elastic Stress Concentration Factor For Case Study**

$$k_{tc} = 0.54 + 0.46 * k_{te} = 0.54 + 0.46 * 4.1 = 2.426$$

**Equation 89: Composite Stress Concentration Factor For Case Study**

<sup>256</sup> (Hart-Smith, 1976)

<sup>257</sup> (Hart-Smith, 1976)

<sup>258</sup> (Hart-Smith, 1976)

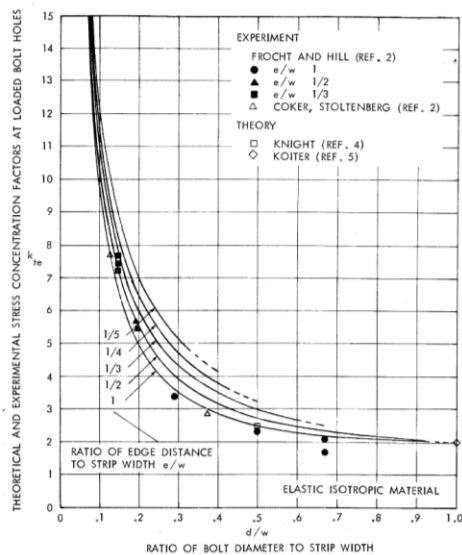


Figure 127: Elastic Stress Concentration Factors<sup>259</sup>

### L.1.2 Bearing

Bearing of the bolt hole is the second failure method which may occur in the FRP deck. Determining the stress distribution across a bolt hole accurately is difficult. However, a cosine distribution of the stress approaches this distribution with decent accuracy.<sup>260</sup> Hence, such a distribution will be assumed.

<sup>259</sup> (Hart-Smith, 1976)

<sup>260</sup> (Chang, Scott, & Springer, 1982)

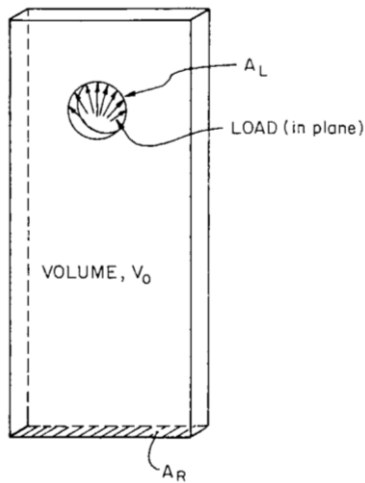


Figure 128: Schematic of Bolt Hole Loading<sup>261</sup>

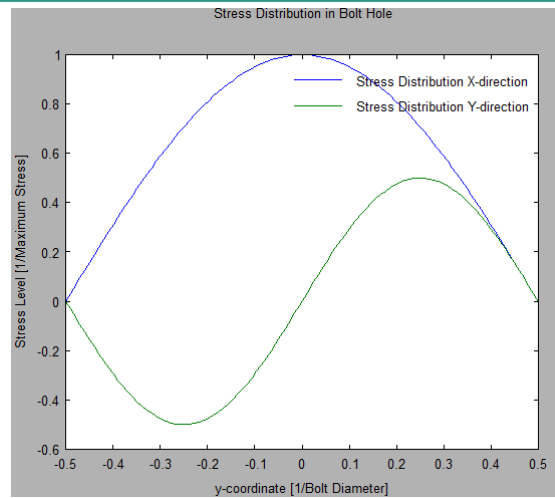


Figure 129: Stress Distribution Along Bolt Hole

In addition to the maximum stresses, the stiffness of the connection is also relevant. All flexibility in the connection will lead to slip between the FRP and the steel. Slippage severely reduces composite action. Therefore, it is desirable to utilize a connection which is as stiff as possible. In addition it is necessary to include the slippage when modeling any part of the structure where composite action is expected. For illustrative purposes, a load displacement curve is presented in Figure 130, where compressive deformation in the bolt and plate have been assumed. The effective depth over which the compressive stress is active is assumed to be 3 times the contact width, where the contact width is assumed equal to the bolt diameter. This is where according to elastic theory, the stress has dissipated to 1/3<sup>rd</sup> of its maximum value.<sup>262</sup> Bending of the bolt has not been included.

<sup>261</sup> (Chang, Scott, & Springer, 1982)

<sup>262</sup> (Bamberg, 2006)



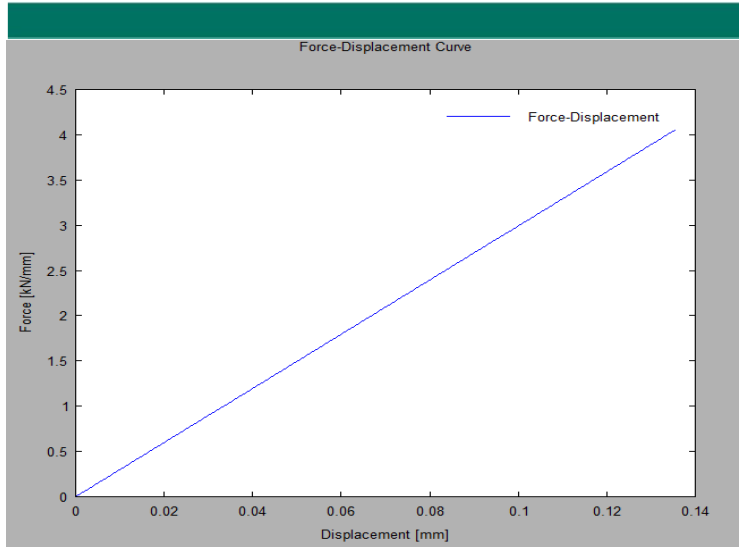


Figure 130: Load Displacement Curve For Bearing<sup>263</sup>

### L.1.3 Unquantified Effects

In addition to the quantified elastic bearing strength and net tension strength which are important to bolted connections, there are some effects which have been determined experimentally. These are difficult to take into account, since no models exist to determine their effects and they were established for specific laminates. Hence they are only qualitatively accounted for.

The first effect is the effect of ply grouping. If multiple lamellas oriented in the same direction are layered against each other in the laminate, the bearing strength is reduced. This effect can be seen in Figure 131. Therefore, it is beneficial to stack the lamellas such that two lamellas oriented in the same direction are never in contact with one another.

<sup>263</sup> This connection assumes a laminate with  $t = 159.2\text{mm}$ ,  $E_1 = 30\text{GPa}$  and  $\nu = 0.31$ . The bolt has properties  $E = 210\text{GPa}$ ,  $\nu = 0.3$ ,  $d = 14$ .

Ply number to centreline <sup>b</sup>	Ply orientation (degrees) <sup>a</sup>				
	Lay-up number				
	1	2	3	4	5
1	+	+	+	+	+
2	0	-	-	-	-
3	-	0	+	0	0
4	0	0	-	0	0
5	90	+	90	90	0
6	0	90	0	0	0
7	+	-	0	+	0
8	0	0	0	-	+
9	-	0	0	0	-
10	0	0	0	0	90
Number of plies	20	20	20	20	20
Percentage of 0/±45/90°	50/40/10	50/40/10	50/40/10	50/40/10	50/40/10

<sup>a</sup>+ and - refer to ±45° ply orientation.  
<sup>b</sup>Lay-ups are all symmetric about the centreline.

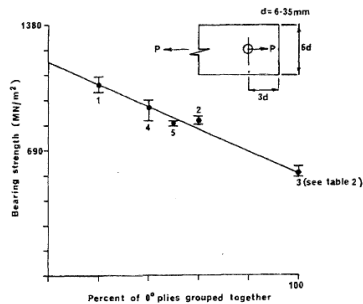


Figure 131: Effect of Ply Grouping<sup>264</sup>

The second effect is that of the stacking order. When considering laminates, the order in which plies are stacked has an influence on the bearing load. When looking at Figure 132, one can see that applying the 0° oriented plies on the outside of the laminate negatively influences the strength. Applying the 0° oriented plies in the interior of the laminate and applying the 90° plies on the outside leads to the highest bearing strength.

<sup>264</sup> (Duthinh, 2000)

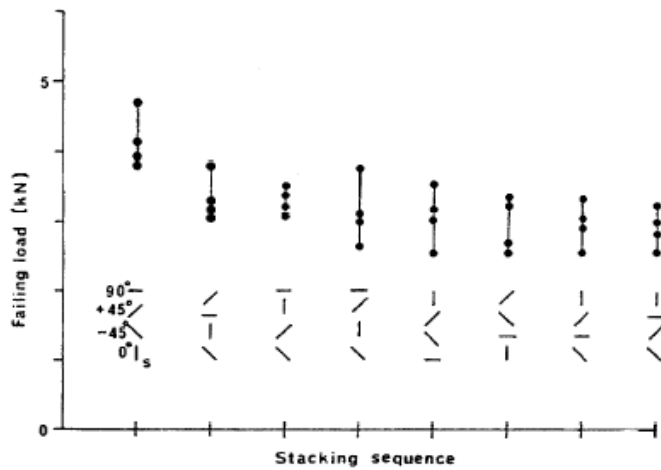


Figure 132: Effect of Stacking Sequence on Bearing Load<sup>265</sup>

A third effect worth mentioning is that of diameter over plate thickness ratio. The effect of this on bearing strength is shown in Figure 133. Notice that in all tested composites, but specifically the glass-epoxy composite, the strength shows a drastic decrease as the relationship between hole diameter and plate thickness increases. Therefore the diameter of the should be chosen such that it does not exceed the thickness of the composite plate.

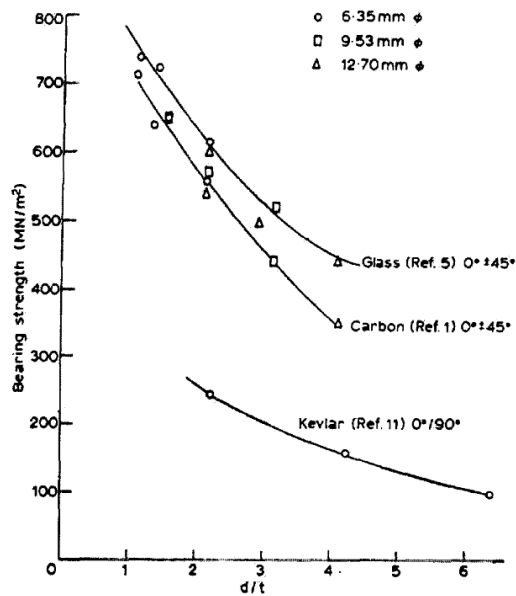


Figure 133: Variation in Bearing Strength as a Function of  $d/t$  Ratio<sup>266</sup>

<sup>265</sup> (Duthinh, 2000)

Fourth and finally, the bolt torque needs to be considered. An increasing bolt torque will increase the bearing capacity of the connection. Creating a level of pretension in the bolt will confine the plate in the z-direction. The Tsai-Wu criterion indicates that a compressive stress through the thickness of the plate will increase the compressive resistance in the bearing direction, as can be seen in Figure 115 on page 186. The effect of this on bolted connections can be seen in Figure 134.

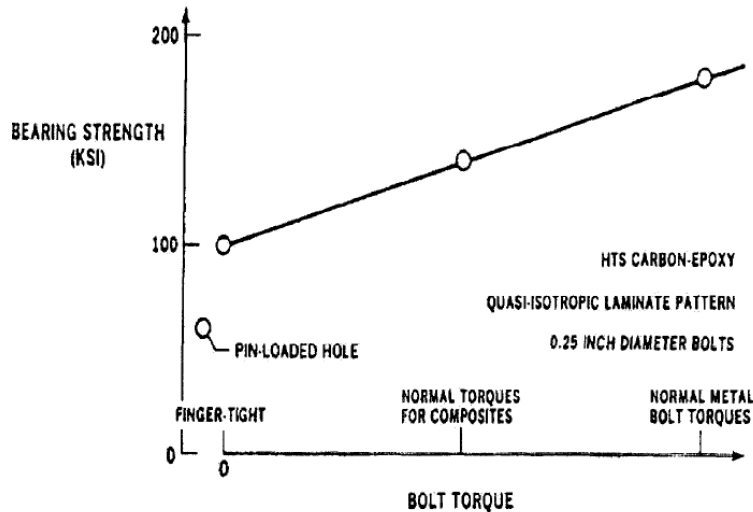


Figure 134: Effect of Bolt Torque on Bearing Strength of Connection<sup>267</sup>

#### L.1.4 Disadvantages of Mechanical Connections

There are several disadvantages to the application of mechanical connections for an FRP to steel connection. Several of these disadvantages are listed below:

1. Access: When applying bolts, access is required to both sides of the joint in order to fasten the bolt. This may be overcome using one-sided bolts such as undercut anchors, blind bolts or hollow bolts.
2. Holes: In order to place a bolt, a hole must be present in each of the two parent components, which overlap. Getting these holes to overlap requires precision throughout the installation process. In order to get the holes to overlap with enough space to fit the bolt through, a tolerance is typically applied.
3. Drilling: When holes are drilled in FRP plates, this may lead to crack formations which weaken the laminate.
4. Stress Concentration Factor: Creating holes in the cross-section as described above will increase the stress in the plate. See L.1.1 Net Tension for more detail.

<sup>266</sup> (Duthinh, 2000)

<sup>267</sup> (Duthinh, 2000)

5. Bearing Stress: The bearing stress between a bolt and FRP plate cannot redistribute the way it does for steel plates, reducing the bearing strength. See L.1.2 Bearing for more detail.
6. Uncertainty: There are several effects of FRP bolted connections which are difficult to account for, such as the effect of ply grouping, stacking order, ratio between thickness and hole diameter, and pretension. See L.1.3 Unquantified Effects for more information.
7. Complexity: Joints add to the complexity of a structure by adding more parts to it; they require the bolt, nut, and washers and sometimes lubricants, locking compounds or gaskets. Sometimes these items are used in varying sizes and qualities throughout the construction, which increases the chance of errors being made.
8. Corrosion: Bolts are typically made out of steel, so that they are prone to rusting. This can lead to weakening of the connection during the structure's lifetime.
9. Construction Time: Bolts are usually installed by manual labor. They take time to install, so that construction may be slowed by having to install the bolts.

## L.2 Adhesive Joints

Besides the mechanical fastening method described above, it is also possible to apply adhesive joints. When considering FRP to FRP connections, adhesive joints are almost exclusively applied. But these joints are not uncommon when considering FRP-steel connections either. There are two mathematical models for determining the strength of adhesive bonds, the linear method and the bond-slip bi-linear method.

### L.2.1 Linear Method

The Linear method simply requires a shear modulus and an adhesive thickness, to determine a stiffness of the adhesive. The stiffness is calculated according to Equation 90.

$$K_{adh} = \frac{G_{adh}}{t_{adh}}$$

Equation 90: Stiffness of an Adhesive Connection<sup>268</sup>

With:

$K_{adh}$ : Stiffness of the Adhesive [N/mm<sup>3</sup>]

$G_{adh}$ : Shear Modulus of the Adhesive Material [MPa]

$t_{adh}$ : Thickness of the Adhesive Layer [mm]

The slip between the two surfaces can be modelled according to Equation 91.

---

<sup>268</sup> (Xia & Teng, 2005)

$$\delta_{slip} = \frac{\tau_{13}}{K_{adh}} = \frac{\tau_{13} * t_{adh}}{G_{adh}}$$

Equation 91: Slip in Adhesive Bond<sup>269</sup>

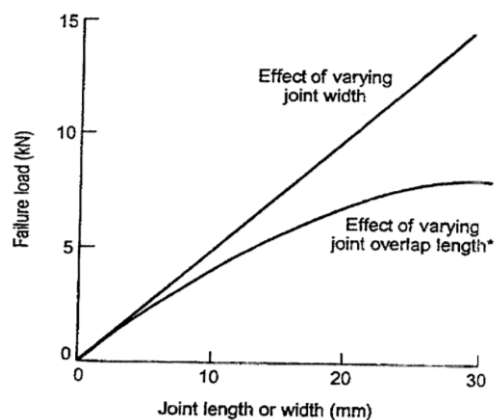
With:

$\delta_{slip}$ : Slip Between the Two Adhered Surfaces [mm]

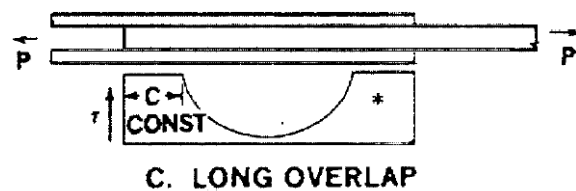
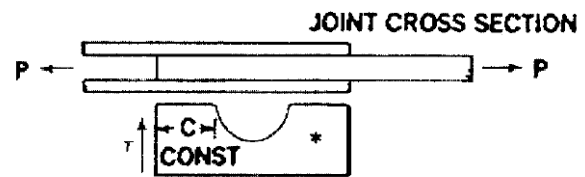
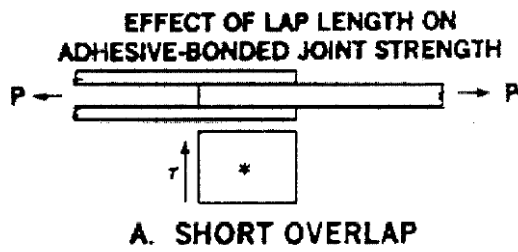
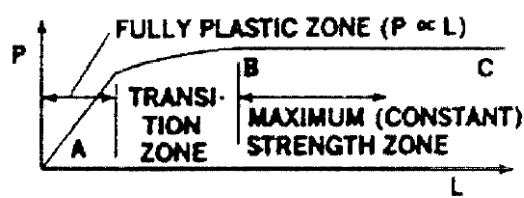
$\tau_{13}$ : Shear Stress in the Adhesive [MPa]

There are four important notes regarding these equations:

1. Adhesive layers with a thickness exceeding 4mm are not realistic. In fact, even in laboratory experiments, bonds intended to be 2mm or thicker consistently undershot their intended thickness.
2. The equations are only valid when in the linear elastic region. However, the shear strength of adhesives typically used to bind steel to FRP is significantly larger than the shear strength of FRP materials. Therefore, bond-slip models need not be applied.
3. The slip presented here disregards the deformation within the steel and FRP. Therefore, the stiffness according to this model is larger than that in reality.
4. The stiffness implied here is only valid for short joints. However, since the shear between the two materials in this case study will be applied in a continuous fashion, as opposed to a localized force, the expectation is that bond length will not be of influence.



<sup>269</sup> (Xia & Teng, 2005)



### L.2.2 Disadvantages of Adhesive Bonds

There are some important disadvantages of adhesive bonds that must be taken into account when choosing whether to apply mechanical or adhesive bonds. Several of those are listed below:

1. **Time to cure:** After joining two components with adhesive, the connection may not be immediately loaded, since the adhesive must cure prior to reaching its full strength. This can cause delays when several dependent components are connected.
2. **Surface Preparation:** Prior to creating an adhesive bond, the two surfaces need to be prepared. This typically includes removing any paint or previous adhesives and cleaning, amongst other things. While this can generally be ensured under factory conditions, on-site preparations are much more difficult to guarantee.
3. **Component Fit:** Components which are to be glued together should have a sufficient contact surface area. This could mean that parts must be redesigned to meet this criteria. When considering a very long bond length, such as the length of a bridge, any deformations of the components during assembly may cause significant gaps between the two components, leading to severely weakened regions of the adhesive.
4. **Disassembly:** disassembling for removal or replacement is not possible without damaging the components. Considering the lack of knowledge regarding long term behavior of FRP, it may be beneficial to retain the ability to remove or replace the deck in the future.
5. **Chemicals:** Due to the chemical nature of adhesives, it is vital to limit human exposure to the adhesives. Sustained or intense exposure to adhesive chemicals may have severe negative side effects on a person's health. Additionally, these chemicals may also be

harmful to flora and fauna, so that disposal of waste products or excess adhesive must be done with care.

6. Verification of Strength: Following the creation of an adhesive bond, it is no longer possible to see the adhesive. This means that it is difficult to verify that the joint was executed according to specifications. Voids, improperly mixed and hence weak adhesive, unbonded regions and the like are difficult to detect.
7. Inspection: Inspecting an adhesive bond faces the same problem as verifying its strength initially: the adhesive layer between the two components cannot be seen. Therefore, damage incurred during the lifetime of the structure, due to moisture, fatigue, UV-exposure, or chemicals is difficult to observe.
8. Experience: Steel-to-FRP connections are relatively new. This means that the long term behavior of adhesive are not yet fully understood. In addition, since many constructors are unfamiliar with steel-to-FRP connections, they tend to prefer the mechanical connections which they have grown accustomed to when designing in steel.

### L.3 Conclusion

The use of adhesive and mechanical joints has been discussed above. The main criteria used to decide which connection to apply are:

- Experience
- Ability to inspect
- Strength Verification

The use of mechanical connections is based on the three criteria above, where experience played the most important role. A design without adhesive connections is preferred since there is a lack of data regarding their strength and long term performance. Due to the concerns arising from this lack of data, a mechanical joint will be applied. However, since FRP has different properties from steel, taking a standard steel-steel connection and simply replacing one component with FRP will not produce an ideal design.



## Appendix M: Contact Between a Cylinder and Groove

The contact stresses between the bolt and FRP should be calculated according to the theory for a cylinder in a larger groove to account for margin required during construction. This theory assumes that initial contact area between the two is a perfect line, but gains width as the two components deform elastically. The maximum stress will occur at the centerline of the contact area, and an elliptical pressure distribution is assumed. This situation is schematically presented in Figure 135. The contact area can be calculated according to Equation 92 and the contact pressure according to Equation 93. Note in Equation 92 that as the radii of the cylinder and groove become equal (the radius of the groove is negative), the contact width tends to infinity. This also means that the maximum bearing force tends to infinity.

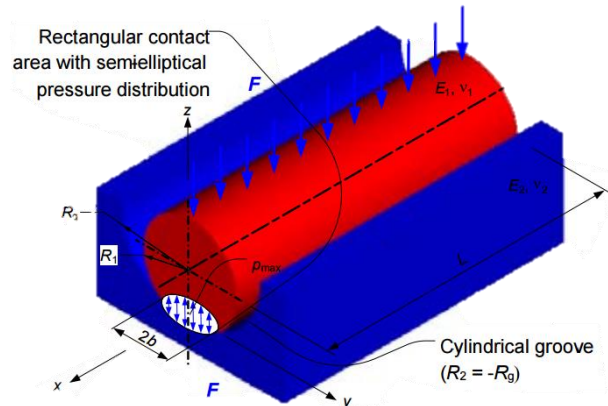


Figure 135: Schematic for Calculating Elastic Stress for a Cylinder in a Groove<sup>270</sup>

$$b = \sqrt{\frac{4F_{bearing} * \left[ \frac{1 - \nu_1^2}{E_{1,bearing}} + \frac{1 - \nu_2^2}{E_{2,bearing}} \right]}{\pi L_{bearing} \left( \frac{1}{R_1} + \frac{1}{R_2} \right)}}$$

Equation 92: Contact Area for Cylinder in a Groove<sup>271</sup>

<sup>270</sup> (Bamberg, 2006)

<sup>271</sup> (Bamberg, 2006)

With:

$b$ : Width of the Contact Region [mm]

$F_{bearing}$ : Force Applied Transferred Between the Two Solids [N]

$E_{1,bearing}$ : Young's Modulus of the Cylinder Material [MPa]

$\nu_1$ : Poisson's Ratio of the Cylinder Material [-]

$E_{2,bearing}$ : Young's Modulus of the Cylindrical Groove Material [MPa]

$\nu_2$ : Poisson's Ratio of the Cylindrical Groove Material [-]

$L_{bearing}$ : Length of the Contact Region [mm]

$R_1$ : Radius of the Cylinder [mm]

$R_2$ : Radius of the Cylindrical Groove [mm]. Note: Radius is Negative for a Groove.

$$p_{max} = \frac{2F_{bearing}}{\pi b L_{bearing}}$$

Equation 93: Contact Pressure for a Cylinder in a Groove<sup>272</sup>

With:

$p_{max}$ : Maximum Contact Pressure Between the Two Materials [MPa]

---

<sup>272</sup> (Bamberg, 2006)

## Appendix N: Calibration Study

Prior to modeling a full sized connection, model accuracy should be demonstrated. In order to do this, previously performed experiments should be mimicked in the model. During this process, several model elements, and physical characteristics were checked.

### N.1 Bolted Laminate Geometry

A series of experiments has been found, which measure the bearing strength of a bolt in a glass fiber reinforced polymer laminate. These experiments include a variety of geometries and laminate buildups which have been tested. As such, this makes for a good basis for creating a model which corresponds with reality. The setup of said experiments is shown in Figure 136. For these experiments, the bolt size was constant at 5mm and the laminates ranged from 1.4 to 4.8 mm in thickness, with varying lamella layups, and given in . The measurements of the specimens are much smaller than applicable for the case study, so that these experiments can only be used as calibration of the model.

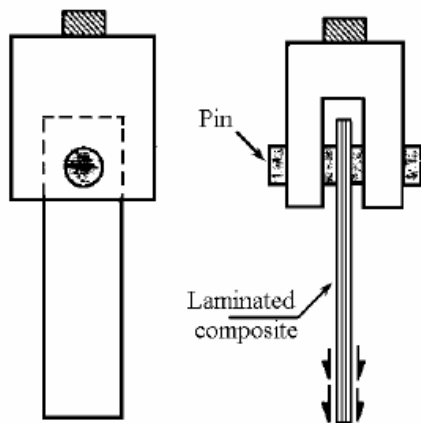


Figure 136: Calibration Experiment Set Up<sup>273</sup>

<sup>273</sup> (Okutan, 2001)

Layups of Experiment Specimens			
Specimen Number	Layup	Lamella Type	Thickness
1	[0/±45]s	UD	4.4
2	[90/±45]s	UD	4.4
3	[0/90/0]s	UD	3.3
4	[90/0/90]s	UD	3.3
5	[90/0]2s	UD	4.8
6	[±45]2s	UD	4.8
7	[0/90]6	Woven	1.4
8	[±45]6	Woven	1.4

Table 53: Layups, Lamella Types, and Thickness of Experimental Specimens

## N.2 Supports and Loading

The boundary condition of the system play an important role in the development of stresses and strains. For the calibration experiment the bolt was held in place, and the laminate was subjected to displacement controlled loading, at a certain distance below the bolt. As such, displacements have been assigned to nodes corresponding to these locations. The model of the bolted laminate is shown in Figure 137 and Figure 138, with assigned displacements indicated by the light blue markers. The ends of the bolt are supported in X direction. To load the model, the end of the plate is subjected to a fixed displacement.

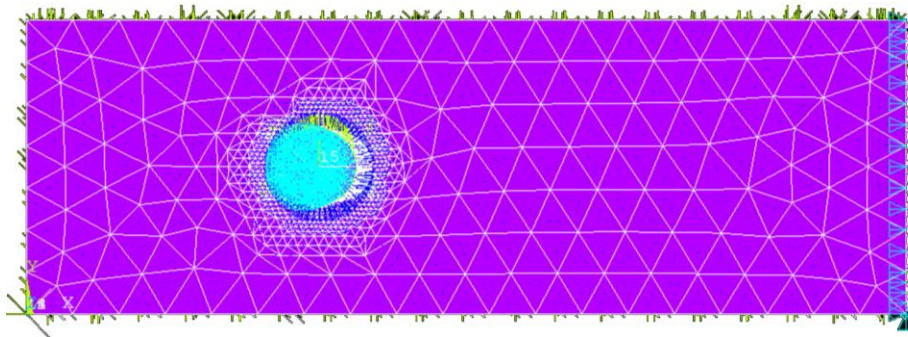


Figure 137: Top view of calibration model

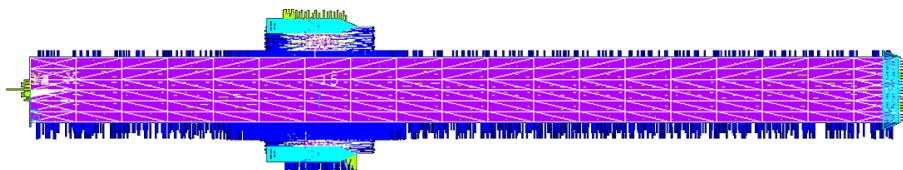


Figure 138: Side view of calibration model

### N.3 Materials

The materials used in this Analysis will be steel and FRP. The FRP is applied in two different varieties; the unidirectional lamellas, and the woven lamellas. The material properties utilized are listed below. The values listed for FRP are based on lamella properties. For the analysis, the lamellas will be individually modeled.

FRP Lamellas			
Property	Unidirectional	Woven	Units
Young's Modulus X	44000	20000	MPa
Young's Modulus Y	10500	20000	MPa
Young's Modulus Z	10500	20000	MPa
Shear Modulus	3740	4000	MPa
Poisson's Ratio XY	0.36	0.25	-
Longitudinal Tensile Strength	800	473	MPa
Longitudinal Compressive Strength	350	300	MPa
Transverse Tensile Strength	50	473	MPa
Transverse Compressive Strength	125	300	MPa
Shear Strength	120	90	MPa

Table 54: Unidirectional FRP Lamella Material Properties

Steel		
Property	Values	Units
Young's Modulus	210000	MPa
Shear Modulus	80000	MPa
Poisson's Ratio XY	0.3	-

Table 55: Steel Material Properties

### N.4 Mesh

The mesh will consist of three element types. These are listed below.

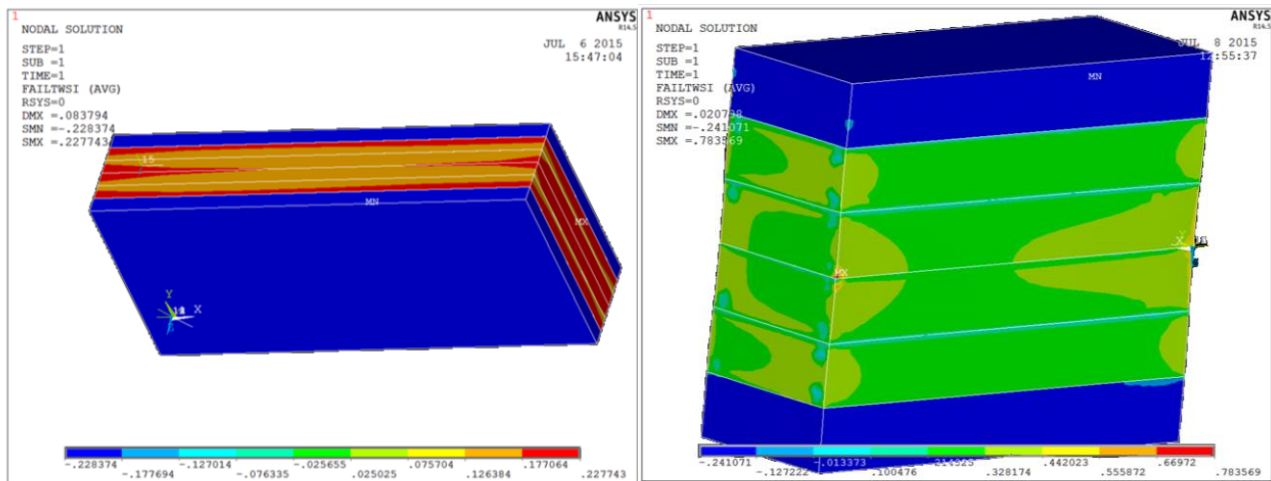
1. SOLID187
  - a. A 3-D, 10 node solid element.
2. TARGE170
  - a. A 3-D target element. This element overlays a solid and acts as the surface which receives contact.
3. CONTA174
  - a. A 3-D contact element. This element overlays a solid and acts as the contact initiating surface.

The solid elements will be used for meshing all of the solid materials. This includes the steel flange, the FRP layer, and the bolt. The target and contact elements will be used as contact pairs. The target element will be used along the concave surfaces, i.e. the interior of the hole in the FRP laminate. The contact elements will be used along the convex surfaces, i.e. the bolt surface.

A mesh refinement analysis must be performed to determine convergence of the model. The fineness of the mesh is especially important in the direct vicinity of the bolt, since large variations in stresses are expected there.

## N.5 Mesh Size

A convergence study regarding required mesh size is performed. To do this a model consisting of a laminate supported at one end and loaded through a uniform displacement at the other. The laminate itself consisted of a  $[0 \pm 45]_s$  buildup. A problem arises here in the sense that mesh refinement does not lead to a converging value of the failure criteria, as shown in Figure 139. Inspection showed that this was the result of edge effects which continues to become more and more localized as elements become smaller. However, using element sizes at which the edge effect is sufficiently smooth is not an option, since these elements would be larger than the bolts used in the experiments which will be mimicked.



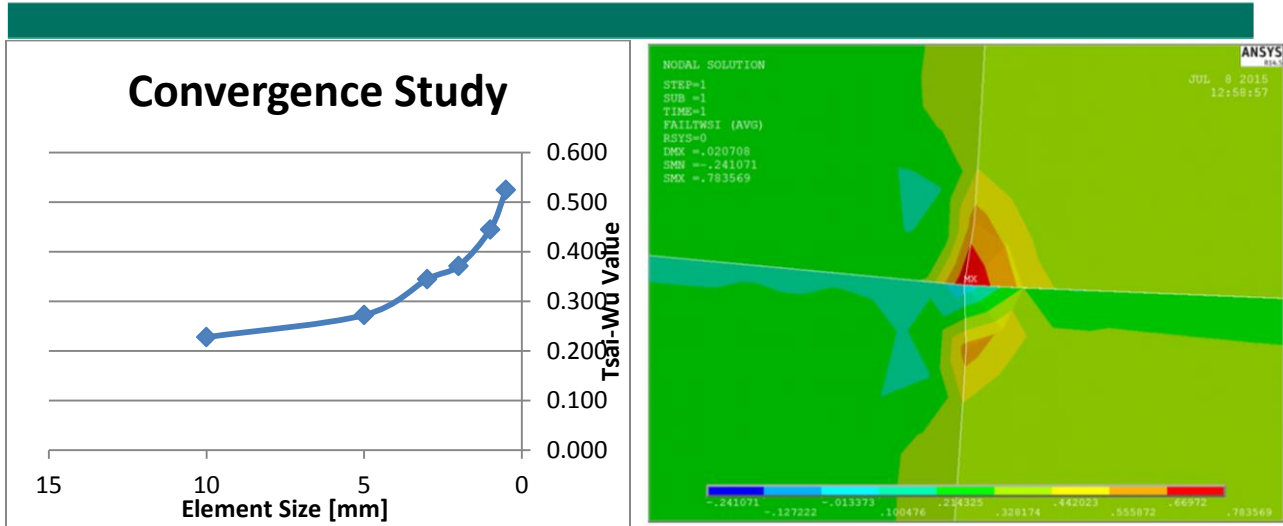


Figure 139: Mesh Size Study (clockwise): (1) Laminate with a large mesh size, (2) Laminate with a small mesh size, (3) Influence of mesh size on failure criterion, (4) Close up view of the problematic region

### N.5.1 End Effect

The Tsai-Wu value is measured as a function of the distance from the edge of the support, with varying mesh sizes. One can see in Figure 140, that independently of the mesh size, the influence of the peak values are damped out approximately 1 mm from the edge. In order to obtain results which correspond to reality, the peaks at the edge should be avoided. Hence, the data within 1 mm from the edge should be avoided as being inaccurate. Looking at Figure 141, one can see that when the end of the laminate is not considered, one can see a Tsai-Wu value distribution without large peaks.

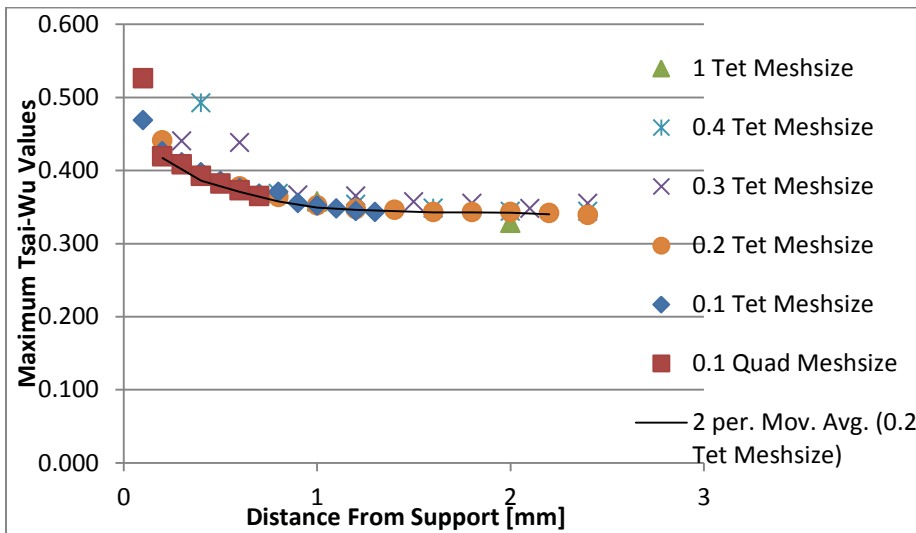


Figure 140: The Tsai-Wu value of a laminate as a function of distance from the support (sizes in mm)

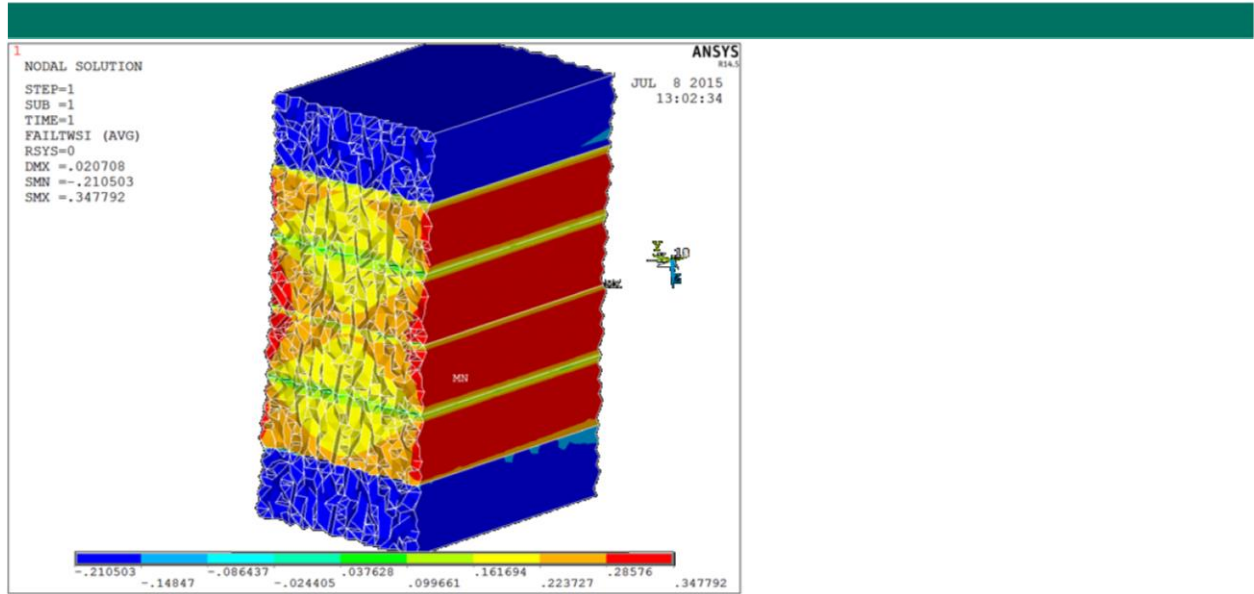


Figure 141: Cross Section of Laminate, where end effect is no longer present

### N.5.2 Global Convergence

With the influence of the edge effect described above, a measure for the global convergence criteria must be established. For this, the simplified uniform laminate has been replaced with the bolted laminate, and two criteria have been decided upon. First the support reaction will be determined. Secondly, the Tsai-Wu value at 1mm distance from the bolt hole will be determined. For the regions of the laminate away from the bolt, a mesh size of 3.2mm was utilized, and refinement around the bolt was increased until convergence was obtained. The results are shown in Figure 142, as a fraction of the value found with the smallest mesh size. The difference in the values obtained between the steps corresponding to a 3 fold mesh refinement and a 6 fold mesh refinement is minimal. Therefore, the mesh was not refined beyond this point.



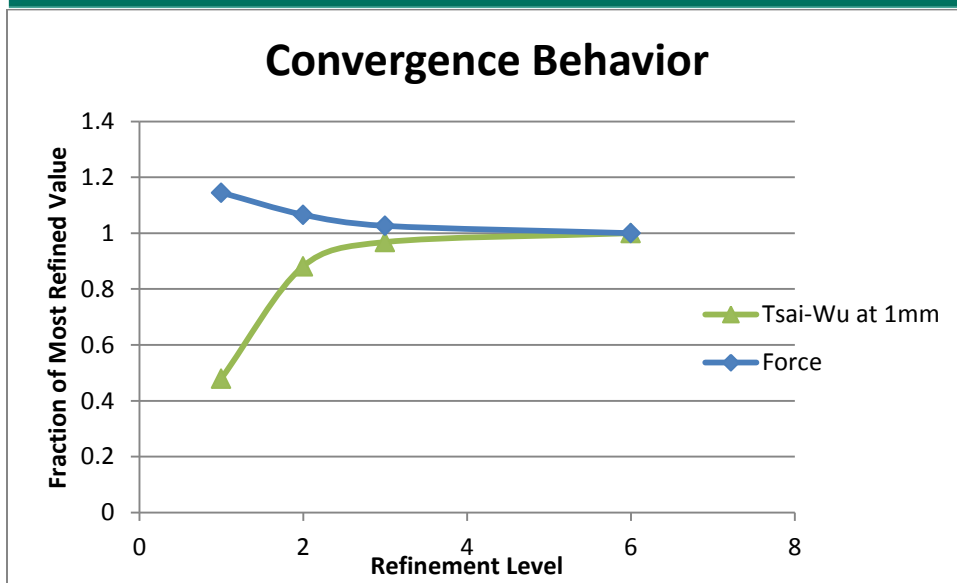


Figure 142: Force and Failure Criteria Convergence Study

## N.6 Results

The data from the calibration models are used to determine the accuracy of the model and will be used interpret the data obtained from a full-scale model. To analyze the data from the small scale models, an accurate method for determining failure should be established. There are several methods for calculating failure which will be examined for accuracy, following which a criterion for failure for the large scale connection will be established.

### N.6.1 Calculation Methods

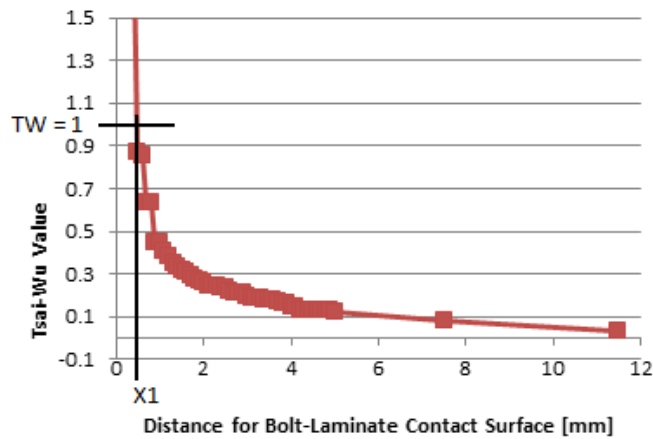
One of the difficulties in analyzing a model is determining when failure occurs. The bolt-FRP interface shown extremely large peak stresses and therefore a large Tsai-Wu value at loads far below the experimental failure levels. Three methods for calculating failure based one measurement distance have been analyzed, each subdivided into 3 subgroups based on cross-sectional location. The three methods are the single point failure, the dual point failure and the distance average methods. The three methods are graphically presented in Table 56. The three subgroups regard where in the cross-section of the laminate the Tsai-Wu Value is measured. The first is at the outermost fiber of the top ply, the second is an average over the laminate cross-section, and the third considers the maximum value over the height of the cross section.

## Failure Calculation Methods

### Graphical Representation of Method

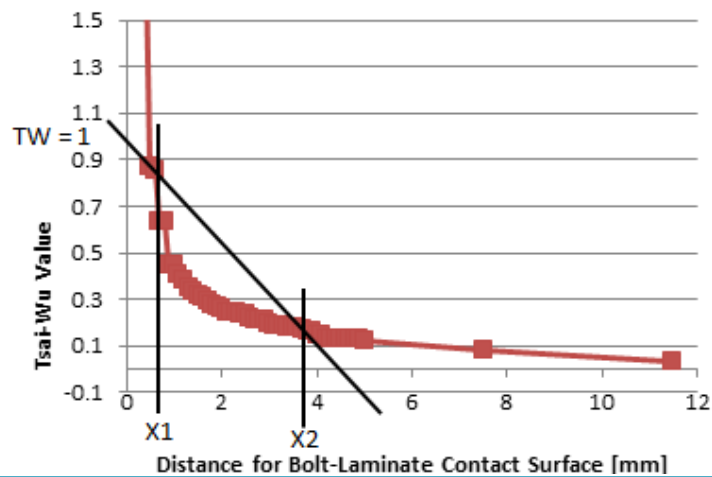
### Explanation

#### Single Point



The single point failure criterion is exceeded when at a predetermined location the Tsai-Wu value exceeds 1.

#### Dual Point



The dual point failure criteria is exceeded when the linear interpolation of two Tsai-Wu values at predetermined distances exceeds 1 at the contact surface.

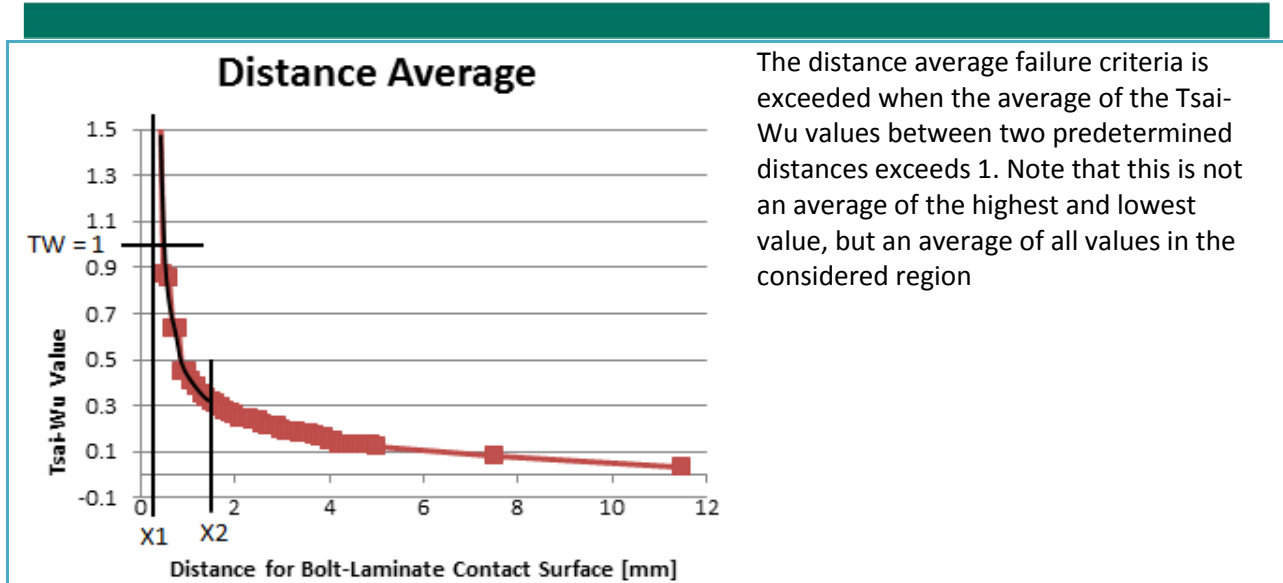
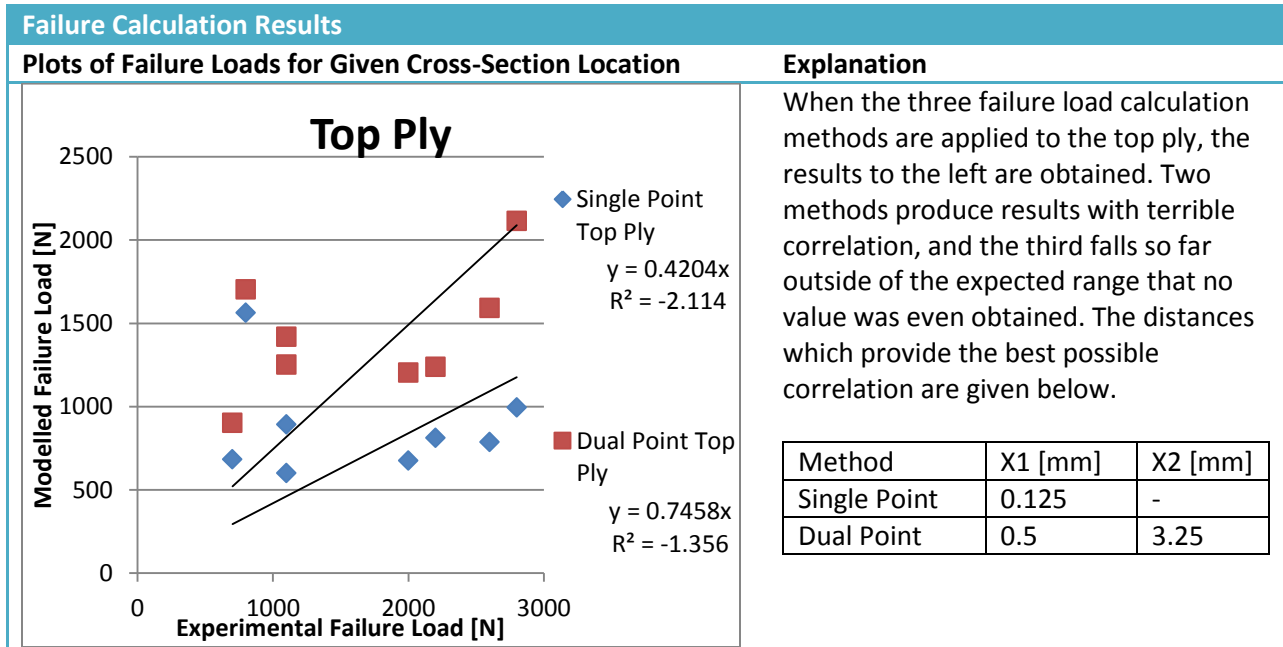


Table 56: Methods For Calculating Model Failure

### N.6.2 Analysis

The model failure loads are plotted against the results of the experimental data in Table 57. The results are presented in for the cross-section based subgroups.



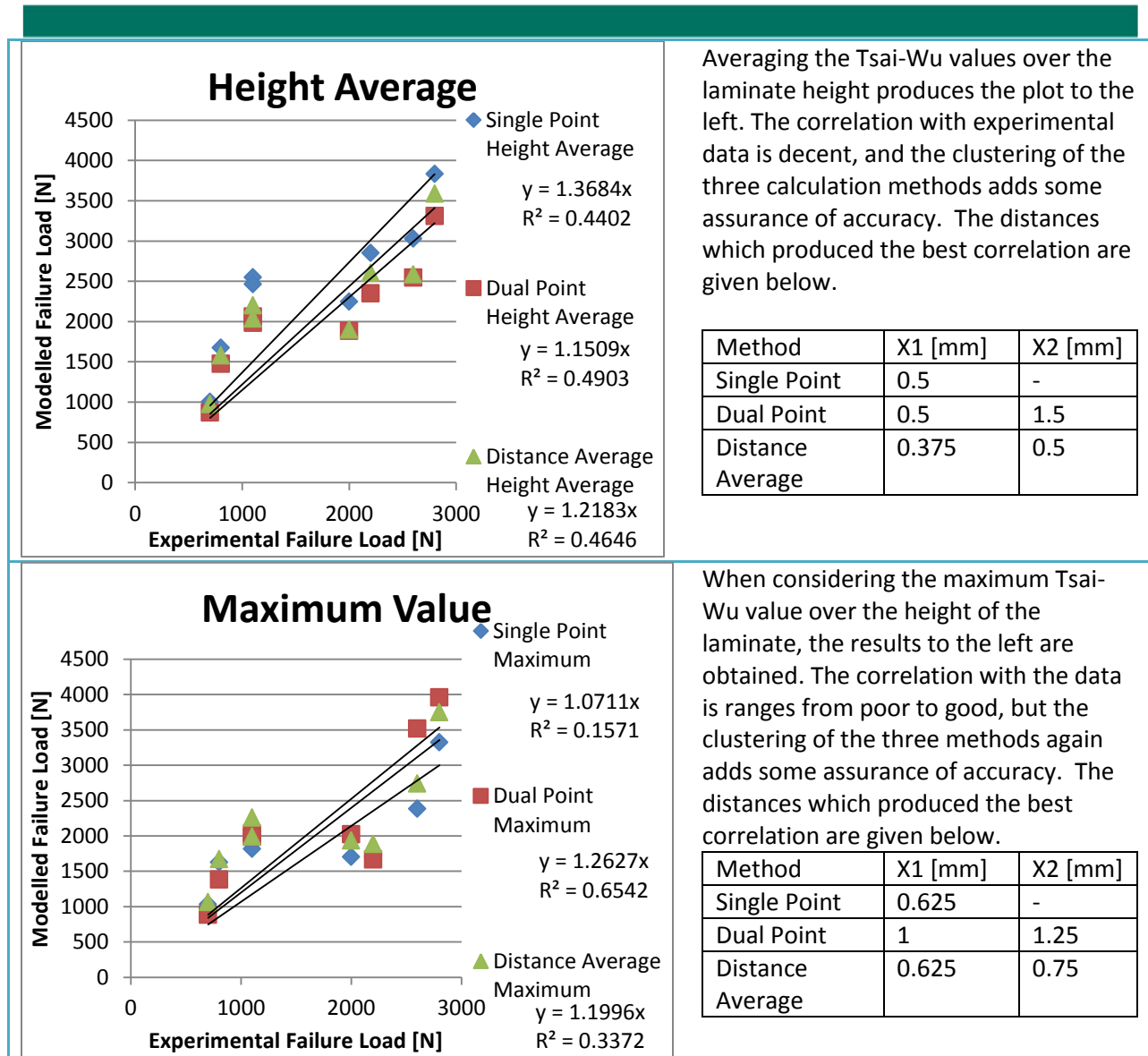


Table 57: Modelled Failure Load Plots for Different Cross-Section Locations

### N.6.3 Conclusions

The analysis done above clearly shows that considering the top fiber of a laminate does not allow for a decent prediction of failure. Considering averages over the height of the laminate provides much better results. The data is clustered about the trend lines, which lay close together and only a bit above the ideal values. The laminate average faces the problem that the considered specimens are relatively thin. However, when scaling the connection up to a size applicable to bridge building, the laminate will become much thicker. One will then face the question of how many plies, or what thickness of the laminate, should be considered when averaging the Tsai-Wu value over the height. The

small scale models have indicated that averaging up to 4 plies produces good results, so that this will be utilized for the full scale model as well.

This uncertainty can be avoided by taking the maximum value over the height of the laminate. Using the maximum value produces a large disparity between the three methods in terms of correlation with experimental values. However, the dual point method in combination with the maximum value approach has shown the best correlation of all combinations. Additionally, the three methods again lie quite close to each other.

For the full scale connection, the dual point method will be used in combination with the maximum cross-sectional Tsai-Wu value. To provide assurance of accuracy, this method will be verified with the remaining maximum value methods, as well as the height average methods. All methods have shown to overestimate the real values by between 7 and 37%, this will be corrected for individually per method. Applying these 6 methods should provide a decent range regarding the actual strength of the full scale connection.

## N.7 Scaling

In order to scale the results to sizes required for bridge building, some input parameters should be altered. Specifically, the distances used to calculate failure should be scaled. For a different set of experiments, and for a simplified failure criteria, the characteristic distances for single and distance averages has been shown to have a linear relationship with hole diameter.<sup>274</sup> This can be seen in Figure 143. However, these lines are not directly applicable to this study for several reasons.

1. Since a simplified failure criterion was used in calculating these lines higher values for the characteristic distances were found.
2. The lines do not intersect at zero so that multiplying by the ratio between the bolt diameters is also not an option.
3. There is no line available for the dual point failure criterion.
4. The range over which the distance are shown to scale linearly with hole diameter is between 6 and 10 mm.

---

<sup>274</sup> (Camanho & Lambert, 2006)

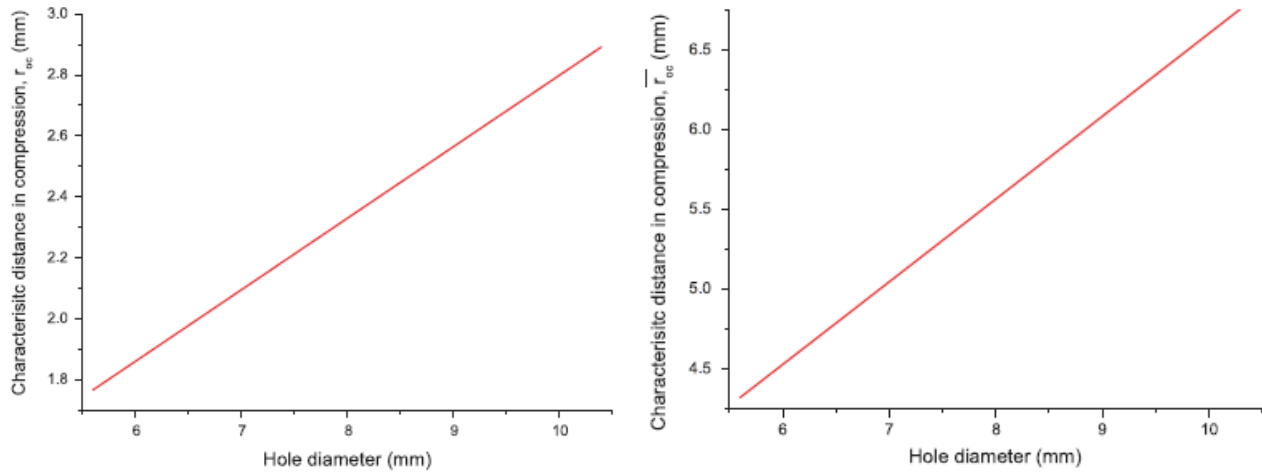


Figure 143: (Left) Original Relationship Between Characteristic Distance and Hole Diameter for Single Point Failure Method, (Right) Original Relationship Between Characteristic Distance and Hole Diameter for Distance Average Method.<sup>275</sup>

To account for the first two points listed above, the lines will be scaled according to ratio between the distances at a 5mm hole diameter. This has been done simple by determining the slope and y-intercept of the lines, and dividing them by the ratio between the characteristic distances for 5mm holes according to these lines and according to the calibration model.

The dual point failure method will be scaled according to the single point method. Calculations have shown that scaling according to the single point method is more conservative than scaling according to the distance average method, although the difference in the two methods is small (less than 6% for all holes up to 38mm diameter). As an example, the original and new lines applied for the distance average method are shown in Figure 144. Note that due to the expanded failure criterion, the lines are much shallower than the original lines.

Regarding the fourth point, assuming that the relationship between the characteristic distances and the hole diameters remains linear is incautious. Calculating for 36mm hole diameters would produce characteristic distances ranging from 5.5 to 12.5mm. While 5.5mm falls within a realistic range, 12.5mm seems very high. The linear relationship has been proven valid for hole diameters in the 6-10mm range. A study is performed to determine the influence of scaling on the failure load and hence to determine a reasonable value to which the measurement distances can be scaled.

<sup>275</sup> (Camanho & Lambert, 2006)

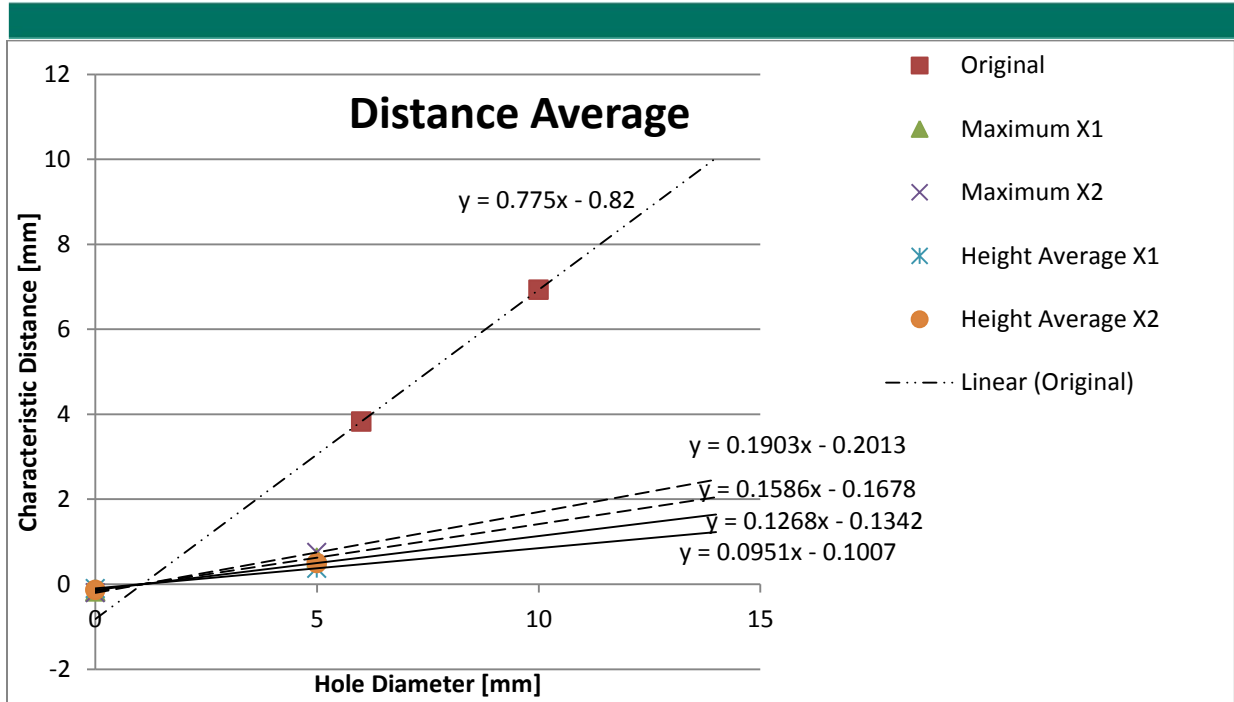


Figure 144: Characteristic Distances for the Distance Average Method

## Appendix O: Joint Influence Studies

As part of the study towards bolted joints, the influence of several parameters has been determined. These parameters are the clearance in the bolt hole, the influence of the head and nut of the bolt, the influence of the splitting tension in the hole, and the influence of the connection strength on the mass reduction of the girders.

### 0.1 Bolt Clearance

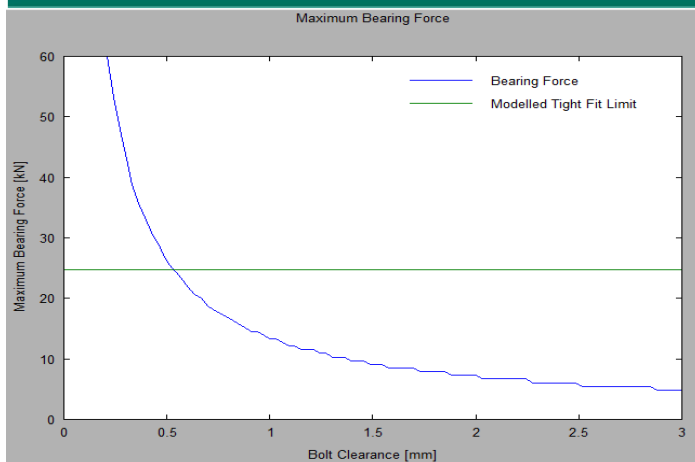
Typically, when designing bolted connections, a clearance is recommended. This is done so that minor misalignments can be compensated for during construction. However, the clearance between the bolt and the hole has a negative impact on stiffness. The connection will slip prior to force development, which has a negative impact on the stiffness of the connection and will reduce composite action between the deck and girder.

Clearance will also reduce the strength of a connection. To achieve clearance the bolt will have a smaller diameter than the hole. This difference in diameter means that the contact region between the two becomes considerably smaller, resulting in much more concentrated stresses. To determine this effect the theory of elastic contact between a cylinder and groove has been applied, as explained in Appendix M: Contact Between a Cylinder and Groove. This theory tends to infinity for grooves and cylinders with equal diameter, i.e. tight fit bolts. Hence the calculated values should purely serve as indicative of the trend. If the strength limit according to the ANSYS model is considered, the bearing strength is still greatly diminished by the clearance. This calculation method shows that a 3mm clearance, as specified by norms for normal holes in steel structures<sup>276</sup>, leads to a reduction of strength by a factor 5. Such a reduction means that designing bolted connections according to steel design norms is not feasible.

---

<sup>276</sup> (NEN 6772 (nl): Technische Grondslagen voor Bouwconstructies - TGB 1990 - Verbindingen, 2000)





**Figure 145: Bearing Strength of a Connection Determined with the Theory of Elastic Contact Between Cylinder and Groove, Tested against Tsai-Wu Criterion.**

To verify the hand calculations an ANSYS model of the situation has been made. The model is similar to the one described in 6.3 Full Scale Joint Model. However, three factors were altered to benefit convergence. The first is that the steel plate was removed, and the displacement which was applied to it was instead applied to the bottom of the bolt. The influence of this on the results is expected to be small. The second change is that the mesh used in this calculation is much coarser. This invalidates several of the failure models, as the Tsai-Wu value has not yet converged at the measurement distances required for these models. Given that the spread in results of the tight fit bolt was exceptionally small, the use of fewer failure models is accepted in exchange for a vast reduction in computational time. The third change is most significant. The model is deemed unstable by ANSYS, as the bolt experiences rigid body motion prior to contact with the laminate. To prevent this from happening, the displacement of the bolt needs to be controlled in x-direction at multiple heights. The location at which to do this was at two thirds of the laminate height (measured from the bottom). In the hand calculations performed in 6.1.2 Preliminary Calculations, this is the location of the neutral axis of the laminate. Hence, the bolt will rotate about this point so that controlling the motion in x-direction about this point will have the smallest influence on the results.

The results of the ANSYS calculation are presented in Table 58. The decrease in strength according to the model, is significantly larger than for the hand calculations. However, whether in reality the reduction is a factor 5 in accordance with hand calculations, or a factor 20 in accordance with FE models is inessential for this case study. Either reduction factor makes a bolted connection so weak that none of the design presented above are feasible.

Method	Strength [N]		
	Clearance	Tight-Fit	Factor
Single Point Maximum	1620	36130	0.045

Single Point Average	1784	28996	0.062
Distance Average Maximum	1647	33291	0.049
Distance Average Height Average	1954	31938	0.061
Dual Point Maximum	1860	29363	0.063
Dual Point Height Average	1768	30954	0.057

Table 58: Connection Strength for a Connection With 3mm Clearance

The reaction force measured at the fictitious support within the bolt is significantly larger than originally expected. In fact, the difference between the force applied to the bolt, and that which is transferred to the laminate, varies between 84% and 6% through the simulation. This implies severe inaccuracy. Therefore, the results displayed below can only be taken to be suggestive of the degree of strength reduction resulting from the bolt clearance.

### 0.1.1 Injection Bolts

To eliminate the negative effects of bolt clearance without having to apply extremely expensive tight-fit holes, injection bolts can be applied. These special bolts include a small hole in the bolt head so that the clearance between the bolt and laminate can be filled through resin injection. A schematic of a typical injection bolt is shown in Figure 146.

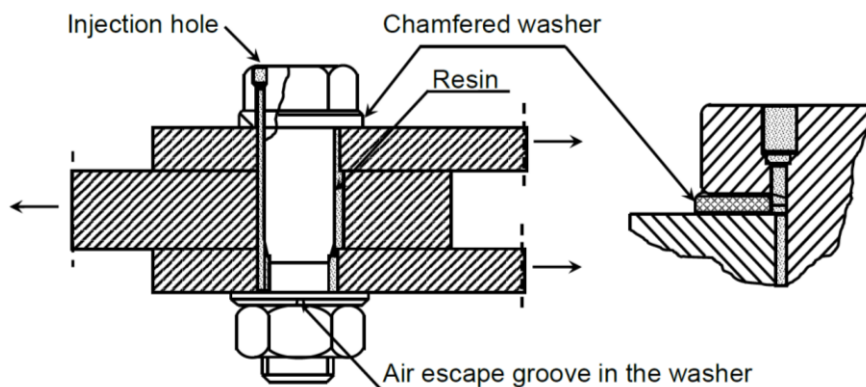


Figure 146: Injection Bolt Schematic<sup>277</sup>

Since the clearance is filled with resin, the initial slip and the peak stresses which arise as a result of the diameter mismatch are eliminated. The bolt is immediately in contact with the resin, so that transfer of load between the two occurs at a smaller displacement. The stress is dispersed within the resin, so that a more uniform stress reaches the laminate. This theory is supported by experiments, which indicate a stiffer and stronger connection as a result of injection bolts.<sup>278</sup>

<sup>277</sup> (Qureshi & Mottram, 2012)

<sup>278</sup> (Qureshi & Mottram, 2012)

Figure 147 shows the different behavior under loading of bolts with clearance, without clearance, and resin injected bolts. Note that the connection has been made according to Figure 148 with high strength friction grip (HSFG) bolts, i.e. pretension bolts. The belief is that FRP is unsuited for HSFG bolts. This is because FRP has a tendency to creep, thereby eliminating any pretension over time. The effect of pretensioning is clearly visible in the first experiment, where the connection withstands 10kN of force prior to initial slip. After the friction has been overcome, the bolt shows a large displacement, prior to making contact with the laminate, and being able to transfer more load. For bolt which are not pretensioned (or the pretension has faded due to creep), the bolts will show this slippage from the outset.

The bolted connection without clearance, shows a stiffer behavior. The initial effects of pretensioning are still visible through the distinct kink in the load displacement curve, but after the friction has been overcome, the bolt behaves much stiffer than the variant with clearance. Note that in both cases the maximum load was 25kN. This was where the experiment was cut-off. This was due to the utilized experimental criteria. The failure criterion was set to 0.15mm displacement (as indicated by the red dotted lines) according to the British norms.<sup>279</sup> The second was the design load of 25kN, which the bolt was cyclically loaded to 10 times to verify consistent behavior. Both criteria had to be reached to stop the experiment.

Finally, the connection with resin-injected clearance is considered. This connection shows a much stiffer behavior than the other two. This is because there is no slip, and load transfer occurs immediately through the resin, which reduces peak stresses. The stiffness is increased so much, that the failure criterion of 0.15mm slip was not reached until the loading was increased well beyond the limit for the other two experiments.

---

<sup>279</sup> (BS EN 1090-2:2008. Execution of Steel Structures and Aluminium Structures Part 2: Technical Requirements for the Execution of Steel Structures, 2008)

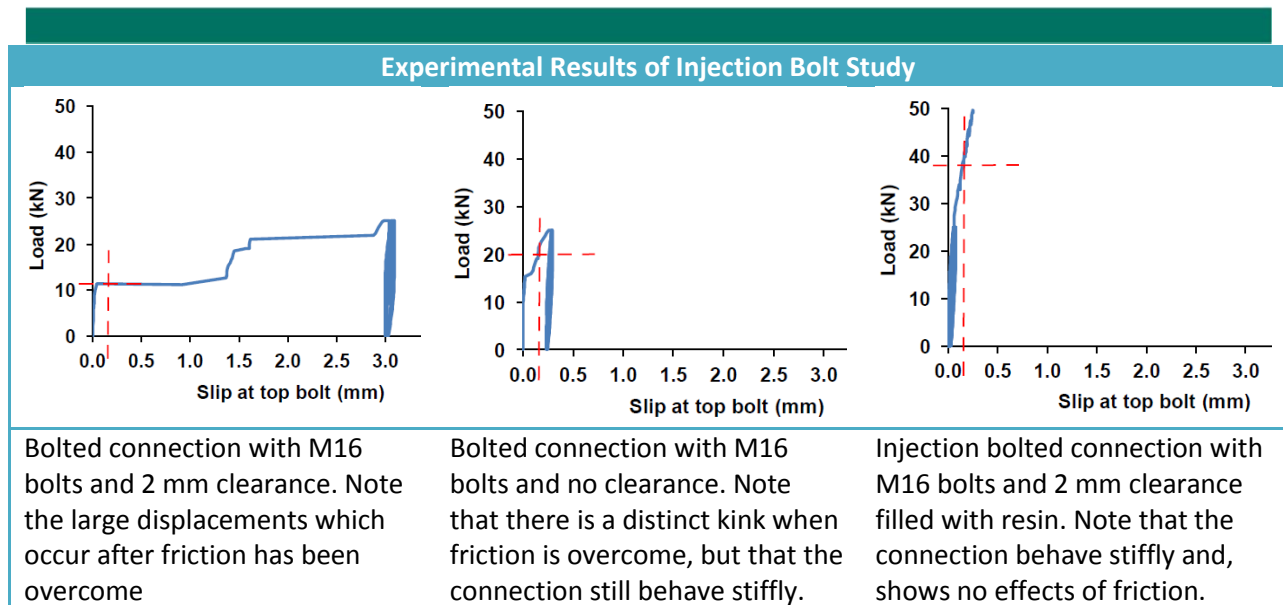


Figure 147: Experimental Results of Various Bolted connections. From Left to Right: (1) Holes with 2mm clearance, (2) Holes with no clearance, (3) Holes with 2mm clearance, resin injected.<sup>280</sup>

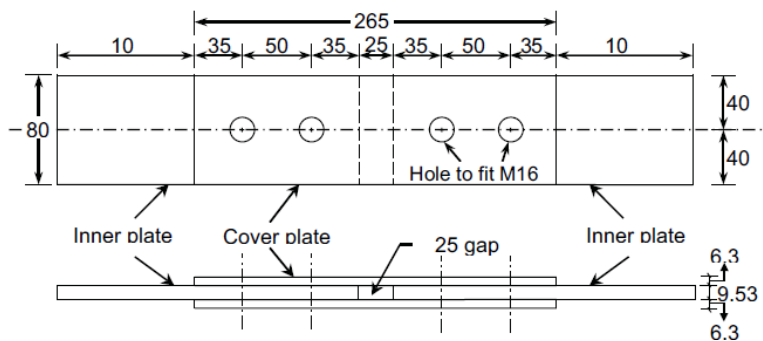


Figure 148: Geometry Setup of Experiments with Resin Injected Bolts<sup>281</sup>

In conclusion, one can see that the stiffness of the injection bolts is far superior to that of the other two connections. When determining experimental failure according to the British norms, the strength and stiffness of injection bolts greatly exceeds that of the non-injection bolted connections, including tight fit holes. Based on these considerations, injection bolts offer a promising alternative to more expensive tight fit holes.

<sup>280</sup> (Qureshi & Mottram, 2012)

<sup>281</sup> (Qureshi & Mottram, 2012)

## 0.2 Bolt Head

For the models above, the bolt head was neglected. The bolt was modelled in such a way that it was free to rotate inside the hole. However, in reality this rotation will be restricted to a certain extent by the washers, nut, and bolt head. When the bolt tries to rotate, these elements will come into contact with the laminate or steel thereby hindering rotation. Allowing the bolt to rotate freely marks the most conservative model for determining the strength of the connection. The degree to which rotation is prevented is dependent several factors, including the sizes of the washers, bolt head, and nut.

Since the rotational stiffness at the end of the bolt is dependent on several variables, it becomes difficult to accurately determine. The extreme situation of perfect rotational fixture has been analyzed, to give an upper bound estimate for the strength of the connection. A schematic of this situation is shown in Figure 149. Combining this model with the hinged model should provide a realistic range for the strength of the connection, and hence how much can be gained in the way of design strength by accurately determining the influence of the washers, head and nut.

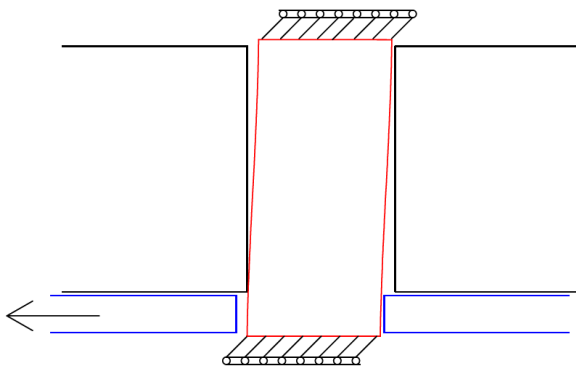


Figure 149: Schematic of a Bolt With Rotationally Fixed Ends

The model used to calculate this situation is nearly identical to the Full Scale model. The main differences are that the bolt has been shortened so that it barely sticks out from the laminate and steel plate, and that the ends are fixed in such a manner that rotation is prevented. Another input which has been altered is that mesh has been made coarser, similar to O.1 Bolt Clearance.

The results obtained for the failure models valid with the coarse mesh, are given in Table 59. The calculation methods invalidated through the coarse mesh are shaded red, and the critical value is shaded in green. All methods in the table are linearly scaled to the measurement distance for 36mm bolts. The strength increases by a factor as a result of modeling it rotationally fixed at its ends. This value far exceeds expectations. In fact, modelling the connection as fixed yields a design failure load which exceeds the hand calculated value upon which the original design was based.

Strength of Rotationally Fixed Bolted Connection			
Method	Fixed [N]	Hinged [N]	Ratio [-]
Single Point Maximum	75379	36130	2.09
Single Point Average	57892	28996	2.00
Distance Average Maximum	73162	33291	2.20
Distance Average Height Average	63574	31938	1.99
Dual Point Maximum	105907	29363	3.61
Dual Point Height Average	63923	30954	2.07

Table 59: Strength of Bolted Connection Schematized as Rotationally Fixed Compared to Hinged Schematization

### 0.3 Tension Effect

In literature there is a dispute regarding the tension which arises in the laminate at the contact interface perpendicular to the direction of loading. Some sources state that the magnitude of this tensile stress is equal to the magnitude of the compressive stress in the direction of primary loading.<sup>282</sup> Finite element models show a factor between these two of anywhere between 0.2 and 5.<sup>283</sup> The assumption that the load has a sinusoidal distribution leads to a factor of 0.25 between the force transfer in the y- and x-direction.<sup>284</sup>

With such variability within literature, the influence of the ratio between these two stresses on the bearing capacity of the connection has been studied. The calculations are done in a manner similar to 6.1.2 Preliminary Calculations. However, in these calculations the tension factor (the ratio of tension over compression) has been made the variable. The tension factor has a significant impact on the bearing strength of a connection. Figure 150 shows that if the tension factor is within the range found in literature, it can change the strength by more than a factor 3.

One can see in Figure 150 that the influence of tension is nearly negligible until the tension factor reaches approximately 0.5. After this, the maximum bearing force drops quickly. Until the tension factor reaches 1.5, the strength reduction is linear with increasing tension factor. After this level, there is a kink and the line becomes a curve. Looking at which ply fails and the components of the Tsai-Wu criterion (see G.4.2 Tsai-Wu Criterion), this can be explained. Near each kink in the curve, a different term of the Tsai-Wu criterion becomes dominant, as shown in Table 60,. The first region is dominated by the terms compressive loading in the x-direction. The ply which fails is oriented at 90 degrees, so that the local 2-axis corresponds to the global x-axis. The second region is dominated by shear loading in the 45 degree ply. The third region is dominated by tension in y-direction, in a 0 degree oriented ply. Hence, for this ply the y-direction corresponds to the local 2-axis.

<sup>282</sup> (Bamberg, 2006)

<sup>283</sup> (Okutan, 2001)

<sup>284</sup> (Chang, Scott, & Springer, 1982)

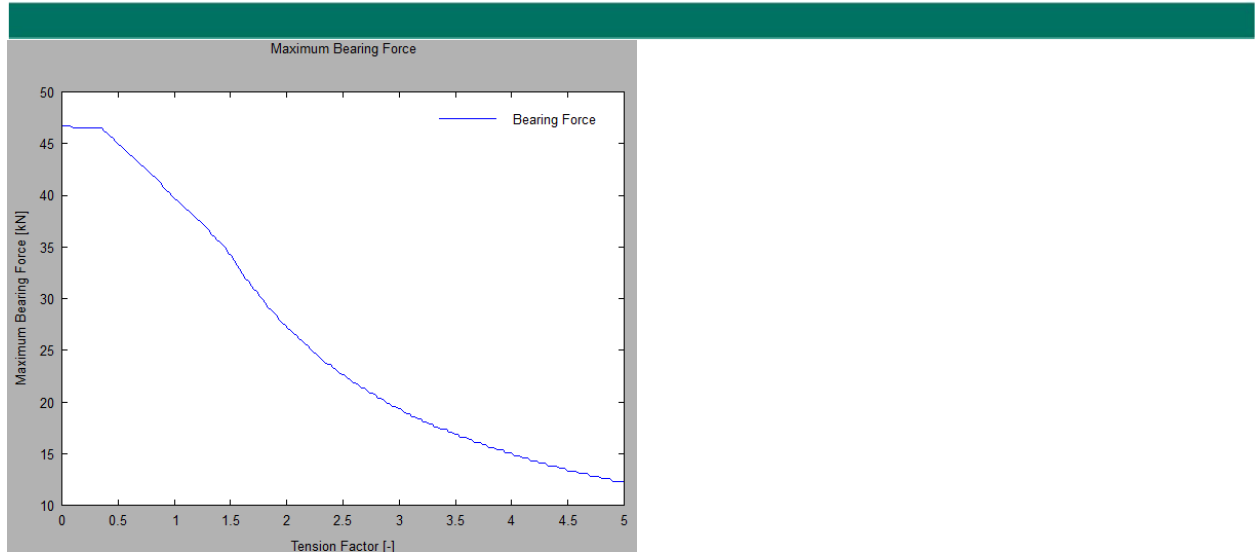


Figure 150: Influence of the Ratio Between Tensile Stress Perpendicular to the Primary Loading Direction and Compressive Stress in the Direction of Loading on the Failure Load of a Bolted Connection

Values of Tsai Wu Terms as a Function of Tension Factor							
Tension Factor	Failure Ply Orientation [°]	Tsai Wu Term					
		$\sigma_1$	$\sigma_2$	$\sigma_1^2$	$\sigma_2^2$	$\tau_{12}$	$\sigma_1\sigma_2$
0.1	90	-0.0262	-0.8728	0.005	1.7986	0.0003	-0.0953
0.75	45	0.0295	-0.2863	0.0064	0.1935	1.0995	0.0352
3	0	0.0632	0.4107	0.0293	0.3983	0.0001	-0.1081

Table 60: Values of Each of the Six Tsai-Wu Terms for the Three Distinct Regions in Figure 150.

#### 0.4 Alternative Materials For Connection

Glass fibers have been chosen in this thesis based on their cost effectiveness. They are 15-40 times cheaper than aramid or carbon fibers, while the performance loss is significantly less. This means that unless specific requirements demand the higher strength and stiffness, the use of E-glass fibers is most economic. For the connections in question, there is a specific requirement for higher strength. Therefore, an analysis has been made of the influence of different fibers on the strength of the connection. The results are presented in Figure 151.

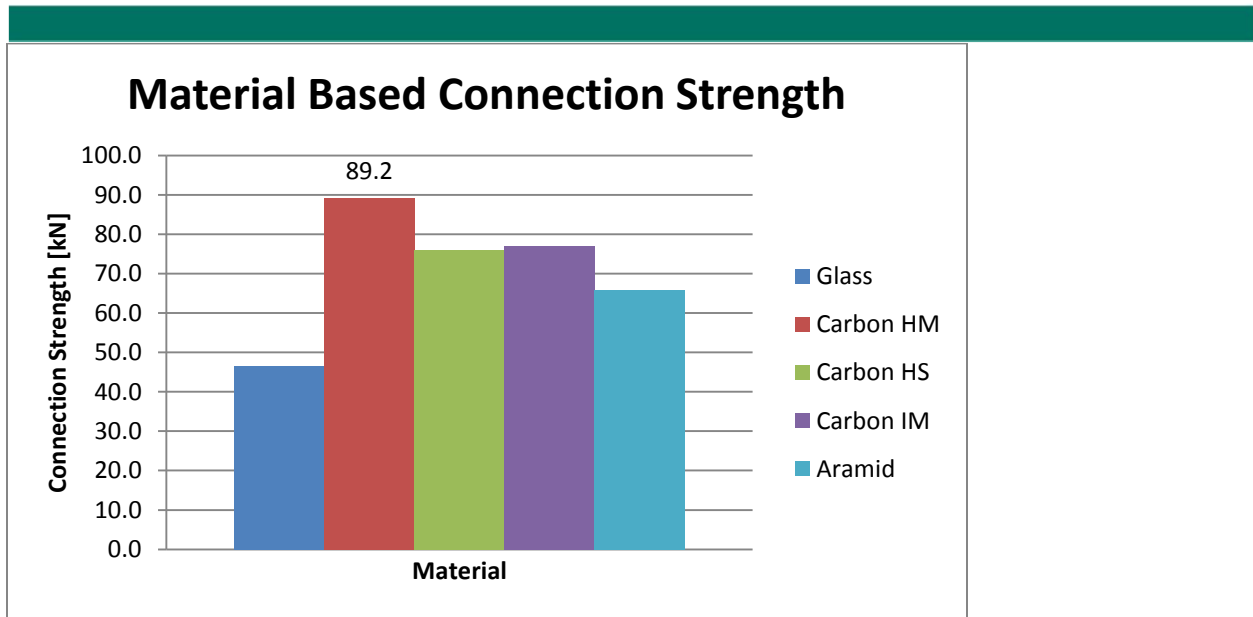


Figure 151: Strength of Bolted Connection Using Different Fiber Types, Based on Hand Calculations

In Figure 151, one can see that the strength of the bolted connection increases greatly when using High Modulus Carbon Fibers. In fact, the strength nearly doubles. However, this comes with a caveat: producing the entire deck with carbon fibers, would lead to a massive increase in shear stress as well. Therefore a proffered solution is to locally strengthen the connection using carbon fibers as opposed to glass fibers. This has never been done according to the author’s knowledge, and would bring along some problems of its own. To create local reinforcement, short fibers would probably be required, which typically allow for a much smaller fiber volume fraction, and are typically applied through the spray lay-up method for which a larger material safety factor is specified.

A way around this problem would be to manufacture the strip of the deck involved in the connection using carbon fibers. In this case, the component could still be created with long fibers, allowing for production methods other than spray lay-up. This method would lead to an increase in the shear stress, but as long as the connection width remains relatively small the increase in shear stress should also remain small.

## 0.5 Comparison to Connections in Concrete

The hand calculations used to determine the strength of bolted connections in FRP were performed elastically. However, when considering dowel connections in concrete calculations performed elastically far underestimate the strength of connections. In concrete, there are two considered failure mechanisms, as shown in Figure 152. These are shear of the dowel and bearing of the concrete. For this chapter only bearing failure will be considered.



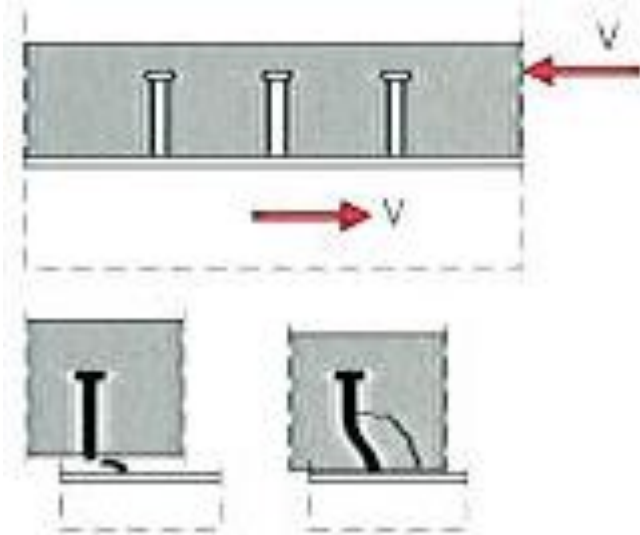


Figure 152: Failure Mechanisms of Dowel connections in Concrete. (Bottom Left) Shear of the Dowel. (Bottom Right) Concrete Bearing Failure<sup>285</sup>

Calculating bearing failure of the concrete elastically will lead to a vast underestimation of the strength. To illustrate this, some values of connections strength have been calculated according to codes, and according to hand calculations. These are presented in Table 61. Note that the values according to the code are design values while the hand calculated strengths are characteristic values. The methods listed under hand calculated strengths explained below:

- Method 1:** The load is assumed to create a normal force and bending moment over the height of the concrete-dowel interface. Additionally, the stress distribution is sinusoidal over the width of the dowel. Failure occurs when at the outer fiber, the maximum compressive stress of the concrete is exceeded.
- Method 2:** Similar to method 1, except that the moment action in the concrete has been excluded.
- Method 3:** The plastic capacity of the concrete cross section in immediate contact with the dowel. This is simply the characteristic concrete compressive strength multiplied by the height and diameter of the dowel.

<sup>285</sup> (Stark & Stark, 2009)

Comparison of Hand Calculated and Norm Based Failure Loads							
Diameter [mm]	Norm [kN]	Hand Calculated Values [kN]			Percentage of Norm [-]		
		Method 1	Method 2	Method 3	Method 1	Method 2	Method 3
16	59	4	20	32	7%	34%	54%
18	70	5	23	36	7%	33%	51%
19	75	5	24	38	7%	32%	50%
20	80	5	25	40	7%	32%	50%
22	90	6	28	44	7%	31%	49%
24	100	6	30	48	6%	30%	48%

Table 61: A Comparison of the Failure Loads of Dowel Connections in Concrete Calculated According to Norms and Simple Hand Calculations.<sup>286</sup>

Table 61 shows that the strength of connections in concrete beams far exceeds the elastic and plastic limits. This is likely due to the confined nature of concrete in front of a dowel. One can see in Figure 152 that rather than local compressive failure occurring at the contact interface, a section of concrete extending some distance from the interface breaks loose from the remainder of the deck. This is why the strength according to the norms can be larger than the strength according to local elastic and plastic calculations.

### 0.5.1 Assumed Values for Calculations of Connections in Concrete

In order to calculate the values above, several values have been assumed. In the interest of reproducibility, these assumptions are given in Table 62.

Assumed Values for Calculation of the Influence of Composite Action		
Item	Value	Units
Young's Modulus Concrete	33	GPa
Concrete Compressive Strength	30	MPa
Dowel Height	66.25	mm
Thickness Steel Flange	15	mm

Table 62: Assumed Values for the Comparison of Various Calculation Methods for the Strength of Connections in Concrete.

### 0.5.2 Relationship Between Connections in Concrete and FRP

The fact that a connection in concrete is significantly stronger than an elastic calculation would indicate, does not mean the same is valid in FRP. There are several points which differ between concrete and FRP which may have an influence on the strength of connections.

<sup>286</sup> Methods and Verification: (Stark & Stark, 2009).

Norm: (NEN-EN 1994-1-1: Design of composite steel and concrete structures - Part 1-1: General rules and rules for buildings, 2005).

Concrete deck are typically thick and solid. An FRP deck typically is of comparable thickness but hollow. The face plates of the deck are typically 10-20mm thick. In this thesis, a finite element analysis was performed on a laminate which was thickened to 66.25mm. This is quite a bit smaller than a typical concrete deck thickness. The difference in thickness will influence the degree of confinement, and hence influence the connection strength.

Concrete has a small degree of plasticity in compression. Concrete can be modelled as a bi-linear material with a plastic region between 1.75 and 3.5‰. FRP lamellas do not show this behavior. However, FRP gains some plasticity from being laminated since some plies will reach their ultimate strength prior to others. The degree to which a laminate shows plasticity is highly dependent on how the laminate is oriented. The different plastic behavior of the two materials will impact the connection strength.

The connections in FRP and concrete are created in different ways. In concrete, the dowel is welded to the steel flange or plate and the concrete is cast around this. For FRP, holes should be drilled through which the bolt can be placed. This means that while in concrete, a connection which fits exactly around the dowel can be expected, in FRP the bolt will not be an exact fit to the hole without expensive preparations. Even if the connection in FRP can be made as a tight fit, the drilling of the hole through the material causes damage and cuts the fibers. These initial defects will likely impact the strength.

The difference between in concrete connection strengths according to the norm and to hand calculations, cannot be directly related to FRP. The materials and their properties vary too greatly. However, the fact that there is such a difference bodes well for the future of mechanical connections in FRP. While experimental verification is required, perhaps the actual strength of bolted connections lies higher than an elastic calculation indicates.

## 0.6 Influence of Connection Strength on Mass

Previous influence studies have shown that there are several factors which can greatly affect the strength of connections. Therefore an analysis has been made of how much the connection strength influences the global design. This has been done by determining the mass of the main girder as a function of the strength of the bolted connection. This has been done in a manner similar to the one described in 5 Laminate Orientation. There are two deviations from that method. First, the criteria that the force through the connection may not exceed the assumed strength. Second, the geometry of the reduced deck height design is used.

The mass of the main girder is determined and compared to the mass of the original design. This has been done assuming either 1, 2 or 4 bolt rows. The results are presented in Figure 151. There are several things worth noting.

1. All three lines have a plateau at higher connection strengths. These plateaus signify the level at which the connection strength is no longer critical, and instead stiffness or (typically) stress becomes critical.
2. The plateau is slightly higher for the 1 and 2 row situations. This is caused by the required connection width, which is set to 600mm for 4 rows, and 300mm for the other two situations.
3. The mass change can become negative. When the connection is too weak, the design becomes so inefficient that realizing composite action between the deck and girders actually requires more mass to be added than that it saves.
4. The calculated strength of 24.6kN falls within the region where the connection governs the design. However, the influence study assuming rotationally stiff ends shows a connection strength of approximately 58kN, which falls within the plateau region of the 4 bolt row connection. Hence, if the rotationally fixed model can be proven to be more accurate, this could result in 20% weight savings on the main girders.

The weight savings with the design without composite action, according to 6.4.2 Redesign with No Composite Action, shows weight savings of nearly 21%. This begs the question, is compositely connecting the deck to the girders economically viable?

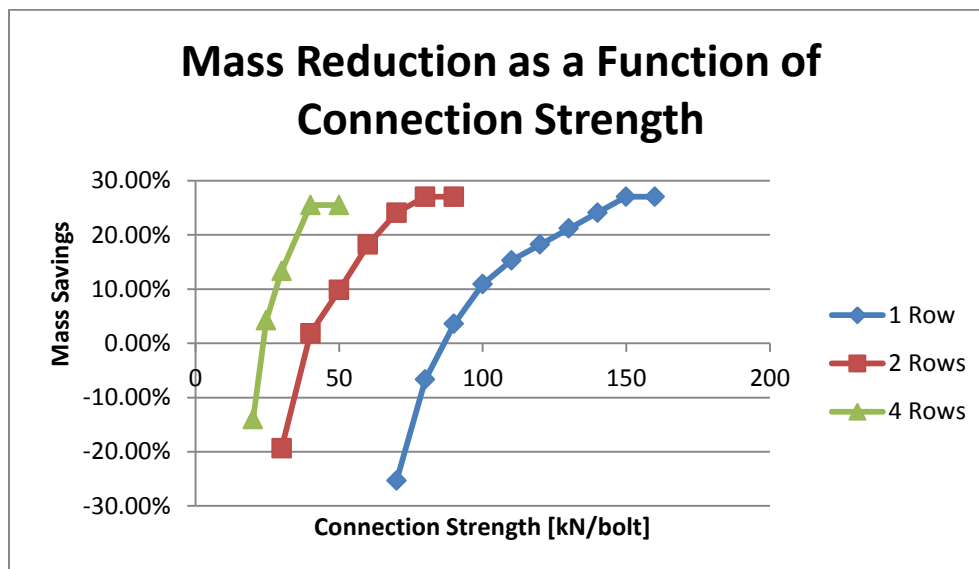


Figure 153: Analysis of the Mass Savings Which can be Achieved in a Deck-Girder System with Composite Action as a Function of Connection Strength

## Appendix P: Comparison to Eurocomp Handbook

The *Eurocomp Design Code and Handbook*<sup>287</sup> is recognized by experts as the design handbook to apply during the design of bolted connections in composites. Therefore Eurocomp method will be applied to the calibration experiments and the full scale model, and will be compared to the previously determined values.

### P.1 Simplifications and Assumptions of Eurocomp

Some assumptions and simplifications have been applied to the Eurocomp. These are listed below:

- Only bearing has been considered
- The bearing stress is determined at 0° from the direction in which the force is applied
- The stress concentration factor  $C_{m,1} = 1.2$  has been applied for symmetric joints
- The stress concentration factor  $C_{m,1} = 2$  has been applied for asymmetric joints
- Basic load case 2 has been utilized
  - The surrounding laminate is under compression
  - The stress distribution factor is dependent on the directionality of the laminate
    - Situation A: Unidirectional, 0°,  $C_{scf} = 1.5$
    - Situation B: Unidirectional, 90°,  $C_{scf} = 1.05$
    - Situation C: Unidirectional, Quasi-Isotropic,  $C_{scf} = 1.25$
- The laminate stiffness properties follow from 4.3.5 Determination of Laminate Properties
- The material factors is set at  $\gamma_m = 3.4$ . based on partial factors as follows
  - $\gamma_{m,1} = 2$
  - $\gamma_{m,2} = 1.7$
  - $\gamma_{m,3} = 1$

### P.2 Comparison of Eurocomp and Calibration Experiments

The Eurocomp handbook is used to determine the failure load of the calibration experiments. The results are presented in Table 63.

$$F_k = \frac{\sigma_k dt}{C_m C_{scf}}$$

$$F_d = \frac{\sigma_k dt}{C_m C_{scf} \gamma_m}$$

Equation 94: Characteristic and Design Failure Loads of a Bolted Connection

<sup>287</sup> (The European Structural Polymeric Composites Group, 1996)

With:

$F_k$ : Characteristic Failure Load of Joint [N]

$F_d$ : Design Failure Load [N]

$\sigma_k$ : Characteristic Failure Stress of Laminate Under Bearing [MPa]

$d$ : Diameter of Bolt [mm]

$t$ : Thickness of Laminate [mm]

$C_m$ : Correction Factor [-]

$C_{scf}$ : Stress Concentration Factor over Width of Bolthole [-]

$\gamma_m$ : Material Factor [-]

Where several components in Equation 94 are defined according to Equation 95.

$$\gamma_m = \gamma_{m,1} \gamma_{m,2} \gamma_{m,3}$$

$$C_m = C_{m,1} C_{m,3}$$

$$\sigma_k = E_r \varepsilon_{c,crit}$$

$$\frac{1}{E_r} = \frac{1}{E_x} \cos^4 \theta + \left( \frac{1}{G_{xy}} - \frac{2\nu_{xy}}{E_x} \right) \sin^2 \theta \cos^2 \theta + \frac{1}{E_y} \sin^4 \theta$$

**Equation 95: Material Factor, Correction Factor, Characteristic Stress and Radial Young's Modulus Required for the Determination of the Failure Load of a Bolted Connection According the Eurocomp Handbook**

With:

$\gamma_{m,1}$ : Partial Material Factor Accounting for Derivation of Material Properties [-]

$\gamma_{m,2}$ : Partial Material Factor Accounting for the Production Process [-]

$\gamma_{m,3}$ : Partial Material Factor Accounting for Environmental Effect and Loading Duration [-]

$C_{m,1}$ : Correction Factor Accounting for Stress Variations over Height of Laminate [-]

$C_{m,3}$ : Correction Factor Accounting for Small Bolt Spacing. Only Relevant for Tangential Stresses [-]

$E_r$ : Young's Modulus in Radial Direction [MPa]

$\varepsilon_{c,crit}$ : Critical Strain of the Laminate in Compression. Specified as 0.002 [-]

$E_x$ : Young's Modulus of laminate in x-Direction [MPa]

$\theta$ : Rotation of the Direction of Loading With Respect to the x-Axis [rad]

$G_{xy}$ : Shear Modulus of the Laminate in the xy-plane [MPa]

$\nu_{xy}$ : Poisson's Ratio of the Laminate [-]

$E_y$ : Young's Modulus of laminate in y-Direction [MPa]

Comparison Between Experiments and Eurocomp					
Experiments			Eurocomp		
Laminate	Thickness [mm]	Experimental Failure Load [N]	Situation	Characteristic Failure Load [N]	Design Failure Load [N]
[0 ±45]s	4.4	2200	C	673	198
[90 ±45]s	4.4	1100	C	399	117
[0 90 0]s	3.3	1100	A	609	179
[90 0 90]s	3.3	2000	B	574	169
[90 0] 2S	4.8	2600	A	735	216
[±45] 2S	4.8	2800	C	388	114
[0 90] 6 woven	1.4	800	A	156	46
[±45] 6 woven	1.4	700	C	145	43

Table 63: Comparison of Experimental Failure Loads and Failure Loads Calculated According to the Eurocomp

Table 63 shows the results of the experiments used during the calibration of the finite element models, and the strengths (characteristic and design) as determined according to the Eurocomp Design Code. The Eurocomp values should be lower since they represent characteristic and design values. However, the difference between the experimental failure load and the design failure load is very large. This indicates that the Eurocomp values are very conservative.

### P.3 Comparison of Eurocomp and Full Scale Model

The full scale bolted joint is also calculated according to the Eurocomp method. The results are presented in Table 64.

Comparison Between Full Scale Model and Eurocomp			
	Eurocomp [N]	Model [N]	Difference
Characteristic	47422	44416	-6%
Design	13948	24906	79%

Table 64: A Comparison Between the Failure Loads of the Full Scale Connection as Calculated by the Eurocomp and the ANSYS Model.

Table 64 shows the failure loads according to the Eurocomp calculation method, as well as according to the ANSYS model. When comparing the characteristic values, the two methods are nearly identical. However, the Eurocomp specifies a higher material safety factor, so that the design strength is much lower than according to the model.

The geometry of the full scale model does not comply with the Eurocomp on all fronts. Specifically, the laminate is thicker in relation to the bolt diameter than allowed by the Eurocomp. This has an impact on the moment in the joint. The hand calculations of strength indicate that the moment

---

reduces the strength of the joint by a factor 4, while the Eurocomp accounts for the eccentricity of single lap joints simply by applying a reduction factor of 2. This simplification might be valid for thin laminates, but as thicknesses increase the reduction factor should increase as well.



## Appendix Q: Model Validation

The finite element model must be validated. The elements to be verified are as follows: the main girders, the crossbeams, the deck, and the connections. First the global model will be presented. The model is based on the geometry according to 6.4.2 Redesign with No Composite Action. The model has been set up parametrically, and the individual elements of the model will be verified with relatively small dimensions, to reduce computation time. The dimensions used for model validation are given in Table 65.

Validation Model Dimensions		
Property	Value	Units
Bridge Length	5000	mm
Bridge Width	3000	mm
Height Main Girders	553.25	mm
Main Girder Flange Width	300	mm
Main Girder Flange Thickness	35	mm
Main Girder Web Thickness	20	mm
Crossbeam Height	353.25	mm
Crossbeam Flange Width	300	mm
Crossbeam Flange Thickness	20	mm
Crossbeam Web Thickness	20	mm
Width of Connection	400	mm
Height Of Connection Laminate	20	mm

Table 65: Altered Measurements for Validation Model. Measurements not Included Remain Unchanged from the Main Model.

The element type used is a shell 181 element. This is a two dimensional, 4-noded element. The material properties of this element can be input by layer, making it ideal for laminate calculations. The steel profiles consist of a single layer, while the deck is layered in accordance with 4.3.5 Determination of Laminate Properties.

The second element type used is an MPC184 element, as shown in Figure 154. This is a multipoint constraint element, where the keyoptions have been set in such a manner that the element becomes a “point-in-plane” connection. This means that the element links the displacement of two nodes in one direction, while allowing relative motion in the other two directions. The relative motion is constrained by a spring stiffness. This element forms the connection between the deck and the girders, where the two are linked together for z-direction displacements, but are allowed to move in the X- and Y-directions. The design assumes that no shear flow is transferred between the deck and the girders. However, allowing free movement of the deck over the girder allows for rigid body motion, so that a spring stiffness should be chosen which prevents rigid body motion, yet does not influence the results of the calculation. The stiffness will be determined in Influence of Connection Stiffness on page 278.

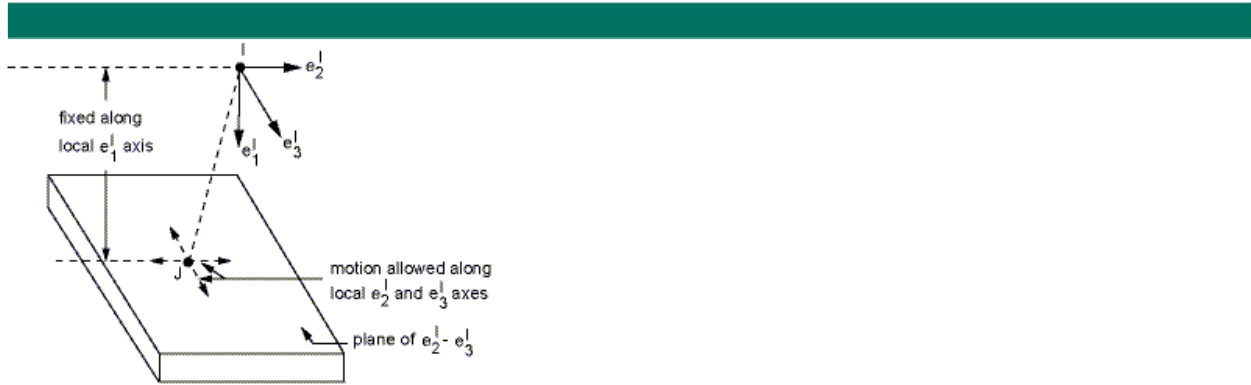


Figure 154: Visualization of an MPC184 Element Set as a Point-In-Plane Connection<sup>288</sup>

## Q.1 Main Girders

To validate the main girders, they have been isolated from the rest of the model. This has been done by assigning the other components of the model dummy material properties. The dummy material properties are given in Table 66.

Dummy Material Properties		
Property	Value	Units
Young's Modulus	0.001	MPa
Poisson's Ratio	0.003	[-]
Shear Modulus	0.001	MPa

Table 66: Material Properties for Dummy Material

The displacement of the main girders under a point load has been calculated by hand and by ANSYS. The hand calculation is based on Euler-Bernoulli beam theory. To account for this in ANSYS, the shear stiffness of steel has been increased by a factor 100, to eliminate the shear deformation. The result is that the deformation according to ANSYS matches quite closely with the deformation according to the hand calculation. This is shown in Figure 155. Note that the stress field does not perfectly correspond to beam theory near the supports and applied load.

<sup>288</sup> (ANSYS, Inc., 2012)

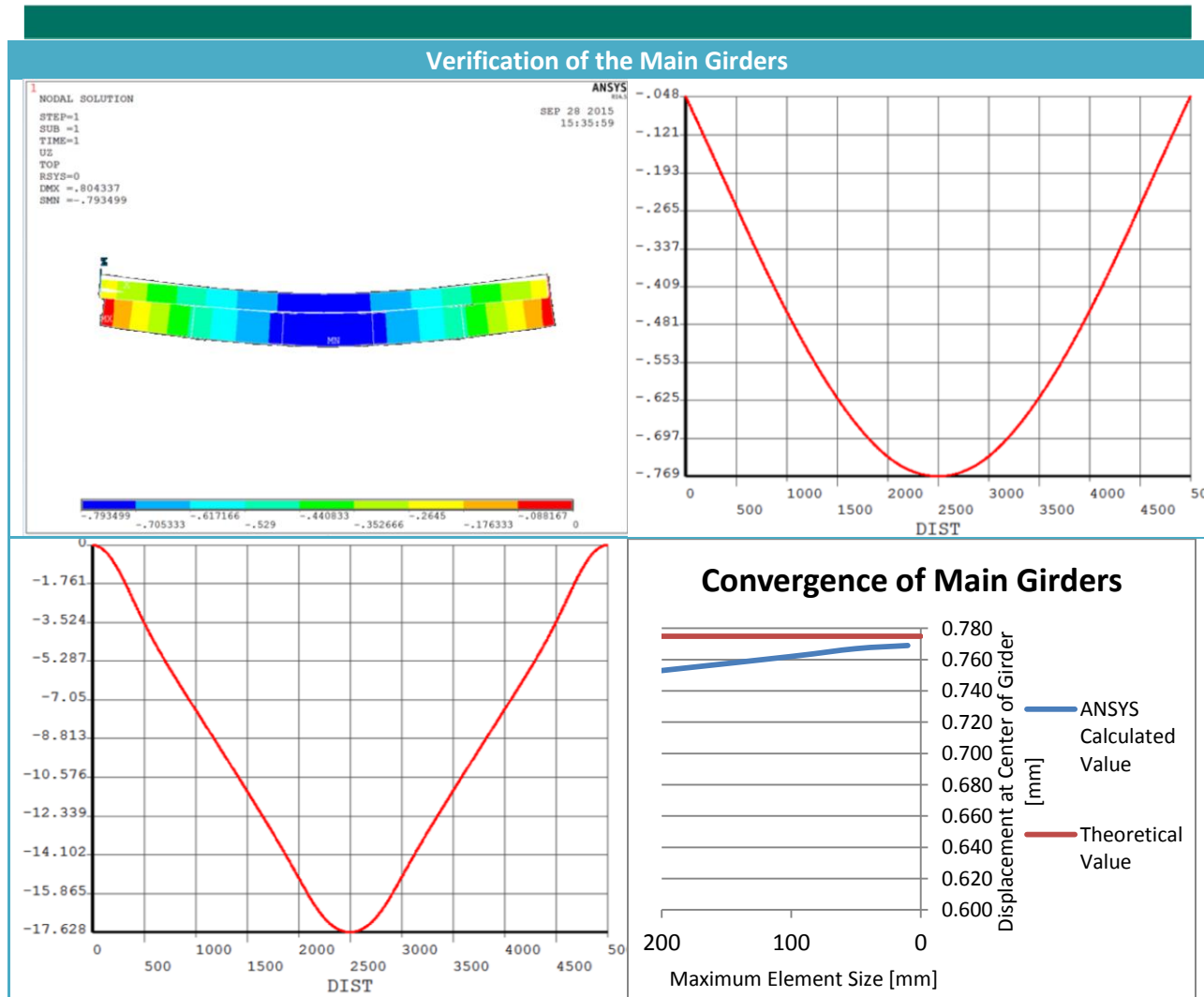


Figure 155: (Top Left): Displacement in Z-Direction [mm]. (Top Right): Displacement Field over the length of the Main Girder [mm]. (Bottom Left): Stress Development Over the Length of the Top Flange of the Main Girder [y-axis: MPa; x-axis: mm]. (Bottom Right): Convergence and Accuracy Study of the Results.

## Q.2 Crossbeams

The cross beams are validated in the same manner as the main girders. The beams are isolated by giving the rest of the structure dummy material properties. Due to the manner in which the model is set up, the beams of the main girder cannot be given material properties, since this would cause two large holes in the flanges of the crossbeams. The thickness of the main girder flanges has been altered to match the flanges of the crossbeams. However, since they still present a local widening of the flange and hence introduce an inaccuracy.

The results of the calculations are presented in Figure 156. The displacement of the system is as expected. Regarding the stress, note that at the location where the main span intersects the

crossbeams, there is a local stress reduction. Additionally, there are some initiation effects near the center of the span and near the supports. Finally, for the convergence analysis, one can see that the difference between the hand calculation and the ANSYS calculation is small; it is 1.9%.

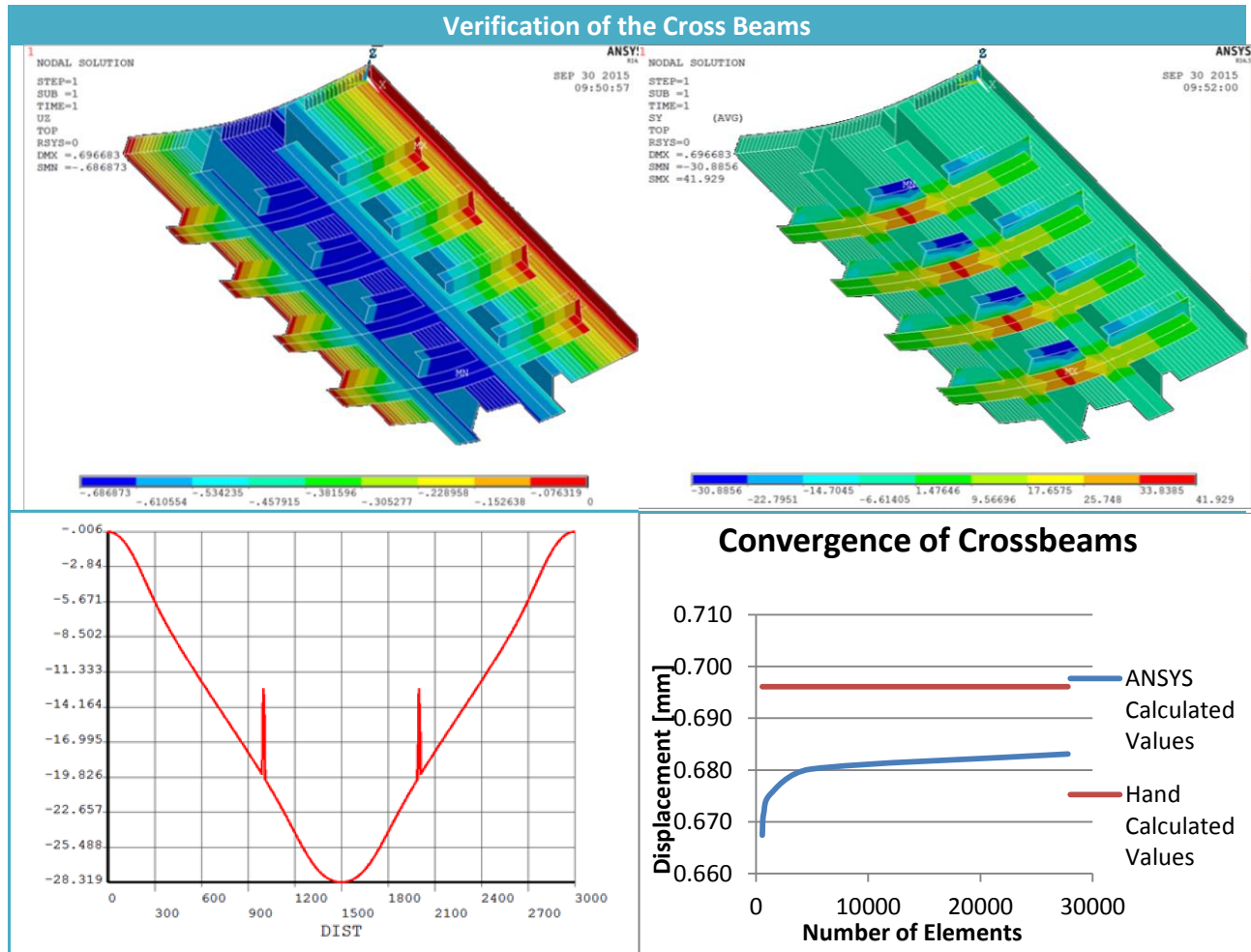


Figure 156: (Top Left) Displacement Field in Z-direction. (Top Right) Stress Field in Y-direction. (Bottom Left) Stress in Y-Direction over the Length of the Top Flange of the 2<sup>nd</sup> Crossbeam. (Bottom Right) Convergence of Displacement at Center-Span of the Crossbeams

### Q.3 Deck

The Deck will be tested in a manner similar to the main and cross girders. It is modelled as a simply supported plate, with a load applied in the middle. However, in this case the load will be applied in the form of a set displacement, and the force required will be measured. This is done because it is easier to apply a set displacement than a uniform load along a line.

An additional difference is that the shear deformations will be accepted. Since the deck is more slender than the girders, the expectation is that the shear deformations will play a smaller role. The

reason that the shear deformations are accepted in the case of the deck but not in the case of the girders is that for laminated materials the shear modulus also influences the Young's Modulus. This follows from classical laminate theory. Therefore the ANSYS results are expected to show a slightly more flexible beam than the hand calculations.

The results of the ANSYS calculation are given in Figure 157. The difference between the hand calculated value and the ANSYS calculated value are 2.44% and 2.18% for displacement and stress respectively.

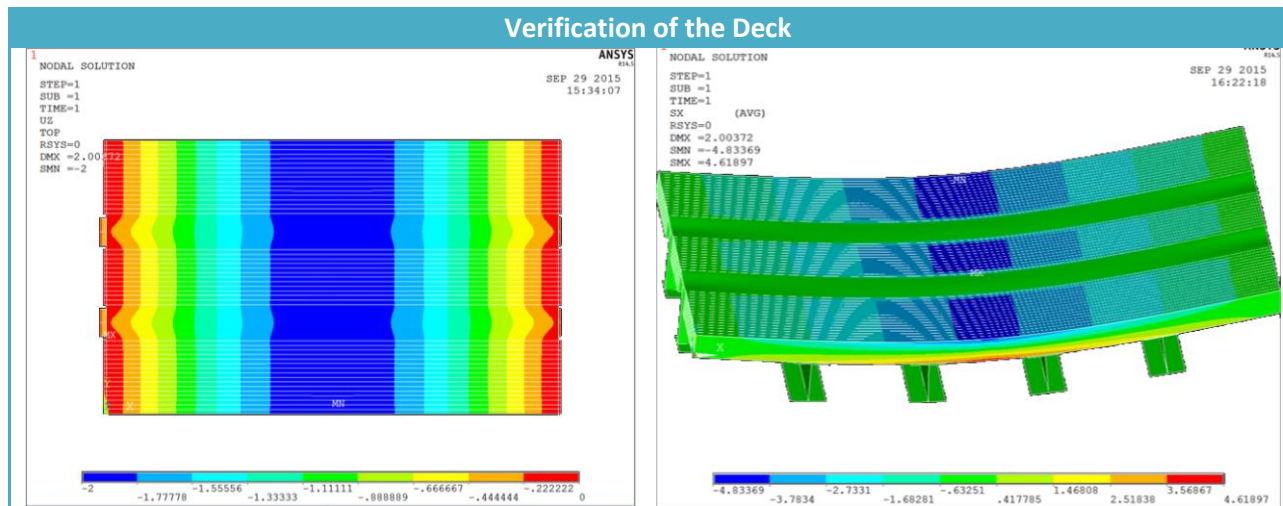


Figure 157: (Left) Displacement Field in Z-direction. (Right) Stress in X-DIRECTION

## Q.4 Connections

There are three components of the deck which should be checked. The first is the free relative motion in the XY-plane of the deck with respect to the steel profiles. The second is the secure connection in the Z-direction. Finally, the influence of the stiffness of the connection should be checked. Note that there are 7 rows of connections along the main girders. This corresponds to the 4 bolts rows which were originally part of the design, as well as a row along the center of the girder, and the outer edges. The connections along the outer edge and the center lines are required to ensure vertical compliance between the girder and the deck.

### Q.4.1 Free Horizontal Motion

The free motion in the XY-plane will be considered first. This is checked by applying a displacement in the X- and Y-direction of the deck. The results are shown in Figure 158. Note that there appears to be a peak stress near the location where the displacement of the deck has been applied. However, the value of this peak stress is order size  $10^{-3}$  MPa. This very slight inaccuracy is tolerable.

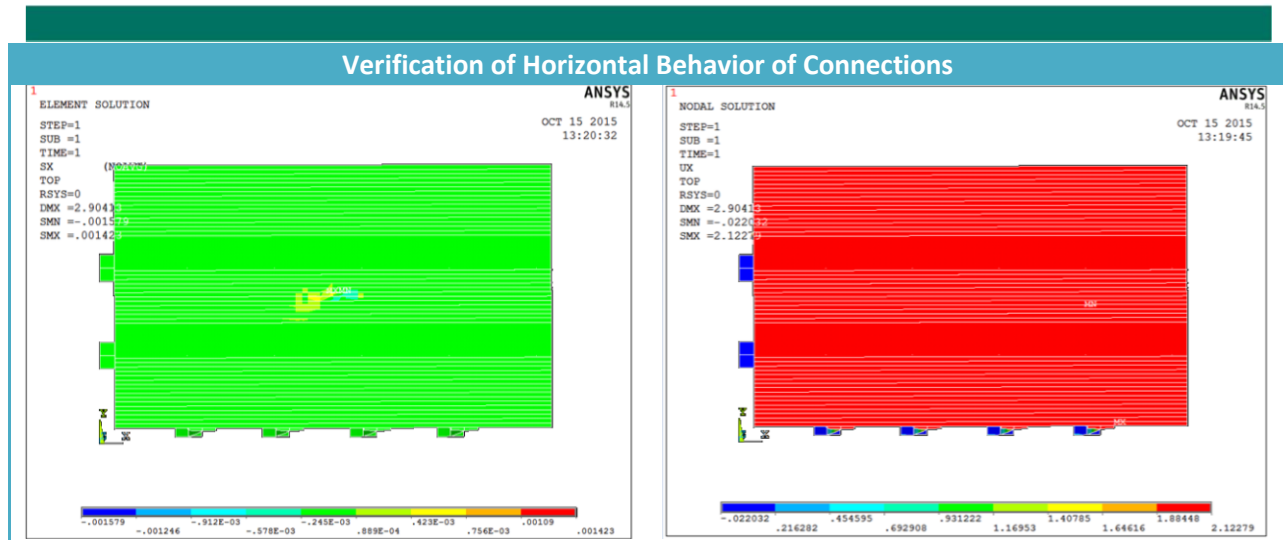


Figure 158: (Left) The Stress Field in the Model [MPa]. (Right) The Displacement Field of the Model in X-Direction [mm].

#### Q.4.2 Restrained Vertical Motion

The behavior of the connections in the Z-direction will be assessed next. The deck should be attached to the girders in Z-direction. To test this, a point in the deck has been assigned a 2mm displacement in Z-direction. The results are shown in Figure 159. Most noteworthy is that as the deck experiences loading in Z-direction, the girders will also experience such loading.

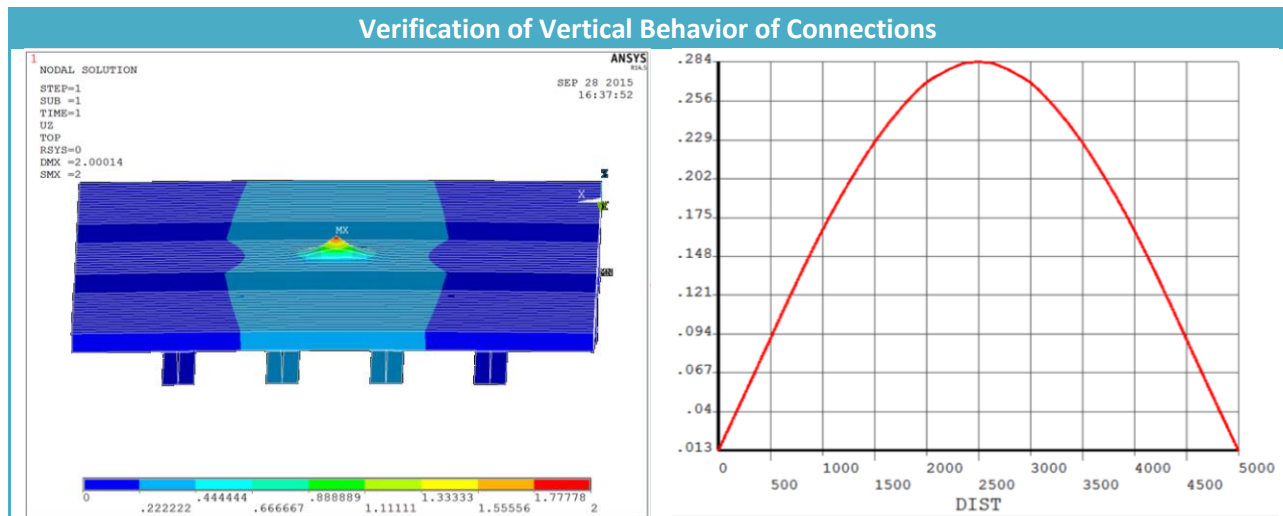


Figure 159: (Left) The Displacement Field in Z-Direction of the Model [mm]. (Right) The Displacement Along the Length of the Main Girder [mm].

#### Q.4.3 Influence of Connection Stiffness

In order to test the influence of the stiffness of the connections, an analysis has been made relating the stiffness of the connection to the displacement of the bridge under a point load. A point load of -100kN in z-direction is applied to each of the main girders at mid-span. The resulting

displacement is calculated for a series of connection stiffnesses. The results are displayed in Figure 160 and Figure 161.

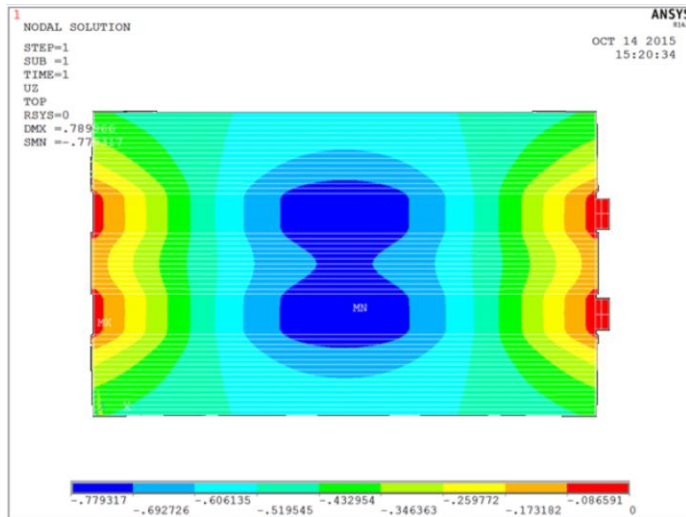


Figure 160: Typical Displacement Field in z-Direction for the Analysis of the Connection Stiffness

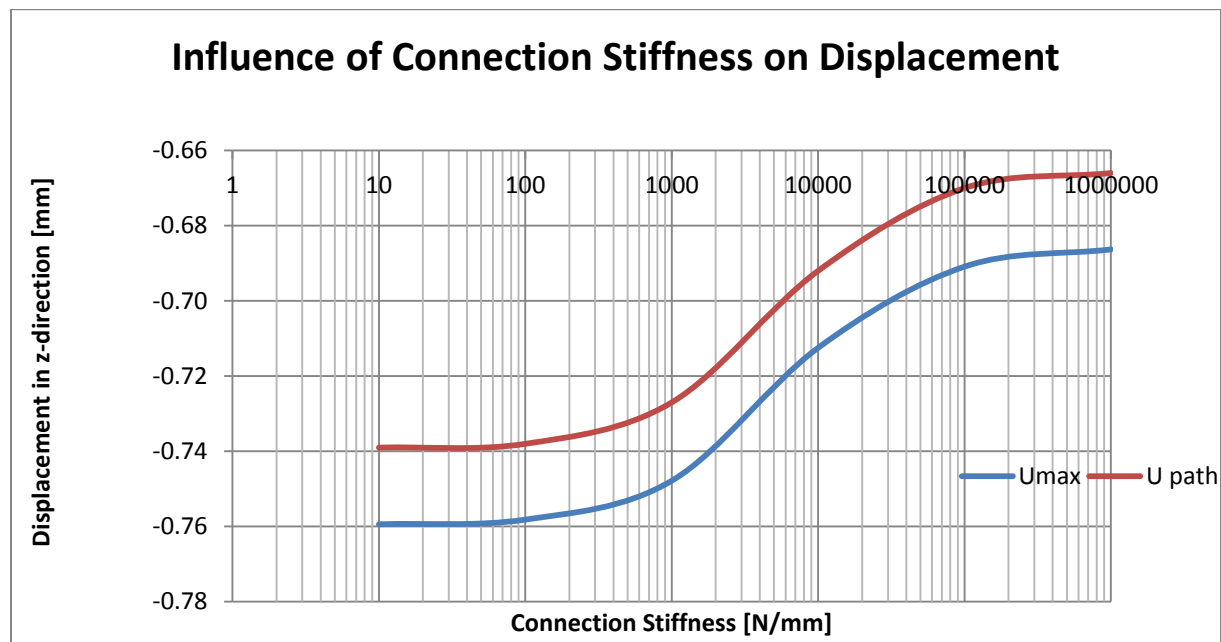


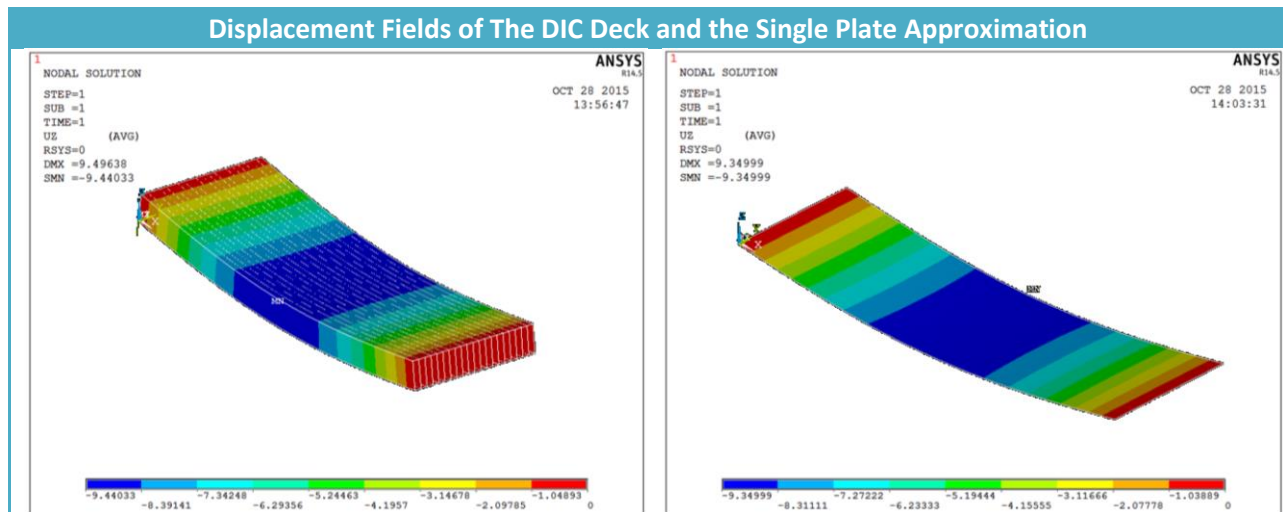
Figure 161: Influence of the Connection Stiffness on the Displacement in z-Direction. U max Represents the Maximum Vertical Displacement in the System. U path Represents the Maximum Vertical Displacement Along the Top of the Main Girder.

Figure 161 shows the influence of the connection stiffness on the displacement of the model. Remember that these calculations have been performed on a smaller variant of the bridge to reduce computational time. Therefore the results of this calculation are not directly applicable to the full scale model, and should only be used as indicative values. For the smaller model, the shear connection has no influence as long as the stiffness remains below the 100N/mm threshold. For the full scale model, the rigid body motions of the deck disappear when a spring stiffness of 0.001N/mm is introduced. Based on the large disparity between these spring constants, the belief is that the spring constant applied in the full scale model has no unwanted influence on the displacement of the structure.

### Q.5 Validation of Plate Approximation

To reduce the number of elements in the model of the bridge, parts of the deck are approximated with a single plate rather than the geometry of the DIC deck. This reduced geometrical complexity allows for the model to be calculated considerably faster. In order to simplify the structure in this manner, the plate approximation should be designed such that its behavior matches that of the original deck.

To ensure that the properties of the plate approximation match those of the DIC deck, the two versions of the deck were isolated and subjected to a load. The load consisted of a 100kN load across the entire surface of the deck. Since the DIC deck has orthotropic properties, the deck is tested in two directions. This is achieved by altering the location of the supports. The displacements of the DIC deck are determined and the single plate is designed so that it matches the displacements for both scenarios. The displacements for the two versions of the deck in both scenarios are shown in Figure 162.





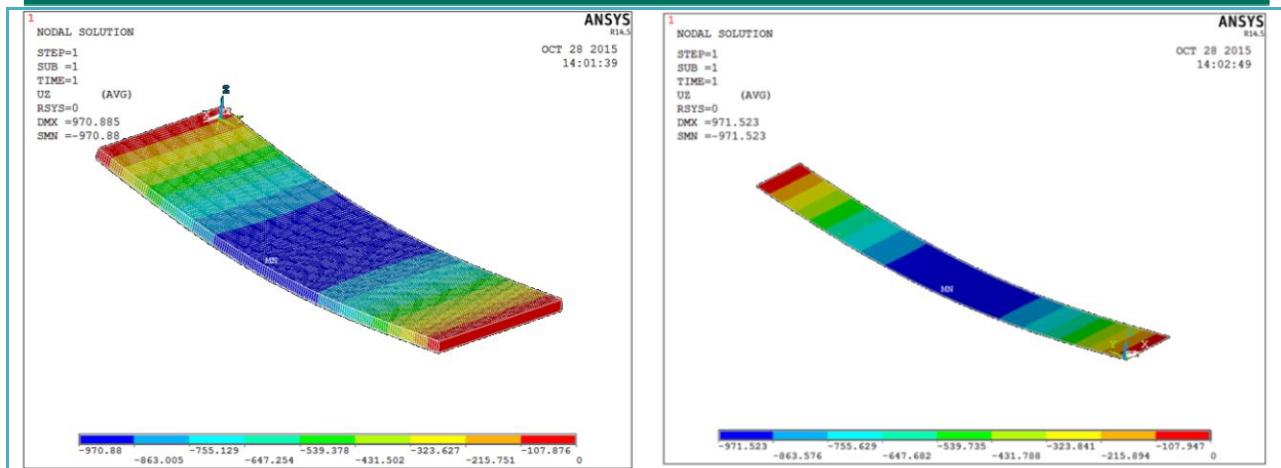


Figure 162: (Top Left): The Displacement Field in Vertical Direction of the DIC Deck Tested in Longitudinal Direction. (Top Right): The Displacement Field in Vertical Direction of the Plate Approximation Tested in Longitudinal Direction. (Bottom Left): The Displacement Field in Vertical Direction of the DIC Deck Tested in Transverse Direction. (Bottom Right): The Displacement Field in Vertical Direction of the Plate Approximation Tested in Transverse Direction.

The displacements of the DIC deck in Figure 162 are determined using the geometry provided by the deck and the material properties as described in 4.3.5 Determination of Laminate Properties. The properties of the single plate are set to mimic the behavior. The single plate is created as a sandwich panel. The outer faces of this panel match the face panels of the DIC deck. The material properties of the filler material between the two face panels is given in Table 67.

Material Properties for Single Plate Filler Material		
Property	Value	Units
Young's Modulus Longitudinal	2820	MPa
Young's Modulus Transverse	282	MPa
Shear Modulus Longitudinal	3086	MPa
Shear Modulus Transverse	29.6	MPa
Poisson's Ratio	0.26	-

Table 67: Material Properties for the Filler Material in the Single Plate Approximation

With the material properties according to Table 67, the displacements given in Table 68 are found. The difference between the two models is sufficiently small that they are acceptable. Hence in locations where the local behavior of the deck is unimportant, the deck can be simplified using the single plate approximation. For regions where local displacements are relevant, the original deck will continue to be utilized.

Displacements of the Two Deck Models			
Scenario	DIC Deck Displacement [mm]	Single Plate Displacement [mm]	Difference [%]
Longitudinal	9.44	9.35	-0.96%
Transverse	970.88	971.52	0.07%

Table 68: Displacements of the DIC Deck and the Single Plate Approximation for Longitudinal and Transverse Load Carrying Situations

## Appendix R: Verification of Loading Distance in Model

In 8.1 Hand Calculations of Girder to Deck Detail, for various laminate thicknesses a distance between the load and the critical cross section is determined which produces the maximum moment in the considered detail. The distance indicated by “L” in Figure 163 represents this distance, minus half of the wheel width<sup>289</sup>. The distance for each laminate thickness is determined using a schematization based on several assumptions. However, the resulting distances, given in Table 69, are also applied in the ANSYS model. For this reason, a check should be performed to see if the assumed distances are correct. Therefore, these distances have been checked against a model where the wheels are applied directly next to the girder.

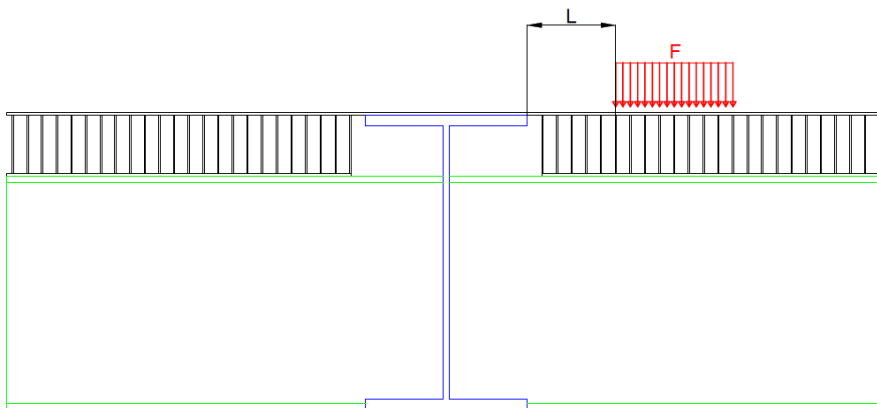


Figure 163: Cross Section of the Main Girder-Deck System. Load F represents a Wheel Load, and L is Dependent on the Thickness of the Laminate.

Distance at Which Wheel Load is Applied	
Laminate Height [mm]	Distance “L” [mm]
11.75	0
20	0
50	230
70	400
135	950

Table 69: List of Distances at Which the Wheel Load is Applied Based on Laminate Thickness.

Since the analysis of the detail focusses on fatigue damage, this is also utilized as the criteria for determining which situation taxes the structure more. The fatigue damage resulting from differing laminate thicknesses are plotted in Figure 164. For the laminates of 20mm thickness or less, the two lines coincide. This is expected, since for these thicknesses the distance at which the load was applied is equal. As the laminate thickness passes the 20mm mark, the cumulative damage which includes L

<sup>289</sup> For thinner laminates the distance L would become negative. However, for these thicknesses L is set to zero.

becomes larger than the damage excluding L. This indicates that applying the wheel load at a distance from the girders creates a situation which is more taxing on the laminate. Hence the decision to apply the load at a certain distance from the edge of the girder is supported.

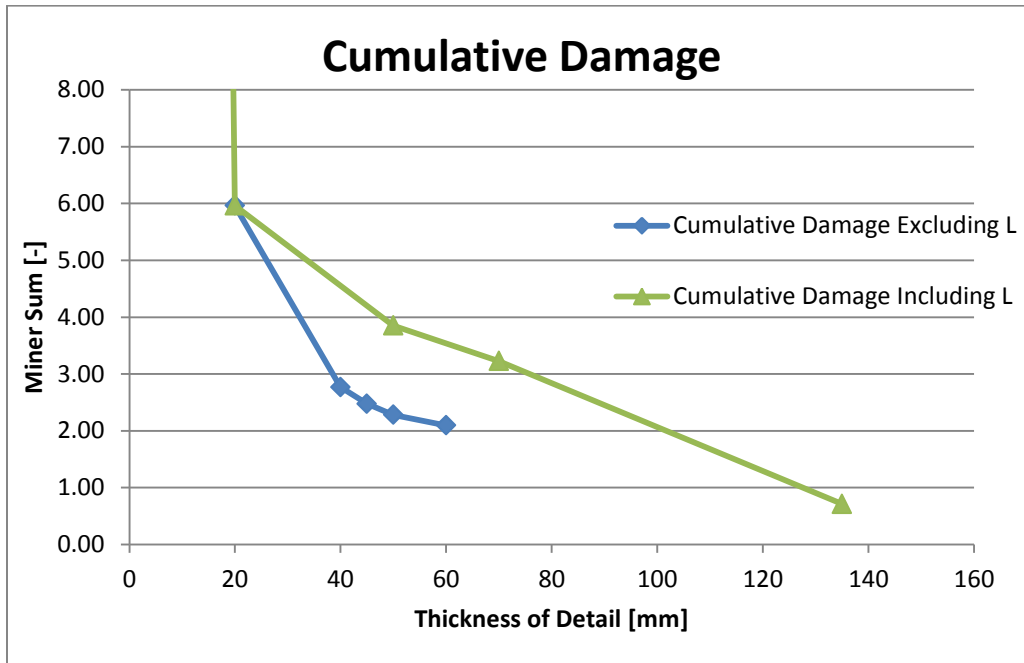


Figure 164: The Cumulative Damage as a Function of the Thickness of the Laminate at the Detail. Two situations are considered. One including the distance L, and one where L is zero.

Applying the wheel load at a certain distance from the girder edge leads to a higher cumulative damage. This has been proven above. However, the distance used in the analysis above is determined based on hand calculations where several simplifications have been applied. For a model which includes more complexities, the likelihood is large that this distance will vary. Based on time constraints, a study towards the distance corresponding to the largest damage has not been performed. The belief is that for thinner laminates and shorter distances any change will be small. This provides an additional motivation to seek a solution with a minimal laminate thickness.

## Appendix S: Influence of Reduced Stiffness of Rear Abutment

Throughout the design process, one of the design criteria applied is that the stiffness of the rear abutment needs to increase by 30% in order to reduce vertical displacements. This leads to an unfair comparison which benefits the current design. This appendix analyzes the influence that this additional design requirement has on the mass of the global structure. The stiffness, section modulus, and mass have been determined according to the methods explained in chapters 5.4 Composite Stiffness of Girders, 5.5 Section Modulus of Connected Cross Section, and 5.6 Mass Change Due to Composite Action, respectively. The results are presented in Table 70. As expected, the lowered stiffness requirement leads to lighter girders.

Influence of Neglecting the Increased Stiffness Requirement					
	High Stiffness			Low Stiffness	
	Current Design	FRP Optimized	Orthotropic	FRP Optimized	Orthotropic
<b>Stiffness [kNmm<sup>2</sup>]</b>	2.20E+12	2.86E+12	2.93E+15	2.24E+12	2.20E+12
<b>Section Modulus [mm<sup>3</sup>]</b>	1.73E+07	2.67E+07	2.62E+07	2.08E+07	1.80E+07
<b>Mass [tonnes]</b>	10.5	10.0	5.6	8.7	3.6

Table 70: The Stiffness, Section Modulus, and Mass of the Rear Abutment for The Current, Optimized FRP, and Orthotropic Designs, with and without the Increased Stiffness Requirement.

## Appendix T: Bibliography

- Allred & Associates Inc. (2015). *What is Carbon Fiber*. Retrieved May 22, 2015, from DragonPlate:  
<http://dragonplate.com/sections/technology.asp>
- American Chemical Society. (1993). *National Historic Chemical Landmarks*. Retrieved April 9, 2015, from Bakelite:The World's First Synthetic:  
<https://www.acs.org/content/acs/en/education/whatischemistry/landmarks/bakelite.html>
- American Chemical Society. (2003, September 17). *National Historic Chemical Landmark*. Retrieved April 10, 2015, from High Performance Carbon Fibers:  
<http://www.acs.org/content/acs/en/education/whatischemistry/landmarks/carbonfibers.html>
- ANSYS, Inc. (2012). ANSYS 14.5 Help. *MPC184 Point-in-plane Joint Element Description*. Pittsburgh, Pennsylvania, United States: SAS IP, Inc.
- Bamberg, P. E. (2006). *Contact Stresses and Deformations*. Salt Lake City: The University of Utah.
- Bank, L. C. (2006). *Composites for Construction: Structural Design with FRP Materials*. Hoboken: John Wiley & Sons, Inc.
- BS EN 1090-2:2008. Execution of Steel Structures and Aluminium Structures Part 2: Technical Requirements for the Execution of Steel Structures. (2008). United Kingdom: British Standards Institution.
- Burgoyne, C., & Head, P. (1993). *Aberfeldy Bridge - and advanced textile reinforced footbridge*. Cambridge: University of Cambridge.
- Calard, V. (2011). *Formulas and Equations for the Classical Laminate Theory*. Paris: Association des Centraliens.
- Camanho, P., & Lambert, M. (2006). *A design methodology for mechanically fastened joints in laminated composite materials*. Amsterdam: Elsevier.
- Chang, F.-K., Scott, R., & Springer, G. (1982). *Strength of Mechanically Fastened Composite Joints*. Ann Arbor: The University of Michigan.
- Civieltechnisch Centrum Uitvoering Research en Regelgeving-onderzoekcommissie C 124. (2003-6). *Vezelversterkte kunststoffen in civiele draagconstructies: Achtergrondrapport bij CUR-Aanbeveling 96*. Gouda: Stichting CUR.

- Company of Proprietors of the Stroudwater Navigation. (2010). *Bonds Mill Bridge*. Retrieved April 14, 2015, from The Company of Proprietors of the Stroudwater Navigation:  
[http://www.stroudwater.co.uk/swmap/map3/bonds\\_mill\\_bridge.html](http://www.stroudwater.co.uk/swmap/map3/bonds_mill_bridge.html)
- Composites World Staff. (2014, January 1). *The fiber*. Retrieved April 15, 2015, from Composites World:  
<http://www.compositesworld.com/articles/the-fiber>
- Core Systems. (n.d.). *New Product! SOLEPAVE*. Retrieved May 22, 2015, from Core Systems:  
<http://www.coregravel.ca/new-product-solepave/>
- Cripps, D. (2015). *Guide to Composites*. Retrieved April 15, 2015, from Net Composites:  
<http://www.netcomposites.com/guide>
- Davalos, J., Chen, A., & Qiao, P. (2013). *FRP Deck and Steel Girder Bridge Systems: Analysis and Design*. Boca Raton: CRC Press.
- Demers, C. E. (1997). *Fatigue Strength Degradation of E-glass FRP Composites and Carbon FRP Composites*. Tuscon: University of Arizona.
- Direct Industry. (2015). *Owens Corning: Multi-end E-glass roving*. Retrieved May 22, 2015, from Direct Industry: The Online Industrial Exhibition: <http://www.directindustry.com/prod/owens-corning/multi-end-e-glass-rovings-37816-259793.html>
- Duthinh, D. (2000). *Connections of Fiber-Reinforced Polymer (FRP) Structural Members: A Review of the State of the Art*. Gaithersburg: NIST.
- Eischen, J., Chung, C., & Kim, J. (1990). *Realistic Modeling of Edge Effect Stresses in Bimaterial Elements*. Raleigh: North Carolina State University.
- Erhard, G. (2006). *Designing with Plastics*. Cincinnati: Hanser Gardner Publications.
- Gemeente Alphen aan den Rijn. (n.d.). *Vervanging Koningin Julianabrug*. Retrieved April 8, 2015, from Alphen aan den Rijn:  
[https://www.alphenaandenrijn.nl/Inwoners/Wonen\\_verbouwen/Nieuwbouw\\_bouwkavels/Bouwprojecten/Alphen\\_aan\\_den\\_Rijn/Vervanging\\_Koningin\\_Julianabrug](https://www.alphenaandenrijn.nl/Inwoners/Wonen_verbouwen/Nieuwbouw_bouwkavels/Bouwprojecten/Alphen_aan_den_Rijn/Vervanging_Koningin_Julianabrug)
- Gondar, P. (2013). *Laser Stake Welded Sandwich Steel Decks for Highway Bridges*. Delft: Delft University of Technology.
- Google. (n.d.). *Koningin Julianabrug, Alphen aan den Rijn, Netherlands*. Retrieved April 4, 2015, from Google Maps:  
<https://www.google.com/maps/place/Kon.+Julianabrug,+Alphen+aan+Den+Rijn,+Netherlands/>

@52.134856,4.6634299,17z/data=!3m1!4b1!4m2!3m1!1s0x47c5daf9611601b7:0xfcec3ba3907e15b8

Gradeci, K. (2013). *Upgrading Old Movable Bridges with FRP Deck Application: The case study of Wilhelminabrig*. Delft: Delft University of Technology.

Gurit. (2015). Gurit Corecell T. *Structural Foam Core*. Switzerland: Gurit Holding AG.

Hart-Smith, L. (1976). *Bolted Joints in Graphite-Epoxy Composites*. Long Beach: NASA.

Hartsuijker, C., & Welleman, H. (2011). *Module: Non-Symmetrical and Inhomogeneous Cross Sections*. Delft: TU-Delft.

Hattink, C. (2014). *DO-Berekening Stalen val*. Amsterdam: Iv-Infra.

Hewson, N., & Parke, G. (2008). *ICE manual of bridge engineering*. London: Thomas Telford Ltd.

Hollaway, L. (2001). *Advanced Polymer Composites and Polymers in the Civil Infrastructure*. Amsterdam: Elsevier Science.

Indian Institute of Technology. (2014, August 18). *Self Consistent, Mori-Tanaka and Halpin Tsai Models*. Retrieved April 16, 2015, from National Programme on Technology Enhanced Learning: <http://nptel.ac.in/courses/101104010/34>

Indian Institute of Technology. (n.d.). *Module 7: Strength and Failure Theories*. Retrieved April 21, 2015, from National Programme on Technology Enhanced Learning: <http://nptel.ac.in/courses/105108124/7>

JFE Engineering Corporation. (2014). *Design and construction of steel/concrete composite deck slab bridges*. Retrieved June 2015, 23, from JFE Engineering Corporation: <http://www.jfe-eng.co.jp/en/products/link/t18.html>

Johnson, R. P. (2012). *Designer's Guide to Eurocode 4: Design of Composite Steel and Concrete Structures*. London: Thomas Telford Limited.

Kable. (n.d.). *Friedberg Bridge, Friedberg, Germany*. Retrieved April 14, 2015, from Roadtraffic Technology: <http://www.roadtraffic-technology.com/projects/friedberg-bridge/>

Kaw, A. K. (2006). *Mechanics of Composite Materials: Second Edition*. Boca Raton: Taylor & Francis.

Knippers, J., & Gabler, M. (2006). *New Design Concepts for Advanced Composite Bridges - The Friedberg Bridge in Germany*.



- Knippers, J., & Gabler, M. (2008). *The FRP road bridge in Friedberg Germany - new approaches to a holistic and aesthetic design*. Stuttgart: University of Stuttgart.
- Kok, L. (2013). *Feasibility study for FRP in large hydraulic structures: Literature Study*. Delft: Delft University of Technology.
- Kolstein, D. (2008). *Fibre Reinforced Polymer (FRP) Structures*. Delft: Delft University of Technology.
- Macdonald, Abbot, & Peterson. (1983). *Volcanoes in the Sea: Geology of Hawaii*. Manoa: University of Hawaii Press.
- Marsh, G. (2006, October 08). *50 years of reinforced plastic boats*. Retrieved April 10, 2015, from Reinforced Plastics: <http://www.reinforcedplastics.com/view/1461/50-years-of-reinforced-plastic-boats/>
- Marshall Cavendish Corporation Staff. (2003). *How It Works: Science and Technology*. Tarrytown: Marshall Cavendish.
- Meikle, J. L. (1997). *American Plastic: A Cultural History*. New Brunswick: Rutgers University Press.
- Naik, N. (n.d.). *Compressive strength of unidirectional composites: evaluation and comparison of prediction models*. Mumbai: Indian Institute of Technology.
- Nettles, A. (1994). *Basic Mechanics of Laminated Composite Plates*. Huntsville, Alabama: NASA.
- Network Group for Composites in Construction. (2013). *Bonds Mill Lift Bridge*. Retrieved April 14, 2015, from Network Group for Composites in Construction: <http://www.ngcc.org.uk/LinkClick.aspx?fileticket=Ej fj87PpEc%3D&tabid=85&mid=458>
- Nijssen, R. (2013). *Composieten Basiskennis*. Delft: Hogeschool Inholland.
- Normcommissie 351 001. (2000). *NEN 6772 (nl): Technische Grondslagen voor Bouwconstructies - TGB 1990 - Verbindingen*. Delft: Nederlands Normalisatie-instituut.
- Normcommissie 351 001. (2002). *NEN-EN 1990: Basis of Structural Design*. Delft: Nederlands Normalisatie Instituut.
- Normcommissie 351 001. (2003). *NEN-EN 1991-1-5: Thermal Actions*. Delft: Nederlands Normalisatie Instituut.
- Normcommissie 351 001. (2003). *NEN-EN 1991-2 (en): Traffic Loads on Bridges*. Delft: Nederlands Normalisatie Instituut.

- Normcommissie 351 001. (2005). *NEN-EN 1991-1-4: General Actions - Wind Actions*. Delft: Nederlands Normalisatie Instituut.
- Normcommissie 351 001. (2005). *NEN-EN 1994-1-1: Design of composite steel and concrete structures - Part 1-1: General rules and rules for buildings*. Delft: Nederlands Normalisatie Instituut.
- Normcommissie 351 001. (2006). *NEN-EN 1993-1-1: Design of Steel Structures*. Delft: Nederlands Normalisatie Instituut.
- Normcommissie 351 001. (2007). *NEN-EN 1993-2: Design of Steel Structures - Part 2: Steel Bridges*. Delft: Nederlands Normalisatie Instituut.
- Normcommissie 351 001. (2011). *NEN-EN 1990+A1+A1/C2/NB: National Annex to Basis of Structural Design*. Delft: Nederlands Normalisatie Instituut.
- Normcommissie 351 001. (2011). *NEN-EN 1991-1-5+C1/NB: National Annex Thermal Actions*. Delft: Nederlands Normalisatie Instituut.
- Normcommissie 351 001. (2011). *NEN-EN 1991-2: National Annex Steel Bridges*. Delft: Nederlands Normalisatie Instituut.
- Normcommissie 351 001. (2011). *NEN-EN 1993-2+C1/NB: Design of Steel Structures - Part 2: Steel Bridges*. Delft: Nederlands Normalisatie Instituut.
- Normcommissie 351 062. (2001). *NEN 6786: Voorschriften voor het ontwerpen van beweegbare bruggen*. Delft: Nederlands Normalisatie Instituut.
- Offereins, S. Koningin Julianabrug te Alphen aan den Rijn. *Concept-DO*. Iv-Infra, Amsterdam.
- Okutan, B. (2001). *Stress and Failure ANalysis of Laminated Composite Pinned Joints*. Izmir: Dokuz Eylul University.
- Peel, L. D. (2005). *Investigation of High and Negative Poisson's Ratio Laminates*. Kingsville: Society for the Advancement of Material and Process Engineering.
- Performance Composites Ltd. (2009, July). *Mechanical Properties of Carbon Fiber Composite Materials*. Retrieved June 10, 2015, from Composite Materials Engineering Specialists in Carbon Fibre: [http://www.performance-composites.com/carbonfibre/mechanicalproperties\\_2.asp](http://www.performance-composites.com/carbonfibre/mechanicalproperties_2.asp)
- Pilling, J. (2005). *Michingan Tech*. Retrieved April 16, 2015, from Halpin-Tsai Equations: <http://www.mse.mtu.edu/~drjohn/my4150/ht/ht.html>

- Prince Engineering. (2015). *FRP Reinforcement for Structures*. Retrieved May 4, 2015, from Prince Engineering: Build on Prince: <http://www.build-on-prince.com/frp-reinforcement.html#sthash.MlmhRXIS.dpbs>
- Purslow, D. (1977). *The Shear Properties of Unidirectional Carbon Fibre Reinforced Plastics and their Experimental Determination*. London: Procurement Executive, Ministry of Defense.
- Qureshi, J., & Mottram, T. J. (2012). *Resin Injected Bolted Connections: A step towards achieving slip-resistant joints in FRP bridge engineering*. London: The University of Warwick.
- Redactie Omroep West. (2010-2015). *Zoeken: Julianabrug*. Retrieved April 29, 2015, from Omroep West: [http://www.omroepwest.nl/search/apachesolr\\_search/Julianabrug](http://www.omroepwest.nl/search/apachesolr_search/Julianabrug)
- Rhijn, R. v. (2012). *Memo Composiet*. Alphen aan den Rijn: Gemeente Alphen aan den Rijn.
- Rijswijk, K., Brouwer, W., & Beukers, A. (2003). *FAO Corporate Document Repository*. Retrieved May 22, 2015, from Application of Natural Fibre Composites in the Development of Rural Societies: <http://www.fao.org/docrep/007/ad416e/ad416e05.htm>
- Roylance, D. (2000). *Laminated Composite Plates*. Cambridge: Massachusetts Institute of Technology.
- Scholze, C. (2015). *FBD600 Asset Bridge Deck - Product data*. Retrieved September 17, 2015, from Fiberline Composites: Create More With Less: <http://fiberline.com/fbd600-asset-bridge-deck-product-data>
- Slayter, G. (1933). *Patent No. US2133235 A*. United States of America.
- Solvay: Asking More From Chemistry. (2015). *Ryton PPS -Engineering Properties*. Retrieved November 10, 2015, from Solvay Markets & Products: <http://www.solvay.com/en/markets-and-products/featured-products/Ryton-Engineering-Properties.html>
- Stapel, E. (2012). *Cramer's Rule*. Retrieved May 20, 2015, from Purplemath: <http://www.purplemath.com/modules/cramers.htm>
- Stapel, E. (2012). *Minors and Cofactors*. Retrieved May 20, 2015, from Purplemath: <http://www.purplemath.com/modules/minors.htm>
- Stark, J., & Stark, R. (2009). *Staal-beton: Toepassing en berekening van staal-beton constructies voor gebouwen volgens Eurocode 4 bij normale temperatuur en brand*. Zoetermeer: Bouwen met Staal.
- Stratford, T. (2012). *The Condition of the Aberfeldy Footbridge After 20 Years of Service*. Edinburgh: University of Edinburgh.

- Surathi, P., & Karbhari, V. M. (2006). *Hygrothermal Effects on Durability and Moisture Kinetics of Fiber-Reinforced Polymer Composites*. La Jolla: University of California, San Diego.
- The Editors of Encyclopaedia Britannica. (2013, October 4). *Sir Joseph Wilson Swan: English Physicist and Chemist*. Retrieved April 10, 2015, from Encyclopaedia Britannica: <http://www.britannica.com/EBchecked/topic/576273/Sir-Joseph-Wilson-Swan>
- The Editors of Encyclopaedia Britannica. (2015). *Aramid: Chemical Compound*. Retrieved April 10, 2015, from Encyclopaedia Britannica: <http://www.britannica.com/EBchecked/topic/32063/aramid>
- The European Structural Polymeric Composites Group. (1996). *Structural Design of Polymer Composites*. London: E & FN SPON.
- Tiwari, N. (n.d.). *Introduction to Composite Materials and Structures*. Retrieved April 21, 2015, from National Programme on Technology Enhanced Learning: <http://nptel.ac.in/courses/112104168/31>
- Torabizadeh, M. A. (2013). *Tensile, compressive and shear properties of unidirectional glass/epoxy composites subjected to mechanical loading and low temperature services*. Mashad: Indian Journal of Engineering & Materials Sciences.
- Tsai, S. W. (1965). *Strength Characteristics of Composite Materials*. Newport Beach: National Aeronautics and Space Administration.
- U.S. Department of Transportation: Federal Aviation Administration. (1996). *Comparative Evaluation of Failure Analysis Methods for Composite Laminates*. Springfield: National Technical Information Service.
- U.S. Environmental Protection Agency. (1997). *Profile of the Plastic Resin and Manmade Fiber Industries*. Washington, DC: U.S. Government Printing Office.
- University of Cambridge. (2008, January). *Dissemination of IT for the Promotion of Materials Science (DoITPoMS)*. Retrieved April 16, 2015, from Mechanics of Fibre-Reinforced Composites: [http://www.doitpoms.ac.uk/tlplib/fibre\\_composites/index.php](http://www.doitpoms.ac.uk/tlplib/fibre_composites/index.php)
- van Beek, L., & Vrielink, J. (2012). *Koninging Julianabrug: Variantenstudie*. De Bilt: Grontmij Nederland, B.v.
- Velzen, C. v. (2012). *Memo: Variantenstudie Koningin Julianabrug*. Alphen aan den Rijn: Gemeente Alphen aan den Rijn.
- Ventsel, E., & Krauthammer, T. (2001). *Thin Plates and Shells: Theory, Analysis, and Applications*. New York: Marcel Dekker, Inc.

VVD, R. (2014, March 5). *Interview Tseard Hoekstra over Renovatie Koningin Julianabrug*. Retrieved April 9, 2015, from VVD Afdeling Alphen aan den Rijn Boskoop Rijnwoude: <http://www.vvd-abr.nl/artikel/interview-tseard-hoekstra-over-renovatie-koningin-julianabrug>

Wikipedia. (2015, February 16). *Moveable Bridge*. Retrieved April 13, 2015, from Wikipedia: [http://en.wikipedia.org/wiki/Moveable\\_bridge](http://en.wikipedia.org/wiki/Moveable_bridge)

Xia, S., & Teng, J. (2005). *Behaviour of FRP-to-Steel Bonded Joints*. Kingston, Ontario, Canada: International Institute for FRP in Construction.

Yuan, H. (2011). *Optimization of Rib-to-Deck Welds for Steel Orthotropic Bridge Decks*. Blacksburg: Virginia Polytechnic Institute and State University.